1997

Structure and tectonic evolution of palaeozoic-mesozoic rocks: Sanandaj-Sirjan Zone, Western Iran

Mohammad Mohajjel Kafshdouz
University of Wollongong

STRUCTURE AND TECTONIC EVOLUTION OF PALAEOZOIC - MESOZOIC ROCKS, SANANDAJ-SIRJAN ZONE, WESTERN IRAN

A thesis submitted in fulfilment of the

requirements for the award of the degree

DOCTOR OF PHILOSOPHY

from

THE UNIVERSITY OF WOLLONGONG

NEW SOUTH WALES

AUSTRALIA

by

MOHAMMAD MOHAJJEL KAFSHDOUZ

MSc (Hons) *University of Wollongong*

School of Geosciences

1997

The contents of this thesis are the result of original research by the author and material contained herein has not been submitted to any other university or similar institution for a higher degree.

M. Mohajjel Kafshgarouz

This thesis is dedicated to my wife.

ABSTRACT

The Sanandaj-Sirjan Zone is part of the Zagros Orogen in western Iran. The study area (June area) occurs in the middle part of this zone and consists of: Permian marble and metadolomite; Middle to Late Triassic marble, metadolomite, schist, quartzite, and amphibolite; Late Triassic - Jurassic phyllite and metaigneous rocks; Late Jurassic to Early Cretaceous intermediate volcanic rocks; and Aptian-Albian limestone.

Two major episodes of deformation are recognisable in the study area and in adjoining regions. The first is characterised by east-northeasterly plunging tight folds with axial plane schistosity and associated prograde amphibolite to greenschist metamorphic facies. The second deformation is the major event and is characterised by west-northwesterly-trending tight folds with an axial plane schistosity dipping steeply towards the north-northeast. These folds are overturned with south-southwest vergence and plunge moderately to the east. Low-grade (greenschist) metamorphism is associated this event. This deformation was caused by dextral transpression with the deformation partitioned into two domains. One domain contains schist and marble, which are ductilely folded and cut by abundant thrusts. In the second domain, a mylonitic foliation is formed in mylonitic rocks and syn-deformational granitic plutons. Dextral shearing is defined by abundant shear-sense indicators. The Galeh-Doz pluton has had its emplacement controlled by S-shaped fissures produced by dextral transpression.

A new subdivision is recognised for the Sanandaj-Sirjan Zone and consists of from southwest to northeast: (1) the radiolarite sub-zone with Late Triassic to Late Cretaceous shallow to deep-marine rocks; (2) the Bistoon sub-zone with Late Triassic to Late Cretaceous shallow-marine carbonates; (3) the ophiolite sub-zone with Late Cretaceous ophiolites; (4) the marginal sub-zone with a Late Jurassic - Early Cretaceous volcanic arc succession deposited in shallow-marine environments; and (5) the complexly deformed sub-zone with the late Palaeozoic - Mesozoic passive margin succession of the northeastern side of Neo-Tethys and overlying convergent margin assemblages. Deformation in the complexly deformed and marginal sub-zones was related to subduction of Neo-Tethyan oceanic crust and was associated with arc volcanism during the Late Jurassic - Early Cretaceous. Subsequently, oblique collision occurred in the Late Cretaceous producing dextral (pure-shear dominated) transpression and deformation partitioning. Collisional tectonics in a regime of dextral transpression was renewed in the Neogene.

ACKNOWLEDGEMENTS

This study was undertaken with the assistance of a scholarship from the Ministry of Culture and Higher Education and the Ministry of Mines and Metals of the Islamic Republic of Iran.

I would like to express my deep appreciation to my supervisor Dr C.L. Fergusson of the School of Geosciences at the University of Wollongong for his excellent comments and supervision of this study. I also acknowledge discussion with other academic members of the school: Dr B. Chenhall, Dr P.F. Carr, and Dr J. Pemberton. I would like to thank Dr J. McLelland (Colgate University) for some useful discussions.

The assistance of the clerical and technical staff of the School, namely Mr A.M. Depers, B. McGoldrick, M. Perkins, D. Carrie, and D. Martin, is acknowledged.

I would like to express my appreciation to the following organisations: Ministry of Culture and Higher Education of Iran, Geological Survey of Iran, Ministry of Mine and Metals of Iran, and authorities of Darijan Marble and Masud-Abad talc mines in the Dorud region. I wish to acknowledge Professor M. Ahmadzadeh the head of Geological Survey of Iran, Dr M. Alavi and Mr A. Vaez and Dr Gezelaiag, for general assistance with this project. I also acknowledge many useful discussions and company in the field with M.R. Sahandi. I appreciate the assistance of A.R. Shahidi, B. Nazari and M. Mahbobidoost for the provision of field facilities.

I deeply appreciate the support of my family who were patient and co-operated with me during my study.

CONTENTS

LIST OF TABLES

LIST OF FIGURES

CHAPTER 1

INTRODUCTION

1.1 LOCATION

The Zagros Orogen of western Iran is a part of the Alpine-Himalayan mountain chain. From northeast to southwest, the Zagros Orogen consists of four parallel tectonic zones: (1) the Urumieh-Dokhtar Magmatic Assemblage, (2) the Sanandaj-Sirjan Zone, (3) the Zagros Fold-Thrust Belt, and (4) the Mesopotamian - Persian Gulf foreland basin (Berberian and King, 1981; Alavi 1991a, 1994). This orogenic belt is the result of closure of Neo-Tethys by consumption of oceanic crust at a northeast-dipping subduction zone below central Iran and subsequent continental collision between the Afro-Arabian and Iranian continental fragments.

The Sanandaj-Sirjan Zone extends for 1500 km from northwest (Sanandaj) to southeast (Sirjan) in the western part of Iran and has a width of 150-200 km (Figure 1.1). This study is concerned with exposed Late Palaeozoic and Mesozoic intensely deformed and metamorphosed rocks in the June area of the north Dorud-Azna region that are located in the central part of the Sanandaj-Sirjan Zone. The study area covers 350 km^2 and is located 300 km southwest of Tehran, 10 km northeast of Dorud and 12 km northwest of Azna (Figure 1.2). These cities are located near the southwestern border of the Sanandaj-Sirjan Zone and are adjacent to some of the high Zagros mountains. Compared to the high Zagros mountains (southwestern Sanandaj-Sirjan Zone and Zagros Fold-Thrust Belt), much of the Sanandaj-Sirjan Zone has a relatively lower relief topography, typically no more than 1400 m. Regional reconnaissance has also been undertaken throughout the northwestern Sanandaj-Sirjan Zone.

1.2 AIMS

The main aims of this thesis are:

(1) to complete a structural analysis of the intensely deformed and metamorphosed rocks in the June area of the Dorud-Azna region (Figure 1.2);

(2) to determine the timing of deformation episodes in relation to tectonic events in the study area;

(3) to find the metamorphic history of the study area and its relationship to different deformation episodes;

(4) to study fabrics of highly deformed intrusions in the study area and their structural evolution;

(5) to establish new tectonic subdivisions of the Sanandaj-Sirjan Zone; and

(6) to determine the tectonic evolution of the Sanandaj-Sirjan Zone, especially during the opening and closure of the Neo-Tethyan oceanic realm.

1.3 METHODS

Field investigations have included regional geological reconnaissance in the northwestern half of the Sanandaj-Sirjan Zone and more detailed geological mapping of the study area. Extensive field work was undertaken in 1994 and 1995. 110 days were spent in the field completing detailed mapping in the study area with a further 65 days of regional reconnaissance. Structural elements have been distinguished and measured at macroscopic and mesoscopic scales. Information on structures, such as style, overprinting and orientation has been collected with observations taken at 1163 stations.

Geological maps of the study area were produced based on aerial photographs at 1:50 000 and 1:20 000 scales. More detailed structural analysis was undertaken

in two well-exposed areas (Papion-Meydanak and Darijune-Bala). 1:20 000 scale aerial photographs were enlarged to 1:7 500 scale and used as base maps for these areas. Structure maps have been drawn and show extensive representative structural data. These include the 1:20 000 scale geological map of the June area (the main map in the rear pocket). All structural measurements were plotted on equal-area lower hemisphere stereographic projections using the computer programs QUICKPLOT and ROCKWARE STEREO. Samples were collected for petrological, structural and radiometric dating purposes. Thin sections of oriented samples were made to study microstructures (fabric and shear sense indicators).

No previous structural work had been done in the study area and the basic geological information is from the only published map of the region, the Khorramabad quadrangle 1:250 000 geological map, which was compiled by Soheili (1992). This map was based on a previous geological map of Berthier et al. (1974) in addition to new information from the 1:100 000 scale geological map of the Shazand region, that includes the June area (Sahandi et al. in press). The latter map was prepared by a group of Geological Survey of Iran field geologists, including the author, in 1984.

1.4 GEOLOGICAL SETTING

In this section, a brief account of the Late Precambrian - Palaeozoic history of Iran is presented, followed by an outline of the geological development of the Sanandaj-Sirjan Zone.

Outline of Late Precambrian - Palaeozoic History of Iran

Iran consists of several continental fragments which have been joined together along suture zones (Stöcklin 1974; Figure 1.3). These fragments have distinct structural trends that have been inherited from different tectonic events. The main

continental fragments (modified after Alavi 1991a) are: (a) the Alborz Belt, with east-west trends that are deflected around the oceanic crust of the southern Caspian Sea, (b) northwest Iran (after Şengör 1990a), with northwest-southeast structural trends, (c) the Central Iran Blocks (also known as the Iranian microcontinent) and the East Iran Belt, both with north-south structural trends, (d) the Zagros Orogen with northwest-southeast trends, and (e) the east-west trending Makran Accretionary Complex. The general term "central Iran" is applied to an amalgam of northwest Iran and the Central Iran Blocks.

The oldest rocks in Iran are exposed in the Central Iran Blocks and also occur in parts of the subsurface of the Zagros Orogen and possibly parts of the Alborz Belt. These rocks were complexly deformed during the Late Precambrian Pan-African (Katangan) orogeny at around 960-600 Ma (Berberian and King 1981; Samani 1992; Samani et al. 1994). This orogeny is considered to be an episode of accretion of various arc fragments terminating at about 600-550 Ma in Arabia (Husseini 1989). In Iran, this compressional tectonic activity ended with the intrusion of granites at about 583 Ma (Samani et al. 1994).

The Pan-African orogenic belt formed at the margin of Gondwana-Land and represents a major episode of crustal growth. Subsequently, during the latest Precambrian to Late Palaeozoic interval, this crust was affected by a major episode of continental rifting followed by platformal sedimentation (Husseini 1989; Samani et al. 1994). The same latest Precambrian - Late Palaeozoic succession is recognised throughout the major crustal fragments of Iran and extends beyond them to include successions in Arabia, Turkey, Jordan, Afghanistan and Pakistan (Berberian and King 1981; Husseini 1989; Boulin 1991). The base of the succession consists of latest Precambrian alkali volcanic and evaporatic rocks and is overlain by a distinctive succession of Cambrian-Permian siliciclastic and carbonate rocks deposited in shallow

marine to continental environments (Berberian and King 1981). Only mild epeirogenic events have affected the succession, as shown by several (non-angular) unconformities that have regional distribution throughout all the various continental fragments of Iran (Berberian and King 1981). Therefore the succession has had a regime of relative tectonic stability as is typical of platform settings. The distinctive nature of the succession is considered good evidence that the Iranian fragments were part of Gondwana-Land and an extension of the Afro-Arabian continental platform in the latest Precambrian - Late Palaeozoic interval (Stöcklin 1974; Berberian and King 1981; Husseini 1989).

Geological setting of the Sanandaj-Sirjan Zone

The Sanandaj-Sirjan Zone was first named by Stöcklin (1968) and described as a northwest-southeast trending belt of metamorphosed rocks occurring at the northeastern border of the Zagros Orogen (Figure 1.1). This zone has been included within larger tectonic units including the Rezaieh-Esfandageh orogenic belt of Takin (1972) and the Esfandageh-Marivan Zone of Nabavi (1974).

Near the southwestern border of the Sanandaj-Sirjan Zone is the major Zagros suture. The suture is marked by Late Cretaceous ophiolite associations which are well exposed in the southeast (Neyriz) and the northwest (Kermanshah). Also, fault-bounded units of thin-bedded pelagic limestone, radiolarite and radiolarian shale, have been traced discontinuously along the Zagros suture zone (e.g. Kazmin et al. 1986; Berberian and King 1981).

Along the northeastern boundary of the Sanandaj-Sirjan Zone, the relationship with northwest and central Iran is difficult to establish because of widespread Tertiary and Quaternary cover. A series of depressions, including Lake Urumieh, Tuzlu Gol, Gavkhuni and Jazmorian depressions, separate the Sanandaj-Sirjan Zone from the

Urumieh-Dokhtar Magmatic Assemblage to the northeast. In the south, the Gavkhuni depression is delineated by some remarkably straight faults (the Abadeh, Shahr-Babak, and Baft faults); some of which have undergone Quaternary right-lateral strike-slip movements (Berberian 1981). In the northwest, steeply dipping faults separate the Sanandaj-Sirjan Zone from northwest Iran and affect Mesozoic and all older rocks (Stöcklin 1974). A faulted contact between the Sanandaj-Sirjan Zone and the Urumieh-Dokhtar Magmatic Assemblage has been recognised in the Esfahan area (Figure 1.1) and is thought to have had dextral strike-slip movement that may have occurred as early as Late Cretaceous time (Tillman et al. 1981).

The Palaeozoic and older units of the Sanandaj-Sirjan Zone are part of the Arabian-Iranian platform that also includes elements of other continental fragments in Iran (see above; Stöcklin 1968). Palaeomagnetic data indicates that the Sanandaj-Sirjan Zone remained part of the Arabian platform until Early Mesozoic times (Berberian and King 1981). Along the Zagros suture, platform conditions terminated during a rift event that created the Neo-Tethyan ocean in the Permian to Triassic interval (Berberian and King 1981; Şengör et al. 1988). Stratigraphic evidence for rifting includes a succession of Triassic mafic volcanic and siliciclastic-carbonate rocks and a thick succession of probable deep-marine strata of Late Triassic - Jurassic age; neither of these units are recognised in the adjoining Central Iran Blocks and northwest Iran (Berberian and King 1981).

In Mesozoic times, the southwestern margin of the Sanandaj-Sirjan Zone faced Neo-Tethys and was part of the passive margin at the northeastern boundary of the Arabian platform. Late Triassic - Jurassic pelagic strata in the southwestern Sanandaj-Sirjan Zone provide the first sedimentary evidence for the appearance of an oceanic environment (Berberian & King 1981). Much of the Sanandaj-Sirjan Zone occurs northeast of the suture and was part of the strip-like Cimmerian continent that formed

by rifting off the northeastern margin of Gondwana-Land during the opening of Neo-Tethys (Şengör 1984; Şengör et al. 1988; Boulin 1991).

The northern margin of the Cimmerian continent had formed earlier by rifting and continental separation in Carboniferous times as Palaeo-Tethys opened; evidence for this event is shown by the presence of ophiolitic fragments at the northern border of the Alborz Belt (Figure 1.3, Şengör 1984, Alavi 1991b, 1992). In Early Mesozoic time, initial collision occurred between the Laurasian and Cimmerian continents in the northern Iran. While oceanic crust of the Palaeo-Tethys in northern Iran was being consumed, the Neo-Tethyan ocean was being created along the Zagros suture possibly due to extension in a backarc environment (Şengör et al. 1988; Şengör 1990a).

During the Late Jurassic - Late Cretaceous interval, a northeast-dipping subduction zone developed at the southwestern boundary of the Sanandaj-Sirjan Zone which became an active continental margin (Berberian and King 1981). Oceanic crust of Neo-Tethys was consumed at this subduction zone which is associated with Late Jurassic - Early Cretaceous andesite in the southern Sanandaj-Sirjan Zone (Berberian and King 1981). In the Late Cretaceous, consumption of all the oceanic crust of Neo-Tethys caused collision between the Cimmerian continent and the Arabian platform resulting in major deformation and metamorphism in the Sanandaj-Sirjan Zone (Berberian and King 1981). Post-collisional Tertiary granite and diorite intrusions occur in the Sanandaj-Sirjan zone (Berberian and Berberian 1981). Despite the Sanandaj-Sirjan Zone being subjected to different phases of Alpine orogeny during Mesozoic and Cainozoic times, the Zagros Fold-Thrust Belt in the southwest, with its thick, continuous, conformable succession of Palaeozoic-Mesozoic-Tertiary shelf deposits, was not deformed into gentle folds and thrust faults until Late Cainozoic times (Stöcklin 1968, 1974; Falcon 1969).

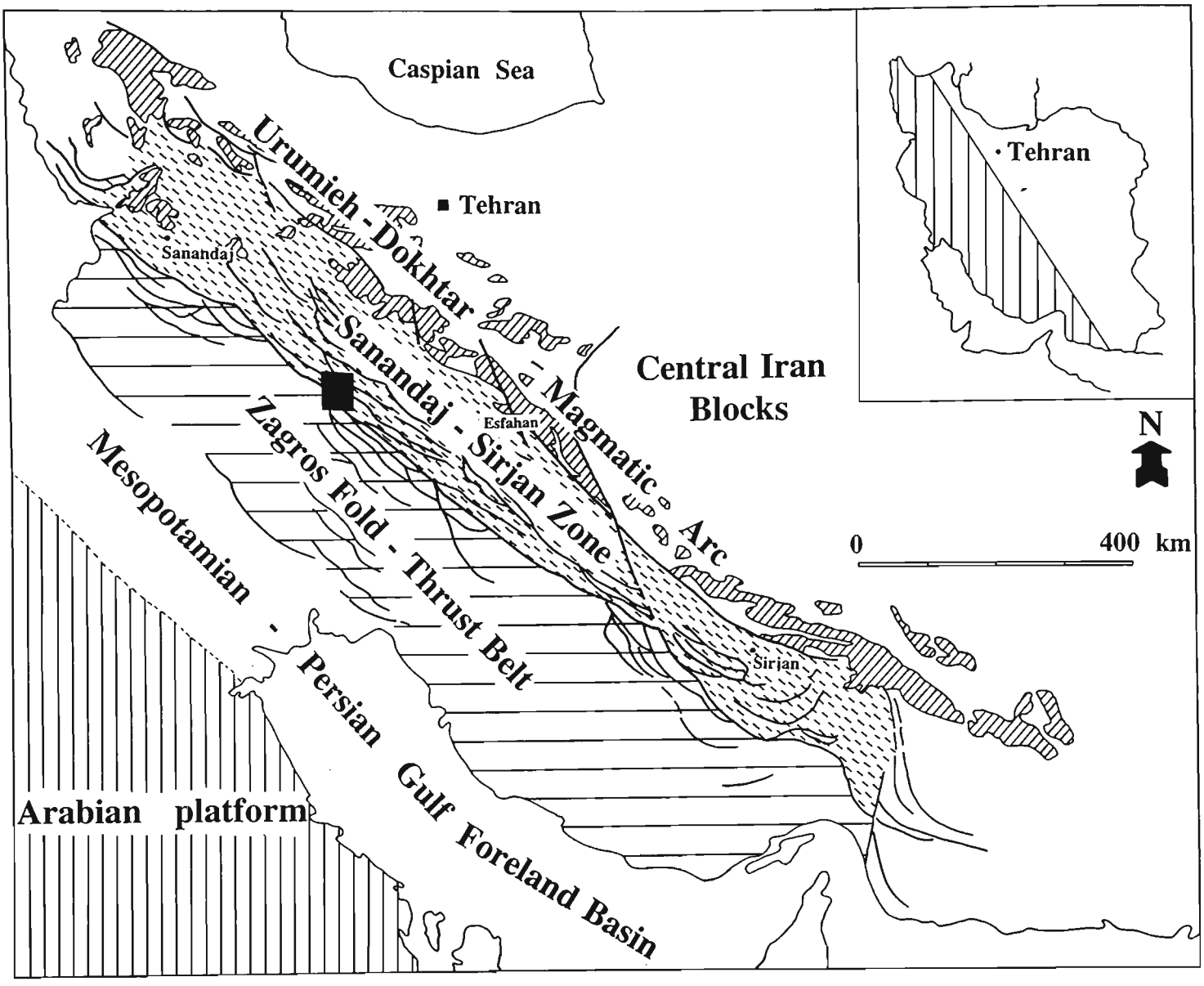

Figure 1.1

Tectonic zones of the Zagros Orogen and location of the Dorud-Azna region of the Sanandaj-Sirjan Zone (simplified from the tectonic map of the Middle East 1:29 000 000, Alavi 1991a).

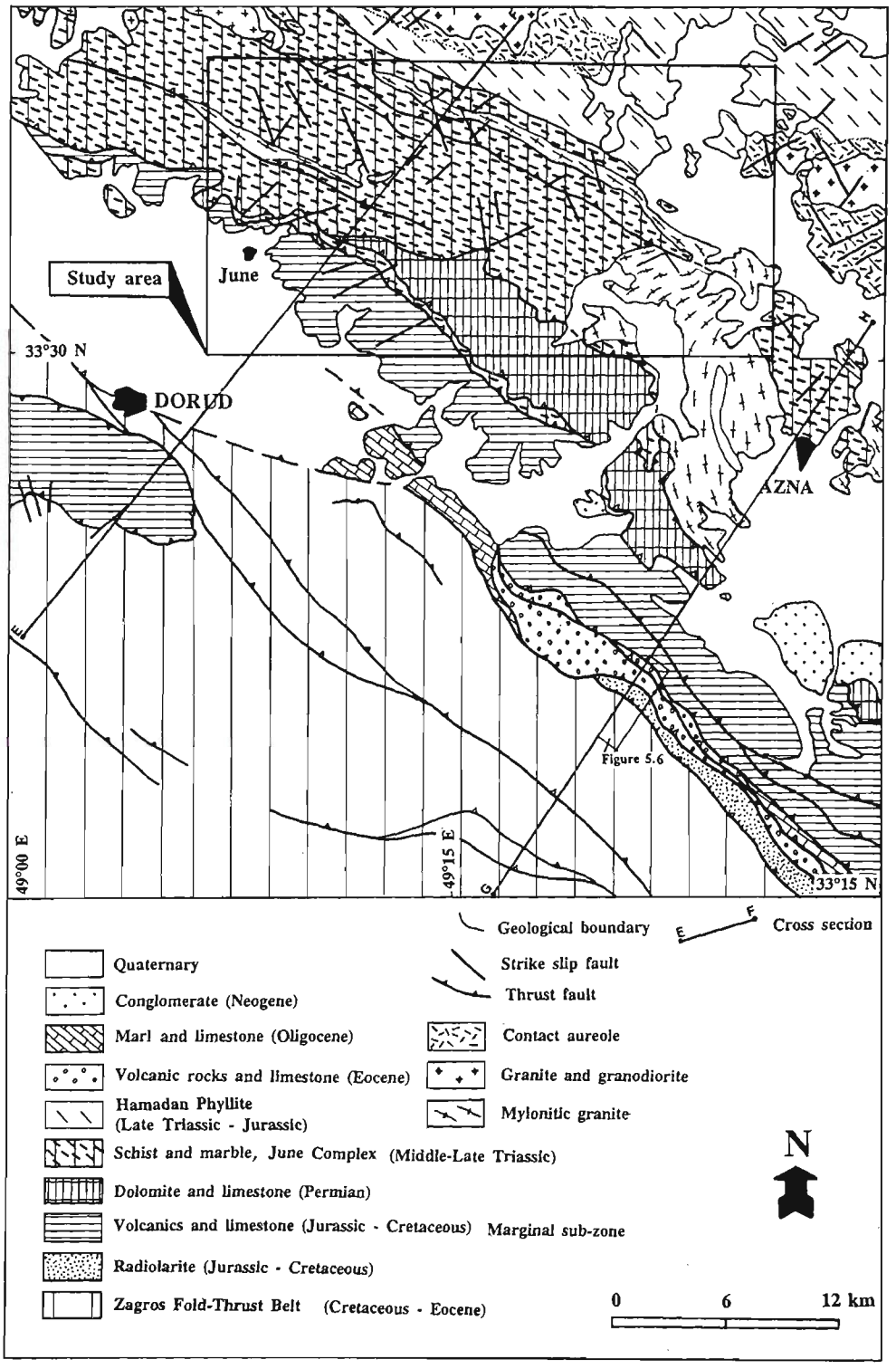

Figure 1.2 Simplified geological map of the Dorud-Azna region. See Chapter 5 for details of tectonic zones and cross sections.

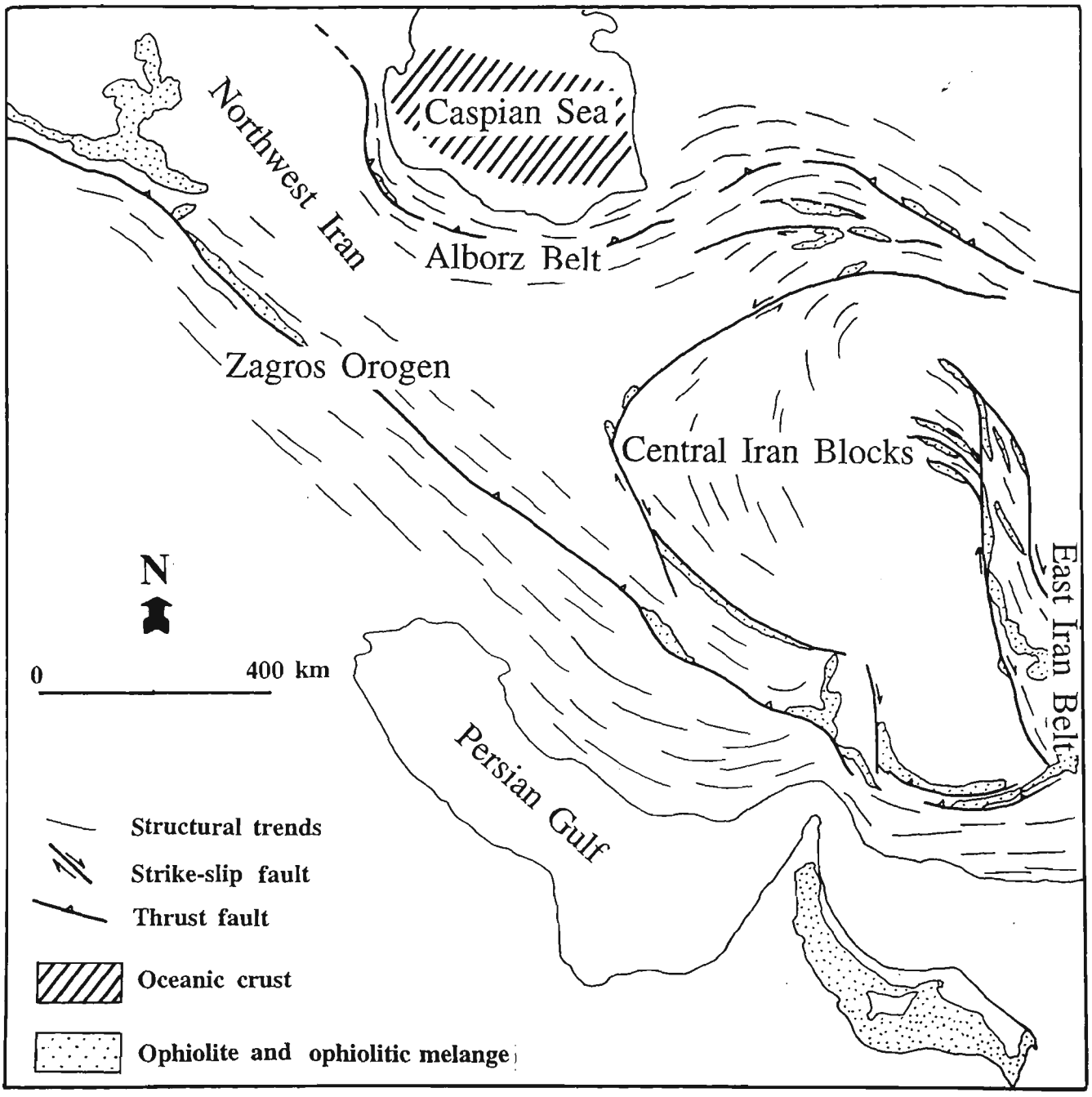

Figure 1.3

Simplified map of Iran and adjacent areas with main structural trends and exposures of ophiolite and ophiolitic melanges.

CHAPTER 2

STRATIGRAPHY OF THE JUNE AREA

2.1 INTRODUCTION

The June area is dominated by metamorphic rocks of Late Palaeozoic and Mesozoic age. The oldest exposed rocks in the study area are a succession of Permian limestone and dolomite (the Kuh-e-June Metacarbonate, new name). The central part of the area is dominated by a succession of metamorphic rocks referred to as the June Complex (new name) and thought to be of Middle-Late Triassic age. This unit is composed of quartzite, metadolomite, schist and marble overlain by greenstone interbedded with marble. In the past these rocks were called the Azna Complex and were considered to form part of a Precambrian unit because of they have higher metamorphic grades than adjoining units (Thiele 1966). Nearly all fossils have been obliterated in these rocks apart from very poor remnants of resistant crinoids preserved in carbonates which indicate that they are Phanerozoic rather than Precambrian. Overlying the June Complex is the Hamadan Phyllite of Late Triassic - Jurassic age (Stöcklin and Setudehnia 1991) and dominated by phyllite. The stratigraphy of the Triassic-Jurassic succession has been difficult to establish owing to intense multiple folding and faulting.

In this chapter a formal stratigraphy of the Dorud-Azna region is presented for the first time. Descriptions of all rock units are included. The succession is correlated with other units of the same age in the northwestern part of the Sanandaj-Sirjan Zone. A brief discussion of the depositional setting of the stratigraphic succession is also included.

Since 1980, the Geological Survey of Iran has been revising existing maps and

producing 1:100 000 scale geological maps throughout the Sanandaj-Sirjan Zone. The study area is a part of the Shazand quadrangle that has been mapped by a group of geologists including the author in 1984 (see Sahandi et al. in press). This mapping has not identified formal stratigraphic units due to the lack of abundant well-preserved age-specific fossils and the intensity of deformation and metamorphism. Instead a preliminary lithostratigraphy has been recognised and equated with various geological periods which in effect have been used as informal lithostrtigraphic terms. The stratigraphy of the June area presented in this chapter is consistent with the preliminary lithostratigraphic usage of Sahandi et al. (in press). Following common practice in Iran the term "marble" is used for metamorphosed limestone whereas metamorphosed dolomite is called metadolomite.

2.2 KUH-E-JUNE METACARBONATE

In the Dorud-Azna region, Permian marble and metadolomite were originally recognised by Thiele (1966) and later they were mapped by Berthier et al. (1974); they, however, were not formally named. The unit is exposed in the south of the study area and is named after the northwesterly trending Kuh-e-June (translated as mountain of June) 6 km east of June (Figure 2.1). These rocks are faulted out 4 km east-northeast of June but, to the southeast they continue along strike out of the study area. No formal type section has been proposed because neither the base nor the top of the sequence are exposed. Instead a representative section is nominated for the area west of Masud-Abad talc mine which is 13 km east-southeast of June (Figures 2.1, 2.2).

The unit comprises marble and metadolomite which are conspicuously light-coloured, commonly white (Figure 2.3a), in contrast to the adjacent green-coloured schist and purple-red volcanic rock. West of the Masud-Abad talc mine, the Kuh-

e-June Metacarbonate is divided into two informal members (Figures 2.1, 2.2, 2.3a) which are described below.

(a) The lower member consists of 200-250 m of thin-bedded to medium-bedded (10-30 cm) grey recrystallised limestone. This unit contains sporadic grey chert bands and nodules which are in the range of 1-10 cm thick (Figure 2.3b). In thin sections cut perpendicular to bedding, lamination is evident and defined by alternating layers of coarser (0.2-0.5 mm) and finer bands (0.05-0.2 mm) of calcite crystals. No sedimentary structures apart from bedding are recognised in the marble. Rarely, poorly preserved fusulinid occur in the marble but have not been identified beyond system level.

(b) The upper member consists of 150-200 m of buff recrystallised dolomite with patches of fusulinid-bearing, dark-grey marble from 1 m up to 10 m across (Figure 2.3c). The metadolomite and the marble patches are internally massive with no bedding or other sedimentary features preserved. The patchy occurrence of these fossiliferous marble outcrops amongst the dolomite is consistent with the dolomitisation having been a secondary process. White calcite veins, 1 mm to 10 cm wide, occur in the marble.

The Kuh-e-June Metacarbonate occupies the core of a map-scale F_2 antiform (Figure 2.1) and therefore the base of the unit is not exposed in the study area. Consistent dips of the succession in the representive section imply that the total thickness is over 400 m. The upper part of the unit is exposed 2 km to the east of Papion where it is faulted against basal quartzite of the Triassic June Complex.

Marble patches in the upper unit have been found 200 m west of the Teadar talc mine (Figure 2.1) and include Fusulinidae and the rhodophytes *Permocalculus* sp.

and *Gymnocodium* sp. which indicate a Late Permian age (Sahandi et al. in press).

The Kuh-e-June Metacarbonate in adjoining map sheets is mapped as a unit of Permian rocks. In the northwestern map sheet (Borujerd), these rocks are only exposed to the west of Borujerd at an isolated mountain that is surrounded by alluvium. They comprise grey marble with an unknown thickness (Hajmolla-Ali et al. 1989). In the southeastern map sheet (Aligudarz), Permian rocks are described as grey marble and metadolomite with an unknown thickness except in some parts where marble is up to 80 m thick (Soheili et al. 1992).

2.3 JUNE COMPLEX

In the Dorud-Azna region, a metamorphosed sequence, consisting of gneiss, mica schist, amphibolite, quartzite and marble, was studied and named the Azna Complex by Thiele (1966). A Precambrian age was inferred for the Azna Complex because of its higher grade metamorphism in contrast to the lower metamorphic grade of surrounding units. Thiele et al. (1968) also correlated these higher grade metamorphic rocks with similar rocks that occur in the southwest of Golpaygan quadrangle which they thought were unconformably overlain by a Permian unit. Recent mapping by Soheili et al. (1992) has demonstrated that these so-called Permian rocks are of Middle-Late Triassic age.

Berthier et al. (1974) mapped the Khorramabad quadrangle and recognised a unit informally referred to as both the "green series" and the "leptynite series" (metasilicic igneous rocks). This unit consisted of intermediate volcanic and volcaniclastic rocks interbedded with marble and included the higher metamorphic grade rocks referred to as the Azna Complex by Thiele (1966). No detailed stratigraphy was established due to the complexity of deformation and the scarcity of age-diagnostic fossils. The "green series" was inferred to be of Permian-Triassic age on the basis of scarce corals

and crinoids in contrast to the Precambrian age inferred by Thiele et al. (1968) for similar rocks in the Golpaygan quadrangle.

The June Complex comprises most of the outcrops in the study area and consists of metasedimentary (quartzite, metadolomite, schist and marble) and greenstone (amphibolite and schist, the "green series" of Berthier et al. 1974). According to the type of metamorphism, the June Complex is divided into two: lower grade and higher grade rocks. The higher grade rocks of the Dorud-Azna region were always thought to be Precambrian (Thiele et al. 1968; Soheili et al. 1992) but it is now realised that they are part of the June Complex of Triassic age.

The name for the complex is taken from June village which is located in the southwest of the study area (Figure 2.1). This complex comprises most outcrops of the Dorud-Azna region and extends along strike both to the northwest and southeast out of this region (see Chapter 5).

The lower grade metamorphic rocks of the June Complex include strongly folded and foliated quartzite, metadolomite, marble and schist interbedded with thin-bedded and medium-bedded grey marble. The higher grade rocks comprise an assemblage of metapelitic rocks including garnet-biotite schist, metasilicic igneous rocks and metabasite (amphibolite and epidote-amphibole schist). The metabasites, which are strongly mylonitised, make up the main part of the higher grade rocks.

Some understanding of the original stratigraphy of the June Complex is obtained from an appreciation of the complex structure of the unit (Chapter 3). Recognition of a map-scale F_1 has been crucial to determining the stratigraphic succession (Figure 2.1). East-northeast of Baraftab-Deraz, a representative stratigraphic column has been constructed for the June Complex on the limb of an F_1 map-scale fold (Figures 2.1, 2.2). It consists of a succession with three units: (a) a lower unit with quartzite, (b) a middle unit with metacarbonate, quartzite and schist, and (c) an upper unit with

metamafic and metasilicic igneous rocks with interbedded marble.

Lower unit

At 3 km northeast of Baraftab-Deraz, quartzite is exposed in the lower part of the June Complex in the core of a map-scale F_1 anticline (Figure 2.1). Here, the base of quartzite is not exposed but is found to the west, 4 km northeast of June where the quartzite has a faulted contact with the Kuh-e-June Metacarbonate. This rock unit is also exposed 2 km north of June and continues along strike to the west out of the study area (Figure 2.1). The quartzite is grey to reddish purple, and is thin-bedded to medium-bedded (20-35 cm) and contains cross bedding (Figures 2.3d, 2.4a). The true thickness of the quartzite is difficult to determine due to the intense deformation but is estimated at 150-200 m. The quartzite is locally interbedded with medium-bedded to thick-bedded (30-50 cm), yellowish-brown, sandy metadolomite with chert bands and nodules. Change of colour in alternating beds is evident (Figure 2.4a).

The composition of quartzite changes up section from pure quartz sandstone to lithic and feldspathic sandstone. Quartz and minor feldspar grains are recrystallised and are aligned along the foliation. Grain boundaries are sutured (see Chapter 4). Muscovite and chlorite also occur and are aligned along the foliation. Lithic fragments in lithic sandstone include fine-grained sedimentary rocks, chert and fragments altered to iron oxides (see Chapter 4).

Middle unit

The middle unit of the June Complex consists of metacarbonate, quartzite, calcschist and schist and is the thickest unit of the succession. It is extensively exposed around the villages of Papion and Meydanak (3 km northeast of June) and continues farther west out of the study area. In the representative section, northeast

of Baraftab-Deraz village, the middle unit contains a distinctive marker horizon called the Darijan Marble Member which divides the middle unit into two parts (Figures 2.1, 2.2).

The lower part in the representative section consists of 200 m of grey thick-bedded metadolomite with chert bands overlying the quartzite. Lower in the section metadolomite is interbedded with quartzite beds (20-50 cm) whereas higher in the section schist bands up to 4 m thick occur. The Darijan Marble Member, named after Darijan marble mine (12 km northeast of June, Figure 2.1) occurs at the top of the lower part of the middle unit (Figure 2.2). This rock has a distinctive light colour and is a key marker horizon that defines the top of the lower unit. It is a white and light-grey, thick-bedded to massive (1-3 m) marble with variable thickness up to 150 m.

Farther west, the lower part of the middle unit near Papion village (Figure 2.1) comprises a sequence up to 600 m thick of dark greenish-grey schist interbedded with fine-grained quartzite and grey to yellowish-brown thick-bedded (up to 1 m) metadolomite with chert bands and nodules and a marker marble horizon. This marker horizon (see the structural map of the Papion-Meydanak district, Chapter 3) consists of 50-100 m of grey to dark-grey intensely folded and foliated thin-bedded to medium-bedded marble (calcschist) with chert bands. In places, chert bands and thin-bedded marble layers have the same thickness (1-3 cm). West of Papion, boudinaged chert bands up to 30 cm thick are exposed.

To the north of Galeh-Gurchak village (3 km northeast of June), the lower part of the middle unit lies between two major thrust faults and has an exposed thickness of up to 400 m. This rock unit is traced from north of June to 4 km east of Serengeh and extends to the southeast out of the study area. It is composed of green to pale-green schist interbedded with well foliated grey marble, thick-bedded to

massive yellowish-brown metadolomite and quartzite.

The upper part of the middle unit in the representative section (northeast of Baraftab-Deraz) consists of metadolomite, marble and schist. This sequence also occurs 800 m north of the Papion village (see the structural map of Papion-Meydanak district, Chapter 3, Figure 3.5). Here, in a composite section more than 1 km thick, this sequence is composed of interbedded yellowish-brown, thick-bedded to massive dolomite with grey and white chert bands and nodules, muscovite schist, chlorite-actinolite schist with interbedded medium-bedded quartzite, grey to white grey, thin-bedded, highly folded and foliated marble with chert bands. Chert bands are best developed to the northwest of Meydanak. To the north of Meydanak occur intensely folded schist and crystalline silicified buff thick-bedded dolomite interbedded with chlorite-actinolite schist (Figure 2.4b, c). These schists were formed from alteration of mafic intrusive rocks. In thin section, the schist comprises chlorite and muscovite that wrap around abundant feldspar. Biotite and hornblende are altered. Chlorite and calcite were produced by alteration of amphibole.

The upper part of the middle unit also extends from Ag-Bolag to the south of Deh-Haji in the northern part of the study area. In this part of the June area, the middle unit consists of alternating thin-layered metasandstone, buff brown medium-bedded metadolomite and green to pale-green schist.

Upper unit

The upper unit of the June Complex consists of a succession of greenstone including amphibolite, epidote-amphibole schist, chlorite-epidote schist and chlorite-actinolite schist with sheet-like metasilicic igneous rocks, biotite-muscovite schist, marble and metadolomite with chert bands. These rocks are exposed around Baraftab-Deraz, Zageh-Bala, Shur-Shur and Bag-Ali villages in the core of the map-scale F_2

antiform (Figure 2.1). The same sequence is exposed farther north around Ag-Bolag, Deh-Mosa and Deh-Haji villages in the northeast of the study area and also is exposed farther east to the south of Bavaki (Figure 2.1). A representative section for the upper unit is located between Meydanak and Zageh-Bala. In the amphibolite, segregation layering is defined by hornblende-rich and plagioclase-rich bands. These bands change in thickness from a few centimetres up to 30 cm. Amphibolite is highly mylonitised and altered (see Chapters 3, 4). Interbedded marble is well-recrystallised and contains lenses of epidote and amphibole.

In the eastern part of the study area and also farther to the north metasilicic igneous rocks are exposed. These rocks are pink and pinkish-red on weathered surfaces and white on fresh broken surfaces. They are fine grained, highly recrystallised and contain porphyroclasts of sericitised plagioclase and alkali feldspar. Foliation is defined by aligned quartz grains and sericite flakes. They have a sheet-like geometry and could represent primary volcanic and/or intrusive rocks.

The upper unit of the June Complex appears to have a transitional contact with the overlying Late Triassic - Jurassic Hamadan Phyllite (see below). The lower contact of the upper unit (June Complex) is taken at the base of the first greenstone. The thickness of the upper unit has estimated at 600 m, although this is not well established due to structural complications in the core of the map-scale F_2. The lower part of this unit is truncated by a syndeformational granite in the northern part of the study area (see Chapter 3).

Correlation of the June Complex

Recrystallisation has largely obliterated fossils in the June Complex. No index fossils have been found in the study area but 15 km northwest of June, southwest of the Tavandasht marble mine, abundant crinoids and corals occur in thin-bedded grey

marble of the middle unit. Foraminifers at the same locality include *Crystelaria* sp., *Glomospira* sp., *Agathammina* sp., *Glomospira densa*, *Textraxis* sp., *Tolypammina* sp., *Endothyra* sp., *Trocholina* sp., *Involutina* sp., *Meandroculina* sp., *Diplotremmina* sp., and *Earlandia* sp., and suggest a Late Triassic (Norian-Rhaetian) age (Sahandi et al. in press). 50 km southeast of June in the Aligudarz area, near Abe-Barik, in the same low-grade rocks, corals and poorly preserved ammonites are found in addition to Ladinian conodonts (Soheili et al. 1992). These preserved fossils in the June Complex of adjoining areas indicate a Middle-Late Triassic age.

Throughout the northwestern part of the Sanandaj-Sirjan Zone, the higher grade of metamorphism and the lack of fossil remnants were the reasons given for the inferred Precambrian age of the upper unit of the June Complex. In the past, the upper unit of the June Complex, with its brown thick-bedded to massive metadolomite with white and grey chert bands and nodules, local pink to red jaspilite lenses and bands in metadolomite in association with metasilicic igneous rocks, was correlated with the Late Precambrian Rizo Formation of central Iran and its equivalents in northwest Iran (Huckriede et al. 1962; Stöcklin and Setudehnia 1991).

2.4 HAMADAN PHYLLITE

The Hamadan Phyllite was introduced as an informal formation by Dehgan (1947). This name has been taken from Hamadan city located 200 km southwest of Tehran in the northwestern part of the Sanandaj-Sirjan Zone. The Hamadan Phyllite is exposed over a distance of 400 km in the northwestern half of the Sanandaj-Sirjan Zone, extending from northeast of Hamadan (Asad-Abad) to the southwest of Golpaygan. The width of the Hamadan Phyllite in the Hamadan area is 100 km which decreases to a width of 10 km to the southwest of Golpaygan and terminates to the west of Esfahan (see Chapter 5, Figure 5.1). No type section has been

introduced for the Hamadan Phyllite. The Hamadan Phyllite is composed of mainly dark-grey to black phyllite and slate that are regularly interbedded with rare medium-bedded to thick-bedded (1-3 m), white and grey marble in the lower part. These rocks comprise a thick sequence of mudstone and were described as "flysch-type" rocks in the Kermanshah quadrangle (Braud 1987). More than 2 km of thickness is estimated for the Hamadan Phyllite which transitionally overlies the Middle-Late Triassic June Complex.

On the Golpaygan 1:100 000 geological map (Mohajjel 1992), the Hamadan Phyllite has been divided into three lithostratigraphic units: a lower unit of phyllite with interbedded medium-bedded to thick-bedded (0.5-1 m) grey marble and metavolcanic rock, a middle unit of monotonous dark grey slate with local interbedded greywacke, and an upper unit of slate with upward-increasing *pentacrinous*-bearing greywacke and quartz sandstone (Figure 2.2).

The lower unit, and lower part of the middle unit, of the Hamadan Phyllite are exposed in the northeastern part of the study area. In the lower unit adjacent to the June Complex, the Hamadan Phyllite consists of phyllite interbedded with crinoid-bearing marble. In the study area, the main body of the Hamadan Phyllite comprises monotonous dark grey phyllite. Complex folding and a intensely developed schistosity has prevented recognition of sedimentary structures in this unit. The lower contact of the Hamadan Phyllite is transitional with the underlying June Complex. The upper contact of the Hamadan Phyllite occurs outside the study area and is an angular unconformity which is overlain by a transgressive basal conglomerate of the Cretaceous (Aptian-Albian) succession (see Chapter 5). Fine-grained igneous rocks of basaltic, basaltic andesitic and silicic composition occur in the transitional zone between the June Complex and the Hamadan Phyllite. These rocks are located in a strike-slip dextral shear zone and are strongly mylonitised (see Chapter 3).

Hamadan Phyllite is intruded by granite and granodiorite plutons with wide contact aureoles. Fossils are rare in the Hamadan Phyllite; where fossil ages have been determined the age range is from Rhaetic-Liassic to late Dogger (Thiele et al. 1968). In the Varcheh area, 60 km northwest of Golpaygan, ammonites and belemnites have been found in the upper part of the Hamadan Phyllite, and indicate a Early Jurassic (Toarcian) age (Kholgi 1984; Vaezipour and Eglimi 1984). A Late Triassic - Jurassic age is assigned to the Hamadan Phyllite (Stöcklin and Setudehnia 1991).

2.5 TEADAR VOLCANIC ROCKS

This rock unit is an informal stratigraphic term which is named after Teadar village located 6 km southeast of June. The Teadar volcanic rocks are exposed in the southwest of the study area and continue both to the northwest and southeast out of the study area. They consist of green, purple and red vesicular andesitic lava, pyroclastic rocks and red shale. Pyroclastic rocks are thin-bedded to medium-bedded (5-30 cm). These non-foliated rocks are metamorphosed to low-greenschist facies (see Chapter 4). Epidote is extensively developed and chlorite and actinolite also occur. Idioblastic plagioclase is altered with either partial or complete replacement by epidote.

The base of the Teadar volcanic rocks is not exposed in the study area and the true thickness is not clear. To the north they have been thrust under the June Complex (Figure 2.1). These volcanic rocks are not dated in the study area but regionally they are part of the succession of the marginal sub-zone (see Chapter 5) which in the adjoining regions are of Jurassic - Early Cretaceous age.

2.6 SURANEH LIMESTONE

This name is taken from Suraneh village located 3 km southeast of June. The Suraneh Limestone is exposed in the southwestern part of the study area and continues to the southeast out of the study area. At Suraneh, it consists of 60 m of grey to light-grey, thick-bedded (0.4-1.5 m), recrystallised limestone containing the resistant foraminifers *Orbitolina* sp. and *Dictyoconus?* sp. that indicate an Aptian-Albian age (Sahandi et al. in press). The Suraneh Limestone has a faulted and sheared contact with the Teadar volcanic rocks which is exposed to the west of Serenjeh village (Figures 2.1, 2.5).

2.7 INTRUSIONS

Both silicic and mafic intrusions are exposed in the study area.

Galeh-Doz pluton

The Galeh-Doz pluton is exposed in the eastern part of the study area. This pluton has intruded the June Complex and a restricted contact aureole is developed. It is a coarse-grained granite which is strongly deformed and mylonitised (see Chapter 3). It contains fine biotite, quartz and very large feldspar crystals (up to 3 cm) giving an augen structure to the rock. The northwestern extension of this synorogenic deformed granite is exposed in a west-northwest trending long (18 km) and narrow (up to 1 km) sheet subparallel to the structural trend (west-northwest) in the northern part of the study area. Another exposure of this rock unit, with the same trend, is in the central of the study area and extends along strike to the west out of the study area (Figure 2.1).

Gabbro and micrograbbo in the June Complex

In the upper unit of the June Complex foliated mafic rocks are present. They are coarse-grained and contain hornblende (0.5-2 mm across) that pseudomorphs pyroxene in addition to plagioclase which is partly altered to sericite. A granular texture is still preserved in these rocks and is consistent with their formation as plutonic rocks. In contrast, other finer-grained amphibolites have had their primary textures completely destroyed. The gabbro and microgabbro rocks have only weakly developed retrograde metamorphism (see Chapter 4). These igneous rocks have not been radiometrically dated but relations between metamorphism and fabrics indicate that they could be syn-D_2 mafic intrusive rocks (see Chapter 5).

Pirkhalil Dolerite

This mafic rock is located at Pirkhalil, 9 km east of June, and has intruded the Kuh-e-June Metacarbonate and the June Complex (Figure 2.1). The Pirkhalil Dolerite is medium to coarse grained and has a porphyritic texture with euhedral plagioclase up to 2 cm long and interstitial pyroxene, hornblende, sphene and magnetite. The rock is not foliated but is highly altered and contains epidote (zoisite and clinozoisite) and chlorite. Other doleritic sills and dykes occur in rock units throughout the study area (Figure 2.4d).

2.8 DEPOSITIONAL ENVIRONMENT OF THE SUCCESSIONS

The Late Permian Kuh-e-June Metacarbonate consists of dolomite and limestone with scattered fusulinids that are consistent with a shallow-marine (shelf) environment. The June Complex is of Middle-Late Triassic age implying that some section is missing between it and the Late Permian Kuh-e-June Metacarbonate. This could either reflect faulting out of some of the succession or the presence of an unexposed

unconformity between the two successions. Therefore it is not known if shallow-marine sedimentation responsible for deposition of the Kuh-e-June Metacarbonate was continuous into the younger June Complex.

The lower unit of the June Complex comprises quartz sandstone containing cross bedding and locally interbedded sandy dolomite; deposition must have occurred at least partly in a shallow-marine environment to account for formation of dolomite but the cross-bedded sandstone may have been deposited in either a shallow-marine or continental setting. The middle unit contains abundant marble, including the Darijan Marble Member, and therefore had a shallow-marine environment of deposition. The increasing proportion of schist in the upper part of the middle unit of the June Complex may reflect a gradual deepening of the depositional environment up section; although still in a relatively shallow-marine setting. The upper unit of the June Complex contains mafic submarine volcanic rocks including basaltic lava partly with pillow structures (Soheili et al. 1992). This unit also contains gabbro and microgabbro intrusions which are possibly associated with D_2 and are therefore unrelated to the syndepositional igneous activity. Silicic igneous rocks occur in association with the mafic volcanic rocks. The presence of thin marble bands in the upper unit of the June Complex indicates that a shallow-marine environment has persisted during the major phase of bimodal igneous activity that affected this part of the succession. Overall, the June Complex records sedimentation in a dominantly shallow-marine setting concluding with a major phase of silicic-mafic igneous activity.

The upper unit of the June Complex is overlain by the Late Triassic - Jurassic Hamadan Phyllite with a thickness of more than 2 km of monotonous mudstone in the lower and middle part, and shallow-marine to continental rocks in the upper part (Mohajjel 1992). This is consistent with accumulation in a trough that was gradually infilled by prograding sedimentation. A deep-marine setting has been inferred for the

middle unit of the Hamadan Phyllite (Braud 1987) but the extent of deformation has precluded detailed sedimentological studies.

At the same time as deposition of the upper part of the Hamadan Phyllite in the northeastern part of the study area, in the southwestern part abundant Jurassic - Early Cretaceous andesitic volcanic rocks were being erupted. These volcanic rocks are included in the marginal sub-zone (see Chapter 5).

Cretaceous (Aptian-Albian) rocks angularly unconformably overlie the Late Triassic - Jurassic Hamadan Phyllite at several places in the northwestern half of the Sanandaj-Sirjan Zone (see Chapter 5). The Aptian-Albian Suraneh Limestone in the southwestern part of the study area indicates a shallow-marine depositional environment.

Plutonic rocks, including the gabbro and the Galeh-Doz pluton, are associated with the second deformation (see Chapter 3). The Pirkhalil Dolerite is post-tectonic and is probably of Tertiary age.

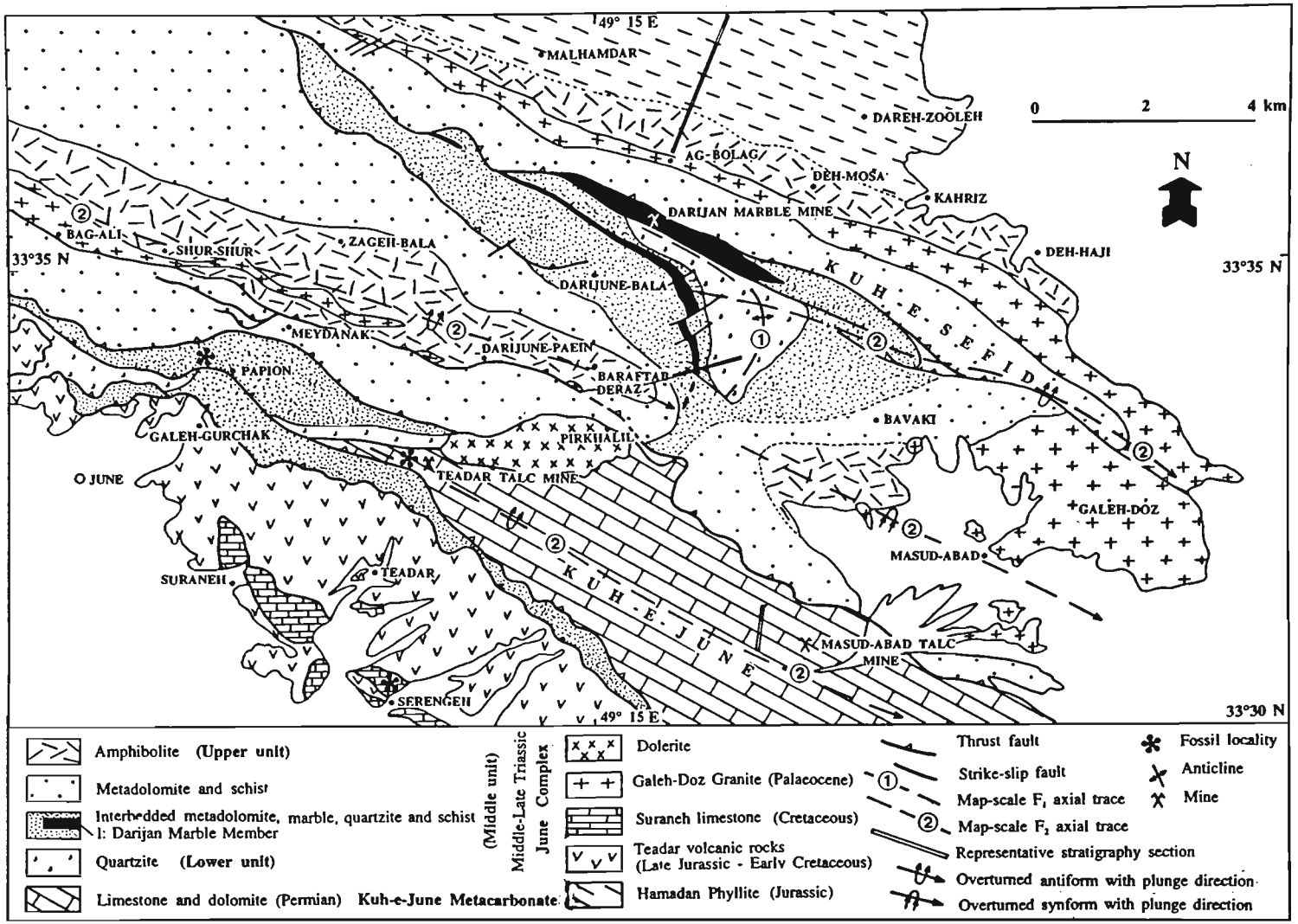

Figure 2.1 Simplified geological map of the June area.

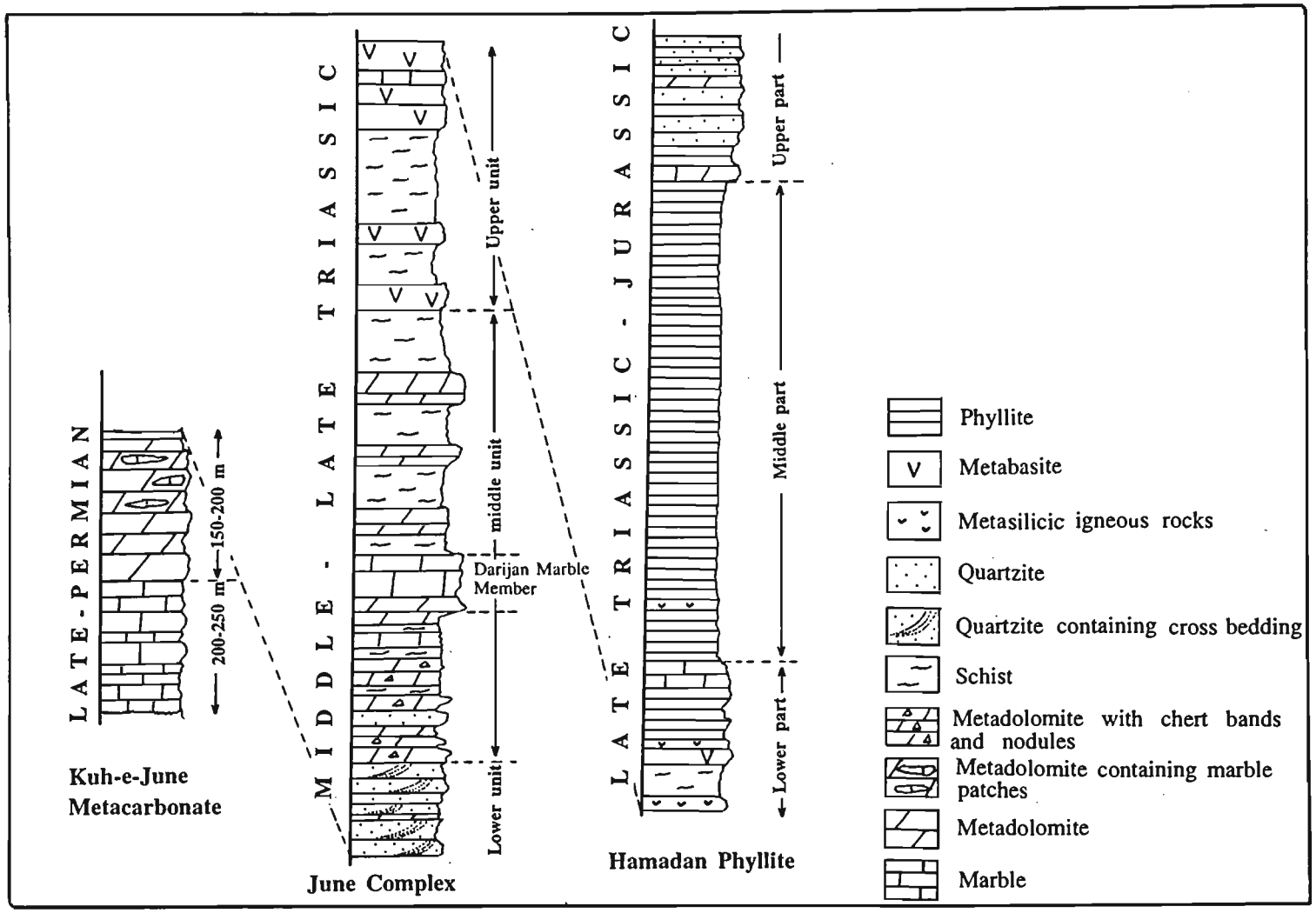

Figure 2.2 Representative stratigraphic columns showing successions occurring in the June area. Top half of the Hamadan Phyllite is not exposed in the June area. (Note that columns are not to scale.)

Figure 2.3

(a) Two rock units of the Permian Kuh-e-June Metacarbonate. On the left side of the photograph (southwest) is a darker unit of limestone and on the right side (northeast) is a light grey dolomite. Bedding dips at 45° to the northeast. Location is to the west of Masud-Abad talc mine. The photograph is about 400 m across.

(b) Permian grey limestone with boudinaged chert bands and nodules. Location is 300 m southeast of Masud-Abad talc mine. Hammer is 32 cm in length.

(c) A patch of dark grey crystalline limestone in yellowish brown massive crystalline dolomite. 200 m east of Teadar talc mine. Hammer is 32 cm in length.

(d) Cross bedding in quartzite (top to the west). Location is 3 km east of Baraftab-Deraz. Coin is 16 mm across.

a
b
c
d

Figure 2.4

(a) Cross-bedded quartzite (top to the right). 3 km northwest of Bavaki. Hammer is 32 cm in length.

(b) Thick-bedded metadolomite with chert bands and well foliated schist. 50 m north of Meydanak. Hammer is 32 cm in length.

(c) Folded interbedded medium-bedded to thick-bedded yellowish brown dolomite and mafic volcanic rock. North of Meydanak, looking towards west. The photograph is 50 m across and a road cuts across the middle of the photograph.

(d) A non-foliated dolerite sill in schist and marble sub-parallel to lithological layering (west of Meydanak). Lens cap is 5.5 cm in diameter.

a
b
c
d

Figure 2.5

(a) Teadar volcanic rocks overlain by limestone. West of Serengeh; looking towards the west. The photograph is 300 m across. Note that a dextral strike-slip fault has displaced the units.

(b) Suraneh Limestone above a faulted contact with the underlying Teadar volcanic rocks. 200 m northwest of Serengeh village. Hammer is 32 cm in length.

a

b

CHAPTER 3

STRUCTURE

3.1 INTRODUCTION

The Zagros Orogen formed by continental collision between the Afro-Arabian continent and the Iranian microcontinent in the Late Cretaceous to Tertiary interval (Dewey et al. 1973; Berberian and King 1981; Alavi 1980, 1994). Widespread thrusting has been attributed to the collision in the Sanandaj-Sirjan Zone (Alavi 1994). This chapter presents a structural analysis of the Sanandaj-Sirjan Zone in the Dorud-Azna region and details a complex structural succession containing both brittle and ductile structures that formed during convergence and subsequent collision.

The study area is complexly deformed and at least four episodes of deformation are recognised and labelled D_1, D_2, D_3 and D_4 respectively. Structural elements associated with each deformation are listed in Table 3.1. The relative timing of different deformation phases has been deciphered from field observation of: overprinting cleavages/foliations, refold patterns, folded lineations and relationships between faults and other structures. The major regional deformation is the D_2 event and it has largely reoriented D_1 structures parallel to D_2 structures making it hard to distinguish between them except where overprinting criteria are found. Extensive transposition is developed in phyllite, schist and calcschist. F_1 and F_2 mesoscopic folds, and their associated axial planar schistosities, have the same style in many areas.

Deformation partitioning has occurred during D_2 with distinct deformation styles and histories occurring in these two different rock suites, namely: (1) schist and marble, and (2) mylonitic rocks. Mylonitic rocks developed during D_2 show

considerable dextral shear. In contrast to S_2 in schist and marble, the steeply dipping mylonitic foliation (S_2) in mylonite rocks contains a strong sub-horizontal mineral stretching lineation. This feature is well documented for the syndeformational granite which is strongly mylonitised. Shear-sense indicators are well preserved in the syndeformational mylonitic intrusions, and other mylonitic rocks, and indicate regional dextral shear. D_2 and younger thrust faults are also developed and had an important role in the deformation process.

3.2 D_1 DEFORMATION

The first deformation is characterised by F_1, S_1 and rare L_1. In most of the area D_1 structures are reoriented sub-parallel to D_2 structures and cannot be easily distinguished. D_1 structures are well documented at some localities in quartzite, schist and marble of the greenschist metamorphic rocks of the June Complex but are difficult to find in the Hamadan Phyllite.

Mesoscopic folds

Few mesoscopic F_1 are exposed in the study area. They commonly have a tight to isoclinal interlimb angle (0°-30°, Figure 3.1) but are locally tighter than isoclinal (mushroom-shaped). Only within thin chert bands in highly foliated marble are F_1 disharmonic (Figure 3.1c) whereas elsewhere F_1 are harmonic. Some F_1 have discontinuous dome-shaped hinges with plunges varying up to 20° and resemble the "pod folds" of Wilson and Cosgrove (1982, p. 84; see Figure 3.1d).

Axial planes dip moderately to steeply (50°-80°) to the east with variable strikes due to later folding. F_1 plunge at 40°-60° to the northeast (Figure 3.2).

S_1

S_1 is developed axial planar to F_1 and is commonly parallel to S_0. It is well developed in schist and thin-layered marble and also occurs in metadolomite and quartzite but is only rarely recognised in phyllite. S_1 is a metamorphic structure as shown by syntectonic mineral growth. In schist, S_1 is defined by alignment of muscovite and biotite flakes whereas in quartzite it is defined by elongate detrital quartz grains that have recrystallised as shown by their polygonal mosaic texture. In phyllite, S_1 is transposed by S_2, but locally at a microscopic scale S_1 is preserved in hinge areas of F_2 microfolds (Figure 3.3). S_1 in amphibolites is defined by a segregation layering with feldspar-rich and amphibole-rich bands (Figure 3.4a). These amphibolites contain relics of aligned metamorphic brown hornblende that are retrogressed to actinolite (see Chapter 4).

L_1

The S_0 and S_1 intersection lineation is rarely observed. In the Bavaki area (Figure 3.5), it is moderately plunging to the northeast subparallel to F_1 (Figure 3.2b).

Macroscopic folds

The macroscopic F_1 in the study area are isoclinal folds with attenuated long limbs and elongate angular hinges. On the basis of the geometry and outcrop patterns of macroscopic F_1 folds, the study area is divisible into two separate eastern and western domains (Figure 3.4b). In the western domain, the macroscopic F_1 have east-west trending axial traces whereas in the eastern domain they have northeast-southwest trending axial traces exposed in interference fold patterns. The Papion and Darijune-Bala folds of the western domain and the refolded outcrop patterns of the Bavaki area in the eastern domain are specifically described.

Papion fold

Around Papion village, a macroscopic F_1 fold couple with a west-northwest trending elongate hinge zone is exposed (Figures 3.5, 3.6). The hinge zone is located 900 m northeast of Papion and extends to the east-southeast. The Papion fold is outlined by a thin marker unit up to 150 m wide of grey marble and calcschist, with chert bands which are intensely folded. The Papion fold has an F_1 axis that is moderately plunging to the east-northeast (Figure 3.7a). This structure is refolded by F_2 with west-northwest trending axial surfaces that are moderately to steeply dipping to the northeast (Figure 3.7a, see D_2).

Darijune-Bala folds

North of Darijune-Bala, macroscopic F_1 are outlined by a closed outcrop pattern formed by a light grey metadolomite unit (Figure 3.8). An S-type F_1 fold couple is located near the western end of the metadolomite and a Z-type F_2 fold couple occurs near the eastern end north of Darijune-Bala. The Z-type fold is the parasitic fold of the map-scale F_2 (see D_2 for more description). The outcrop pattern indicates fold interference between a Z-type F_2 couple and a S-type F_1 couple (see Ramsay 1967, p. 158; Marshak and Mitra 1988, p. 366).

Bavaki folds

Northwest of Bavaki, the structure is dominated by a map-scale F_1 anticline (Figure 3.4b). This anticline is difficult to decipher on its limbs but the hinge area is recognised as part of an interference fold pattern developed from superimposition of map-scale F_2. Cross bedding, preserved in quartzite of the lower unit of the June Complex, indicates younging directions. A quartzite unit has been traced along the

hinge area of this F_1 anticline. 3 km northeast of Baraftab-Deraz (Figure 3.5), bedding in the western limb of the anticline dips steeply to the east but, younging is to the west. In the northern limb, quartzite dips moderately to steeply to the north-northeast with younging in the same direction (Figure 3.5). The observed changes in the orientation of younging directions indicate that the early fold is an anticline.

One kilometre northwest of Bavaki, quartzite is exposed in a macroscopic F_1 with a northeast-southwest trending axial trace (Figure 3.5). The northwestern limb of this structure is vertical or dips steeply to the northwest or southeast. Cross bedding found in this limb indicates younging to the northwest. The southeastern limb is vertical or dips steeply to the southeast.

3.3 D_2 DEFORMATION

This deformation produced the dominant structures in the study area and developed by intense folding of S_0 and S_1. F_2 and the axial plane schistosity (S_2) are the most abundant structures formed during D_2. Tight to isoclinal F_2 folds are exposed at mesoscopic and macroscopic scales. Widely developed mylonitic fabrics in crystalline rocks were formed during D_2 and are described after analysis of structures in marble and schist units.

Mesoscopic folds

West-northwest trending F_2 folds are well developed in the study area. They are more common in thin-layered marble than in thick-bedded and massive metadolomite and quartzite (Figure 3.9). F_2 folds are less common in phyllite except where it contains interbedded marble or sandstone. Folds in thick-bedded dolomite and marble with chert bands are mostly recognised by folded chert bands. F_2 folds are tight to isoclinal with angular hinges in schist and calcschist whereas angular to

rounded hinges occur in quartzite and metadolomite (Figure 3.9a). Some F_2 are intrafolial and are bounded on either side by planar surfaces (lithological layering parallel to S_2, Figure 3.9c). Axial planes of these folds have moderate to steep dips to the northeast with axes plunging moderately to the east (Figure 3.10).

The style of mesoscopic F_2 varies in relation to changes in lithology. Low amplitude folds with parallel geometry occur in competent quartzite and dolomite (Figure 3.9b), whereas folds with high amplitudes and short wavelengths occur in schist and calcschist (Figure 3.9a, d, e). Amplitude-to-wavelength ratios are typically variable. High ratios also occur in folds in ductilely folded thin-bedded marble (Figure 3.9d, e) and in interbedded schist and marble (Figure 3.9f). F_2 folds have narrow angular hinges and long planar limbs. Folds in competent metadolomite have rounded Class 1C profiles and in less competent thin-bedded marble, schist and phyllite have mostly Class 3 profiles. Quartzite layers have rounded Class 1B and 1C profiles.

Chert bands with various thicknesses in marble and metadolomite display different characteristics during deformation. Thin chert bands are folded and thick chert bands are boudinaged parallel to S_2. In some isoclinal folds where chert bands are highly folded, the hinge areas are exposed as pod-shaped hinges with very highly attenuated limbs (Figure 3.9h).

Within some exposures the style of F_2 indicate highly ductile behaviour of schist and marble during folding. 700 m west of Meydanak (Figure 3.5) complex polyclinal folds were produced due to extreme ductile folding (Figure 3.11). These structures were formed where highly ductile marble was bounded by thick stiff layers of metadolomite.

S_2

An S_2 axial plane schistosity is well developed and has an almost constant west-northwest strike throughout the study area. In fine-grained incompetent layers (schist, calcschist and phyllite), S_2 is better developed than in competent metadolomite and quartzite (Figure 3.12a). In interbedded schist and quartzite layers, S_2 changes its orientation as it passes from stiffer quartzite to softer schist layers (cleavage refraction).

S_2 is defined by the alignment of white mica and chlorite in schist, aligned amphibole in metabasic rocks and aligned sericite and chlorite in phyllite (see Chapter 4). In quartzite, S_2 is defined by alignment of ellipsoidal quartz grains with mica flakes. S_2 is generally parallel to the compositional layering. On F_2 limbs, S_0 and S_1 are commonly transposed parallel to S_2 except in hinge zones of F_2 where lithological layering is trending north-south. At these localities, compositional layering is sub-parallel to S_1 and is cut by the S_2 foliation which has a crenulation morphology (Figure 3.12b).

Lineations

A widespread intersection lineation (L_2^1) between S_1 and S_2 is developed sub-parallel to F_2 in schist. This intersection lineation plunges gently to moderately to the east (e.g. Figures 3.10b, 3.12c). An intersection lineation (L_2^0) between lithological layering and S_2 is developed (Figure 3.12d). This intersection lineation is also gently to moderately plunging to the east sub-parallel to F_2.

Boudinage and pinch-and-swell structures

Abundant boudinage and pinch-and-swell structures are associated with F_2. Competent metadolomite and quartzite layers in incompetent marble and schist (Figure

3.13a, d) and competent metabasite in incompetent marble (Figure 3.13b) contain boudinage and pinch-and-swell structures. Chert bands in metadolomite and marble are also boudinaged.

First generation boudins were refolded and the shape of boudins and pinch-and-swell structures were modified during D_2. Boudinage and pinch-and-swell structures have been modified in two ways: (1) by folding, and (2) by thrusting (Figure 3.14). According to experimental work (Sengupta 1983), the nature of modification of pre-existing boudinage and pinch-and-swell structures relates to the competence of the boudins relative to the host rock, and the width-to-thickness ratio of the boudins. During layer-parallel shortening of boudinage and pinch-and-swell structure, where the competence contrast between the boudins and matrix is relatively large, the shape of the individual boudins is retained during subsequent deformation involving both folding and thrusting (Figure 3.14d). In contrast, in some cases the competence contrast was less and during folding the shape of the boudins have been modified into trapezoidal forms (Figure 3.14a).

Asymmetrical boudinage and pinch-and-swell structures are found in metadolomite and chert bands, within schist and marble units, and adjoining layers are also cut by these shear fractures. Shear senses are consistently dextral and a model for their development is discussed below (see 3.4 Structure of the Mylonitic Rocks).

Fold interference patterns

Interference structures result from the superimposition of differently oriented generated fold sets (Ramsay 1967). In the study area, interference patterns at macroscopic and mesoscopic scales result from superimposition of F_1 and F_2 folds. Two dimensional interference patterns range between types 2 and 3, patterns H and I of Ramsay (1967, p. 531).

The first fold axial surfaces and F_1 are strongly folded by the new generation folds (F_2). Mesoscopic interference patterns are developed in different rock types. They are well exposed in the north-trending limb of the Papion parasitic F_2 folds (see below). At this locality, interference patterns are exposed in calcschist and marble (Figure 3.15a). Axial planes of F_1 are folded by F_2 with vertical or northeasterly steeply dipping axial planes (Figure 3.15b).

Macroscopic interference patterns are mostly exposed at the hinge area of the map-scale F_2 (3 km northeast of Baraftab-Deraz, Figure 3.5). Quartzite in the core of the map-scale F_1 (Figure 3.4b) is exposed in a boomerang-shaped interference pattern (type 2 of Ramsay, 1967). Other macroscopic interference patterns in the Bavaki area (see D_1) were produced by macroscopic F_2 superimposed on F_1 and forming crescent-type interference patterns of Ramsay and Huber (1987, p. 496).

The observed mesoscopic and macroscopic interference patterns in the study area reveals a variation of the principal shortening direction during the deformation history. Changes of the principal shortening direction is a common phenomenon in all orogenic zones, particularly in those areas where the total crustal compression has been large (Ramsay and Huber 1987).

The axial variation of the second folds depends on the tightness and size of the hinge zone of the first folds (Ramsay 1967, p. 538-546). For example, if the first folds are isoclinal and hinges are very narrow then only one dominant axial direction will develop for the second fold axes. The isoclinal F_1 plunge moderately, with a variation in plunge direction between east and northeast (Figure 3.2). F_2 plunge moderately to the east and have a constant orientation throughout the study area (Figure 3.10a) that is close to the axial direction of F_1 (Figure 3.15b).

Macroscopic folds

The study area is dominated by a map-scale isoclinal west-northwest-trending F_2 antiform (Figure 3.5). Lithological layering and axial plane schistosity associated with this fold dip steeply towards the north-northeast and the axis plunges moderately to the east.

The isoclinal map-scale F_2 antiform is overturned with vergence to the southwest. The southwestern limb is attenuated and several north-northeast dipping thrust faults are developed (Figure 3.5, cross sections AB and CD). The map-scale F_2 has a high amplitude and short wavelength and contains parasitic folds: Z-types on the northeastern limb, S-types on the southwestern limb and M-types in the hinge area. On the northeastern limb of the map-scale F_2, in the Darijune-Bala district, a Z-type parasitic fold exists (Figure 3.8) and on the southwestern limb the Papion F_1 fold is refolded as an S-type parasitic fold (Figure 3.6). 1400 m east of Baraftab-Deraz M-type parasitic folds are exposed. Stratigraphically, the succession in the main F_2 antiform is younging into the core of the structure with the middle unit of the June Complex (metadolomite and schist) on the limbs and the upper unit of the June Complex in the core (amphibolite). This arrangement indicates that the main F_2 antiform is downward facing, although local way-up structures can only be identified in the lower unit of the June Complex (cross-bedded quartzite) in the cores of F_1 anticlines. Thus it appears that this fold affects the lower overturned limb of a major F_1 anticline (see Figure 3.5).

The macroscopic F_2 have relatively moderate to steeply dipping northeastern limbs and narrow, steeply dipping to vertical, southwestern overturned limbs dipping to the northeast which indicates an overall vergence to the southwest. In general, macroscopic F_2 are tight to isoclinal with rounded to angular hinges. Some of these folds are described here in detail.

Darijune-Bala parasitic folds

North of Darijune-Bala village a Z-type F_2 antiform-synform couple is exposed (Figure 3.8). These folds are located in the northeastern upright limb of the map-scale F_2. Parasitic F_2 are inclined folds with axial planes dipping at 57°/033° and axes plunging at 53°/067° (Figure 3.10a, c).

Papion parasitic folds

Papion parasitic S-type folds are located on the overturned limb of the map-scale F_2 to the east of Papion village (Figure 3.5). An example of these folds is shown in the block diagram in Figure 3.7a. These parasitic F_2 are overturned with axial planes dipping at 66°/033° and axes plunging at 47° to the east (Figure 3.10a, c). Another S-type fold, located 1 km southwest of Papion village, is cut and transported to the south in a thrust sheet with rotation of the trend of the axial planes to an east-west direction (Figure 3.5). This S-type fold is folded by weak northeast-trending F_4 (Figure 3.5).

The parasitic F_2 folds at Papion are tight with angular to rounded hinges containing abundant mesoscopic structures, Z-type mesoscopic F_2 in the west-northwest trending limbs, S-type in north-south trending limbs and M-type in hinge zones (Figure 3.7b). Transposition along S_2 occurs in the west-northwest trending limbs.

Kuh-e-Sefid antiform

This antiform is located in the northeastern part of the study area. It is a west-northwest trending structure that forms a high mountain in the region and extends from Abbas-Abad at its eastern extremity to the Darijune mine (500 m north of

Darijune-Bala, Figure 3.5). The overturned southern limb of this antiform is displaced by the northeast-dipping Cheshmeh-Narges thrust (see cross sections MN and LO, main map in the pocket).

Kuh-e-June antiform

This structure is located 6 km to the east of June (Figure 3.5). The Kuh-e-June antiform is a close overturned antiform with southwest vergence. It has a long straight northeastern limb and a short overturned southwestern limb. The southwestern limb is attenuated and partly truncated by thrust faults which transport it to the southwest (Figure 3.5, cross section AB). To the north of Teadar village, carbonate of the Kuh-e-June antiform is thrust over the June Complex. This thrust fault is traceable to the southeast out of the study area, terminating 7 km southwest of Azna. The northern limb of the Kuh-e-June antiform is tectonically overlain by the June Complex. The Kuh-e-June antiform is terminated to the west-northwest, 4 km east of June.

Faults

Faulting throughout the study area has contributed to the complex nature of the outcrop pattern with dominant west-northwest trending and north-northeast dipping thrust faults (Figure 3.5). Thrust faults are mostly developed along the overturned limbs of F_2 folds. In the southwestern part of the mapped area, along the west-northwest trending overturned limb of the map-scale F_2 antiform, thrust faults are at low angles or are even horizontal.

In the southwestern part of the study area, the metamorphosed and complexly deformed June Complex is thrust (Galeh-Gurchak thrust) over the Teadar volcanic rocks.

Galeh-Gurchak thrusts

Two conspicuous subparallel thrust faults occur along the southern contact of the June Complex with the Teadar volcanic rocks. These two parallel thrusts are well exposed 2 km north of Teadar (Figures 3.5, 3.16). They dip gently to the northeast (Figure 3.17a). Striations and groves are well developed on the fault planes and are all plunging to the north and northeast (Figure 3.17a). The hanging wall of the northeastern fault the Kuh-e-June antiform contains Permian rocks and is thrust over Triassic rocks (June Complex). Northwest of the southwestern fault is the June Complex which is thrust over the Teadar volcanic rocks. Along this fault a wide shear zone (100-300 m) is developed and it contains S-C planes that have a shear sense consistent with thrust transport (Figure 3.17b).

Cheshmeh-Narges thrust

This fault occurs in the northern part of the study area and is 24 km in length extending from Abbas-Abad at its southeastern extremity to the northwest of the mapped area (Figure 3.5). The fault plane dips (40°- 55°) to the northeast, but to the south of the Kuh-e-Sefid antiform it dips steeply to the northeast (Figure 3.17c). In its eastern part, this fault displaces the overturned southwestern limb of the Kuh-e-Sefid antiform over the Galeh-Doz pluton. Striations on the fault plane plunge 55°/027° and indicate transport in a north-northeast direction (Figure 3.17c). A dextral strike-slip separation of 1200 m is observed on the marble-granite contact and indicates a net slip of 2700 m along this part of the fault (Figure 3.18). In the Abbas-Abad area, the Cheshmeh-Narges thrust fault cuts S_2 in the Galeh-Doz pluton. 5 km northwest of Darijune-Bala, white massive metadolomite in the hanging wall of this fault is thrust over schist in the footwall (Figure 3.17d, cross section CD, Figure

3.5).

Fault north of Kuh-e-June

The Permian Kuh-e-June Metacarbonate is in fault contact with the overlying Middle-Late Triassic June Complex to the north of the Kuh-e-June antiform (Figure 3.5). 3.5 km east-southeast of Papion this fault is dipping at 60° to the north and contains down-dip striations. In contrast to other faults in the study region, this fault juxtaposes stratigraphically older rocks in the footwall block against younger rocks in the hanging wall block. This pattern is anomalous for the D_2 deformation as F_2 folds have a consistent southwest vergence and associated thrust faults are developed along the overturned F_2 limbs (see cross sections in Figure 3.5). One possibility is that this fault formed prior to D_2, perhaps during an earlier phase of extension (see Chapters 5 and 6), and was reactivated as a thrust during D_2 and D_1.

3.4 STRUCTURE OF THE MYLONITIC ROCKS

The mylonitic rocks in the study area were produced in ductile shear zones indicating strain softening with crystal plastic deformation mechanisms (e.g. White et al. 1980). Protomylonite and ultramylonite were produced by recrystallisation and neomineralisation. Shear sense has been widely determined at the scale of the outcrop and in oriented thin sections and consistently indicates dextral displacement. Kinematic indicators (Hanmer and Passchier 1991) such as composite planar fabrics (S-C fabrics, Berthe 1979), shear bands and mica fish (Lister and Snoke 1984), porphyroclast fracture patterns (Simpson and Schmid 1983), asymmetric augen structures, including σ-type and δ-type porphyroclast systems (Passchier and Simpson 1986) are recognised. Shear-sense indicators on the mesoscopic scale were observed on planes approximately perpendicular to the foliation and parallel to the mineral

lineation, generally on sub-horizontal planes. They were also observed in thin sections along the XZ plane of the strain ellipsoid and for this purpose, the oriented samples were cut perpendicular to the shear zones (foliation) and parallel to the movement direction (mineral lineation).

Four major types of mylonitic rocks occur in the study area: (1) mylonitic granite, (2) mylonitic amphibolite, (3) calcite mylonite, and (4) mylonitic metasilicic igneous rocks.

Mylonitic granite

The main exposure of the mylonitic granite (Galeh-Doz pluton) is located at the eastern extremity of the mapped area and extends to the southeast out of the study area towards Azna (Figure 3.5, see Chapter 5). A long sill-like body of this mylonitic granite, 18 km in length and up to 1 km in width, is joined to the northern part of the pluton and extends to the west-northwest. Another exposure of the mylonitic granite (Shur-Shur sill) is exposed around Shur-Shur village in the central part of the study area and extends to the west out of the study area (Figure 3.5). The Shur-Shur pluton has a sheet-like geometry that is extended west-northwest subparallel to the general trend of S_2. Isolated patches of the mylonitic granite are also exposed around Baraftab-Deraz, southeast of Zageh-Bala and north of Ag-Bolag (Figures 3.5, 3.19).

The Galeh-Doz pluton consists of microcline, plagioclase, biotite, quartz and muscovite. The main mass of the Galeh-Doz pluton has more mafic minerals, including biotite, than its west-northwest extension and also the Shur-Shur sill. Augen of feldspar porphyroclasts, as long as 32 mm, were measured in the X direction of the finite strain ellipsoid.

Foliation

The mylonitic granite consists of a compositional layering parallel to S_2. The layering is formed by interbanded quartzo-feldspathic and mafic layers. The foliation is defined by biotite sub-parallel to quartz ribbons and feldspar. A strong lineation is produced by parallel alignment of elongate grains of feldspar. Quartz occurs in ribbons as polygonised grains and in pressure shadows at the end of feldspar porphyroclasts. Quartz porphyroclasts are recrystallised to sub-grains with sutured boundaries. Neocrystallised fine quartz grains occur at quartz grain boundaries and at the borders of quartz ribbons. Undulatory extinction is developed in the quartz ribbons. Elongate feldspar grains define the foliation and are wrapped around by quartz ribbons. Deformation twins in plagioclase minerals are commonly bent (see Chapter 4).

The dominant mylonitic fabric in the granite is developed parallel to the axial plane schistosity of the isoclinal F_2 folds in the country rocks of the study area and therefore is considered to be S_2. In the Galeh-Doz pluton, 5 km southeast of Masud-Abad, just outside the study area (Figure 2.1), mylonitic granite is interlayered with well recrystallised marble and schist and S_2 in the wall rocks is sub-parallel to the mylonitic foliation in the deformed granite. At Masud-Abad, F_2 isoclinal folds and associated axial planar S_2 are well developed in schist and marble adjacent to the granite (see the main map in the pocket).

Locally, an older foliation is observed in the Galeh-Doz mylonitic granite near to wall rocks, for example, at Masud-Abad an early fabric in the mylonitic granite is evident and is isoclinally folded (Figure 3.20a). The axial plane of these folds is parallel to the axial plane schistosity (S_2) of the wall rocks. The steeply dipping mylonitic S_2 is curved in the Galeh-Doz pluton. From Masud-Abad to the northeast, the S_2 mylonitic foliation swings in trend from the north-south to an easterly strike

(see the main map in the pocket). South of Masud-Abad, the foliation strikes northwest-southeast. At Abbas-Abad the S_2 foliation in the granite is folded around the Kuh-e-Sefid F_2 antiform. The west-northwest trending extension of the Galeh-Doz pluton, the Shur-Shur sill and other exposures of the deformed granite also contain the pervasive west-northwest trending mylonitic foliation (S_2). This foliation is vertical or dipping steeply to the northeast (Figure 3.20b).

Stretching lineation (L_m)

In the Galeh-Doz pluton, a strong sub-horizontal to gently plunging stretching lineation is present (Figure 3.20c). In the main mass of the pluton, this lineation plunges 20°-30° to the northeast (Figure 3.21a) and in the west-northwest extension of the Galeh-Doz pluton and the Shur-Shur sill it is subhorizontal or plunging gently to both the northwest and southeast (Figures 3.19, 3.21b, d). The stretching lineation is contained within the strong mylonitic foliation (S_2) and is defined by elongate and extended biotite, quartz ribbons and feldspar porphyroclasts (Figure 3.20d). The mylonitic S_2 defines the orientation of the XY principal plane of strain and the stretching lineation indicates the X direction of the finite strain ellipsoid (Berthe et al. 1979).

1500 m to the southeast of Malhamdar (Figure 3.5), in the west-northwesterly trending extension of the Galeh-Doz pluton, a significant component of stretching is shown by a sub-horizontal to gently-plunging stretching lineation which is indicated not only by stretched feldspar and quartz ribbons but also by long cylindrical rods (Figures 3.21b, 3.22). The cylindrical rods consist of tourmaline surrounded by plagioclase (Figure 3.22a). Aggregates of tourmaline in the core of the rods are also elongated along the stretching direction. Thus the rods must have formed either before or during mylonitization (Figure 3.22d). The rods have a radius up to 6 cm

and the length is in the range 10 to 40 cm, although lengths as long as 2.5 m have been observed. Widths in the Y and Z directions are about the same (Z = Y) indicating a pure constriction (see the graph in Figure 3.22).

1200 m to the south of Deh-Haji village (Figure 3.5), the aggregated tourmaline minerals have been stretched in both the X and Y directions of the strain ellipsoid (Figure 3.23a, b) and therefore the rock is a LS tectonite.

Pinch-and-swell structures also occur in the mylonitic granite (Figure 3.13c); the extension direction indicated by these structures is sub-parallel to the stretching lineation (L_m) on S_2.

Shear-sense indicators

Dextral shear deformation is indicated by porphyroclast asymmetries. Asymmetric augen structures (σ-type) are defined in horizontal exposures (Figure 3.23c). Feldspar augen occur in a fine-grained matrix and have asymmetric tails of fine-grained recrystallised material of the same composition as the porphyroclast (cf. White et al. 1980). Tails are extended along the foliation plane and are asymmetrically distributed around the porphyroclasts. Recrystallised asymmetric tails indicate a dextral shear sense (Figure 3.23c). A broken and pulled apart feldspar porphyroclast has had fibre growth in the cavity indicating the X-direction which is consistent with dextral shearing (Figure 3.23d).

Amphibolite mylonite

West-northwest-trending amphibolite mylonite is located in the core of the map-scale F_2 antiform and, in the northeast around the Malhamdar, Deh-Mosa and Deh-Haji villages north of the west-northwest extension of the Galeh-Doz pluton (Figure 3.5). In the core of the map-scale F_2, this rock unit extends from Baraftab-Deraz in

the centre of the mapped area to the west around Zageh-Bala, Shur-Shur and to the west-northwest it continues out of the study area (Figure 3.5).

A metamorphic segregation layering composed of plagioclase-rich and amphibole-rich layers is present in the amphibolites (Figure 3.24a). The segregated layers show both fine-grained and coarse-grained bands. The segregation layering in the amphibolite is tightly to isoclinally folded (Figure 3.4a). The axial planes of the folds are parallel to the gross mylonitic foliation (S_2) with a west-northwest orientation steeply dipping to the north-northeast.

The stretching lineation (L_m) in the mylonitic S_2 is defined by elongate plagioclase and amphibole (Figure 3.24b) and is sub-horizontal or gently plunges to the northwest or southeast. Also, subhorizontal mechanical striations (Figure 3.24c) occur in the mylonitic foliation indicating strike-slip displacement (cf. Berthe et al. 1979). Pinch-and-swell structures exist along the (S_2) indicating extension subparallel to the stretching lineation (Figure 3.24d). Parallelism of the stretching lineation, striation and also the extension direction as defined by pinch-and-swell structures, are evidence demonstrating subhorizontal extension of the amphibolite unit in a west-northwest direction.

Shear-sense indicators in the amphibolite mylonite

Shear-sense indicators in amphibolite mylonite include: asymmetric augen (Figure 3.24b), S-C structures, displaced broken grains and en echelon shear fracture boudins. These all indicate a dextral shear sense.

S-C structures

Composite C- and S-surfaces (Berthe et al. 1979) are developed in amphibolite mylonite. The angular relationships between these two surfaces define the sense of

shear in the rock. Mica-fish structure (type-II S-C mylonite of Lister and Snoke 1984) is developed in mylonitic amphibolite and is defined by amphibole (Figure 3.25a, c, d). The S-planes are indicated by aligned hornblende with tails extended along the C-planes. They are linked by thin trails of amphibole fragments (Figure 3.25a, d); some of these are extensively developed producing stair-step features from one grain to the next (Figure 3.25d).

Displaced broken grains

Displaced broken grains (after Simpson and Schmid 1983) are observed on a microscopic scale in the amphibolite mylonite. These structures are used for determining shear sense in mylonitic rocks (Simpson and Schmid 1983; Takagi 1986). Feldspars that were unable to deform plastically, have fractured with displacement having occurred along these fractures. The sense of shear along the microfractures, that are oriented oblique to the shear plane, is opposite to the over-all sense of the shear in rock. The style of book-shelf type rotation in the amphibolite mylonite reflects dextral shear (Figure 3.26).

Asymmetric boudins

At one locality near Zageh-Bala, asymmetric boudins occur on both limbs of an isoclinal F_2 and were produced by syn-deformational (syn-D_2) strike-slip shear. The isoclinal F_2 is developed in interbedded metabasite and marble (Figure 3.27). During D_2, the isoclinal fold was produced and continued compression, normal to the limbs of the fold, resulted in the limbs being extended (e.g. Ramsay 1967; Price and Cosgrove 1990, p. 426). During this process, competent layers were fractured at a high angle to the extension direction. Shear fractures cut the axial plane (S_2) indicating that they formed during the later stages of D_2 folding (Figure 3.27).

Dextral displacement on these shear fractures has consistently offset both limbs of the fold.

The boudinage at this locality is an example of shear fracture boudinage (after Gosh 1993, p. 411-418) and several models, involving opposite senses of shear, can explain their formation. Firstly, Gosh has shown how an extension parallel to the layer has produced synthetic shear fractures with displacement along them. The boudins are rotated as a result of sliding along the shear fractures so that the boudins after deformation are arranged in an en echelon pattern (Figure 3.27). This model would account for the formation of asymmetric boudins in Figure 3.27 and other examples in the schist and marble units (Figure 3.28a, see section 3.3 D_2 Deformation). These structures would therefore all indicate dextral shear.

The second model as proposed by Goldstein (1988) is distinct from the first model although it would produce the same shear sense. In this model, prior to shearing layering was inclined at less of an angle than the boundaries of the shear zone (Figure 3.27, inset). Extension fractures formed at a moderate angle to the shear zone boundary and subsequent shearing resulted in reactivation of the extension fractures with synthetic displacement and formation of asymmetric boudinage. This model also indicates a dextral sense of shear for asymmetric boudinage in the study area.

In the third model (after Hanmer 1986), displacement between blocks has resulted from rigid-body back rotation of individual boudins, i.e. for a sinistral layer-parallel shear the blocks are rotated in a counter-clockwise direction. Here, foliation between the boudins should have a sigmoidal pattern (see Hanmer 1986, p. 117); but no curved segments exist in the boudins shown in Figure 3.27 and consequently, this model is not considered to be the case.

Calcite mylonite

Calcite mylonite is well developed in some parts of the study area. Under the microscope, the calcite mylonite is composed of very fine-grained calcite and recrystallised dolomite porphyroclasts. Porphyroclasts have wings consisting fine-grained dolomite grains and strong foliation is produced by the elongation and alignment of calcite minerals and by pressure solution as shown by concentration of graphite and insoluble residues along foliation planes. Asymmetric recrystallised tails indicate dextral shear sense along the mylonitic foliation (Figures 3.25b, 3.28b). Hinges of microfolds are preserved as pods due to strong transposition along the mylonitic foliation (Figure 3.25b). Some dolomite fragments are strongly twinned and others are recrystallised.

The mylonitic foliation in calcite mylonite is S_2 (Figure 3.28b). 200 m to the southwest of Darijune-Bala, highly folded, foliated and mylonitised marble and metadolomite are exposed. They are composed of calcite ribbons and mostly dolomite fragments that are wrapped around by the calcite ribbons. The stretching direction is sub-parallel to the strike of the mylonitic foliation and it is defined by tails on the dolomite fragments (Figure 3.28b). This indicates that flattening was approximately parallel to the shear plane and that the stretching direction is sub-horizontal (west-northwest).

An anastomosing geometry is observed on a mesoscopic scale (Figure 3.28b), and is considered a criterion for non-homogeneous strain (Simpson and Schmid 1983). The anastomosing planes correspond to shear planes (C-planes) between which the dolomite fragments are arranged obliquely. The dolomite fragments appear as asymmetric augen, demonstrating the sense of shear (Figure 3.28a). In a thin section cut parallel to stretching lineation and perpendicular to mylonitic foliation, δ-type asymmetric tails occur in the calcite mylonite (Figure 3.25b).

Mylonitic metasilicic igneous rocks

Along the northern border of the mylonitic granite, within the Hamadan Phyllite, fine-grained mylonitic metasilicic igneous rocks are exposed with a west-northwest trend (see the main map in the pocket). The mylonitic foliation (S_2) in this fine-grained silicic ultramylonite (see Chapter 4, Figure 4.4b, c) is parallel to the axial planes of tight to isoclinal F_2. A strong stretching lineation in S_2 is subhorizontal or gently plunging either to the west-northwest or to the east-southeast.

3.5 D_3 DEFORMATION

The third deformation is characterised by locally developed F_3 folds and S_3 crenulation cleavage. Complex structures including deformed lineations are produced due to superimposition of D_3 on previous deformations.

F_3

F_3 folds are upright, close to open in competent rocks and close in phyllite. The axial plane is mostly vertical or steeply dipping to the north-northeast indicating vergence to the southwest (Figure 3.29a, b). Hinges are moderately plunging to the east-northeast (Figure 3.29c). F_3 folds have low amplitudes and long wavelengths. Profiles of F_3 in phyllite range between Class 1B and Class 2 but in metadolomite, marble and quartzite they have Class 1B profiles. 1400 m north and 800 m southwest of Dareh-Zooleh (Figure 3.5), F_3 are well exposed. A macroscopic scale F_3 is observed 100 m southwest of Darijune-Bala where a synform-antiform fold couple is evident in metadolomite and marble.

S_3

S_3 is an axial planar crenulation cleavage and is developed in phyllite and schist. In competent rocks, such as metadolomite, S_3 is developed as a spaced cleavage (Figure 3.29d). S_3 is vertical or dips steeply to the northeast (Figure 3.29c).

Deformed lineation

The intersection lineation between S_1 and S_2 has behaved as a passive linear feature as described by Ramsay and Huber (1987, p.481) and was rotated during formation of younger folds (F_3). 800 m to the south of Dareh-Zooleh close to open asymmetric F_3 are exposed in phyllite. At the F_3 hinge, L_2 is observed on the folded S_2 (Figure 3.30). The axial plane crenulation cleavage (S_3) is vertical or dips steeply to the north-northeast. The angle between the F_3 hinge line and L_2 (α) on the hinge zone is 32° and remains constant around the hinge. This indicates that F_3 folds were produced by flexural slip folding (after Ramsay 1967, p. 463).

Faults

Timing of D_3 thrust faults are generally identified by cross-cutting relations with S_2. These faults are associated with brecciation. 200 m west of Meydanak, two thrust faults are clearly recognised (Figure 3.31a). In the fault planes, breccia contains angular fragments of metadolomite and quartzite. The distinct fault planes are dipping to the northeast and contain striations indicating north-trending dip-slip motion. The net slip direction on the southern thrust fault is indicated by a striation lineation plunging 20° to the north. Striations on the northern thrust fault plunge 39° to the north. The map offset of two grey marble markers indicates a strike separation of 130 m on the southern thrust fault (Figures 3.6, 3.31a). 300 m southwest of Darijune-Bala a thrust fault is gently dipping to the northeast and is

cutting S_2 (Figure 3.31b).

Two sets of steeply dipping strike-slip faults occur: the northeasterly trending set (010°-040°) are sinistral and the northwesterly trending set (320°-350°) are dextral. They are mostly developed in the northern limb of the map-scale F_2 (Figure 3.5 and the main map in the pocket). The strike-slip faults displace S_2 and D_2 thrust faults. A general north-south direction of shortening (σ_1) is indicated for these two fault sets and therefore they are considered as part of the third deformation event in the area.

3.6 D_4 DEFORMATION

In contrast to the previous deformations, the last deformation is recognised by northeast-southwest trending folds, and conjugate dextral and sinistral kinks that are developed in schist and phyllite. This deformation is superimposed on previous deformations.

F_4

F_4 are open, upright folds with axes plunging both to the northeast and southwest (Figures 3.31c, 3.32a) and lacking an axial plane cleavage. They are well recognised in schist and metaigneous rocks. The best outcrop where F_4 structures are evident is located along the road 2 km northeast Azna (Figure 5.1). In this area S_1, sub-parallel to bedding, is folded to produce F_4.

Two kilometres southwest of Bavaki, a macroscopic F_4 occurs with a northeast-trending axial trace (Figure 3.5 and the main map in the pocket).

Kinking

In strongly deformed metamorphic terrains containing polyphase folding, kink bands commonly represent the last phase of folding (Suppe 1985, p. 340). Within

the study area dextral and sinistral kink bands occur in schist and phyllite. 300 m west of Meydanak conjugate kink bands are well exposed. Kink bands are produced by post D_3 foliation-parallel compression.

3.7 DISCUSSION

Structures in the poly-deformed rocks in the study area have been produced in several deformation periods related to distinct tectonic events. West-northwest trending tight to isoclinal F_1 plunge moderately to steeply to the east-northeast and have an axial plane schistosity (S_1) moderately to steeply dipping to the east with various strikes. D_1 structures have been obliterated or strongly reoriented by pervasive D_2. D_1 was the product of shortening in a north-northeast - south-southwest direction and is related to subduction that occurred during Late Jurassic - Early Cretaceous times (see Chapters 5 and 6). This deformation is represented by a general uplift in the Sanandaj-Sirjan Zone and formation of a well known angular unconformity overlain by a basal conglomerate of middle Cretaceous age (Aptian-Albian, see Chapter 5).

D_2 is the result of oblique collision of the Afro-Arabian continent with the southwestern part of central Iran (Sanandaj-Sirjan Zone) in Late Cretaceous times (see Chapter 6). The major deformation (D_2) is the product of dextral transpression (see below) with north-northeast - south-southwest shortening and substantial dextral shearing in a west-northwest direction. D_2 has been partitioned with two distinct styles of deformation occurring in two separate major groups of rock types (see below). F_2 are tight to isoclinal folds with a pervasive axial plane S_2 schistosity and are the most abundant structures in the study area.

D_2 has also been associated with major north-northeast dipping thrust faults that at least in the southwestern part of the study area are gently dipping. F_2 folds have

a high amplitude and short wavelength implying a relatively deep depth to the level of folding during D_2. The thrust faults have transported these more "thick-skinned" folds to their present structural level during major uplift associated with D_2 transport to the south-southwest. In the later stages of deformation thrusts have cut the overturned southwestern limbs of the major antiforms. Therefore, D_2 is the result of buckling and imbricate thrusting of the thick Late Palaeozoic and Triassic-Jurassic succession (see Figure 3.5, cross sections AB and CD).

Locally observed F_3 are coaxial with F_2 and AS3 are co-planar with AS2 indicating that during D_3, the same shortening direction of both D_1 and D_2 was maintained. For D_4 shortening was almost perpendicular to the shortening direction of the previous deformations.

Deformation partitioning

Deformation partitioning has been observed at a macroscopic scale in polydeformed orogenic belts, with progressive localisation of strain during several deformation stages (e.g. Worley and Wilson 1996), and in a single deformation event (Bergh and Karlstrom 1992). Deformation partitioning in the study area has occurred on a macroscopic scale during D_2 and has formed two interleaved high-strain domains that are controlled by rock type (Figure 3.33a). These domains are: (1) marble and schist units, and (2) crystalline mylonitic rocks.

The domain with schist and marble units is strongly folded (F_2 isoclinal folds) and the axial plane S_2 schistosity is regionally developed. In addition, thrusts have displaced units and indicate a north-northeast - south-southwest compression direction that is consistent with the orientation of F_2 and S_2. The flattened shapes of the map-scale F_2 are consistent with a vertical stretching in this domain although this was not strong enough to develop a stretching lineation. Dextral shearing is not represented

except by occasional asymmetric boudins (Figure 3.28a). These features are consistent with an overall pure shear type of deformation in this domain.

Mylonitic rocks of the second domain are composed of more competent rocks than for the first domain and include amphibolite and metasilicic igneous rocks. These rocks are characterised by steeply dipping mylonitic foliation (S_2) and a west-northwesterly trending subhorizontal stretching lineation in the mylonitic foliation. Dextral shearing is well illustrated by widespread shear-sense indicators. They indicate that D_2 has a major component of dextral shearing parallel to the west-northwest trend of the structural grain in the study area. The geometry of the syn-D_2 Galeh-Doz pluton also indicates that it developed during the episode of dextral shearing (see below). In contrast to the first domain, the second domain shows evidence for intense dextral simple shear demonstrating that almost totally effective deformation partitioning has occurred between both domains.

Transpression

Transpression is considered as a strike-slip shear accompanying horizontal shortening and vertical lengthening in the shear plane (Sanderson and Marchini 1984). Tectonic transpression has been illustrated at obliquely convergent plate boundaries (Tikoff and Teyssier 1994; Teyssier et al. 1995). The type of transpression is controlled by the values of α, the angle between the direction of plate convergence and the contractional flow apophysis, and the angle Θ, which is the angle between the maximum horizontal axis of the incremental strain ellipsoid and the trend of the plate boundary (see Figure 3.33b; after Tikoff and Teyssier 1994).

Tikoff and Teyssier (1994) have applied their model of tectonic transpression to the present-day zones of oblique plate convergence and have recognised pure-shear dominated (e.g. Sumatra) and simple-shear dominated (e.g. California)

transpression. In zones of transpression the deformation is strongly partitioned into domains of pure-shear dominated deformation and simple-shear dominated deformation. The latter is represented by the development of major strike-slip faults as has occurred in California. From the theory devised by Tikoff and Teyssier (1994), it is clear that as the percentage of the partitioning between pure-shear dominated and simple-shear dominated domains is increased the value of Θ is decreased. In thrust-dominated transpression, where the percentage of partitioning is close to 100%, the angle Θ will be very close to the zero (see also Curtis 1997). These regions do not contain major strike-slip faults. Curtis (1997) mapped the Heritage Range in West Antarctica and recognised strong partitioning between two domains, one with reverse geometry (folds and thrusts), and one with dextral strike-slip shearing striking parallel to the regional structural grain (i.e. $\Theta = 0$, $\alpha = 70°$). Overall, the region was affected by pure-shear dominated dextral transpression with efficient deformation partitioning in a zone of highly oblique convergence associated with Gondwanan orogeny.

In the study area, there has been strong partitioning between two domains as indicated by the development of mylonitic rocks dominated by dextral strike-slip shearing and another domain dominated by pure shear deformation in the schist and marble units. This is somewhat similar to the deformation pattern recorded by Curtis (1997). The shear zones in the mylonitic rocks are parallel to the plate margin along which the oblique convergence has occurred (see Chapter 6). In the study area, no strike-slip faults, parallel to the trend of the shear zones, have been observed. The contractional component consists of the development of F_2 folds, with south-southwest vergence, steeply dipping axial plane schistosity and abundant thrust faults dipping to the northeast at 30°-60°. Thrust faults have strikes that are either subparallel to the trend of the orogen or are at an angle of <10° to that trend (Figures 3.17a, c, 3.33a).

The axial plane schistosity of F_2 in schist and marble units is parallel to the mylonitic foliation in the mylonitic rocks. This indicates that the contraction direction is perpendicular to the direction of dextral shearing, and as for the Heritage Range in Antarctica (Curtis 1997) Θ is very close to or equal to zero.

It is therefore suggested that the study area has been situated in a pure-shear dominated transpressional tectonic regime and that a highly oblique shortening direction was responsible for this deformation (see Chapter 6).

Temporal and structural setting of the Galeh-Doz pluton

Syntectonic plutons have been studied in several orogenic belts. Mechanisms of emplacement of syntectonic plutons have been described for the following processes: transcurrent shear with local pull-apart extension (Hutton 1982, 1988; Guineberteau et al. 1987; Choukroune and Gapais 1983), transpression (Murphy 1987; Castro 1986) and ductile thrusting (Brun and Pons 1981; Burg and Wilson 1988; Tobisch and Paterson 1990, Paterson et al. 1990).

Paterson and Tobisch (1988) have summarised the general characteristics of syntectonic plutons. These characteristics are all applicable to the Galeh-Doz pluton and include: (1) the strong steeply dipping foliation in the country rocks continues into the pluton with the same orientation, (2) the strong subhorizontal stretching lineation existing in the country rocks, such as amphibolite mylonite and other mylonitic rocks, continues in the pluton, (3) synkinematic contact metamorphism exists (see below), (4) the pluton margin is highly mylonitised, and (5) the shape of the pluton is concordant with regional structure and it is extensively stretched along the strike of the foliation containing the subhorizontal stretching lineation.

Although the foliation has been dextrally rotated during shearing (see below), the consistency of the mylonitic foliation trajectories within the Galeh-Doz pluton

demonstrates that no strain heterogeneities were produced due to pluton intrusion as described in some syntectonic plutons (e.g. Brun and Pons 1981; Patterson et al. 1991). It is concluded that the mylonitic granite has been intruded syn-kinematically with D_2. No pervasive magmatic foliation (Paterson et al. 1989), or a primary flow foliation formed from ballooning (Hutton 1988), is recognised in the pluton because of the presence of the intense mylonitic foliation (S_2). Pluton boundaries are subparallel to the mylonitic S_2 and the pluton is elongate along the stretching direction (west-northwest).

To the southeast of Galeh-Doz, near the contact of the schist with deformed granite a weak contact metamorphic effect is evident and defined by growth of muscovite and biotite in S_2. The same weak contact effect is observed along the west-northwest-trending extension of the Galeh-Doz pluton. Porphyroblasts have not been observed in the weak contact aureole of the Galeh-Doz pluton.

It is concluded that the mylonitic granite has been strongly sheared and mylonitised by dextral shearing and has the same foliation as the main foliation in the marble and schist units and is subparallel to the axial planes of tight to isoclinal F_2 which occur in the wall rocks.

Tectonic model for emplacement of the Galeh-Doz pluton

A tectonic model for the emplacement of the Galeh-Doz pluton has to account for the pervasive dextral shearing and also the sigmoidal shape of the pluton. In this context, the hypothesis is suggested that the ascent and emplacement of the Galeh-Doz pluton was controlled by: (1) development of a major cavity at 45° to the west-northwest dextral shear zone, (2) buoyancy-controlled magma intrusion along the cavity, and (3) dextral rotation of the central part of the widening pluton (Figure 3.34a). A similar model was used to explain the ascent and emplacement of several

syntectonic plutons in the Hercynian belt in Spain (Castro 1986).

The Galeh-Doz pluton may have initiated as a tensional controlled fissure at 45° to the west-northwest trending dextral shear zone (Figure 3.34a, stage 1), as is well established for en echelon vein systems (cf. Ramsay 1967, p. 83-91; Ramsay and Huber 1987, p. 23-24, 48-52). As the fissure opened it was simultaneously filled with granitic magma (Figure 3.34a, stages 2, 3 and 4). As the Galeh-Doz pluton was intruded it was deformed and extended in the west-northwest direction parallel to S_2 and the subhorizontal stretching lineation was developed throughout the pluton (Figures 3.20, 3.34b).

Continuing dextral shearing caused rotation of the central part of the pluton as has been documented in en echelon sigmoidal gash veins (Ramsay and Huber 1987, p. 23-24, 48-52) and also in the syntectonic granites of the Hercynian belt of Spain (Castro 1986). In the central part of the pluton, S_2 and L_m have been dextrally rotated producing a structure resembling the geometry of a δ-type porphyroclast (Passchier and Simpson 1986). Thus the dominant steeply dipping mylonitic S_2 of the northwestern extension of the pluton changes its strike through the main mass of the Galeh-Doz pluton (Figure 3.34c).

3.8 CONCLUSIONS

Several generations of folds with various interference patterns were produced during plate convergence and subsequent oblique collision in the study area (see Chapter 6). D_1 consists of well-developed S_1 with various strikes dipping to the east and F_1 plunging moderately to the east-northeast. D_2 is the major deformation, characterised by strongly developed S_2 dipping steeply to the north-northeast and F_2 plunging moderately to the east. S_2 is a strong mylonitic foliation in the mylonites including syntectonic plutons. F_3 is locally developed and is coaxial with F_2 and

characterised by axial plane crenulation cleavage.

Since the time of collision, the west-northwest-striking Sanandaj-Sirjan Zone has been affected by oblique convergence (see Chapter 6). D_2 progressive shortening was broadly synchronous with progressive dextral shearing. Deformation partitioning is reflected by the different responses of the rock units to the dextral transpressional deformation. Schist and marble units were intensely folded with southwest vergence and contain thrust faults that are subparallel to the trend of the S_2 and dipping to the north-northeast. In contrast, the syn-tectonic plutonic rocks, amphibolites and other mylonites have a regional S_2 foliation containing a subhorizontal west-northwest-trending stretching lineation. The mylonitic foliation is sub-parallel to the regional S_2 schistosity in schist and marble units. The geometry of structures indicates that both pure-shear dominated and dextral simple-shear dominated deformation played major roles in the D_2 deformation history.

Deformation episode	S Surfaces	Lineations	Folds
D_1	S_1 axial plane schistosity **AS1** axial plane	L_1 intersection lineation (S_1, S_0)	F_1
D_2	S_2 axial plane schistosity **AS2** axial plane	L_2^1 intersection lineation (S_2, S_1) L_2^0 intersection lineation (S_2, S_0)	F_2
----------	----------	----------	
mylonitic elements	S_2 mylonitic foliation	L_m stretching lineation	
D_3	S_3 axial plane cleavage **AS3** axial plane	L_3^2 intersection lineation (S_3, S_2)	F_3
D_4	**AS4** axial plane		F_4

Table 3.1 Structural elements in the study area.

Figure 3.1

(a) Tight F_1 fold in fine-grained quartzite interbedded with thin-layered and partly boudinaged metadolomite. 3 km east of Darijune-Bala. Compass is 12 cm in length.

(b) Tight to isoclinal F_1 fold in marble. 2 km east of Bavaki. Pen is 14 cm in length.

(c) Disharmonic F_1 folds. White chert bands are strongly folded in highly foliated marble. Minor refolding is seen above the lens cap. 500 m southeast of Baraftab-Deraz. Lens cap is 5.5 cm across.

(d) Isoclinal F_1 in well foliated marble; axial plane is sub-vertical and hinges die out along their length. 500 m southeast of Baraftab- Deraz. Coin is 16 mm across.

a
b
c
d

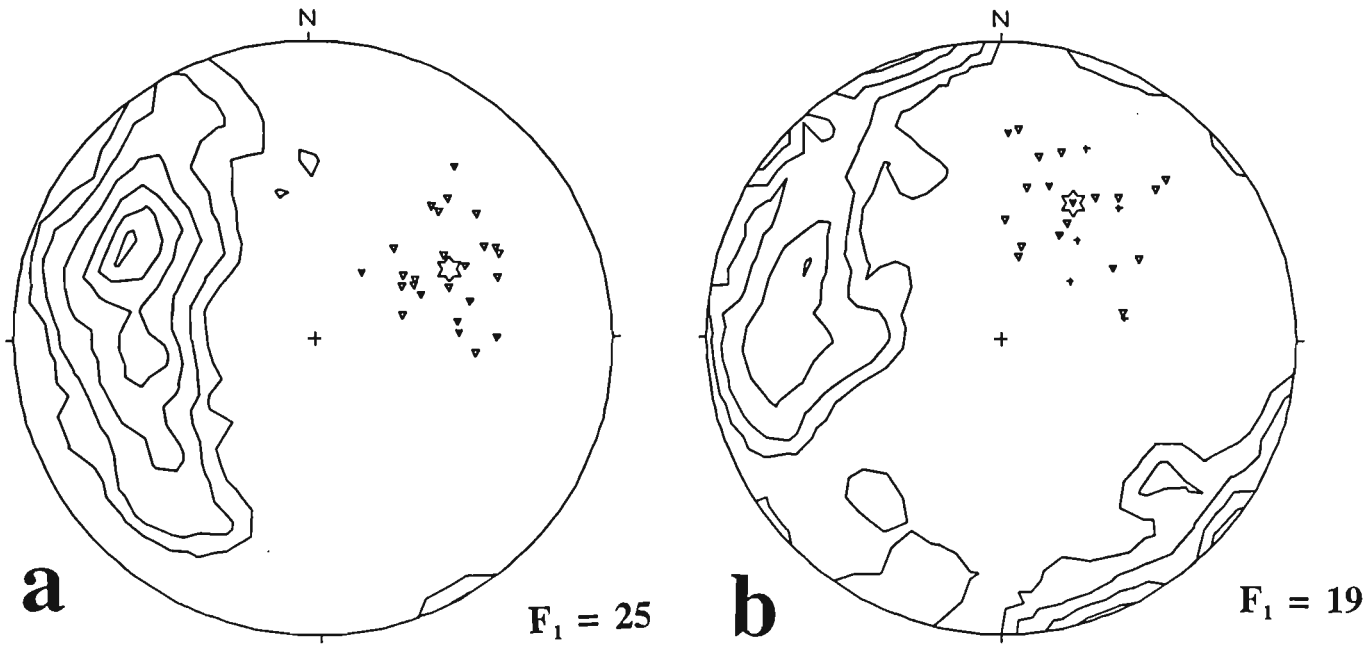

Figure 3.2

(a) Lower-hemisphere equal-area stereographic projection of D_1 structural elements measured on the Papion fold. AS1 and S_1 poles (92) are contoured at 1, 2, 4, 6, 8, and 10% per 1% area. F_1 = triangles and average is shown by star is 48°/063°.

(b) Lower-hemisphere equal-area stereographic projection of D_1 structural elements measured in the Bavaki area, eastern half of the study area. AS1, S_1, and S_0 poles (130) are contoured at 1, 2, 4, and 6% per 1% area. F_1 = triangles and average is shown by star is 47°/028°, L_1 = crosses.

Figure 3.3

Relic S_1 preserved amongst well-developed S_2.

(a) Garnet-muscovite schist with S_2 wrapped around a sub-idiomorphic syn-D_2 garnet porphyroblast. 2 km northeast of Teadar, June Complex, middle unit, sample number 847 (plane polarised light, 1.6 mm in length and 1.1 mm in width).

(b) Chlorite-epidote-actinolite schist produced from retrograde metamorphism of an amphibolite. Note that the actinolite formed from alteration of hornblende and is preserved in a relic microlithon. S_1 is perpendicular to the well-developed S_2. S_2 is defined by chlorite and actinolite. 200 m northeast of Meydanak, June Complex, upper unit, sample number 30 (crossed polarised light, 1.6 mm in length and 1.1 mm in width).

(c) Muscovite-actinolite schist. S_1 is folded to produce isoclinal F_2 with well developed axial plane S_2. 2 km southwest of Dareh-Zooleh, June Complex, upper unit, sample number 472 (crossed polarised light, 1.6 mm in length and 1.1 mm in width).

(d) Relic microlithon with S_1 developed in phyllite and wrapped around by S_2. 1400 m west-northwest of Ag-Bolag, Hamadan Phyllite, sample number 143 (plane polarised light, 1.6 mm in length and 1.1 mm in width).

a
S1
S2
b
S1
S2
c
S1
S2
d
S1
S2

Figure 3.4

(a) Tight to isoclinal F_2 fold in amphibolite. The folded layering (S_1) consists of differentiated feldspar and amphibole-rich layers. The mylonitic foliation (S_2) is parallel to the axial plane of the fold. 300 m southwest of Zageh-Bala. Hammer is 32 cm in length.

(b) Structural domains of D_1 and axial trace of the macroscopic F_1 and map-scale F_2 in the June area.


a

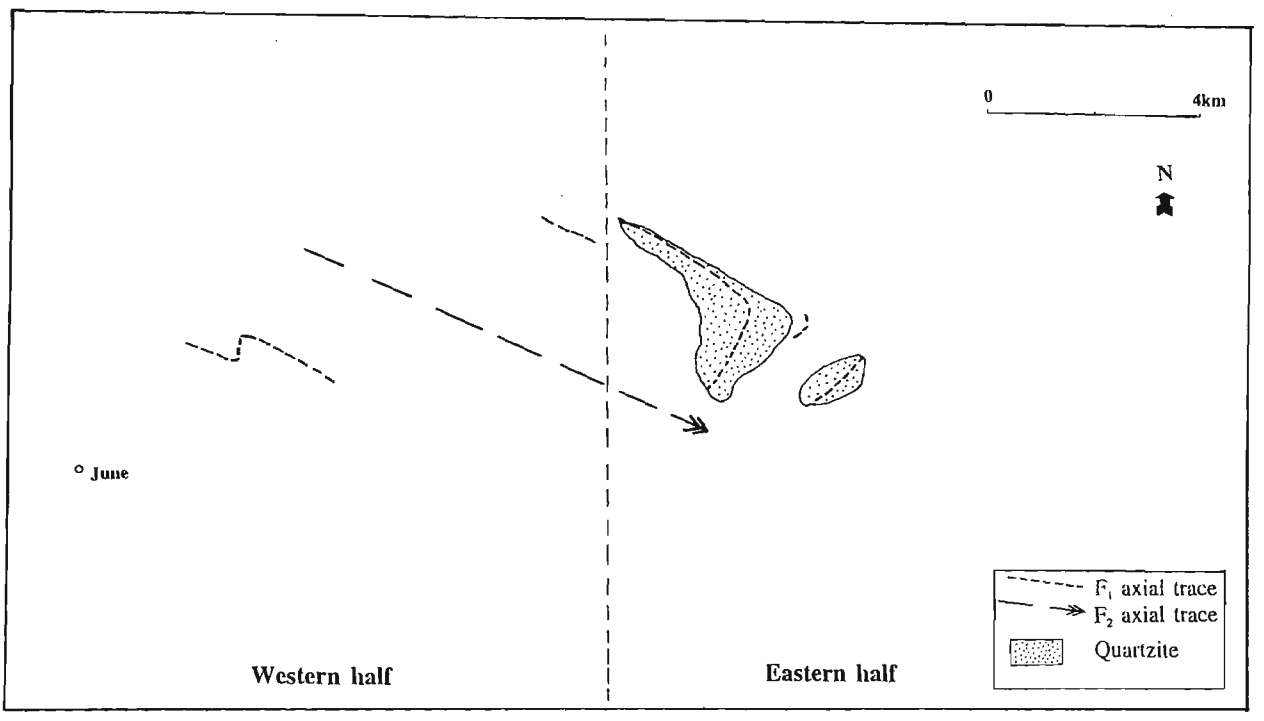
0
4km
N
° June
Western half
Eastern half
F1 axial trace
F2 axial trace
Quartzite

b

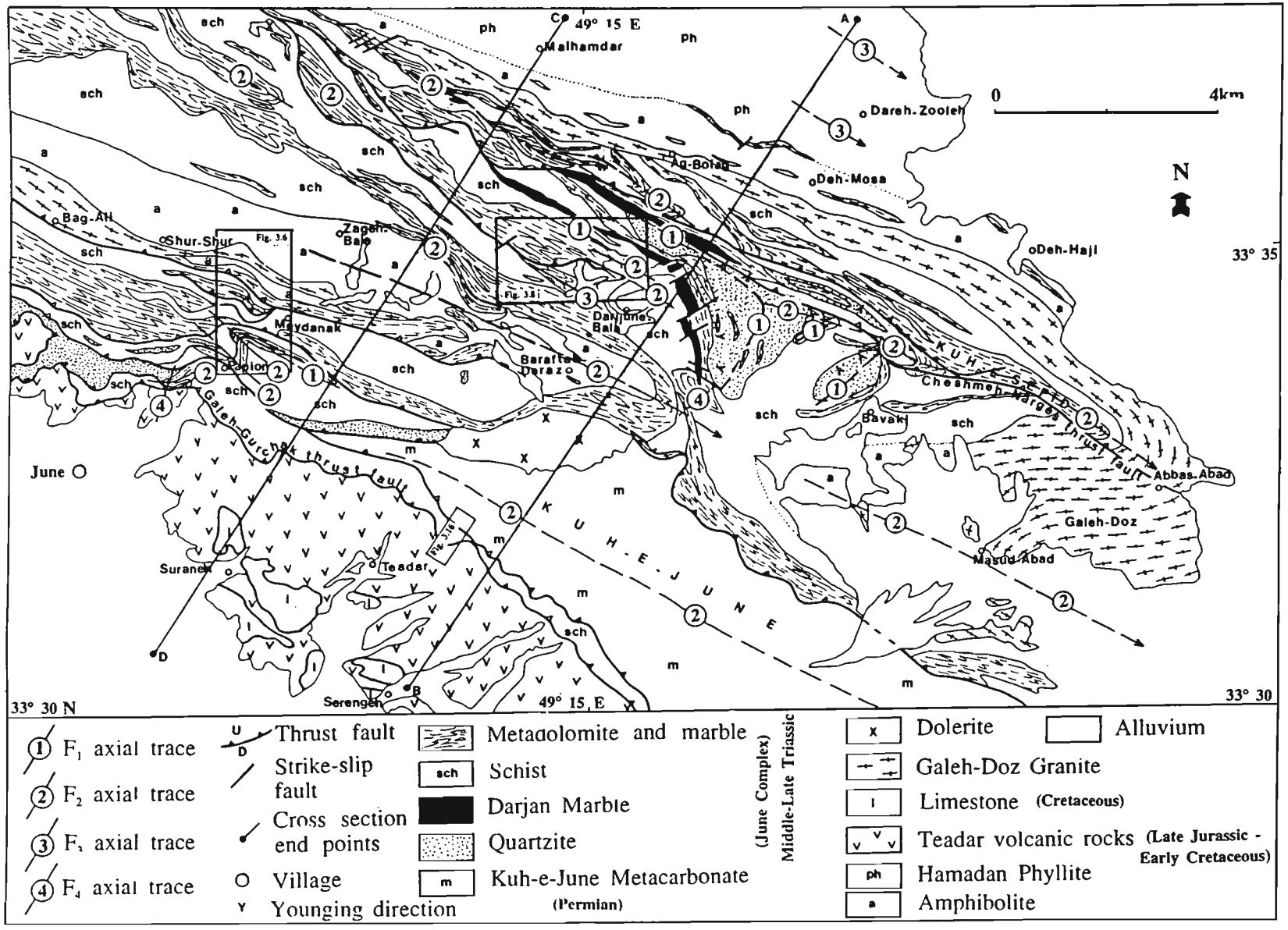

Figure 3.5 Major structures and units in the June area (for detail see the main map).

See next page for cross section AB and CD (note that horizontal scale = vertical scale).

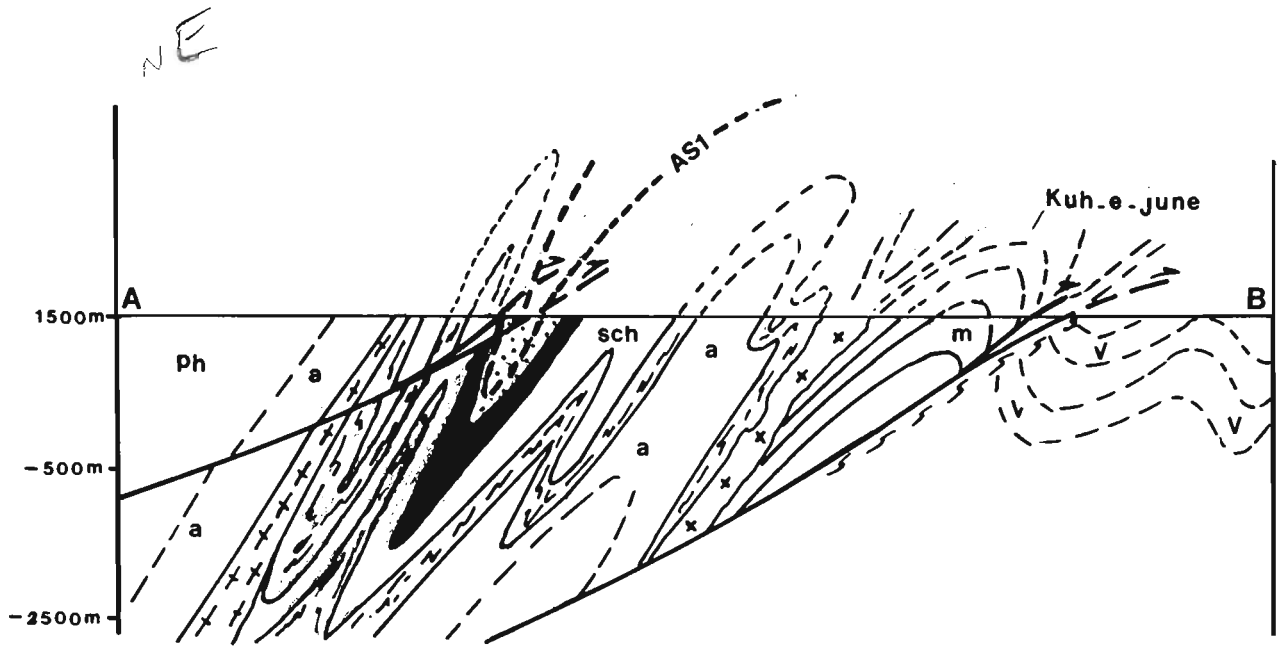
NE
SW
AS1
Kuh-e-june
A
B
1500m
-500m
-2500m
Ph
a
sch
a
m
V
V
V
a
a

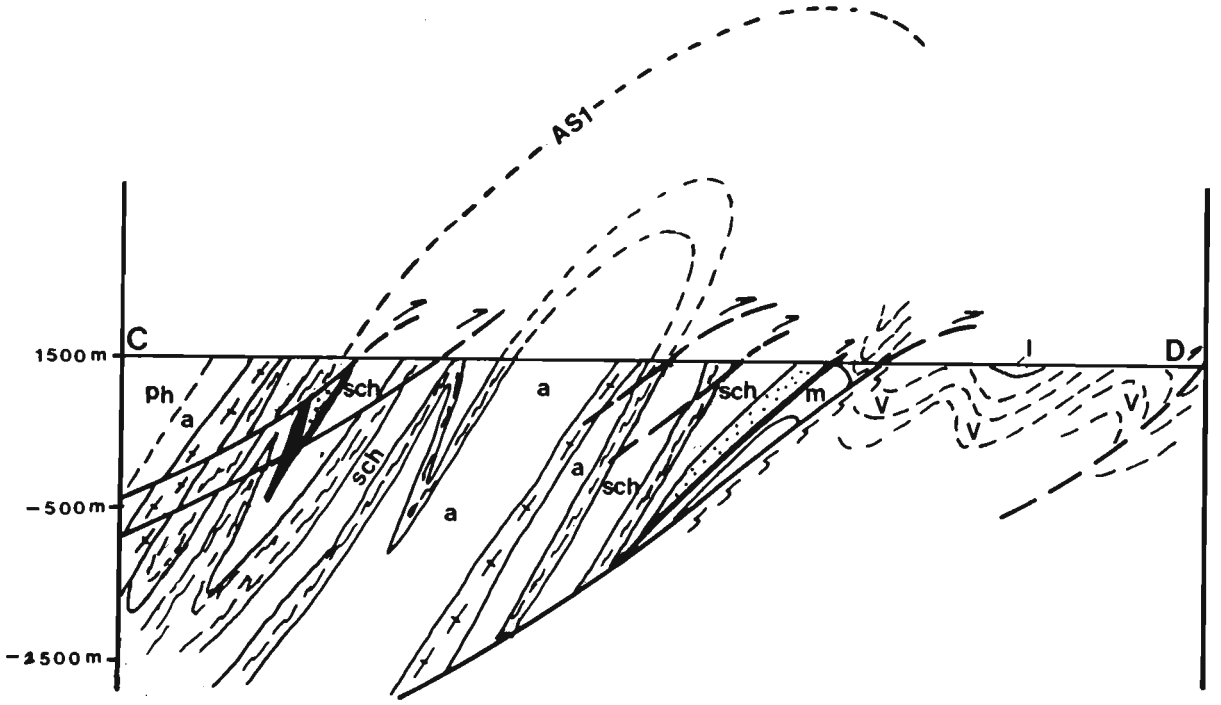
AS1
C
D
1500m
-500m
-2500m
Ph
a
sch
sch
a
a
sch
sch
m
V
V
V
a
a

Figure 3.6 Structure map of the Papion-Meydanak district.

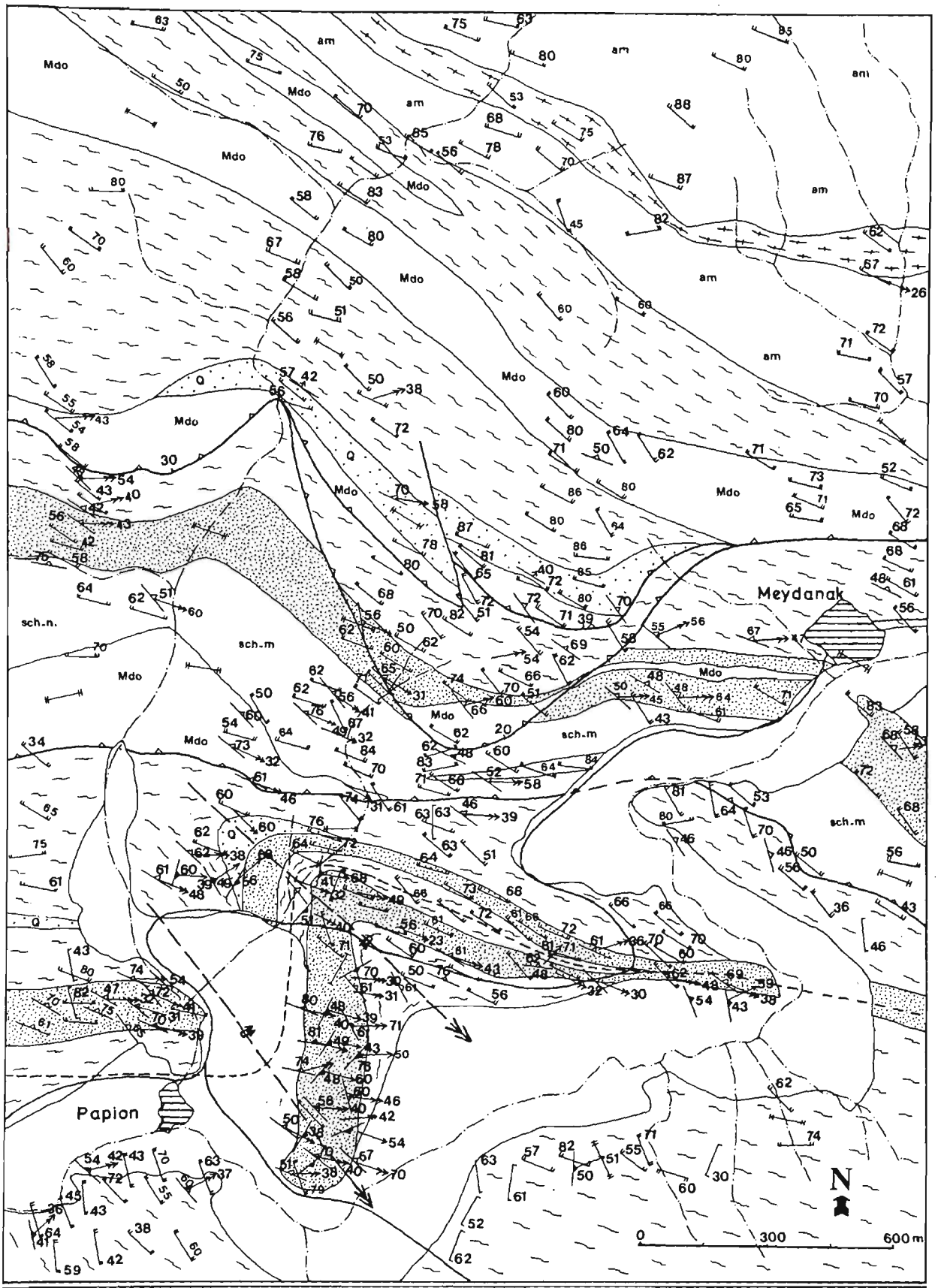
Mdo
am
sch.n.
sch.m
Q
Meydanak
Papion
N
0
300
600 m
Schist
Marble
Metadolomite
Quartzite
Alluvium
Gneiss
Amphibolite
Schist and marble
F2 overturned antiform
F2 overturned synform
F1 axial trace
Strike-slip fault
Thrust fault
Geological contact
Village
Creek
Road
AS1
AS2
S1
S2
F1
F2
F3

Figure 3.7

(a) Schematic block diagram showing the Papion F_1 fold refolded by F_2.

(b) The isoclinal Papion F_1 fold is folded by S-type F_2 folds (same scale as for (a)). Outcrop trace of folds from 1:20 000 scale air photo and location of S-, Z- and M-type mesoscopic F_2 in the macroscopic S-type folds. The index shows plunge direction cross-section of the folds.

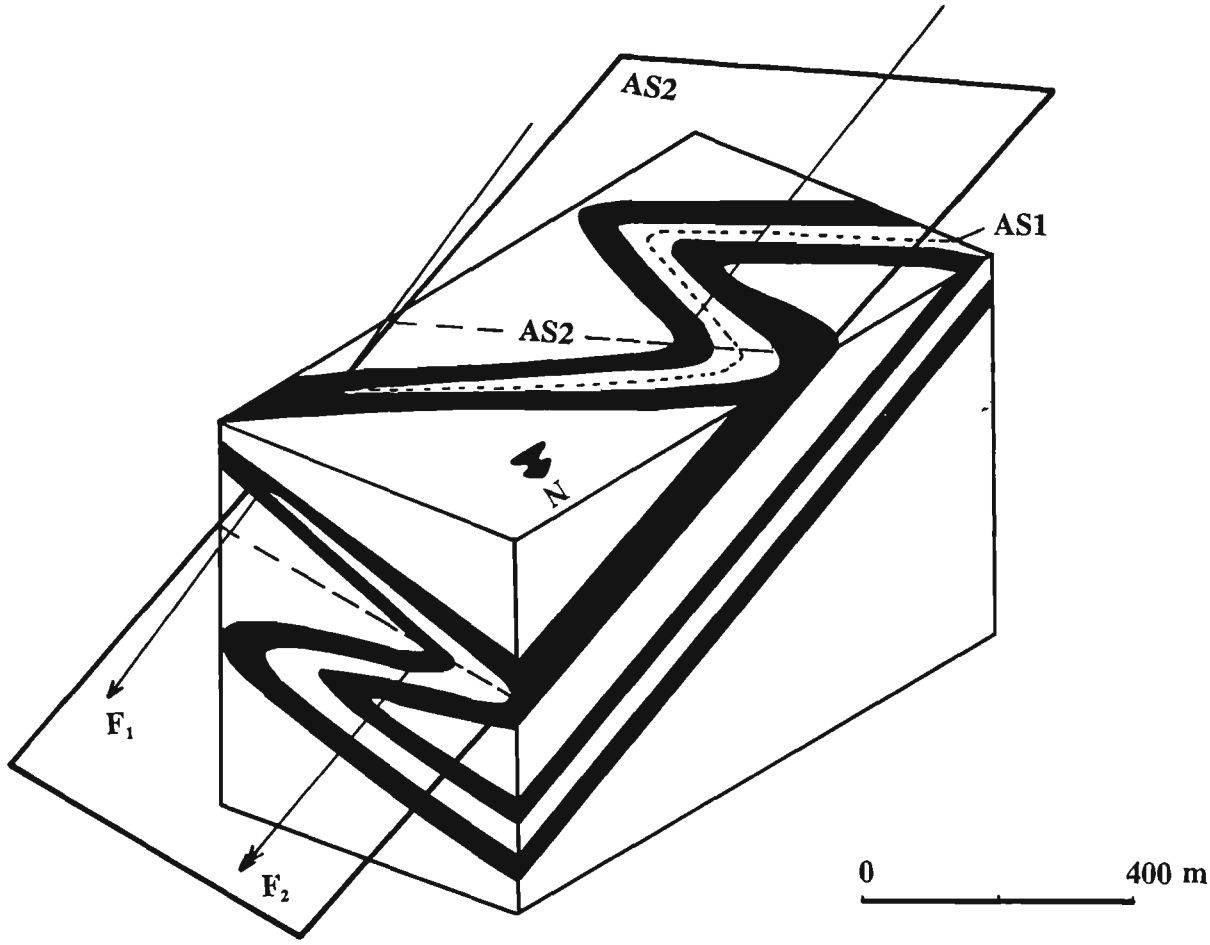

a

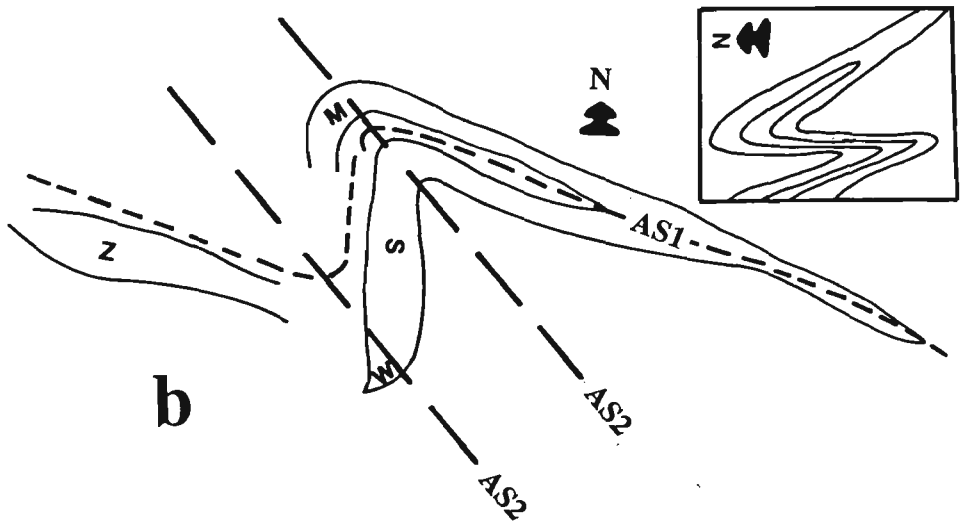

b

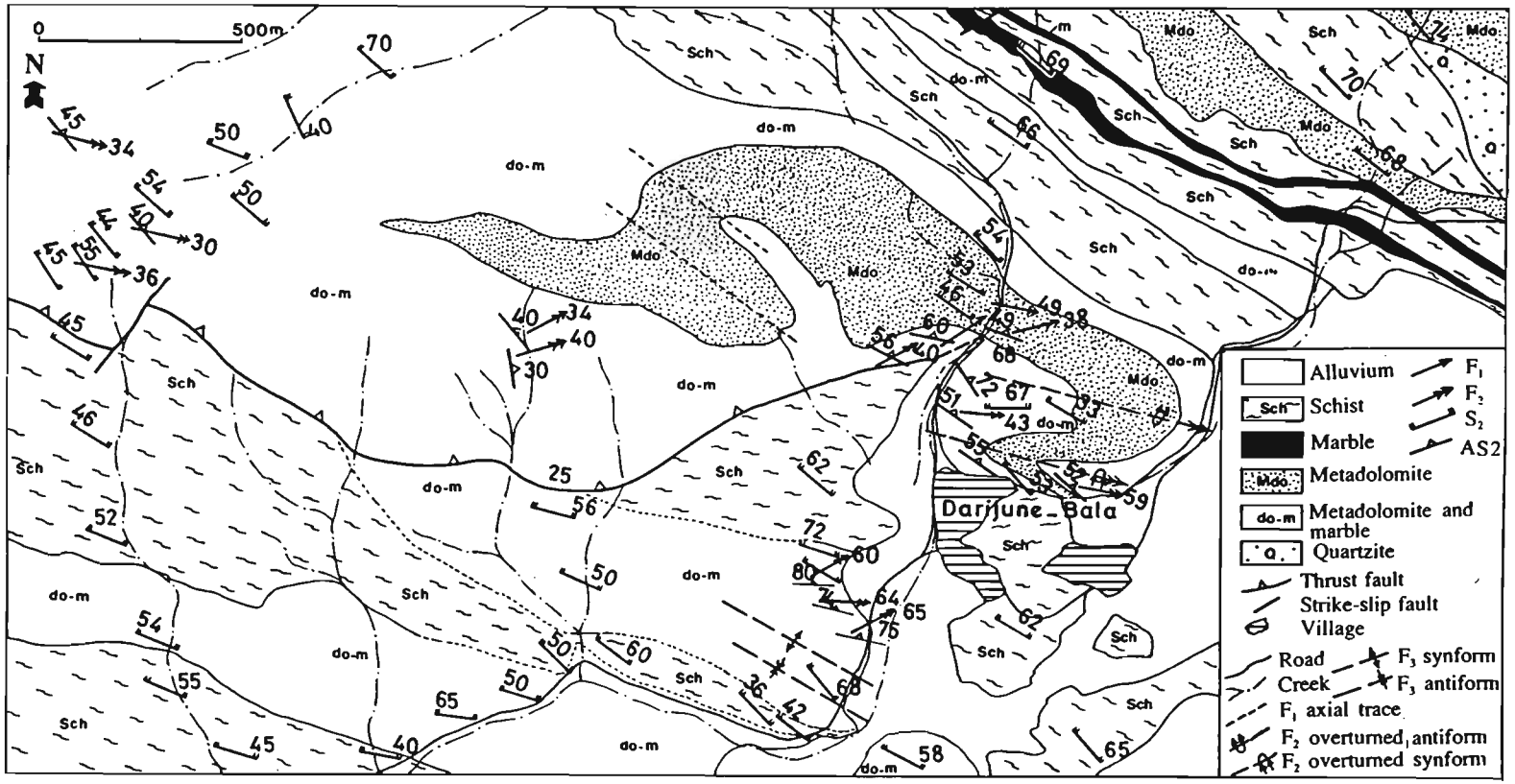

Figure 3.8 Structure map of the Darijune-Bala district.

Figure 3.9

(a) Tight F_2 in schist. 30 m west of Deh-Mosa talc mine. Hammer is 32 cm in length.

(b) Tight cylindrical F_2 in quartzite. Lower unit of the June Complex, 3 km west of Bavaki. Hammer is 32 cm in length.

(c) Intrafolial fold. Middle unit of the June Complex, 2 km west-southwest of Papion. Pen is 14 cm in length.

(d, e) Isoclinal F_2 folds in marble. 1 km east-northeast of Papion. Scales: coin is 16 mm across and lens cap is 5.5 cm across.

(f) Tight angular F_2 in schist and calcschist. The face of the outcrop is perpendicular to the hinge line. 500 m west of Papion. Lens cap is 5.5 cm across.

(g) Well developed F_2 in thin-layered marble (dark upper half) and slightly folded thick-layered metadolomite (light lower half). 1.5 km southwest of Papion. Hammer is 32 cm in length.

(h) Metadolomite with chert bands. Chert bands are strongly folded in a manner that they form very thin layers in limbs and thicker pods in hinges. 500 m southwest of Meydanak. Hammer is 32 cm in length.

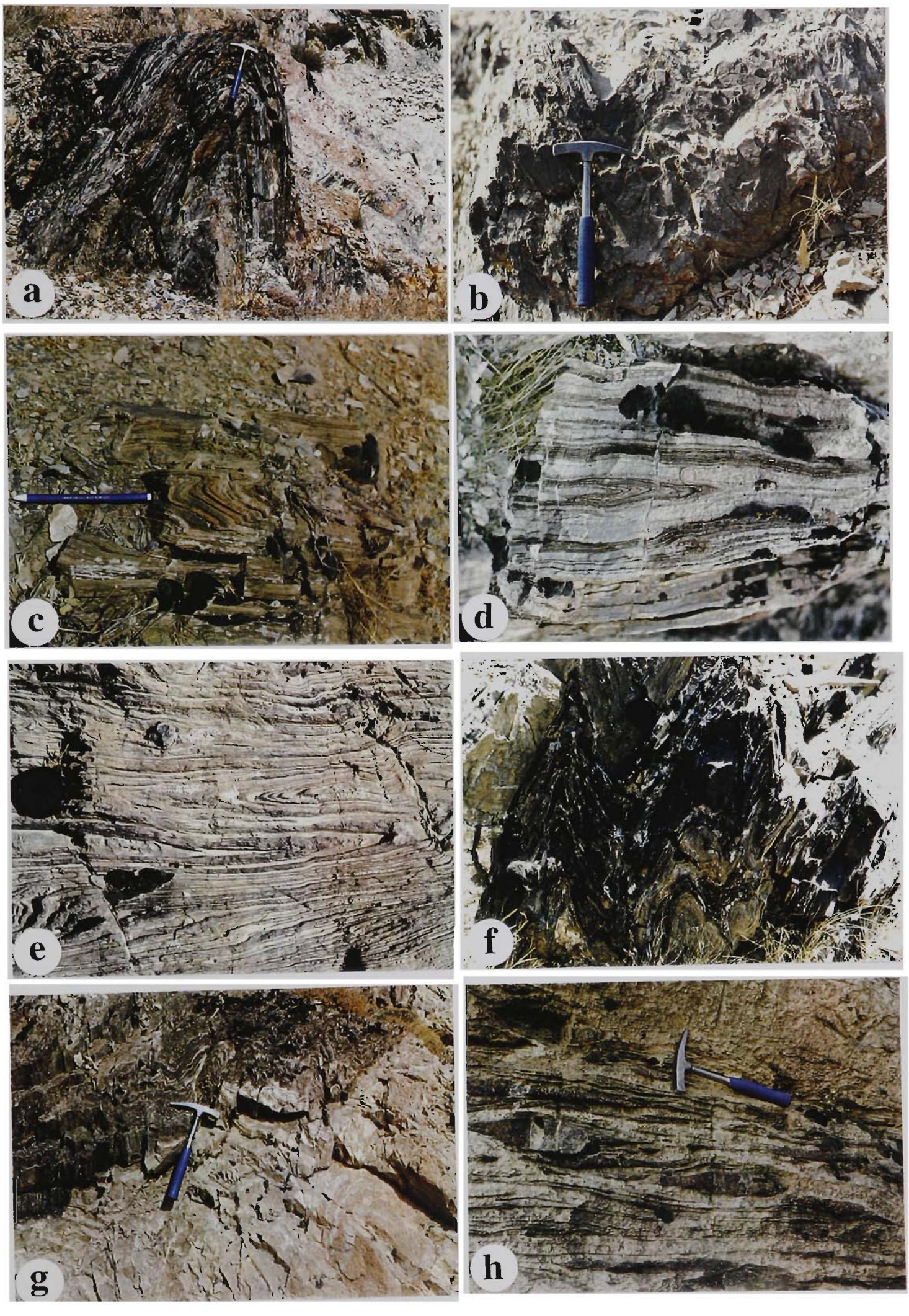
a
b
c
d
e
f
g
h

Figure 3.10

Lower-hemisphere equal-area stereographic projections of D_2 structural data measured in the study area.

(a) F_2 is contoured at 1, 2, 4, 6 and 8% per 1% area. The mean orientation is 62°/67°.

(b) L_2^1 Intersection lineation (S_2 - S_1) in Papion parasitic folds. The mean orientation is 47°/95°.

(c) AS2 and S_2 are contoured at 1, 2, 4, 6, 8 and 10% per 1% area. The mean orientation is 64°/034°.

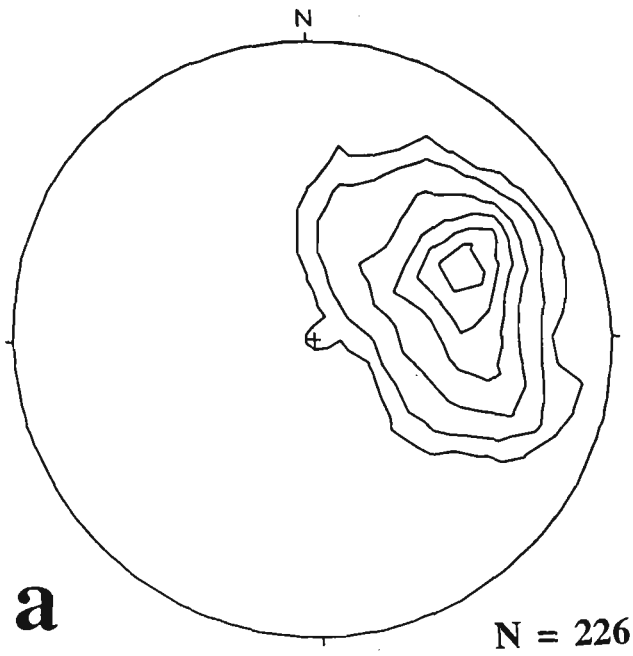

a

N = 226

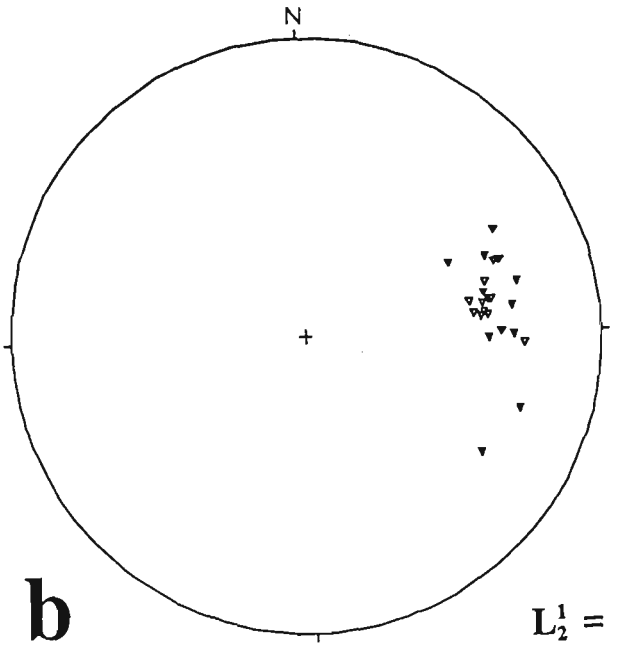

b

L_2^1 = 24

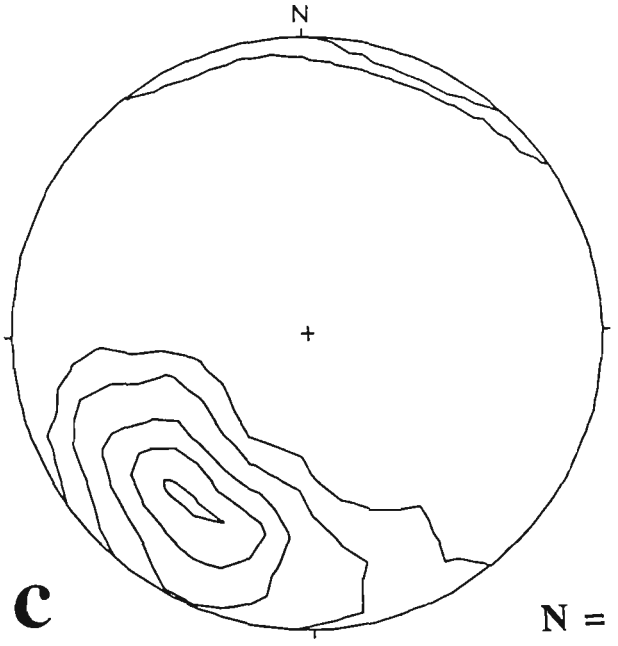

c

N = 994

Figure 3.11 Complex F_2 structures (see text). 700 m west of Meydanak. Lens cap is 5.5 cm in diameter.


AS2
AS2
AS2
AS2

Figure 3.12

(a) Tight F_2 in quartzite. Axial plane foliation dips moderately towards the north. Intersection lineation of S_0 and S_2 is evident on the hinge surface. Hammer is 32 cm in length.

(b) Well developed S_2 cuts lithological layering in the hinge area of the mesoscopic F_2.

(c) Intersection lineation of S_1 and S_2, plunging 35° to the east parallel to pen (Figure 3.10c). 300 m north of Papion. Pen is 13 cm in length.

(d) S_1 subparallel to S_0 and cut by S_2. Note the intersection lineation on the lower surfaces of the layers. Quartzite of the lower unit of the June Complex. 2 km west-southwest of Papion. Hammer is 32 cm in length.

a
b
c
d

Figure 3.13

(a) Isoclinal F_2 fold. Pinch-and-swell structure occurs in competent metadolomite and incompetent marble. 1 km west of Darijune-Bala. Lens cap is 5.5 cm in diameter.

(b) Pinch-and-swell structure in marble and amphibolite. Competent amphibolite is boudinaged along the S_2 foliation and marble has flowed into the neck. 100 m north of Masud-Abad. Pen is 14 cm in length.

(c) Pinch-and-swell structures in the Galah-Doz pluton. The pervasive foliation in schist and mylonitic granite is S_2. Mylonitic granite has intruded into schist and has been extended along L_m. 500 m northeast of Masud-Abad. Hammer is 32 cm in length.

(d) Pinch-and-swell structures in metadolomite (white layer). Marble has flowed into the neck. This structure is sub-parallel to S_2. 500 m southwest of Meydanak. Hammer is 32 cm in length.

a
b
c
d

Figure 3.14

(a) Folded boudins in thin metasandstone layer. 1500 west northwest of Darijune-Bala. Middle unit of the June Complex. Hammer is 32 cm in length.

(b) Folded pinch-and-swell structure. Metasandstone layer is folded along the pinches. Swells are either folded (hinge zone of right-hand fold) or bended (left limb of the left-hand fold). All swells are rotated sub-parallel to S_2. 200 m northwest of Darijune-Bala. Coin is 3 cm in diameter.

(c) Deformed pinch-and-swell structures. The swells are separated from pinches. The swells are in an imbricate or en echelon arrangement. 200 m northwest of Darijune-Bala. Lens cap is 5.5 cm in diameter.

(d) Folded boudins and pinch-and-swell structures in competent metasandstone layer. The folded layer is thrust over the adjacent boudin. Strong foliation is S_2, dipping steeply to the north-northeast. 1500 m west- northwest of Darijune-Bala. Lens cap is 5.5 cm in diameter.

a
b
c
d

Figure 3.15

(a) Type 3 interference patterns produced by coaxial superimposition of F_2 on F_1. 200 m east of Papion, coin is 16 mm in diameter.

(b) Schematic block diagram presents the general orientation of the F_1 and F_2.


a

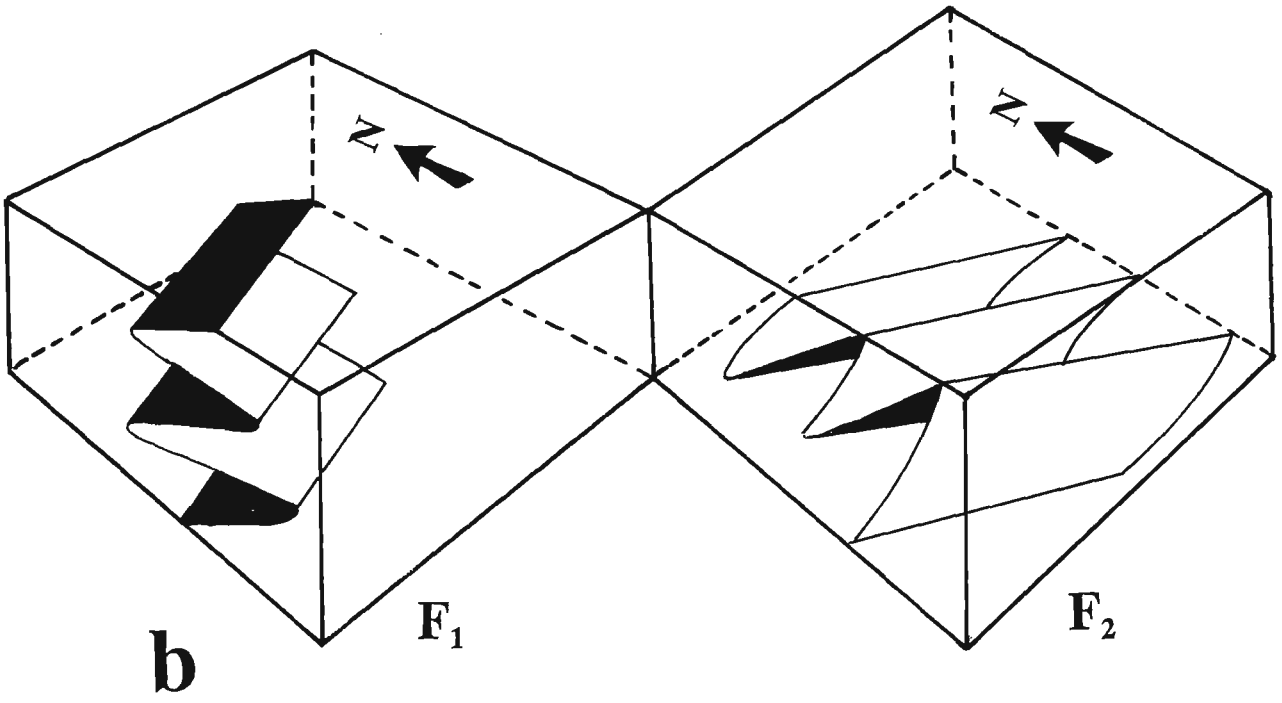
N
N
F1
F2
b

Figure 3.16 The parallel Galeh-Gurchak thrust faults. 2 km northeast of Teadar. Photo is 800 m across. See Figure 3.5 for location.

Figure 3.17

(a) Fault plane of the Galeh-Gurchak thrust fault exposed 1 km to the northeast of Teadar. It dips 30° to the northeast. Hammer is 32 cm in length. Inset shows an equal-area stereographic projection of striations on the Galah-Gurchak thrust fault. They are plunging at 33°/024°.

(b) Shear zone of the Galeh-Gurchak thrust fault. S- and C-planes are developed indicating a right-over-left sense of displacement (northeast over southwest). Lens cap is 5.5 cm across.

(c) Cheshmeh-Narges thrust fault on the southwestern limb of the Kuh-e-Sefid antiform. View is towards the east. Hammer is 32 cm in length. Inset shows an equal-area stereographic projection of striations on the Cheshmeh-Narges thrust fault. They are plunging at 53°/027°.

(d) Cheshmeh-Narges thrust fault. 5 km northwest of Darijune-Bala, looking west. Fault length on photo is 1 km.

a
b
c
d
S
C
N
N

Figure 3.18 Schematic block diagram presenting the orientation and displacement along the Cheshmeh-Narges thrust fault. The inset shows the amount of dextral strike separation.

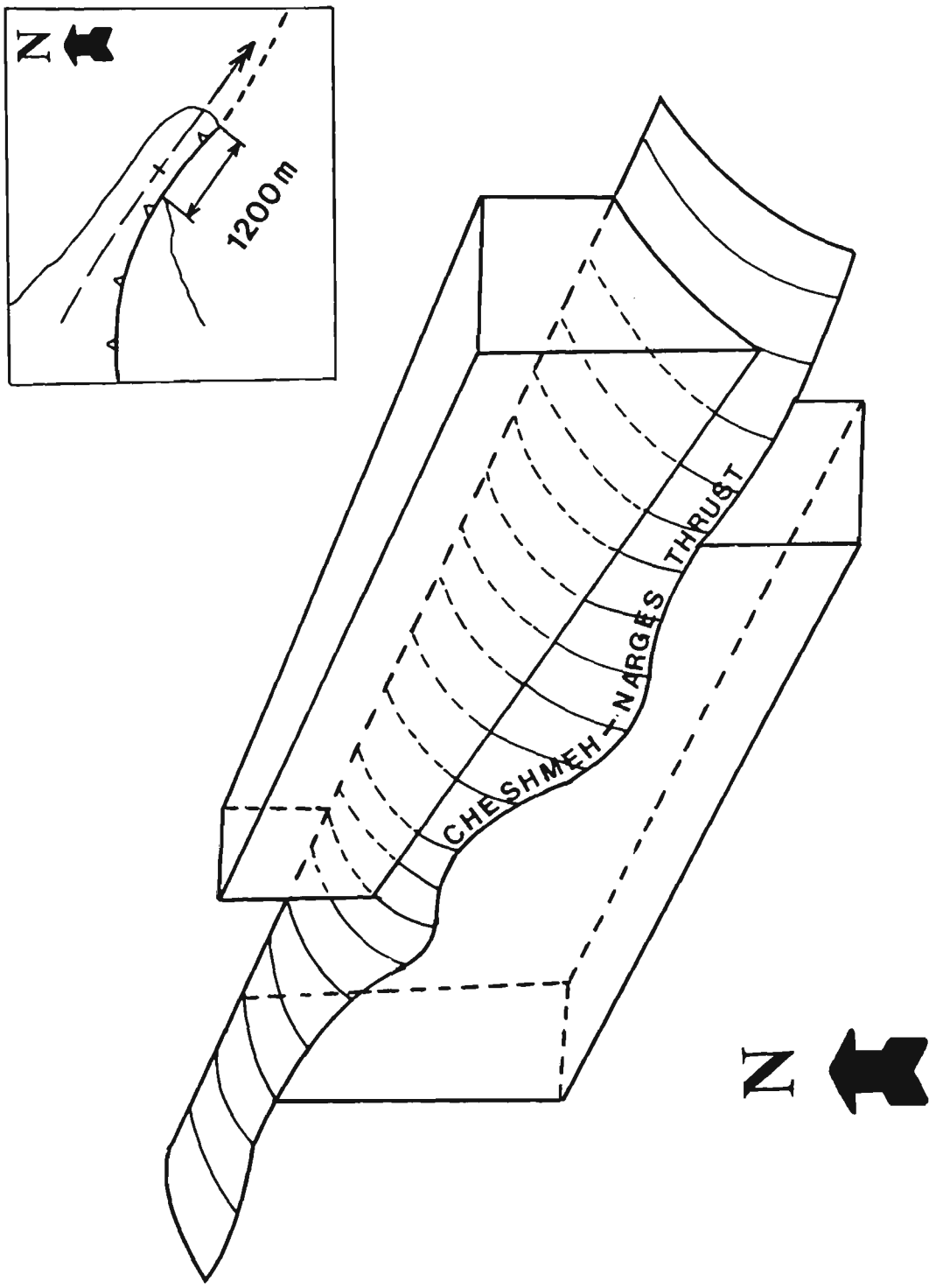
N
1200m
CHESHMEH-NARGES THRUST
N

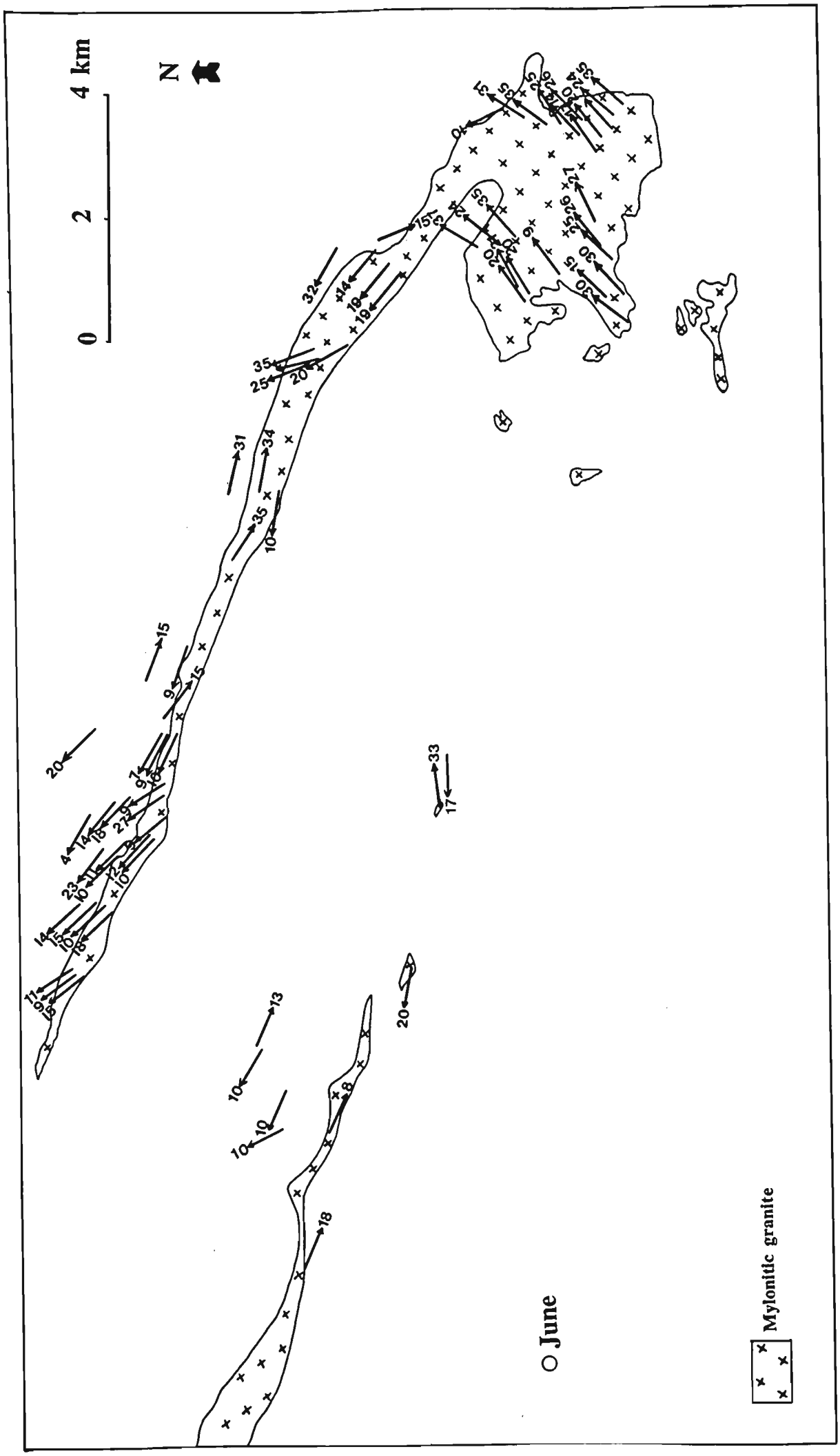

Figure 3.19 Orientation of the stretching lineation (L_m) in mylonitic granite of the June area.

Figure 3.20

(a) Foliation in mylonitic granite developed close to the wall rocks. This foliation is tightly folded with an axial plane parallel to the strongly developed S_2 existing throughout the mylonitic granite. 100 m north of Masud-Abad. Lens cap is 5.5 cm in diameter.

(b) Lower-hemisphere equal-area stereographic projection of mylonitic S_2 in the west-northwestern extension of the Galeh-Doz pluton. Average S_2 shown by great circle is 67°/050°.

(c) L tectonite. Mylonitic granite of the Galeh-Doz pluton. 1 km east of Masud-Abad. Pen is 14 cm in length.

(d) Three dimensional view of the ultramylonite close to the wall rock (Masud-Abad). The right-hand, front, vertical plane is perpendicular to S_2 and contains the subhorizontal stretching lineation. Sample number 171.

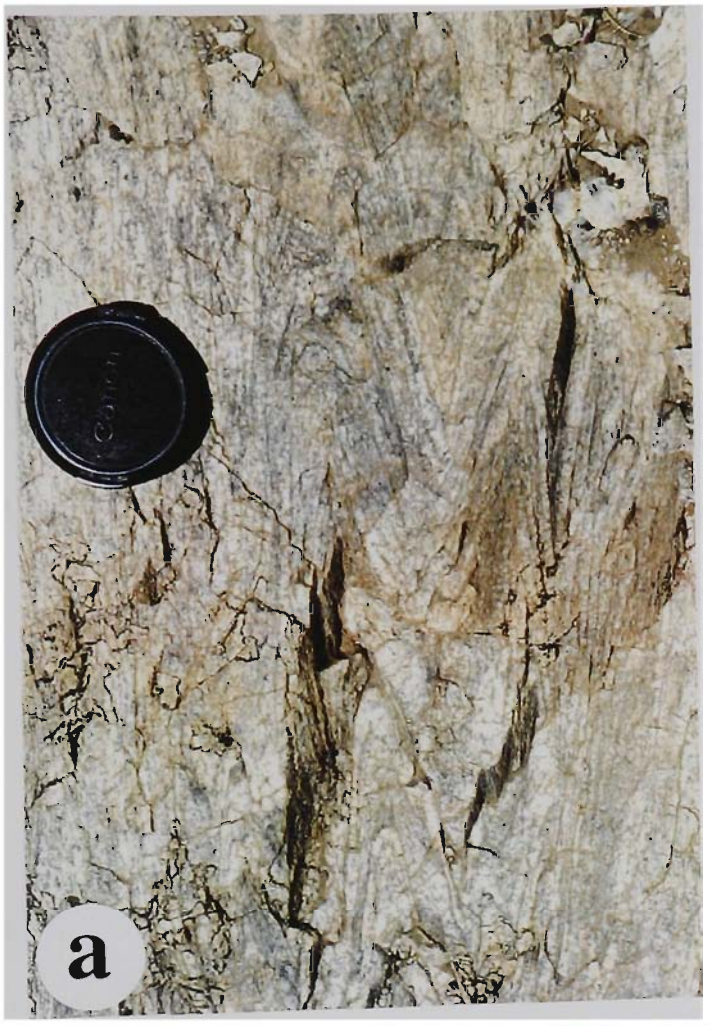

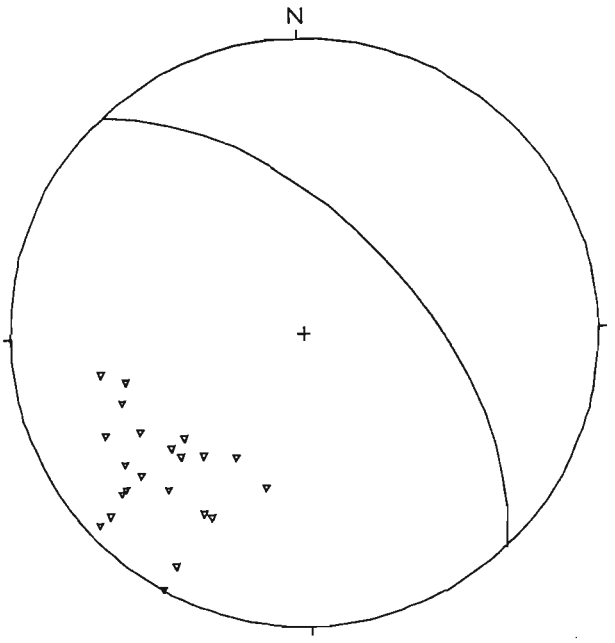

S_2 = 21

b

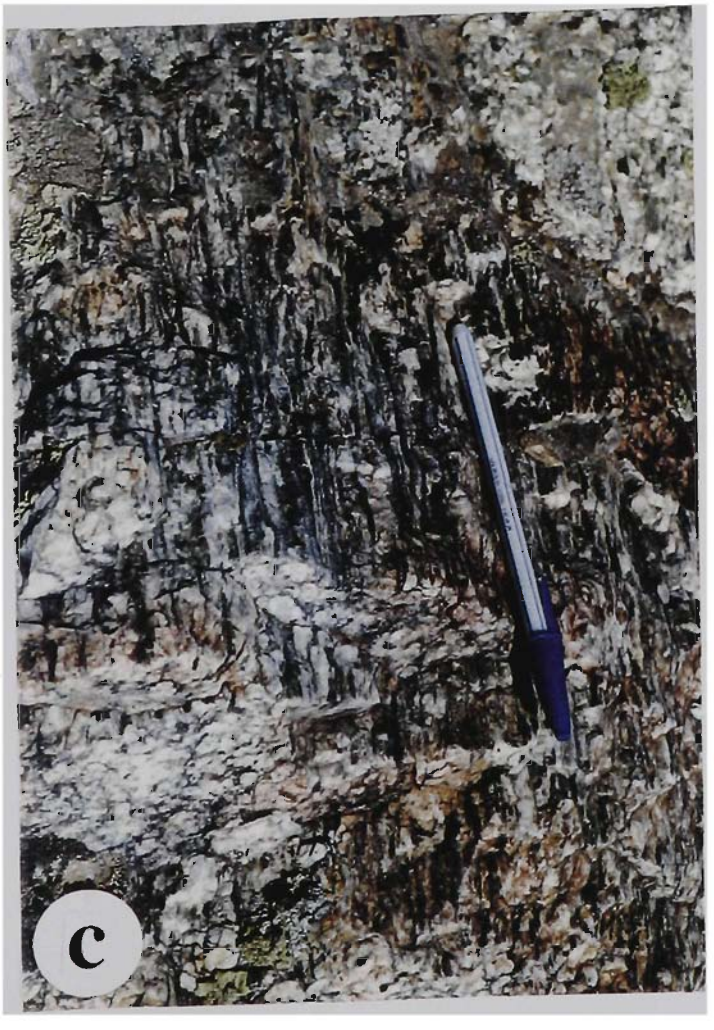

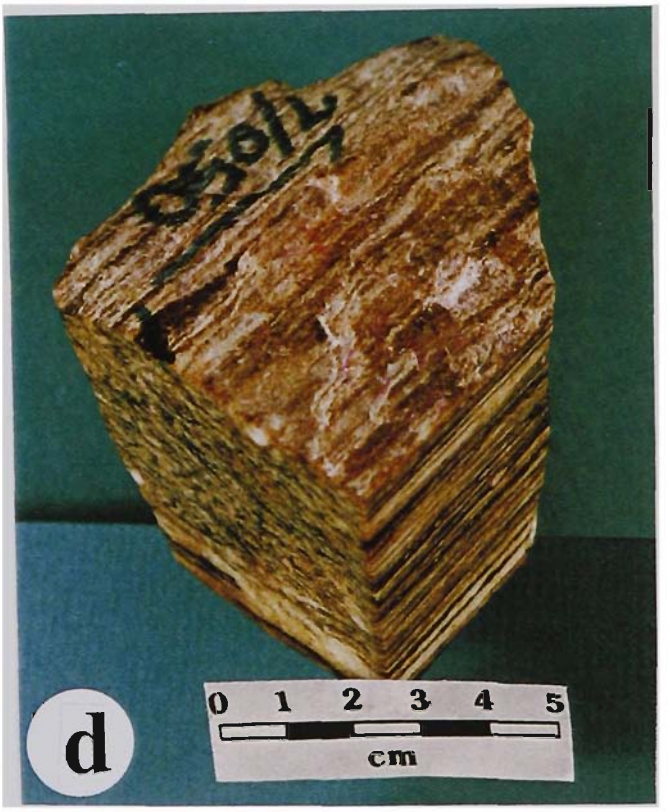

Figure 3.21 Equal-area stereographic projections of:

(a) stretching lineation (L_m) measured in mylonitic granite (Galeh-Doz pluton) and the mean orientation is 17°/052.

(b) stretching lineation measured in mylonitic granite (west-northwest extension of the Galeh-Doz pluton) and the mean orientation is 15°/323°.

(c) stretching lineation measured in all mylonitic rocks of the study area.

(d) stretching lineation measured in amphibolite mylonite.

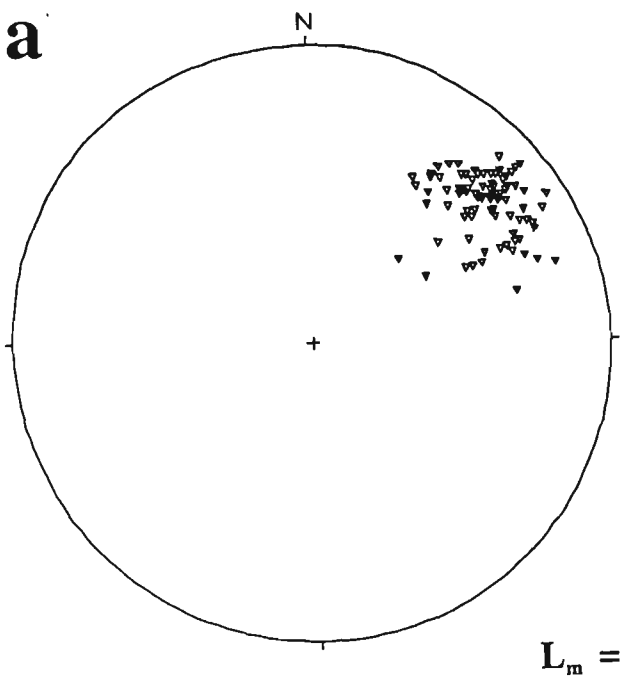

$L_m = 105$

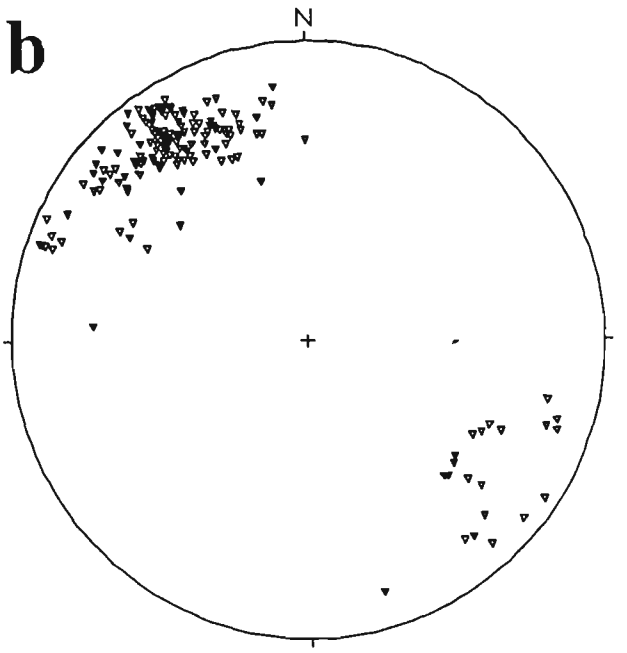

$L_m = 169$

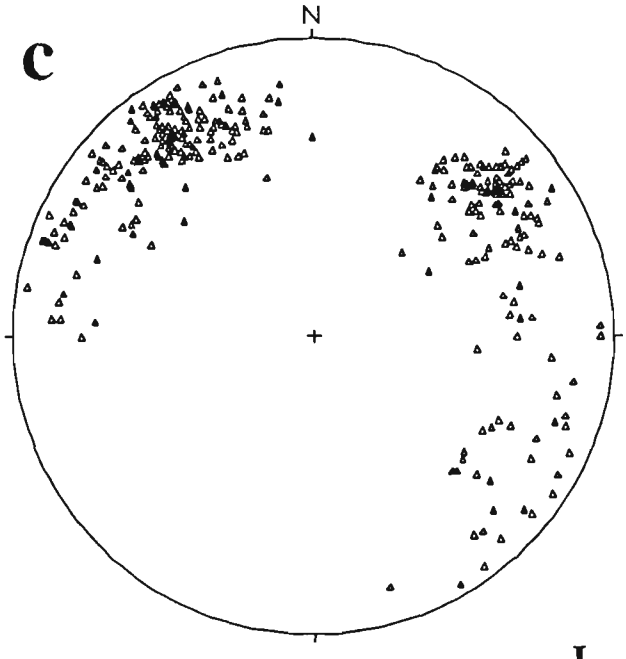

$L_m = 310$

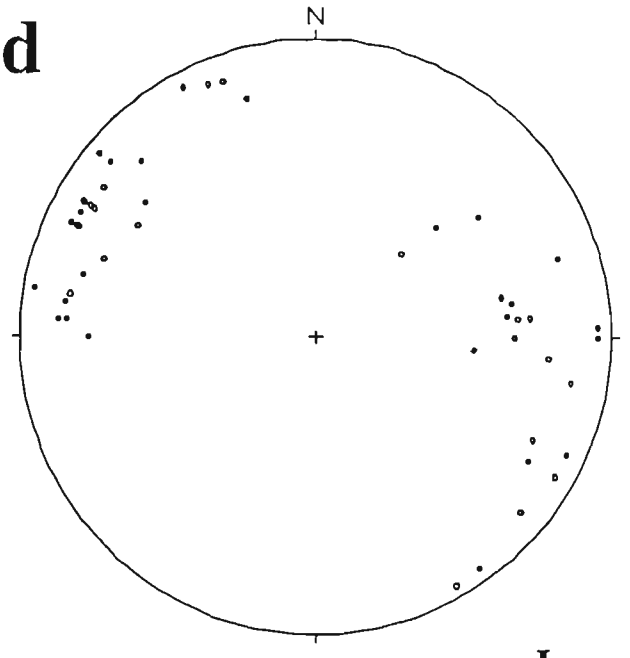

$L_m = 50$

Figure 3.22 Tourmaline rods parallel to the stretching lineation in the west-northwestern extension of the Galeh-Doz pluton, 1500 m south of Malhamdar.

(a) A single rod. Note the segregation of tourmaline minerals in the central part of the circular crosscut. Pen is 12 cm in length.

(b) Distribution of rods in the mylonitic granite. Pen is 12 cm in length.

(c) Tourmaline rods in mylonitic granite. Pen is 12 cm in length.

(d) An isolated tourmaline rod which is parallel to the stretching lineation. Tourmaline inside the rod is stretched along the stretching direction. Sample number 998.

(e) The graph shows 67 measurements of tourmaline rods in the Z and Y directions of strain ellipsoid.

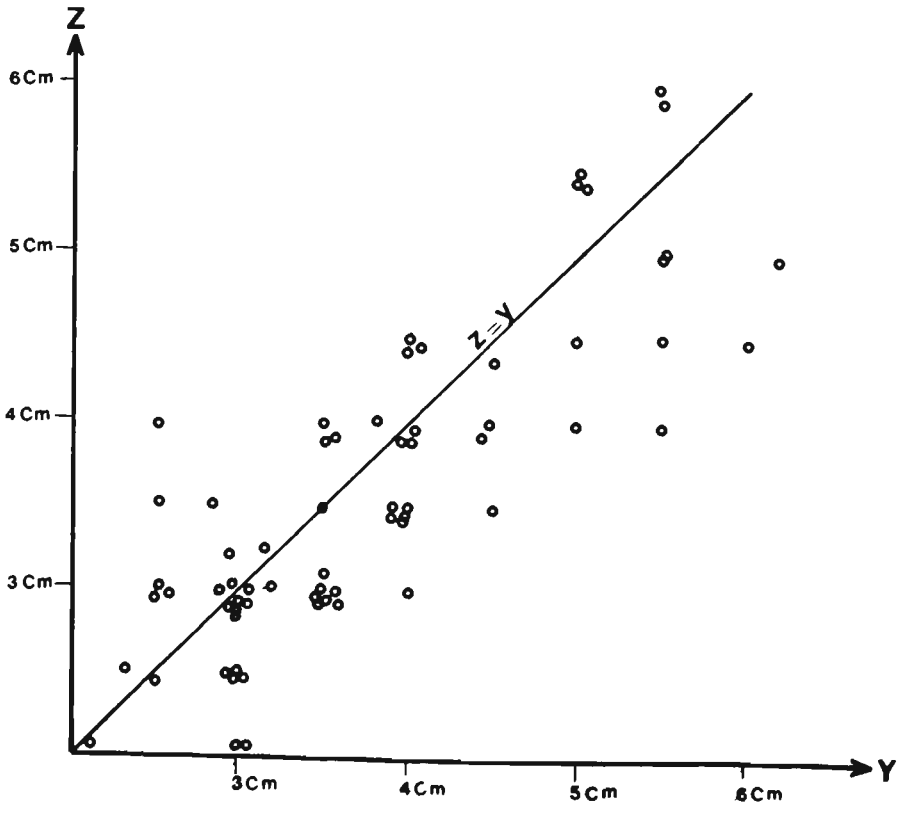


a

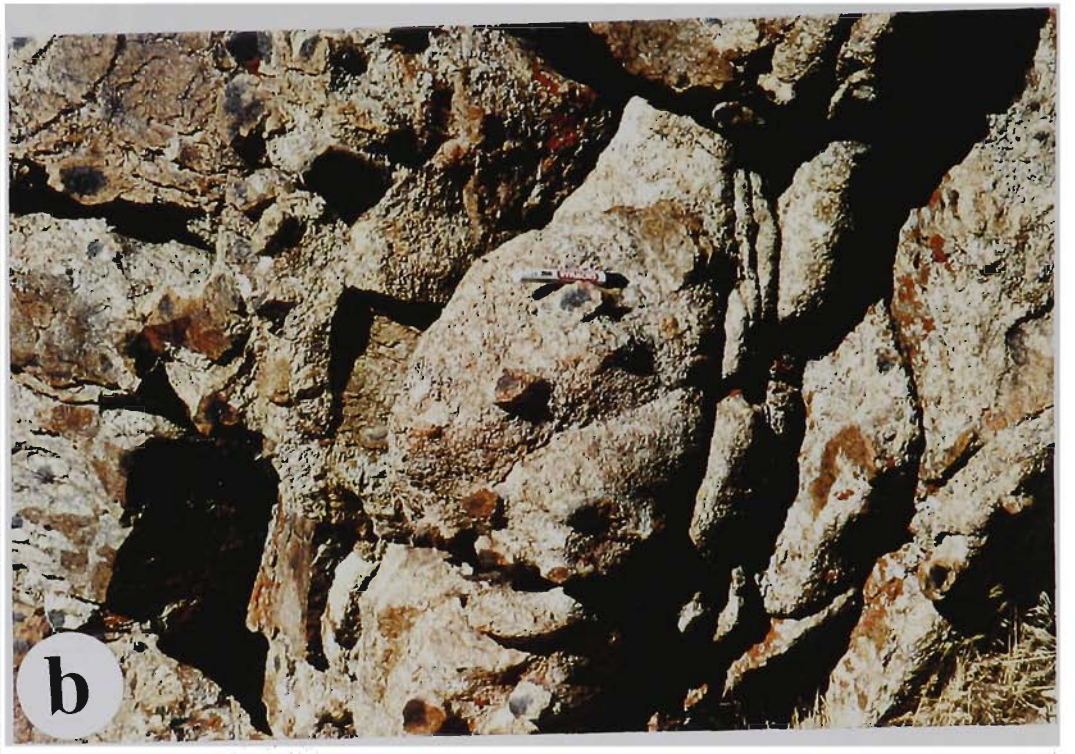
b

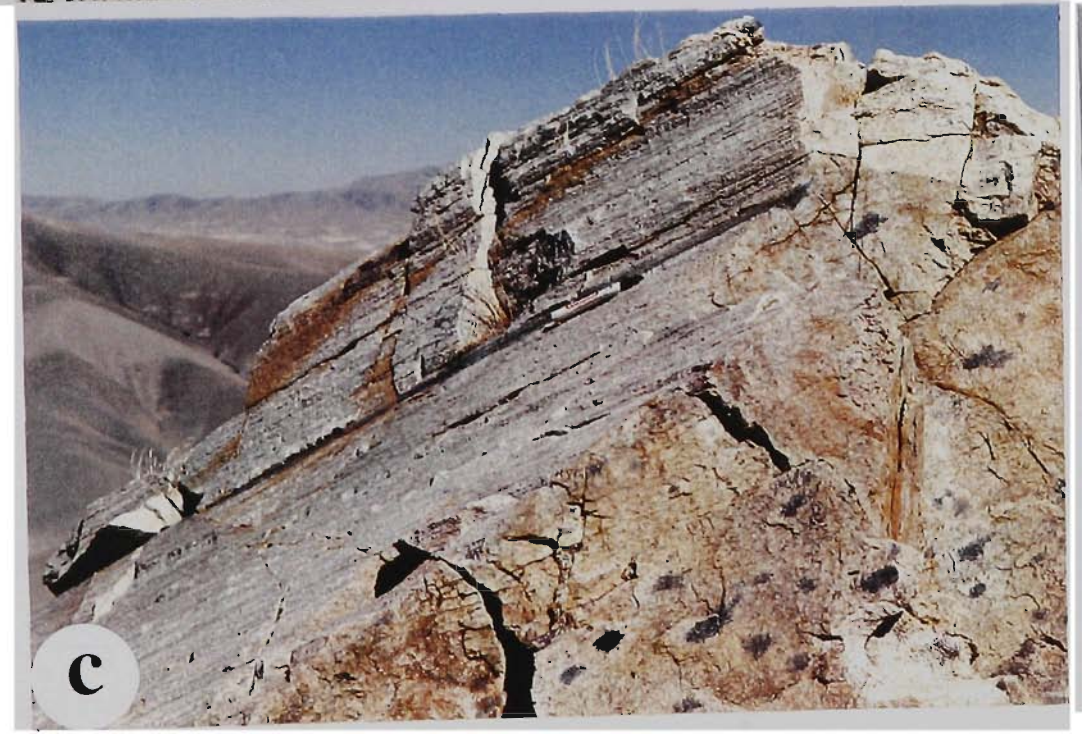
c


STAEDTLER
inch
d

Figure 3.23

(a) LS tectonite. Mylonitic granite. Segregated tourmaline minerals show ellipsoids along the foliation (right of the lens cap) on the vertical cut face that is perpendicular to both foliation and stretching lineation. Ellipsoids also occur on the horizontal cut face that is perpendicular to foliation and parallel to stretching lineation. 400 m south of Deh-Haji. Lens cap is 5.5 cm in diameter.

(b) Schematic block diagram showing stretching lineation in the mylonitic foliation (S_2) and ellipsoids of segregated tourmaline both in horizontal and vertical cut faces.

(c) Dextral shear sense is defined by σ-types feldspar porphyroclasts. The surface is cut parallel to the stretching lineation and perpendicular to the foliation. Galeh-Doz mylonitic granite. Coin is 16 mm in diameter.

(d) S- and C-planes defined by a fractured plagioclase porphyroclast. Antitaxial fibre growth indicate the extension direction along the X axis of the strain ellipsoid. This structure indicates dextral shear sense. Sample number 1052 (crossed polarised light, 1.6 mm in length and 1.1 mm in width.

a

c

d
C
S

b
S2
L2

Figure 3.24

(a) Mylonitic amphibolite. Amphibole-rich bands are interlayered with feldspar-rich bands subparallel to a mylonitic foliation. Segregation layering is parallel to the mylonitic foliation. 200 m southwest of Zageh-Bala. Pen is 14 cm in length.

(b) Pinch-and-swell structure in mylonitic amphibolite. Extension direction is parallel to S_2. Hammer is 32 cm in length.

(c) Mylonitic amphibolite in three dimensions. The top part of the specimen is parallel to the stretching lineation and perpendicular to S_2. σ-type feldspar porphyroclasts on this surface indicate a dextral sense of shear. The vertical left -side of the specimen shows the sub-horizontal stretching lineation. 1 km southwest of Zageh-Bala. Sample number 813 and it is 12 cm across.

(d) Sub-horizontal striation and groves parallel to the stretching lineation on a vertical surface in the C-plane. Mylonitic amphibolite, 2 km southwest of Zageh-Bala. Hammer is 32 cm in length.

a
b
11
c
d

Figure 3.25

Shear sense indicators. Displacement is shown at the top right corner of each photograph.

(a) Mica-fish structure developed by actinolite due to dextral shear. Sample number 472, plane polarised light. 4 mm in length and 2.5 mm in width.

(b) δ-type asymmetric porphyroclast developed by dextral shear in calcite mylonite. Sample number 32, plane polarised light. 4 mm in length and 2.5 mm in width.

(c) Well-developed mica-fish structures in epidote-amphibole schist indicating dextral shear. A σ-type asymmetric plagioclase porphyroclast is developed. Sample number 813a, crossed polarised light. 4 mm in length and 2.5 mm in width.

(d) Mica-fish in sheared amphibolite indicate dextral shear. Sample number 106, plane polarised light. 4 mm in length and 2.5 mm in width (black circles are air bubbles).

a
1T
b
1T
c
S
C
1T
d
S
C
1T

Figure 3.26 Antithetic shears. Displacement is shown at the top right corner of each photograph.

(a) Sheared greenschist. Hornblende porphyroblast broken by parallel fractures. These fractures are separated and sinistrally displaced due to dextral shear. Note that the chlorite fibres in fractures have grown subparallel to the C-plane. Sample number 472, crossed polarised light. 1.6 mm in length and 1.1 mm in width.

(b) Book-shelf displacement along a fracture in altered plagioclase due to dextral shear. The sheared rock is an epidote chlorite schist. S_2 schistosity is defined by alignment of epidote and chlorite and has wrapped around the plagioclase porphyroclast. Note the σ-type porphyroclast with stair-stepped structures and chlorite fibres in fracture and tails of the plagioclase porphyroclast. Sample number 813, crossed polarised light. 1.6 mm in length and 1.1 mm in width.

(c) Ultramylonite. Groundmass is highly recrystallised and consists of quartz and feldspar. The plagioclase porphyroclast is broken into several pieces and fractures are filled by the recrystallised grains. Sinistral displacement along the fractures is produced due to dextral shear. Coarser polygonal grains occur in the recrystallised tails. Sample number 352, crossed polarised light. 4 mm in length and 2.5 mm in width.

(d) Sheared amphibolite. Altered plagioclase porphyroblast is displaced along a fracture. Note the development of small epidote grains along this fracture, which is cut by the secondary parallel fractures. Sample number 422, crossed polarised light. 4 mm in length and 2.5 mm in width.

a
1T
b
1T
c
1T
d
1T

Figure 3.27 An isoclinal F_2 in interbedded marble and metabasite. The more competent layers (metabasite) are stretched sub-parallel to the S_2 in a west-northwest direction as shown by domino-style offsets (see text). Note that the fractures cut both limbs of the fold. Location is 400 m southwest of Zageh-Bala. Lens cap is 5.5 cm in diameter. The inset shows the model presented by Goldstein (1988).


11

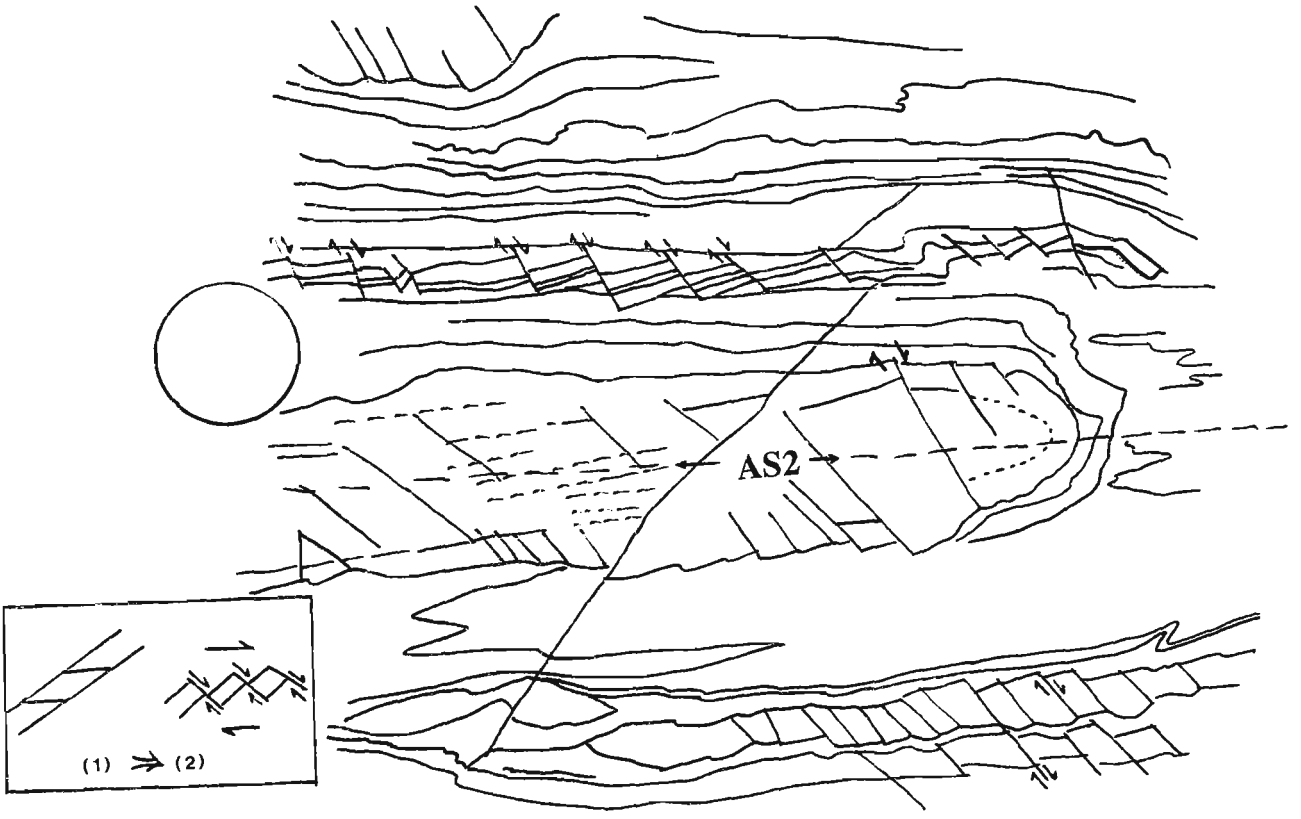
AS2
(1) ⇉ (2)

Figure 3.28

(a) Boudins in competent metadolomite parallel to S_2. Note the asymmetric boudin in the centre of the photograph and also the much smaller asymmetric boudins in thin-layered metadolomite above the lens cap which are displaced dextrally along small shear fractures. The shear fractures cut S_2, lithological layering and boudinage. 600m southeast of Shur-Shur. Lens cap is 5.5 cm in diameter.

(b) Calcite mylonite. Porphyroclasts are metadolomite fragments. 200 m southwest of Darijune-Bala. Coin is 16 mm in diameter.

a
b

Figure 3.29

(a) Close F_3 and associated S_3 (axial planar) crenulation cleavage. Hamadan Phyllite, 800 m southwest of Dareh-Zooleh. The rule is 15 cm in length.

(b) Open F_3 fold in folded S_2. The axial plane crenulation cleavage (S_3) is sub-vertical. Hamadan Phyllite, 1400 m north of Dareh-Zooleh. Hammer is 32 cm in length.

(c) Lower-hemisphere equal-area stereographic projection of F_3 folds. Triangles = AS3 (7) - great circle = average AS3 74°/030°. Crosses = F_3 (10), star = average F_3, 40°/085°.

(d) S_3 in a thin-layered marble. Middle unit of the June Complex, 1 km southwest of Papion. Hammer is 32 cm in length.

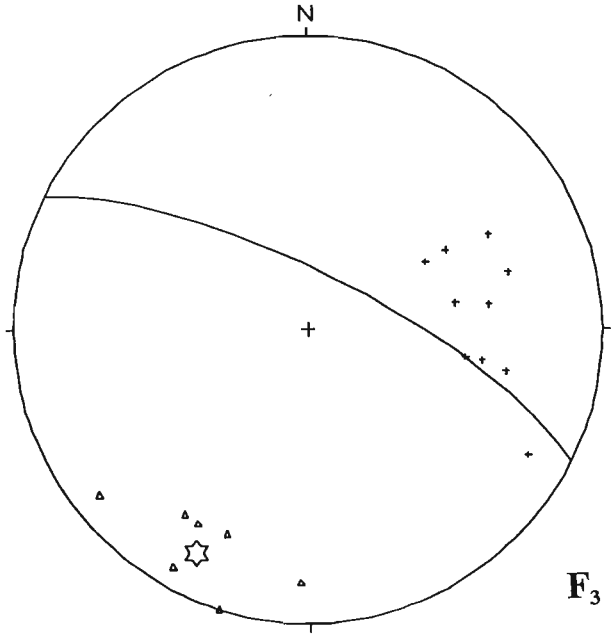

c

$F_3 = 10$

Figure 3.30

(a,b) Intersection lineation between S_1 and S_2 (sub-parallel to F_2) folded by F_3. AS3 dips steeply to the north. F_3 plunges moderately to the east (40°/085°). The trend of the intersection lineation between S_1 and S_2 is 302° and the intersection lineation between S_2 and S_3 is E-W. Coin is 16 mm in diameter.

(c) Schematic presentation of the folded lineation.

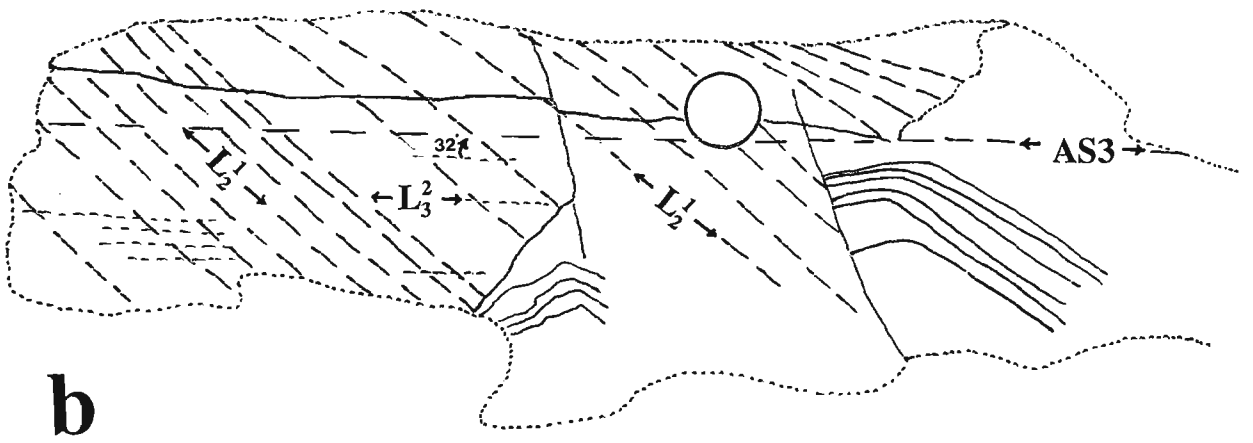

b

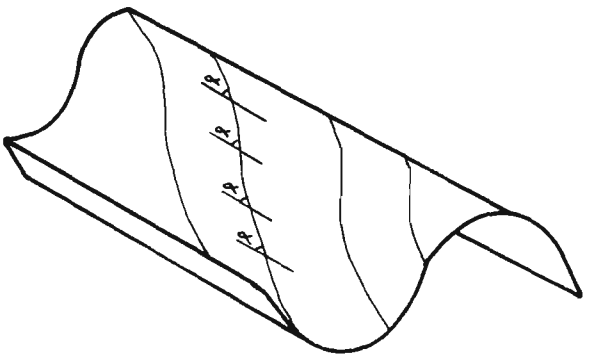

c

Figure 3.31

(a) Post-D_2 thrust faults, dipping to the northeast. Note the displaced metadolomite band along the southern thrust. 200 m west of Meydanak, looking west. Photograph is 400 m across.

(b) Minor thrust fault displacing S_2. 2 km southwest of Darijune-Bala. Hammer is 32 cm in length.

(c) Broad open upright F_4 in schist. 1 km north of Azna. Hammer is 32 cm in length.

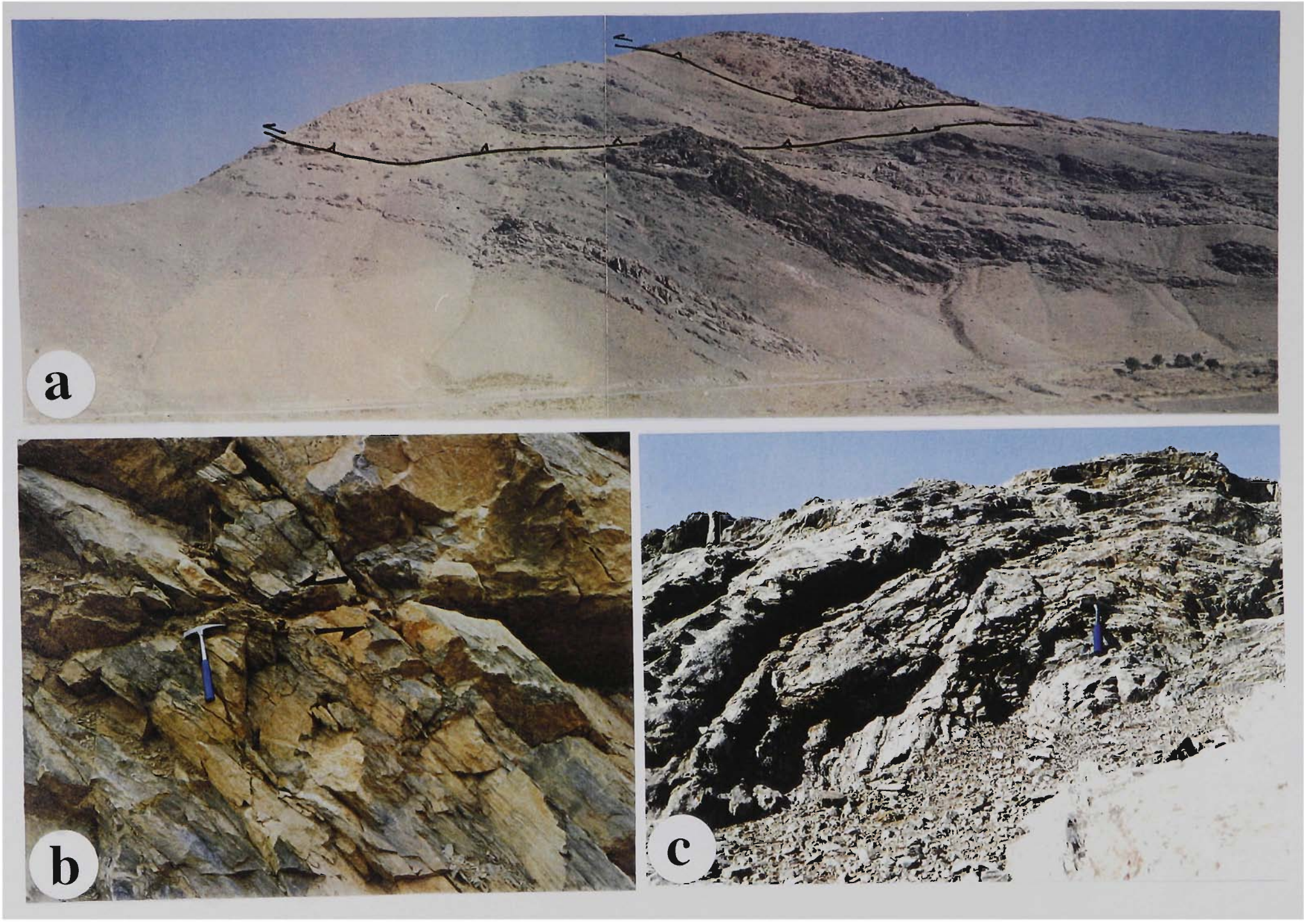
a
b
c

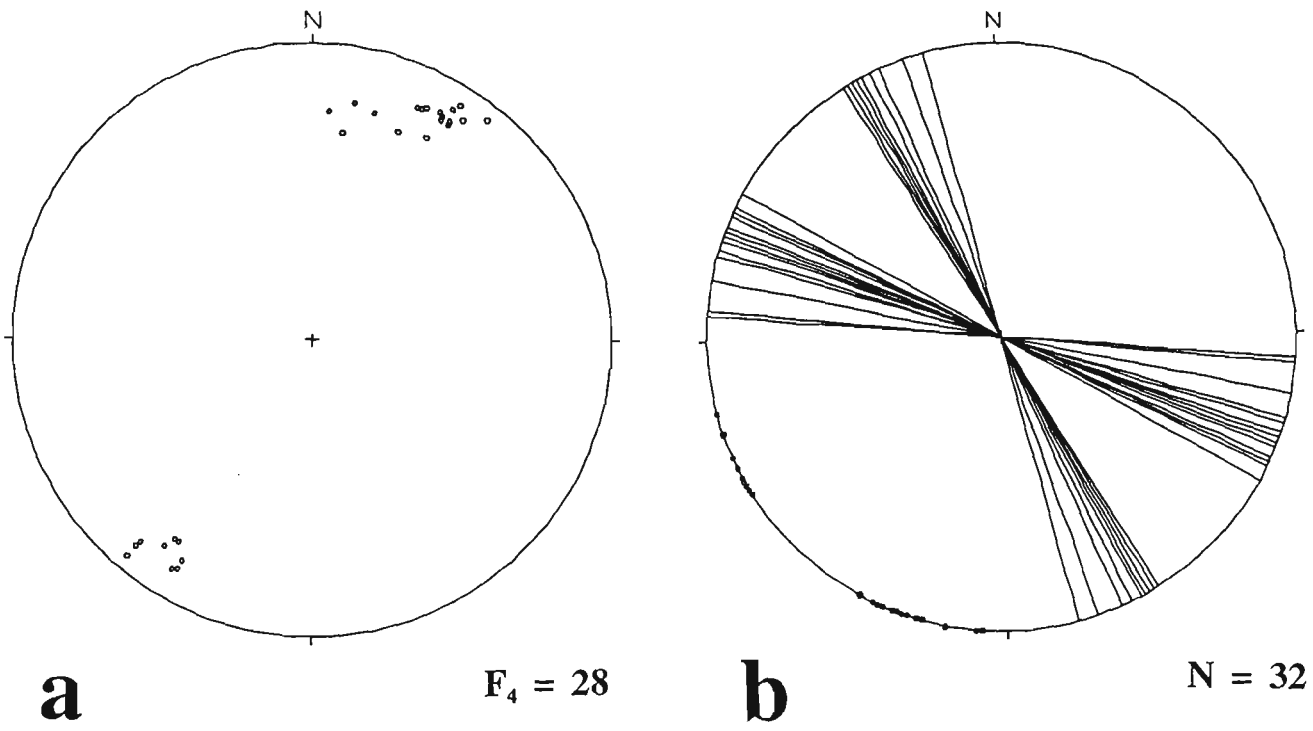

Figure 3.32

(a) Equal-area stereographic projection of F_4 axes. The mean orientation is 07°/028°.

(b) Equal-area stereographic projection of kink bands (poles, great circles) measured in the Papion area (005°-030° sinistral and 060°-076° dextral).

Figure 3.33

(a) General structure map of the June area showing two domains of deformation partitioning: (1) schist and marble rock units, and (2) mylonitic rock units.

(b) Graph showing the relationship between the angle of plate motion (α), the orientation of the instantaneous strain axes (Θ) and the percentage of deformation partitioning (after Tikoff and Teyssier 1994). For the June area $\alpha > 70°$ and $\Theta < 10°$.

(c) Model for partitioning in a pure-shear dominated zone of transpression ($\alpha > 70°$ and $\Theta < 10°$) after Tikoff and Teyssier 1994).

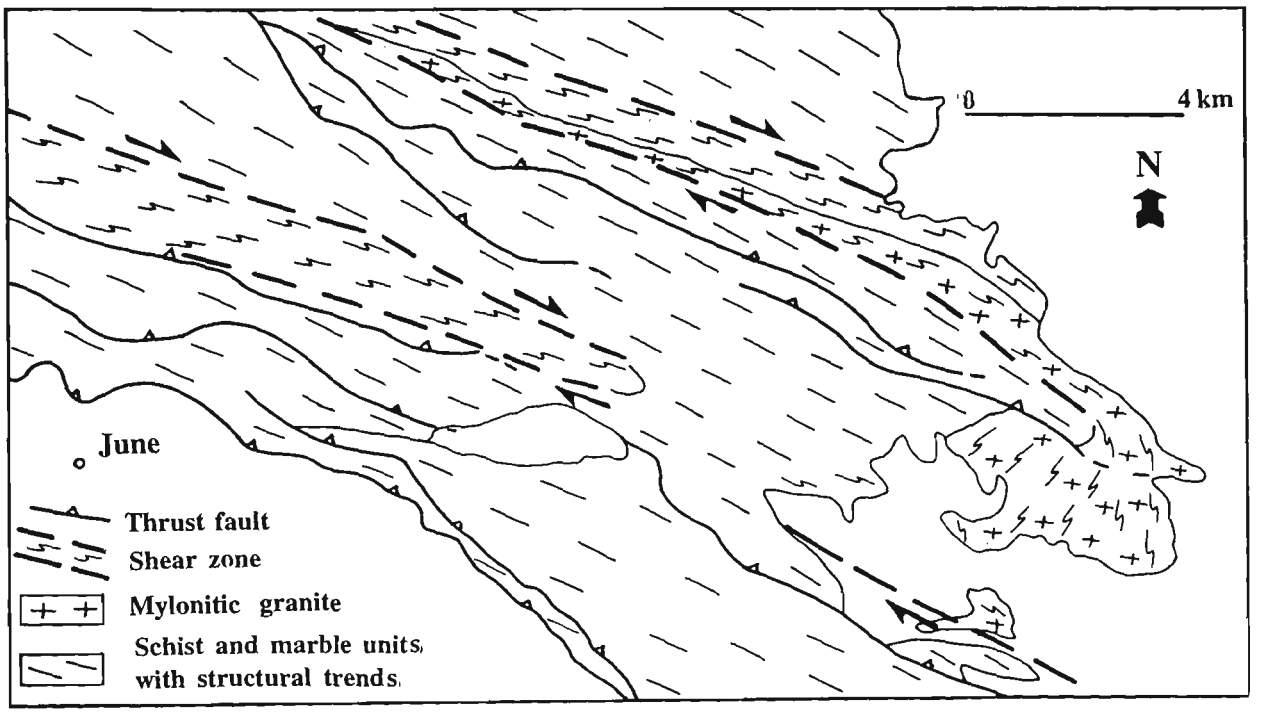
0
4 km
N
June
Thrust fault
Shear zone
Mylonitic granite
Schist and marble units with structural trends

a

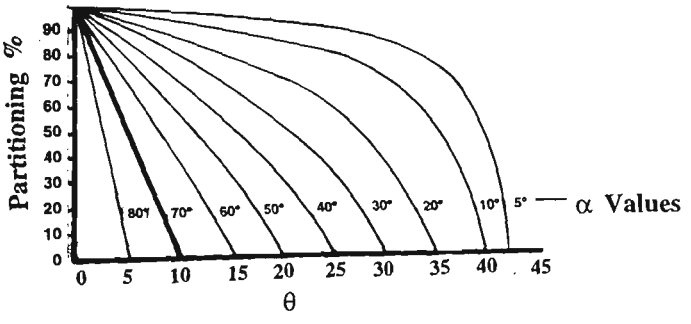
Partitioning %
90
80
70
60
50
40
30
20
10
0
80°
70°
60°
50°
40°
30°
20°
10°
5°
α Values
0
5
10
15
20
25
30
35
40
45
θ

b

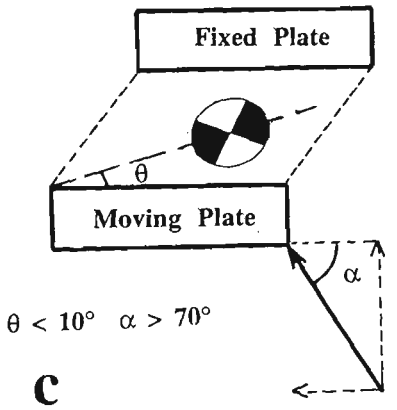
Fixed Plate
θ
Moving Plate
α
θ < 10° α > 70°

c

Figure 3.34

(a) Schematic en echelon extension fissures in a shear zone. Numbers indicate the stages of development.

(b) Map of the Galeh-Doz pluton in the Dorud-Azna region.

(c) Schematic block diagram shows the stretching lineation and mylonitic foliation in the mylonitic granite and amphibolite in the June area.

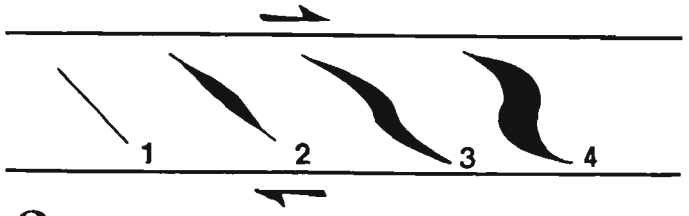
1
2
3
4

a

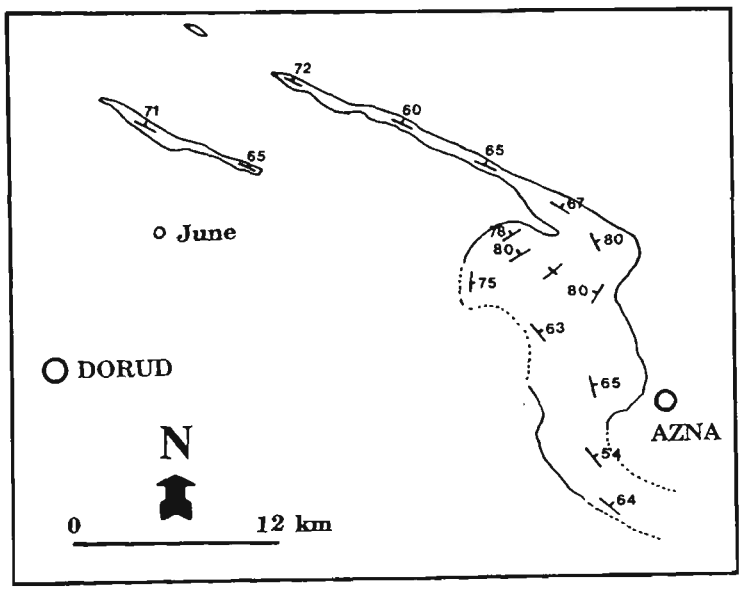
72
71
60
65
65
67
June
78
80
80
75
80
63
DORUD
65
AZNA
N
54
64
0
12 km

b

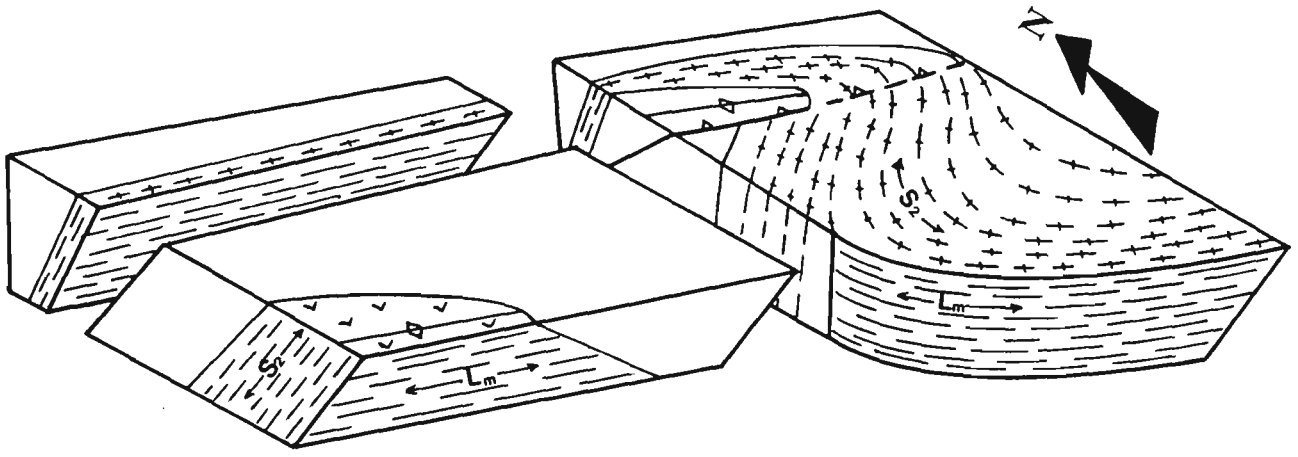
N
S_2
L_m
S_2
L_m

c

CHAPTER 4

METAMORPHISM AND MICROSTRUCTURE

4.1 INTRODUCTION

Detailed field studies, combined with petrographic data, indicate that rocks within the June area have suffered the imprint of both prograde and retrograde metamorphism. This chapter summarises the following: (1) the zonation of metamorphic minerals in the study area; (2) the relationship of metamorphism to the stages of deformation in the study area; (3) the effects of contact metamorphism in the study area and in parts of the northwestern Sanandaj-Sirjan Zone; and (4) the timing of metamorphism. Two distinct phases of regional metamorphism have been identified on the basis of petrographic criteria. The first phase was a prograde metamorphism that was associated with D_1, whereas the second phase was a retrograde metamorphism which affected the prograde metamorphic rocks during D_2. Dynamic metamorphism also occurred in mylonite zones during D_2. Only an overview of metamorphic P-T conditions is presented as a detailed analysis was beyond the scope of this study which has concentrated on structural and tectonic aspects of the Sanandaj-Sirjan Zone.

4.2 REGIONAL METAMORPHISM

The highest grade metamorphic rocks are located in the core of the map-scale F_2 antiform in the central part of the June area (Figure 4.1). Metamorphic grade decreases away from this structure. The highest grade metamorphic assemblages occur in metabasite which changes from amphibolite to greenschist facies metamorphism within the study area. Metamorphic zones are based on variations in

mineral assemblages. The metamorphic zonation for the more important metamorphic minerals is shown in Table 4.1 and the areal extent of metamorphic zones is shown in Figure 4.1.

Zone 1

Rocks in this zone are characterised by the presence of muscovite and chlorite in metapelitic and psammitic rocks and abundant chlorite and epidote in intermediate volcanic rocks. Zone 1 is divided into two sub-zones on the basis of the presence or absence of subidioblastic garnet. Zone 1 rocks in the Hamadan Phyllite all belong to sub-zone 1a that contains no garnet (Figure 4.1, zone 1 phyllite).

In the northeast of the study area, pelitic rocks of the Hamadan Phyllite (zone 1a) contain well developed S_2 which is a spaced compositional foliation with alternating quartz-rich and muscovite-rich laminae. Zone 1a schist has a mineral assemblage of muscovite, quartz and albite. The schistosity (S_2) is defined by abundant muscovite. Plagioclase grains are elongate along S_2 and are wrapped around by muscovite producing an anastomosing fabric. Plagioclase is very fine (up to 0.05 mm across) and contains deformation twins with tapered terminations. Idioblastic opaque minerals are grown over S_2 and are therefore post D_2. S_1 is rarely developed in zone 1 schist and where found is defined by muscovite.

In the Teadar volcanic rocks of the southwestern part of the study area (Figure 4.1), zone 1a mineral assemblages are characterised by the presence of epidote, chlorite and occasionally actinolite. Plagioclase is altered to epidote (zoisite-clinozoisite). Recrystallisation and undulatory extinction occur in quartz. Apart from patches with incipiently aligned metamorphic minerals no metamorphic preferred orientation was observed. No foliations have been observed in these rocks.

Zone 1b rocks are characterised by muscovite, chlorite and the presence of

garnet in pelitic rocks. They occur between the metavolcanic rocks (Teadar volcanic rocks) in the southwest of the study area and the Hamadan Phyllite in the northeast apart from the more restricted areas with zone 2, 3 and 4 mineral assemblages (Figure 4.1). Rock types in this sub-zone include: schist, metasandstone, quartzite, metadolomite and marble. No metabasite has been found in this sub-zone. Schist in zone 1b include both coarse and fine-grained varieties. In coarse-grained schist, muscovite bends around quartz and plagioclase and is locally kinked. Quartz grains are elongate along the foliation and plagioclase is enclosed by muscovite. In garnet-muscovite schist, subidioblastic garnet is enclosed by anastomosing mica grains aligned along S_2. No inclusion trails have been observed in the garnet porphyroblasts (Chapter 3, Figure 3.3a).

Metasandstone consists of recrystallised quartz grains with sutured boundaries and slightly altered plagioclase and pelitic rock fragments (Figure 4.2a, b). Rare muscovite grains are aligned parallel to elongate quartz (Figure 4.2a). Quartzite consists of elongate quartz grains with serrated boundaries that contain very fine recrystallised quartz (Figure 4.2c). In marble and metadolomite, calcite and dolomite grains are recrystallised and contain abundant twins.

Zone 2

Zone 2 rocks are characterised by the presence of biotite, abundant muscovite, quartz and plagioclase but no primary chlorite (Table 4.1). All of zone 2 occurs in the upper unit of the June Complex near the contact with the Hamadan Phyllite (Figure 4.1). Most of the zone 2 rocks are phyllite and fine-grained schist (Chapter 3, Figure 3.3d). Although they have a finer grain size than the zone 1b coarse-grained schists their higher metamorphic grade is shown by the presence of biotite and the absence of chlorite. Garnet is rarely present and its scarcity may reflect

minor compositional differences in comparison to zones 1b and 3. In this zone, a domainal structure is well developed with strong mineral alignment in cleavage domains (S_2) that are separated by microlithons (see Chapter 3, Figure 3.3d). Chlorite occurs as an alteration product of biotite.

Zone 3

Metabasite in this zone is marked by the presence of medium-grained idioblastic to subidioblastic hornblende with blue-green pleochroism, abundant epidote, plagioclase and sphene. Retrogression has resulted in replacement of most of the hornblende by actinolite, which itself is mostly replaced by chlorite. Plagioclase is replaced by epidote (zoisite-clinozoisite). In areas of intense retrogression in zone 3, the metabasite is a chlorite-epidote schist that has a mineral assemblage of plagioclase + chlorite + epidote + quartz ± calcite ± sphene. Plagioclase is mostly altered in its cores with some grains totally altered. Alteration products of plagioclase include sericite, epidote and calcite. Calcite occurs along fractures; here it is recrystallised and contains parallel and crossed twins.

In metasedimentary rocks, schist is coarse grained and contains biotite, garnet, plagioclase and graphite. Plagioclase is relatively fine but is coarser (0.1-0.3 mm) than in zones 1 and 2. These plagioclase grains are lenticular in shape and anastomosed by biotite. Plagioclase includes both unaltered and other grains that are altered to sericite.

S_2 schistosity in garnet-biotite schist is defined by aligned biotite and quartz ribbons (Figure 4.2d). Garnet and plagioclase porphyroblasts are enclosed by quartz ribbons and mica flakes (Figure 4.2d). No inclusion trails are observed in the garnet porphyroblasts. Garnet is not commonly altered but a small amount of chlorite is present along some fractures and also in the pressure shadows of some garnet

porphyroblasts. S_1 is not identified in pelitic schists of zone 3.

Subidioblastic garnets have pressure shadows. In contrast, idioblastic garnets have no pressure shadows and on both sides of the garnet porphyroblast, the foliation is terminated at the contact of the garnet with no overgrowth on S_2 (Figure 4.2d). This indicates that the garnets are syn-D_2; this type of microstructure has been described by Bard (1980, p. 92).

Zone 4

The only rocks in this zone are metabasite and coarse crystalline marble. Amphibolite is typically a layered xenoblastic rock with coarse-grained hornblende-rich and plagioclase-rich laminae. The main minerals consist of idioblastic to subidioblastic hornblende and subidioblastic plagioclase. Hornblende has green to brown pleochroism (Figure 4.3a) and some grains contain simple twins. Aligned hornblende grains define the S_1 foliation. Albite and pericline twins are abundant in the larger plagioclase grains. In places, amphibolite has large plagioclase porphyroblasts over 1 cm long. These plagioclase porphyroblasts are completely altered to calcite. Epidotised plagioclase bands are aligned parallel to S_2.

Marble is interlayered with amphibolite and is well recrystallised, coarse grained with a polygonal texture. Calcite contains common twins. The marble also contains hornblende, actinolite, epidote and chlorite (sample number 102).

The prograde amphibolite occurs as remnants in a well foliated greenschist which has developed by retrograde metamorphism (e.g. sample number 972). Within these remnants the prograde hornblende is partly altered to needles of actinolite, especially along grain boundaries (Figure 4.3b). The retrogressive foliated greenschist consists of abundant actinolite, epidote and chlorite. In some samples the actinolite has been altered to chlorite (Figure 4.3c). In the retrograde schists, plagioclase

porphyroblasts and plagioclase in the groundmass are totally altered to epidote (Figure 4.3d). Retrograde actinolite and chlorite are all oriented along S_2 (Figure 4.3c). Retrograde sphene is present and is aligned subparallel to amphibole-rich laminae. The mineral assemblage consists of actinolite + epidote + chlorite ± sphene.

4.3 METAMORPHISM AND ITS RELATION TO THE DEFORMATION STAGES

D_1

In zone 4 metabasite, S_1 is defined by hornblende which is overprinted by S_2 (Figure 4.3b and Chapter 3, Figure 3.3b). In zone 1b garnet-muscovite schist and phyllite, the remnants of S_1 are identified where they are preserved in microlithons (Chapter 3, Figures 3.3a, d). S_1 in zone 3 metabasite is defined by remnants of actinolite in microlithons (Chapter 3, Figure 3.3c). In zone 1b quartzite, S_1 is defined by elongate quartz grains and alignment of rare mica flakes (Figure 4.2c).

D_2

In metabasite, where retrograde metamorphism is identified, S_2 is defined by aligned actinolite and chlorite (Figure 4.3a, b, c). Plagioclase and hornblende porphyroblasts, that are associated with D_1, are also locally aligned along S_2 within S_2 cleavage domains (Figure 4.3a, b).

In schist, S_2 is defined in zones 1 and 2 by abundant aligned muscovite and in zone 3 by abundant aligned biotite. The timing of garnet porphyroblast growth with respect to the well-developed schistosity (S_2) is established from the textural relationships seen in thin sections. Garnet porphyroblasts in garnet-biotite schist and muscovite schist carry no inclusion trails and are wrapped around by S_2. Therefore,

the microstructural evidence indicates that the garnets have grown during D_2 and are co-existing with biotite.

Dynamic metamorphism was also significant for D_2. In metasedimentary rocks (quartzite, metasandstone and muscovite schist), dynamic deformation is defined by undulatory extinction, sutured boundaries, and mosaic textures (e.g. Figure 4.2a). Quartz porphyroclasts have serrated boundaries (Figure 4.4a). Dynamic metamorphism has also formed mylonite and ultramylonite in amphibolite and metasilicic igneous rocks. These rocks are extensively recrystallised. In ultramylonite, feldspars have been broken and spaces between dislocated grains are occupied with small subgrains (Figure 4.4b). Plagioclase porphyroclasts occur in a very fine-grained strongly recrystallised foliated groundmass (Figure 4.4c). In syn-D_2 granite, the mylonite fabric is defined by: (1) recrystallisation of quartz porphyroclasts, (2) quartz grains are aligned in quartz ribbons parallel to the strong foliation (Figure 4.4d), (3) aligned mica flakes, and (4) fractured and bent deformation twins in plagioclase porphyroclasts (Figure 4.5a).

D_3

The third generation schistosity (S_3) is a crenulation cleavage that in cleavage domains is defined by the rotation of S_2 muscovite as well as some new growth of muscovite grains along S_3 (Figure 4.5b, c). In quartzite, S_3 is a spaced cleavage and is marked by zones of recrystallisation (Figure 4.2a).

4.4 CONTACT METAMORPHISM

In the northwestern Sanandaj-Sirjan Zone several syn- and post-kinematic granite and granodiorite plutons have been emplaced (see Chapter 5). Deformed syn-kinematic plutons are characterised by weak contact aureoles (e.g. Galeh-Doz pluton

in the study area, see Chapter 3). The thermal effect of these deformed plutonic rocks on the wall rocks is defined by a coarser grain size of micas in schist (S_2 schistosity) compared to schists away from the granites. Marbles are also coarser grained near these plutonic rocks.

Contacts of some post-kinematic plutons are faulted and no contact aureoles have been recognised (e.g. Borujerd Granite, see Chapter 5, Figure 5.10), but elsewhere hornfels are well developed. Based on previous reconnaissance study (Mohajjel 1992), contact metamorphic rocks of these plutons are divisible into two zones. In Hamadan Phyllite, the zone close to the pluton is characterised by decussate, well-formed andalusite, cordierite and, locally, sillimanite. The outer zone consists of cordierite and andalusite-bearing spotted schists.

4.5 AGE OF METAMORPHISM

From the microstructural evidence outlined above, the prograde metamorphism (M_1) and first deformation episode (D_1) were synchronous. S_1 is observed in the Middle-Late Triassic June Complex and the Late Triassic - Jurassic Hamadan Phyllite, but it has not been identified in the Teadar volcanic rocks and the Suraneh Limestone. The retrograde metamorphism (M_2) was simultaneous with D_2 as shown by the widespread development of retrograde mineral assemblages along S_2. The fact that retrograde metamorphism was simultaneous with D_2 indicates that at least some of the cooling of the metamorphosed rocks (M_1) occurred by unloading and upward transport of the rocks due to intense folding and associated thrusting during the D_2 event (see Chapter 3; see Jamieson and Beaumont 1988 for an explanation of this process).

4.6 METAMORPHIC FACIES AND PRESSURE TEMPERATURE CONDITIONS

In the study area, S_1 has been formed during compressional deformation associated with low- to medium-grade regional metamorphism. This foliation is defined by biotite and muscovite in metapelitic rocks. This assemblage has been overprinted by S_2 which is defined by muscovite in the same rocks and biotite and muscovite in Zone 2.

During the first deformation event, the rocks reached peak metamorphic conditions in the amphibolite facies based on a mineral assemblage of hornblende-plagioclase in metamorphosed basic rocks. No pyroxene has been observed in these rocks. The maximum temperature was possibly up to around 650° C and a maximum possible pressure of 7 kb (Turner 1981; Vernon 1976, p. 21). This indicates approximate depths of 10-30 km (after Yardley et al. 1990, p. 4). The epidote-amphibolite facies (M_1) of zone 3 has been produced at temperature somewhere around 500°C (Turner 1981). The prograde (M_1) metamorphic rocks range from greenschist through to amphibolite facies and retrograde metamorphism (M_2) ranges from low greenschist (zone 1) through to the upper greenschist facies (zone 3). The temperature of formation of the greenschist facies is generally taken at between 300°-500°C with pressures around 3-4 kb (Gillen 1982, p. 67). The formation of biotite in metasedimentary rocks (zone 3) indicates a temperature of around 400°C (Turner 1981).

4.7 CONCLUDING DISCUSSION

The metamorphic mineral assemblages indicate that the Late Palaeozoic - Mesozoic successions of the June area were metamorphosed at relatively low to medium pressure and temperature conditions (see above). The Middle-Late Triassic

June Complex is metamorphosed at a higher grade whereas the Late Triassic - Jurassic Hamadan Phyllite is metamorphosed at a lower grade. Low-grade metamorphism effects the Cretaceous rocks which are located in the southwest of the study area. Deformed granitoid intrusions are widely developed in the Dorud-Azna region (Figure 4.1). The Galeh-Doz pluton occupies the eastern part of the study area and also the Shur-Shur sill is exposed in the western part (see Chapters 2 and 3). Highly deformed granitic plutons, such as the Galeh-Doz pluton, were intruded into Middle-Late Triassic rocks whereas more widespread non-deformed granitic plutons were intruded into the Hamadan Phyllite with the development of pronounced contact aureoles (see Chapter 5). Evidence for syntectonic emplacement of granitoids has been discussed in Chapter 3. This evidence indicates that the emplacement of the mylonitised granite was a syn-D_2 event.

In some orogenic belts, low-pressure metamorphism with anticlockwise pressure-temperature-time paths have been found in association with compressional deformation and have been explained by crustal thickening without substantial erosion (Collins and Vernon 1991; Lux et al. 1986). In low-pressure terrains, granitoids are commonly emplaced as syntectonic intrusions in the higher grade metamorphic rocks and yet they appear to post-date tectonism in the lower grade parts of the same terrain (Collins and Vernon 1991). Generally, in low-pressure metamorphic terrains more than 80% of the area containing high-grade rocks is occupied by granitic rocks (e.g. Collins et al. 1991). It has been inferred that the source of the heat for high-grade metamorphism was provided by these granitic rocks (Collins et al. 1991). In the study area, however, prograde metamorphism was a syn-D_1 event and unrelated to the intrusion of deformed granites during D_2. The prograde metamorphism is thought to have been associated with a subduction-related orogeny during the D_1 event (see Chapters 5 and 6) and occurred at mid-crustal depths. The metamorphosed rocks

were uplifted and cooled during the subsequent tectonic event associated with D_2. It is conceivable that the syn-D_2 intrusions produced the heat associated with the low grades of regional metamorphism during M_2 (see Chapters 3 and 5).

Rocks	Metasedimentary			Metabasite			
Zone	1	2	3	1	2	3	4
Minerals							
quartz	x	x					
plagioclase	x	x	x	x	x	x	x
white mica	x	x					
chlorite	x			x			
biotite		x	x				
garnet	x	x	x				
epidote				x	x	x	
actinolite					x	x	
hornblende						x	x

Table 4.1 Zonal distribution of important metamorphic minerals in metasedimentary rocks and metabasite in the June area.

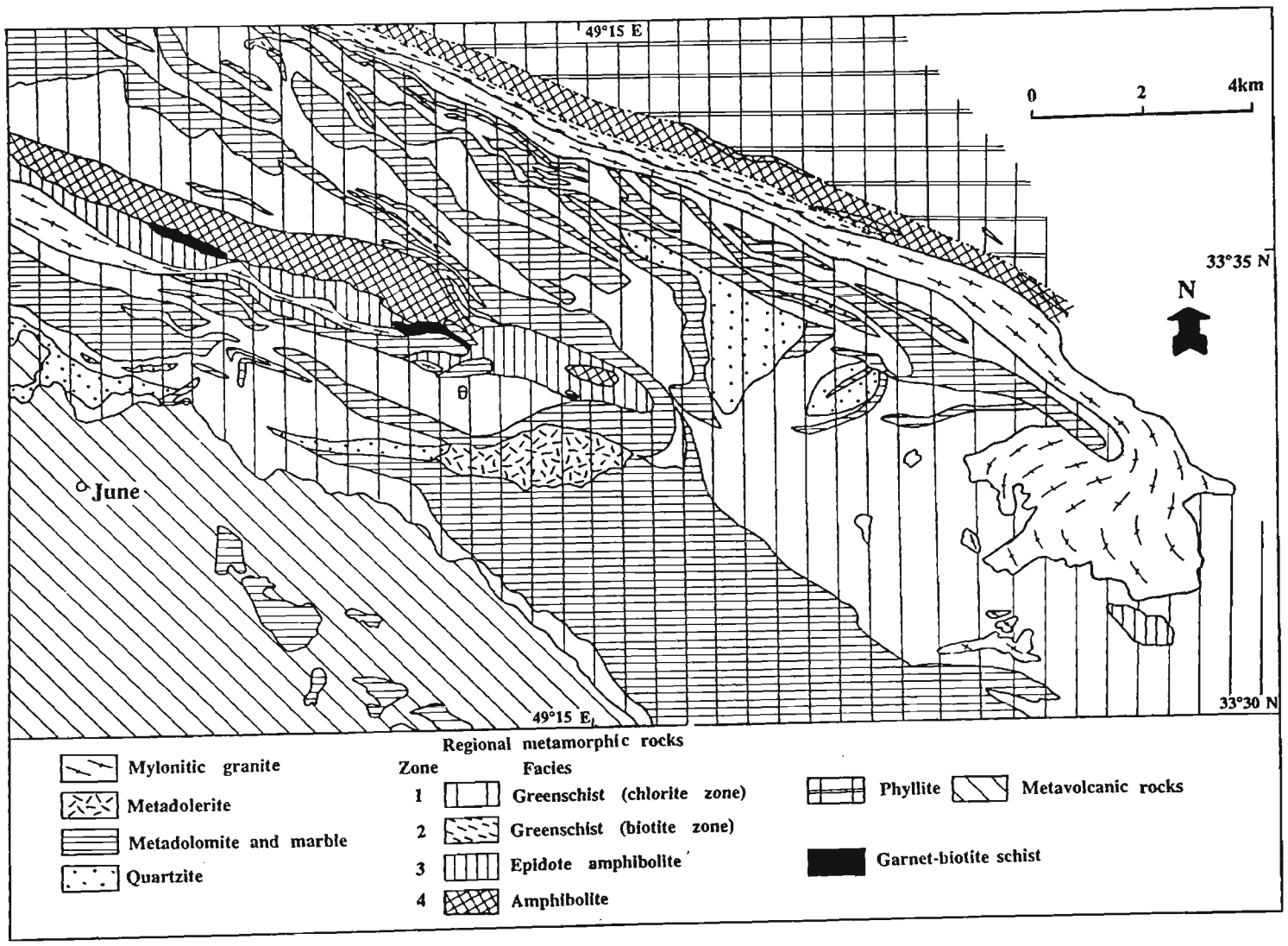

Figure 4.1 Areal extent of the metamorphic zones in the June area.

Figure 4.2

(a) Spaced zones of recrystallisation define S_3 in quartzite. S_2 is defined by flattened grains with local sutured grain boundaries. Sample number 150 (crossed polarised light, 1.6 mm in length and 1.1 mm in width).

(b) Metasandstone. Grain types include altered plagioclase and iron-oxide stained former lithic fragments. Undulatory extinction occurs in quartz grains. Sample number 63 (plane polarised light, 4 mm in length and 2.5 mm in width).

(c) Polygonal mosaic with serrated boundaries in quartzite. S_1 is defined by stylolitic seams formed by pressure solution. Sample number 470 (plane polarised light, 1.6 mm in length and 1.1 mm in width).

(d) Garnet porphyroblast with no inclusion trails. S_2 is defined by the muscovite, biotite and quartz ribbons. To the left of the garnet, plagioclase grain is sinistrally displaced due to dextral shear. Sample number 134 (plane polarised light, 1.6 mm in length and 1.1 mm in width).

a
S_3
S_2
b
c
S_1
d
S_2

Figure 4.3

(a) Hornblende with brown pleochroism. Retrograde pale-green actinolite is developed at hornblende margins. Sample number 401 (plane polarised light, 1.6 mm in length and 1.1 mm in width).

(b) The same photomicrograph as (a) under crossed polarised light. 1.6 mm in length and 1.1 mm in width.

(c) Well-developed retrograde metamorphism in a chlorite-epidote-actinolite schist. A former hornblende porphyroblast has been altered to actinolite and the actinolite itself is altered to chlorite. S_2 is defined by alignment of actinolite. Note that the orientation of actinolite fibres at the margin of the altered porphyroblast is parallel to S_1. Sample number 1089 (plane polarised light, 1.6 mm in length and 1.1 mm in width).

(d) Retrograde chlorite-epidote schist with a porphyroblast completely altered to coarse epidote. Sample number 813 (plane polarised light, 4 mm in length and 2.5 mm in width).

a
b
S1
S2
c
S1
S2
d

Figure 4.4

(a) Mylonitic muscovite schist. Quartz porphyroclast is recrystallised to grains with serrated boundaries. In contrast, on the right side of the photomicrograph an altered plagioclase porphyroclast shows no recrystallisation. Sample number 848 (crossed polarised light, 1.6 mm in length and 1.1 mm in width).

(b) Mylonite. A broken plagioclase porphyroclast has fractures filled by the fine recrystallised grains. Sample number 488 (crossed polarised light, 1.6 mm in length and 1.1 mm in width).

(c) Well-rounded plagioclase porphyroclast in ultramylonite. Sample number 352 (crossed polarised light, 1.6 mm in length and 1.1 mm in width).

(d) Microcline porphyroblast (right side of the photomicrograph) and quartz ribbons with recrystallised quartz grains. Sample number 1052 (crossed polarised light, 4 mm in length and 2.5 mm in width).

a
S2
b
S2
c
S2
d
S2

Figure 4.5

(a) Fractured and bent deformation twins in plagioclase. Note the small sinistral displacement along the microfaults. Sample number 33 (crossed polarised light, 1.6 mm in length and 1.1 mm in width).

(b) The same rock as (c), showing muscovite along the S_3. Sample number 19 (crossed polarised light, 4 mm in length and 2.5 mm in width).

(c) Crenulation cleavage (S_3) developed in muscovite schist. S_2 is a segregation foliation. Sample number 66 (crossed polarised light, 4 mm in length and 2.5 mm in width).

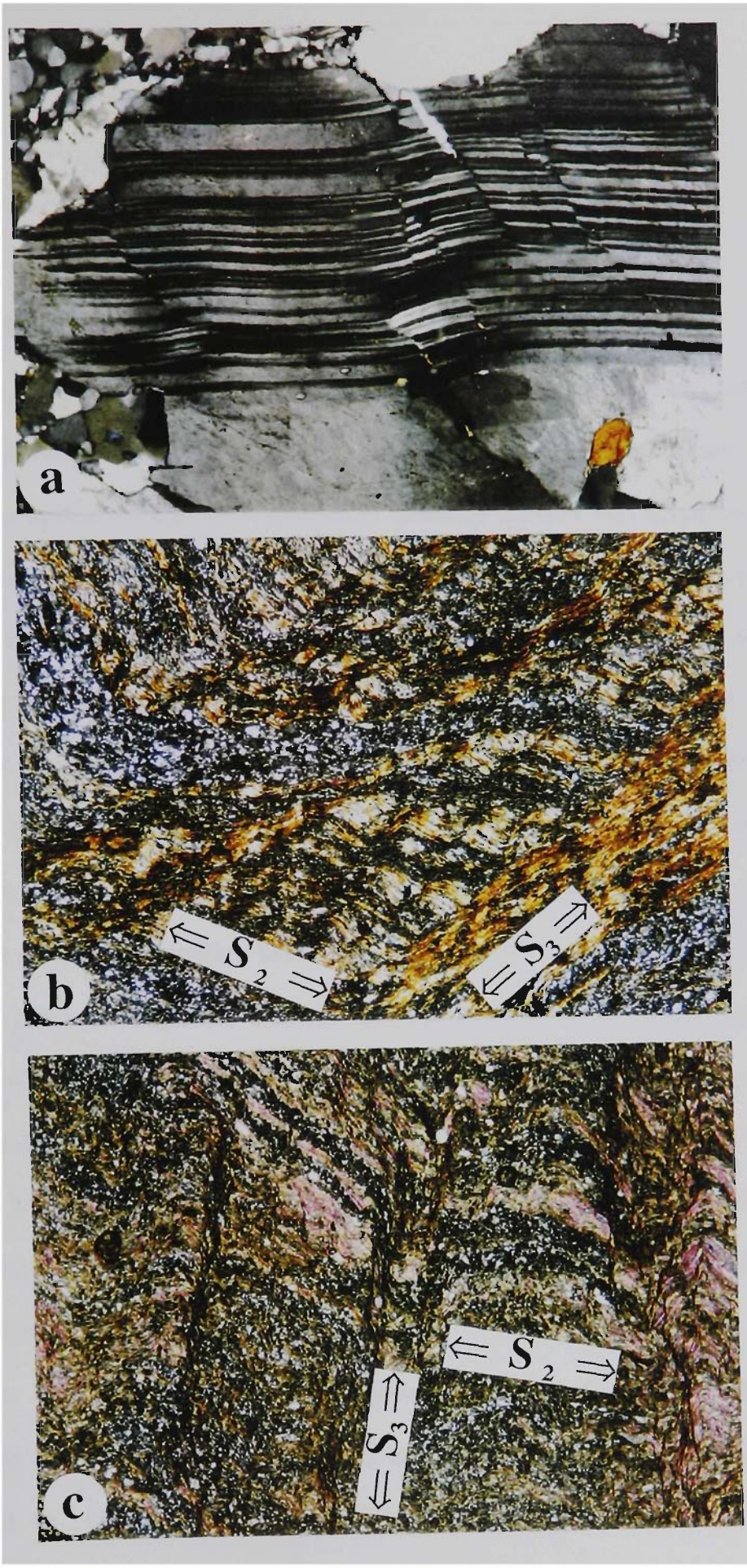
a
b
S_2
S_3
c
S_2
S_3

CHAPTER 5

SANANDAJ-SIRJAN ZONE

5.1 INTRODUCTION

The Zagros Orogen developed from continental separation and subsequent collision between the Arabian platform and the Iranian microcontinent. It is part of Tethyan orogenic collage that developed between Eurasia and dispersed fragments of Gondwana-Land (Şengör 1984). From the northeast to the southwest the Zagros Orogen consists of the Urumieh-Dokhtar Magmatic Assemblage, the Sanandaj-Sirjan Zone and the Zagros Fold-Thrust Belt (Alavi 1991a, 1994, see Chapter 1, Figure 1.1).

The Urumieh-Dokhtar Magmatic Assemblage consists of intrusive and extrusive rocks of Eocene-Quaternary age that are 50 km wide and up to 4 km thick. They extend along the entire Zagros Orogen (Reyer and Mohafez 1972; Berberian and Berberian 1981). Recently, based on geochemical evidence (Moradian 1997), the Urumieh-Dokhtar Magmatic Assemblage has been divided into three parts: (1) the "Urumieh-Nain" part in the northwest, (2) the "Nain-Baft" part in the centre, and (3) the "Baft-Dokhtar" part in the southeast. The southeastern part of the Urumieh-Dokhtar Magmatic Assemblage is still active and is associated with the ongoing subduction of Indian Ocean crust (White and Ross 1979; McCall and Kidd 1982; McCall 1985).

The Sanandaj-Sirjan Zone is located southwest of the Urumieh-Dokhtar Magmatic Assemblage. It has a length of 1500 km and a width up to 200 km from northwest to southeast Iran (Figure 5.1). The rocks of this zone are mostly of Mesozoic age. Palaeozoic rocks are rarely exposed in the northwestern part of the Sanandaj-Sirjan Zone whereas they are common in the southeastern part (Berberian

1977; Sabzehei 1992).

The Sanandaj-Sirjan Zone is characterised by metamorphic and complexly deformed rocks associated with abundant deformed and undeformed plutons in addition to widespread Mesozoic volcanic rocks. Radiolarites and ophiolites are exposed in several places along the southwestern border of the zone. These units separate the Sanandaj-Sirjan Zone from the Zagros Fold-Thrust Belt.

The Zagros Fold-Thrust Belt lies to the southwest of the Sanandaj-Sirjan Zone on the northeastern margin of the Arabian platform. It consists of a Phanerozoic succession with a stratigraphic thickness of up to 10 km. This succession is folded into kilometre-scale simple anticlines and synclines (Stöcklin 1968; Falcon 1969, 1974). The Zagros Fold-Thrust Belt has also been referred to as the Zagros Simply Folded Belt by Alavi (1994). In the past the southwestern part of the Zagros Orogen has been divided into two structural units: (a) a broad simply folded belt (200-300 km wide) including macroscopic elongate anticlines and synclines formed by late Cainozoic orogeny, and (b) a narrow imbricated belt up to 80 km wide uplifted by thrust faults in Late Cretaceous orogeny (Stöcklin 1968; Falcon 1969, 1974; Berberian and King 1981). The imbricated belt was also known as either the "high Zagros" or the "crush zone" (Wells 1969; Nabavi 1974) and much of this belt is now included with the Sanandaj-Sirjan Zone (see below).

The Zagros Fold-Thrust Belt is an active belt which is currently shortening and thickening due to the collision of the Arabian peninsula with central Iran. Seismically-active, blind thrust faults dominate the deeper levels of the Zagros Fold-Thrust Belt (Berberian 1995). Maps of earthquake epicentres in Iran show that abundant seismic activity has affected the Zagros Fold-Thrust Belt (Berberian 1981; Jackson and McKenzie 1984). Seismic activity is greatly reduced to the northeast across the southwestern border of the Sanandaj-Sirjan Zone.

In his review of the Zagros Orogen, Alavi (1994) recognised the dismembered nature of the Zagros suture within the Sanandaj-Sirjan Zone but on the whole considered that the zone was characterised by a common stratigraphic assemblage and structural style. He considered that the stratigraphic assemblage of the Sanandaj-Sirjan Zone was also generally applicable to the Zagros Fold-Thrust Belt. Detailed mapping and reconnaissance work reported in this thesis, in addition to review of previous work, indicate that the Sanandaj-Sirjan Zone is more appropriately divided into several sub-zones with distinctive stratigraphic successions rather than being considered as parts of a single entity (cf. Alavi 1994). In this chapter the new structural zonation is introduced and described along with the stratigraphy, depositional environments and structure of each sub-zone. The new subdivision of the Sanandaj-Sirjan Zone is based on the Palaeozoic and Mesozoic rock assemblages; the Cainozoic rocks are not included in the subdivision and are described generally for the whole zone. This account necessarily concentrates on the northwestern part of the Sanandaj-Sirjan Zone where the writer's field experience is based. The aim is to synthesis the geology of the Sanandaj-Sirjan Zone in the light of new detailed and reconnaissance work undertaken for this project and provide constraints for tectonic evolution of the region.

The Sanandaj-Sirjan Zone, on the basis of Phanerozoic history, has been considered as the most tectonically active zone in Iran (see Chapter 1). Especially in the southeastern part of the zone, deformation and metamorphism has been attributed to a number of "orogenies" by different authors. Orogenic episodes have been recognised for the Late Precambrian (Stöcklin 1968; Thiele et al. 1968; Berberian 1977), Early Palaeozoic (Nabavi 1974; Berberian and Nogole 1974), Late Palaeozoic (Thiele et al. 1968; Berberian 1977; Davoudzadeh and Veber Diefenbach 1987; Şengör 1990a), but the full extent and significance of these events has yet to

be fully determined. It is considered that the major deformation and metamorphic events that affected the Sanandaj-Sirjan Zone were associated with the opening and closing of Neo-Tethys during the Mesozoic era (this opinion is also advocated by Alavi 1994).

5.2 TECTONIC SUBDIVISION

The northwest-southeast trending Sanandaj-Sirjan Zone consists of several elongate sub-zones (Figure 5.1). Each sub-zone is characterised by its own stratigraphy and structural identity. From southwest to the northeast these sub-zones are: (1) radiolarite sub-zone, (2) Bistoon sub-zone, (3) ophiolite sub-zone, (4) marginal sub-zone, and (5) complexly deformed sub-zone.

Radiolarite sub-zone

The radiolarite sub-zone extends discontinuously along the southwestern margin of the Sanandaj-Sirjan Zone in Iran and also has equivalent units occurring as far westwards as the eastern Mediterranean Sea (Cypress, Greece, southern Italy, Bernoulli et al. 1990) and southeastwards in Oman (Hawasina Complex, Kazmin et al. 1986; Bechennec et al. 1990). In the northwestern extremity of the Sanandaj-Sirjan Zone, the radiolarite sub-zone is up to 35 km wide and is 250 km long and extends from southwest of Borujerd to the northwestern border of Iran and beyond to the western Taurides (Antalya) of southern Turkey (Kazmin et al. 1986). Another part of this sub-zone is well exposed 200 km farther to the east-southeast of Kermanshah, 20 km south of Azna (Figure 5.1). In the southeastern extremity of the Sanandaj-Sirjan Zone, near Neyriz, another part of the sub-zone occurs and is 150 km long and up to 15 km wide. Traces of the radiolarite sub-zone also occur in places along the southwestern contact of the Sanandaj-Sirjan Zone between Azna and Neyriz

(Shahrekord quadrangle, Zahedi et al. 1992; Eglid quadrangle, Houshmandzadeh et al. 1975; Figure 5.1).

In the Kermanshah region (Figure 5.2), the succession of the radiolarite sub-zone is divided into a lower unit dominated by limestone and an upper unit with abundant chert (after Braud 1987; see Figure 5.3). The lower unit has a variable thickness of 50-400 m and itself is divided into lower and upper parts. The lower part consists of thick-bedded (1-1.5 m) oolitic limestone with abundant intraclasts of algal fragments and boudinaged white chert bands and nodules. Crinoids and gastropods are abundant and indicate a shallow-marine environment. Foraminifers, including *Galeanella*, indicate a Late Triassic age for the lower part of the lower unit (Braud 1987). The upper part of the lower unit consists of thin-bedded to medium-bedded (20-80 cm) bioclastic limestone with chert nodules and locally interbedded red chert near the top (Figure 5.3). A Jurassic age based on microfossils including *Valvulinella jurassica* is indicated for the upper part of the lower unit (Braud 1987).

The upper unit consists of radiolarian chert, marl and shale. Radiolarite beds are red-brown and range in thickness from 10 to 20 cm. These beds are interbedded with red, green and yellow radiolarian marl and shale. Thin-bedded micritic limestone occurs in the upper half of the unit interbedded with chert and red shale. These limestones contain foraminifers including *Globotruncana* that indicate a deep-marine environment of deposition and a Cretaceous age (Shahidi and Nazari in press). The age of the upper unit is therefore constrained by these limestones that are restricted to the higher stratigraphic levels of the unit; therefore a general late Jurassic - Cretaceous age is inferred for the unit. The thickness of this unit is not clear due to tight folding and repetition by thrust faults, but it is probably in excess of 300 m (Figure 5.3).

Olistoliths occur in the radiolarite succession along the southwestern border of

the radiolarite sub-zone. 60 km south-southeast of Kermanshah Campanian-Maastrichtian olistoliths are exposed and consist of light-grey limestone blocks (Figure 5.4a) that were most likely derived from the Campanian-Maastrichtian Tarbur Formation of the Zagros Fold-Thrust Belt (Motiei 1993, p. 209). The age of the olistoliths indicates that they must occur at the highest stratigraphic levels of the upper unit although structural complications prevent mapping of stratigraphy in these areas.

The succession of the radiolarite sub-zone of the Kermanshah region is folded with a change from upright gentle folds, in the northeast, to overturned, close to tight folds with southwest vergence in the southwest (Figure 5.4b). The tight folds have abundant faults, gently dipping to the northeast, that affect the overturned limbs of folds in the vicinity of the southwestern border of the radiolarite sub-zone. The sense of overturning of the folds indicates that these faults are thrusts (Figure 5.5). The Late Triassic to Late Cretaceous succession of the radiolarite sub-zone is thrust over the Maastrichtian-Palaeocene Amiran Formation of the Zagros Fold-Thrust Belt (Figure 5.5, Braud 1987; Shahidi and Narazi in press). Abundant clasts of radiolarite and ophiolitic components occur in conglomerates of the Amiran Formation and indicate uplift of the radiolarite sub-zone, presumably along bounding thrust faults, occurred in the Maastrichtian (Braud 1987; Shahidi and Narazi in press).

In the southwestern extremity of the Sanandaj-Sirjan Zone a similar succession of radiolarite occurs around the Neyriz area (Figure 5.1) and was formerly included in the Zagros "crush zone" (Wells 1969; Berberian and King 1981). This succession was called the "Pichakun Series" by Ricou (1971, 1974). They were divided into two parts: (a) a lower part of varicoloured, thin-bedded radiolarian chert with interbedded oolitic limestone turbidites that include olistoliths of Late Triassic limestone, and (b) an upper part of red chert lacking turbidites but with interbedded basalt and olistoliths

of Triassic limestone. The upper part of the "Pichakun Series" was named the "Bakhtegan beds" by Hallam (1976). A Middle Jurassic age was indicated for the highest layers of the lower part and a Late Jurassic - Cretaceous (Senomanian) age determined for the upper part on the basis of foraminifers by Ricou (1974). The lower part of the radiolarite succession in the Neyriz region contains olistoliths of megalodontid limestone; the olistoliths have large thick-shelled benthic fossils and calcareous algae indicating a shallow-marine depositional environment (Hallam 1976). These limestone olistoliths contain abundant foraminifers, ostracods, algae and crinoids which indicate a Late Triassic age (Sabzehei and Eshragi 1995). Hallam (1976) concluded that the olistoliths and associated turbidites in both the lower and upper parts were deposited in the deep-marine radiolarite succession by mass-flow processes and were derived from the platform carbonates of the Zagros Fold-Thrust Belt. He further suggested that these mass-flow deposits were dislodged by motion along steeply dipping normal faults in the source area in the Jurassic and Cretaceous.

The Neyriz radiolarites are intensely folded and sheared. They occur in several thrust sheets with thrust faults dipping to the northeast consistent with fold vergence implying that they have been transported over shelf/platform carbonates of the Zagros Fold-Thrust Belt (Alavi 1994, p. 230). The Campanian-Maastrichtian Tarbur Formation, which is mainly a component of the Zagros Fold-Thrust Belt, overlies the radiolarite above an angular unconformity to the south of Neyriz (James and Wynd 1965; Hallam 1976; Ricou 1974). Therefore, the age of thrusting is constrained to the Turonian-Campanian interval.

Along the southwestern margin of the Sanandaj-Sirjan Zone, 20 km south of Azna, this sub-zone is up to 5 km wide and 100 km long (Figures 5.1, 5.6, after Soheili et al. 1992). In this area red chert is interbedded with dark-red to brown radiolarian shale. Pale-green micritic limestone, altered andesite and spilite with

amygdales of calcite are also present. In this area foraminifers, including *Oligostegina* sp. and *Globotruncana* sp., occur in micritic limestone and radiolarians, including *Amphipyndax* cf. *pseudoconulus* (Pessagno) and *Cryptoamphorella* cf. *sphaerica*, occur in red chert (Soheili et al. 1992). These fossils indicate a Late Cretaceous (Campanian) age (Soheili et al. 1992) and a pelagic environment of deposition. Here, the radiolarite sub-zone lies in a thrust sheet that contains intensely folded rocks with southwest vergence and is thrust over Senomanian limestone of the Zagros Fold-Thrust Belt (Figure 5.7, cross section GH). It is truncated at a faulted contact with an overlying succession of Eocene marly limestone. The timing of thrusting is poorly constrained in the Azna region and is post-Senomanian and pre-Eocene.

The succession of the radiolarite sub-zone formed in a basin commencing with shallow-marine deposition followed by gradually increasing water depths resulting in deposition of radiolarite, radiolarian shale and marl (Figure 5.3). The mafic to intermediate volcanic rocks associated with the radiolarites at Neyriz and south of Azna are relatively minor components of the succession and their magmatic affinities are unknown. They could represent minor magmatic activity associated with opening of the main sedimentary basin. The Triassic olistoliths of the Neyriz region have been related to extensional events in the Jurassic-Cretaceous by Hallam (1976) but, instead, they could be related to sea-level fluctuations and minor tectonic instability on the passive margin of the Arabian platform (cf. formation of Cow Head Group megabreccias of the Cambrian-Ordovician passive margin in western Newfoundland, James and Stevens 1986; Williams and Hiscott 1987).

The Cretaceous olistoliths of the Kermanshah region were derived from the platform preserved in the Zagros Fold-Thrust Belt and were transported to the northeast by submarine mass flows and debris slides during basin subsidence. This

implies that the basin of deposition that formed the succession of the radiolarite sub-zone formed in the vicinity of the autochthonous succession of the Zagros Fold-Thrust Belt. The dislodgment of olistoliths and debris flows in the Late Cretaceous indicates some tectonic instability in the foreland at this time (see Discussion).

Bistoon sub-zone

The Bistoon sub-zone is located northeast of the radiolarite sub-zone in the Kermanshah region (Figures 5.1, 5.2) and has previously been referred to as the "inner carbonate platform" by Kazmin et al. (1986). This sub-zone is discontinuous along the southwestern part of the Sanandaj-Sirjan Zone and its full extent outside the Kermanshah region has yet to be established (Figure 5.1).

At the northwestern extremity of the Sanandaj-Sirjan Zone in the Kermanshah region (Figures 5.1, 5.2, 5.3), the Bistoon sub-zone is characterised by a thick-bedded and massive limestone succession that is continuous from the Late Triassic to the Late Cretaceous (Braud 1987). These ages were obtained from abundant index microfossils, including foraminifers, reported in the succession by Braud (1987). The Late Triassic rocks consist of 300 m of thick-bedded and massive reefal limestone overlain by 200-300 m of Lias-Dogger dolomite and grey to dark-grey thin-bedded to thick-bedded limestone that is in places fetid and contains abundant intraclasts and fossil fragments. The upper part of the succession consists of Cretaceous thick-bedded and massive limestone of unknown thickness. The Late Cretaceous micritic limestone contains *Globigerina* ooze that indicates pelagic deposition in contrast to shallow-marine deposition for the Late Triassic - Early Cretaceous part of the Bistoon sub-zone (Braud 1987).

At Kuh-e-Sheerez, 40 km east of Kermanshah (Figure 5.2), radiolarite beds occur interbedded with Cretaceous rocks of the Bistoon sub-zone (Braud 1987;

Shahidi and Nazari in press). It is inferred that the Bistoon sub-zone developed at the northeastern border of the radiolarite sub-zone consistent with its common structural location. The succession of the Bistoon sub-zone is overlain angularly unconformably by early Eocene rocks (Figure 5.3).

The Bistoon succession comprises a topographically elevated massive limestone unit that is difficult to resolve structurally unless age-specific fossils are found. 20 km northeast of Kermanshah (Figure 5.2), folds and abundant northeast-dipping imbricate thrust faults have been recognised by Shahidi and Nazari (in press). At Bistoon Mountain the succession forms a disjointed cliff face over 1500 m high. The Bistoon sub-zone is thrust southwards over the radiolarite sub-zone northeast of Kermanshah and south of Kuh-e-Garin (Figures 5.2, 5.7 cross sections AB and CD).

An allochthon of the Bistoon sub-zone overlying the Zagros Fold-Thrust Belt occurs 20 km southwest of Borujerd (interpretation based on the mapping of Hajmolla-Ali et al. 1989; see Figures 5.2, 5.7 cross section CD) and indicates that thrust slices of Bistoon sub-zone have locally overridden and passed beyond the radiolarite sub-zone. This allochthon has been thrust over the Eocene Kashkan and Shahbazan Formations and Oligocene Asmari Formation of the Zagros Fold-Thrust Belt. This indicates that thrusting was active during the Tertiary. Another allochthon of the Bistoon sub-zone, known as the Garin unit (Braud 1987; Hajmolla-Ali 1989), is located 15 km west of Borujerd at Kuh-e-Garin (Figures 5.1, 5.2). 25 km west of Norabad, the Garin unit is thrust at least 15 km over late Neogene conglomerate (interpretation based on mapping of Shahidi and Nazari in press; see Figures 5.2, 5.7, cross section AB, 5.8). This indicates that thrusting has been active into the late Neogene in the southwestern Sanandaj-Sirjan Zone.

Ophiolite sub-zone

Ophiolites and ophiolitic melange are located along the southwestern margin of the Sanandaj-Sirjan Zone and are restricted to two areas; Kermanshah and Neyriz (Figure 5.1). In the Kermanshah region, ophiolites are exposed along northwest-trending thrust faults (Figure 5.7, cross sections AB and CD). 40 km east-northeast of Kermanshah, south of Sahneh (Figure 5.2), ophiolites are well preserved with ultrabasic rocks at the base consisting of harzburgite, peridotite, dunite and serpentinite (Braud 1987). Harzburgite is abundant and is mostly altered to serpentinite. The ultrabasic rocks are cross-cut by common veins containing magnesite, zeolite, antigorite and chrysotile. These ultrabasic rocks are overlain by gabbro which in turn is overlain by pillow lava.

Near Harsin and west of Norabad (Figure 5.2) ophiolitic melange occurs in imbricated thrust sheets (Shahidi and Nazari in press). Components of the ophiolitic melange include: pillow lava (Figure 5.9a), spilite, red-purple shale and micritic pelagic limestone with interbedded chert (Figure 5.9b, c). The sedimentary rocks are strongly folded and broken up by many small faults (Figure 5.9b, c). The pelagic limestone contains foraminifera including *Globorotalia wilcoxensis, Globorotalia centralis,* and *Globorotalia spinulosa*, which indicate an early-middle Eocene age (Shahidi and Nazari in press).

Two K-Ar radiometric ages have been determined for rocks associated with the ophiolite in the Sahneh area: (1) an age of 86.3 ± 7.8 Ma on a leucodiorite, and (2) an age of 81.4 ± 3.8 Ma on hornblende from a diabase dyke cutting the same leucodiorite (Braud 1987). These ages imply that the ophiolite of the Kermanshah region formed in the Senonian in contrast to the younger age (Eocene) determined from the micritic pelagic limestone blocks from ophiolitic melange. These blocks are regarded as having been incorporated into the melange after the development of

the ophiolite and were derived from the Eocene volcanic-sedimentary unit that occurs in the Kermanshah region (see Cainozoic Successions below).

The ophiolites of the Kermanshah region are thrust over the Bistoon sub-zone, the radiolarite sub-zone and also over a Palaeocene-Eocene succession (see below). 10 km east of Harsin the ophiolites are separated from the overlying Palaeocene-Eocene rock succession by an angular unconformity. In the adjoining Zagros Fold-Thrust Belt conglomerates in the Maastrichtian-Palaeocene Amiran Formation contain abundant clasts derived from ophiolite and indicate thrust emplacement of the ophiolite at this time (Braud 1987). The thrusting and associated uplift also accounts for the angular unconformity at the base of the overlying Palaeocene-Eocene succession of the Kermanshah region.

Ophiolites in the Neyriz region are considered a typical succession of oceanic crust (Hynes and McQuilian 1974; Sabzehei and Eshragi 1995). The base of the succession consists of dunite, harzburgite, lherzolite and layered gabbro. Thin bands of chromite occur in dunite. The upper part of the succession consists of sheeted dykes, basalt pillow lavas and overlying deep-marine radiolarite and pelagic limestone with Senonian - early Maastrichtian radiolaria (Sabzehei and Eshragi 1995). Samples from igneous rocks of the Neyriz ophiolite have been dated by the K/Ar method at 87.5 ± 7.2 Ma indicating a Senonian (Late Cretaceous) age for the igneous rocks of the ophiolite (Lanphere and Pamic 1983). The Neyriz ophiolite is exposed in several thrust sheets (Alavi 1994). Ophiolites in the thrust sheets of the Neyriz region were transported over Late Cretaceous (Albian-Cenomanian and locally Turonian) rocks of the Zagros Fold-Thrust Belt. They are overlain unconformably by shallow-marine reef limestone of the Campanian-Maastrichtian Tarbur Formation (James and Wynd 1965; Hallam 1976; Ricou 1974). Thrust emplacement of the ophiolites is therefore constrained to the Turonian-Campanian interval.

The presence of metamorphic soles associated with the ophiolites along the Zagros Suture has been mentioned in general by Knipper et al. (1986, p 231). A radiometric age of 94 ± 7.6 Ma has been reported from amphibolite of the metamorphic sole in the Neyriz region (Lanphere and Pamic 1983). No structural and metamorphic analysis has been undertaken on these metamorphic rocks that occur in the Neyriz and Kermanshah regions.

Both the Kermanshah and Neyriz ophiolitic complexes are similar in composition and age to the ophiolite-radiolarite complex of the Oman Mountains (Stöcklin 1974; Moores et al. 1984; Cawood et al. 1990). The radiometric age of the Semail Ophiolite is 90 ± 3 Ma (Lanphere 1981; Knipper et al. 1986). It has been suggested that the Neyriz and Oman ophiolites were located along the same belt (Hallam 1976) and that obduction of the ophiolites at Neyriz occurred at the same time as obduction of the Semail Ophiolite in Oman (Dewey et al. 1973; Glennie et al. 1973; Le Metour 1990).

The Semail Ophiolite in Oman is the highest thrust sheet of a stack that includes in structural order below the ophiolite: the inner carbonate platform (correlated with the Bistoon sub-zone of the Kermanshah region by Kazmin et al. 1986), the Hawasina Complex (correlated with the radiolarite sub-zone by Hallam 1976; Bernoulli et al. 1990), the Hajar Supergroup and conformably overlying Aruma Group (equivalents of the passive margin of the Zagros Fold-Thrust Belt, Glennie et al. 1974; Bernulli and Weissert 1987; Cawood et al. 1990). Two distinct phase of of thrusting have been observed in the southeast Oman mountains (Cawood et al. 1990). The first thrust phase was a 5 million year period lasting between the late Campanian and early Maastrichtian. The Maastrichtian Qahlah Formation unconformably overlies the flanks of ophiolite. Therefore the age of unconformity is very similar to that at Neyriz. The second phase of thrusting affected the

Maastrichtian and Tertiary successions and also reactivated the Late Cretaceous thrust system in mid-Tertiary times (Cawood et al. 1990).

The Semail ophiolite has a metamorphic sole with amphibolite facies and underlying greenscist facies rocks. Amphibolite has been radiometrically dated at 90 ± 3 Ma (Lanphere et al 1986). Their present-day structural position is the result of their juxtaposition during ophiolite emplacement (El-Shazly and Coleman 1990).

Marginal sub-zone

The marginal sub-zone is located to the southwest of the complexly deformed sub-zone (Figure 5.1) and is stratigraphically distinctive because it contains abundant Late Jurassic - Early Cretaceous volcanic rocks (Figure 5.3). In contrast to the ophiolite and Bistoon sub-zones the marginal sub-zone has been identified throughout the Sanandaj-Sirjan Zone. The stratigraphy of this sub-zone has been described for several regions from northwest to southeast. These include: Kermanshah (Braud 1987), Nahavand (Alavi and Mahdavi 1994), Aligudarz (Soheili et al. 1992), Golpaygan (Mohajjel 1992), Shahrekord (Zahedi et al. 1992), Eglid (Houshmandzadeh et al. 1975), Neyriz (Sabzehei et al. 1991) and Hajiabad (Berberian 1977). Only the northwestern part of the sub-zone will be described below.

The marginal sub-zone is extensively exposed in the northwestern part of the Sanandaj-Sirjan Zone. 60 km east-northeast of Kermanshah, north of Kangavar (Figure 5.2), this sub-zone has a succession over 1000 m thick and contains interbedded recrystallised bioclastic limestone, andesitic lava, andesitic tuff and spilite (Braud 1987). The limestone contains gastropods and crinoids indicating a shallow-marine environment. South of Kangavar (Figure 5.2), interbedded recrystallised limestone in andesitic lava contain lamellibranchs and pseudocyclammines of Late Jurassic age (Malm; Braud 1987). Farther southeast in the Nahavand area (Figure

5.2), a succession of a slightly younger age consists of red to purple pyroclastic rocks and porphyritic and non-porphyritic dacite and andesite interbedded with recrystallised limestone of Early Cretaceous age (Mahdavi et al. 1992). 30 km south of Aligudarz (Figure 1.2), sandstone, shale and thin-bedded limestone is interbedded with marl containing a Late Jurassic - Early Cretaceous fauna (Soheili et al. 1992). All these successions are representative of the Late Jurassic - Early Cretaceous volcanic and shallow-marine succession of the marginal sub-zone.

15 km northwest of Sahneh in the Kangavar region (Figure 5.2), the Jurassic volcanic rocks are overlain by an angular unconformity at the base of a Cretaceous (Albian-Aptian-Cenomanian) succession with 120-150 m of basal dark-red, highly ferruginous, quartz sandstone containing a marker conglomerate horizon, 40-50 cm thick, with iron oxide pisoliths (Figure 5.9d). The sandstone is overlain by Albian-Aptian, in places Cenomanian, limestone. The age of this succession was determined by Braud (1987) and Shahidi and Nazari (in press). 40 km southwest of Golpaygan, at Kuh-e-Sorkh, an angular unconformity has been recognised between Jurassic volcanic rocks and an overlying Early Cretaceous succession (Mohajjel 1992). A basal conglomerate, above the unconformity, contains well-rounded and sorted clasts of quartzite, mica schist, metadolomite and marble, and is overlain by grey sandy and oolitic biomicrosparite containing abundant Neocomian-Infravalangian faunas (Mohajjel 1992). The unconformity is considered equivalent to that of the Kangavar region and the difference in age is thought to reflect the diachronous nature of the erosional surface. In contrast to the underlying succession no volcanic activity has been recognised in the younger succession of the marginal sub-zone.

The rocks of this sub-zone are folded in gentle to close folds with overturned southern limbs indicating vergence to the southwest. No axial plane cleavage is developed in the rocks and only one episode of folding is evident. The style of

deformation is much simpler than that occurring in the complexly deformed sub-zone to the northeast (see below). Metamorphic grade of the marginal sub-zone is normally sub-greenschist facies grade.

Thrust faults have transported rocks of the marginal sub-zone over the ophiolite, radiolarite and Bistoon sub-zones and also over the Zagros Fold-Thrust Belt (Figures 1.2, 5.2, 5.7). 30 km south of Borujerd a nappe structure (thrust sheet) has been recognised (the Chagalvandi nappe of Hajmolla-Ali et al. 1989) with rocks of the marginal sub-zone thrust at least 20 km over Miocene rocks of the Zagros Fold-Thrust Belt (Figures 5.1, 5.2, 5.7 cross sections CD and EF). At the base of this nappe is a tectonic melange, 50-100 m thick, with components of Eocene limestone containing abundant calcite veins, dolomite, dolomitic limestone, spilite, purple shale and radiolarite. This rock assemblage is strongly sheared with abundant fractures that are either horizontal or gently dipping to the southwest. The nappe structure is overlain by Pliocene conglomerate. Therefore, thrusting of the nappe is at least post-Miocene and predates the Pliocene. The time of thrusting of the marginal sub-zone to the south-southwest is poorly constrained between the Late Cretaceous and continuing up until the Pliocene.

Complexly deformed sub-zone

This sub-zone lies along the northeastern border of the marginal sub-zone and contains the most complexly deformed and metamorphosed rocks in the Sanandaj-Sirjan Zone (Figure 5.1). The abundance of schist, phyllite, and amphibolite, distinguishes this sub-zone from the marginal, Bistoon, radiolarite sub-zones and even the Zagros Fold-Thrust Belt (Figure 5.3). The sub-zone is characterised by several deformation episodes, some of which were synchronous with metamorphism and intrusion of abundant plutonic rocks.

The complexly deformed sub-zone is divided into two regions to the northwest and southeast of the Dehshir fault (Figure 5.1). In the eastern region, complexly deformed and metamorphosed Palaeozoic rocks have been reported to occur in several places from southeast of Sirjan to Neyriz (Berberian and King 1981; Berberian 1977). As briefly mentioned in Chapter 1 these Palaeozoic rocks have been related to several orogenic events including Hercynian and older orogenies. Alavi (1994) disputed the veracity of these orogenic episodes and suggested that all orogenic activity in the Sanandaj-Sirjan Zone was related to the opening and closing of Neo-Tethys. It was not possible to examine the reported occurrences of pre-Triassic orogeny in the southeastern Sanandaj-Sirjan Zone during the course of this project. Until more detailed work has been undertaken in these areas the older reports, which were all based on limited observations, will not be taken into account in this synthesis which is consistent with the review of Alavi (1994).

Stratigraphy of the northwestern complexly deformed sub-zone

In a few places along the northeastern border of the Sanandaj-Sirjan Zone, non-metamorphosed Late Precambrian - Early Palaeozoic rocks are exposed (Figure 5.1). These successions are stratigraphically equivalent to those in central Iran and the Alborz Belt and have been identified 60 km northeast of Eglid (Houshmandzadeh et al. 1975), 45 km north and northeast Golpaygan (Thiele et al. 1968), and in the Takab region (Alavi-Naini et al. 1982).

Northwest of the Dehshir fault in the complexly deformed sub-zone, Middle and Late Palaeozoic rocks are restricted to the Aligudarz, Dorud-Azna, and Nahavand areas (Figure 5.1). 35 km southeast of Aligudarz, non-metamorphosed Devonian, Carboniferous and Permian unmetamorphosed limestones with abundant fossils are exposed (Soheili et al. 1992). In the Dorud-Azna region (Figure 1.2), Permian rocks

consist of recrystallised dolomite and fossiliferous limestone (see Chapter 2). In the Nahavand area, Carboniferous detrital limestone, containing corals and gastropods, are interbedded with quartz sandstone (Alavi and Mahdavi 1994). Overlying Permian strata include dark grey, thin-bedded, fossiliferous recrystallised limestone and massive dolomite (Alavi and Mahdavi 1994).

The June Complex and its equivalents form a continuous belt along the northeastern side of the marginal sub-zone in the northwestern part of the complexly deformed sub-zone (Figure 5.1). The June Complex of the study area is representative of these rocks. The base of the Middle-Late Triassic June Complex is a quartz sandstone and is overlain by dolomite and limestone, which in turn are overlain by a mafic volcanic unit of basalt, basaltic andesite, and silicic igneous rocks with interbedded shale and limestone (see Chapter 2).

Elsewhere the equivalents of the June Complex are known by different names (e.g. in the Eglid region - Toutak, Koli Kosh and Surian Complexes, Houshmandzadeh et al. 1975; in the Shahrekord region - undifferentiated metamorphic rocks, Zahedi et al. 1992; in the Aligudarz region - Abe-Barik unit, Soheili et al. 1992). In the Aligudarz area, the Abe-Barik unit consists of andesitic amygdaloidal pillow lavas and limestone with schist in the upper part which were previously thought to be of Permian age (Thiele et al. 1968). In the Nahavand area (Figure 5.1), a sequence of Middle to Late Triassic - Early Jurassic basaltic and basaltic andesitic lava flows, locally with pillow structures, are interbedded with thin-bedded, well foliated marbles which have thin, upward-increasing, slate layers (Alavi and Mahdavi 1994).

In the northwestern complexly deformed sub-zone a large region is underlain by the Late Triassic - Jurassic Hamadan Phyllite. The Hamadan Phyllite is located to the northeast of the June Complex and its equivalents (Figure 5.1). Much of the Hamadan Phyllite is considered to form a turbidite succession that is transitional to

the underlying igneous rocks of the June Complex (see Chapter 2).

The Hamadan Phyllite is separated from an overlying Cretaceous succession by an angular unconformity that has been recognised from Esfahan to Hamadan in the northwestern part of the complexly deformed zone (Figure 5.10). The lacuna across the unconformity encompasses the early Cretaceous prior to deposition of Aptian-Albian strata. A conglomerate occurs at the base of the Aptian-Albian succession above the unconformity. The basal conglomerate is observed in several places in the complexly deformed sub-zone (e.g. Golpaygan, Mohajjel 1992; Aligudarz, Soheili et al. 1992; Shazand, Sahandi et al. in press; Esfahan, Zahedi et al. 1978, Shahrekord, Zahedi et al. 1992; Figure 5.10). 20 km southwest of Golpaygan at Hendeh village, the Cretaceous succession is exposed in a tight syncline and the basal conglomerate is 15 m thick (Mohajjel 1992). It consists mainly of quartzite clasts (> 90%) with 10-20 cm diameters and in places clasts are as large as 50 cm across. All clasts are ellipsoidal and aligned along the pervasive foliation. This foliation affects both overlying and underlying (Hamadan Phyllite) successions.

The Cretaceous succession above the unconformity throughout the northwestern complexly deformed zone (in part after Mohajjel 1992) consists of:

(1) reddish conglomerate interbedded with red sandstone and shale with local andesitic lava near the top of the succession;

(2) yellow-orange, sandy dolomite grading upward to sandy limestone containing local concentrations of iron;

(3) a thick sequence of grey, Orbitolina-bearing, thickly to massively bedded limestone interbedded with yellow and olive-grey limestone (Aptian-Albian); and

(4) olive-green shale interbedded with thin-bedded to thick-bedded Late Cretaceous limestone.

These Cretaceous rocks were deposited in continental, shallow-marine and locally in

the upper part in deeper marine environments. The andesitic lavas are restricted in extent and are the only volcanism of this age in the whole Sanandaj-Sirjan Zone.

Structure and metamorphism of the northwestern complexly deformed sub-zone

The structure of the study area (see Chapter 3) is considered representative of much of the structure of the northwestern complexly deformed sub-zone (Figure 5.1). In this synthesis, the detailed results from the study area are incorporated with regional reconnaissance undertaken by the writer along with limited previous detailed structural analysis (e.g. Berberian and Alavi-Tehrani 1977) and re-interpretation of 1:100 000 geological maps that exist for most of this region. In a recent synthesis, Alavi (1994) argued that the structure of the region was dominated by thin-skinned thrust slices (duplexes and imbricate thrust systems) with the intensity of deformation increasing to the northeast. In fact, many of the so-called thrusts and nappe structures were not verified by the present work.

From a regional perspective, a major Late Cretaceous - Palaeocene deformation has affected the region and produced northwest to west-northwest trending folds, faults and foliations/cleavages of the style documented in the study area (D_2, see Chapter 3). Map-scale folds associated with this deformation are tight to isoclinal typically with vergence to the southwest. These structures are well displayed in Cretaceous rocks of the complexly deformed sub-zone. These Cretaceous rocks unconformably overlie the Late Triassic - Jurassic Hamadan Phyllite (see above). These structures are reported in several regions in the northwestern complexly deformed sub-zone.

30 km southwest of Hamadan (Figures 3.2, 5.10), in the Kuh-e-Khangormaz, the Aptian-Albian succession has a basal 20-30 m conglomerate and sandstone that unconformably overlies the Hamadan Phyllite. These Cretaceous rocks are exposed in a map-scale syncline with an axial plane trending west-northwest (Amidi and

Majidi 1977; Eshragi, in press). In the Malayer region (Figures 3.2, 5.10), the same Cretaceous rocks are folded with west-northwesterly trending map-scale folds overlying the Hamadan Phyllite with a quartz sandstone containing the basal conglomerate (Amidi and Majidi 1977; Jafarian in press). In the Shazand area (Figure 5.10), the Cretaceous rocks are isoclinally folded and foliated in a map-scale syncline with a west-northwest trending axial plane and vergence to the south-southwest (Sahandi et al. in press).

In the Golpaygan region (Figures 5.1, 5.10), one of these map-scale folds, is 80 km long and up to 5 km wide, with an overturned southwestern limb indicating vergence to the south-southwest (Mohajjel 1992). The axial plane dips steeply to the north-northeast. An axial plane foliation is strongly developed in Cretaceous rocks and the same fabric also affects the underlying Hamadan Phyllite. The same map-scale structures are also observed in adjoining regions (Zahedi et al. 1978; Soheili et al. 1992). All these map-scale folds are correlated with the map-scale F_2 in the study area. Locally, the unconformity between the Cretaceous succession and the underlying Hamadan Phyllite is faulted; these faults are probably related to folding of the unconformity with strain incompatibilities across the contact resulting in localised brittle deformation.

Alavi (1994) inferred that Cretaceous rocks of the Malayer area were a thin nappe thrust over the underlying phyllite and by inference implied that this relationship was common in the northwestern complexly deformed zone. He has failed to recognise the major unconformity between the two successions and has been misled by local faulted contacts, an example of which is shown in a photograph in his paper (Alavi 1994, p. 224). It is clear that the Cretaceous succession and the underlying Hamadan Phyllite have been folded, with associated faulting, in a regional deformation event that affected a largely intact stratigraphic succession (see Figure

5.10).

The structures in the Cretaceous rocks are mapped into the adjoining Hamadan Phyllite in various areas. A major episode of northwest-oriented folding and associated greenschist facies metamorphism was documented in the Hamadan Phyllite of the Hamadan region by Berberian and Alavi-Tehrani (1977). This deformation produced an axial plane schistosity that is steeply dipping to the northeast and correlated with the regional Late Cretaceous - Palaeocene deformation (Berberian and Alavi-Tehrani 1977). Reconnaissance work by the author 35 km southeast of Hamadan (Figure 5.2) has established that the regional Late Cretaceous - Palaeocene deformation is the major deformation in the Hamadan Phyllite and is characterised by tight to isoclinal folds with strongly developed axial plane schistosity. The folds are moderately plunging to the east. Associated axial planar schistosity is north-northwesterly-trending and dips steeply to the east-northeast. A younger deformation in this area is characterised by crenulation cleavage which is sub-parallel to the main schistosity as has been found in the study area (see Chapter 3).

25 km south-southeast of Hamadan, strongly mylonitised syntectonic granite is exposed (Figure 5.2). The strong foliation in this pluton is sub-parallel to the main schistosity in the country rocks (Figure 5.11a, b). This syntectonic granite is considered a possible equivalent of the Galeh-Doz pluton in the study area and has probably had a similar history of generation and emplacement. S- and C-planes in this rock indicate dextral shearing as documented in the study area (Figure 5.11b). On the basis of limited structural analysis, Braud (1987) suggested that the major deformation in the northwest-trending Hamadan Phyllite and Cretaceous succession, found 60 km northeast of Kermanshah, was attributed to the Late Cretaceous - Palaeocene regional deformation.

The upper constraint to the timing of the northwest-trending regional deformation

in the Hamadan Phyllite and Cretaceous succession of the northwestern complexly deformed zone is provided by abundant granite intrusions of Palaeocene age (Valizadeh and Cantagrel 1975, see below). A regional metamorphic event is generally associated with this deformation as shown by the development of axial plane schistosity with new growth of muscovite and in places biotite. This indicates an overall greenschist to sub-greenschist facies metamorphic event as has been described for the study area (see Chapter 4).

Throughout the northwestern complexly deformed sub-zone the Cretaceous succession only has been affected by a single major deformation. The underlying angular unconformity at the base of the Cretaceous succession provides evidence of regional uplift and tilting of Hamadan Phyllite in the late Jurassic - early Cretaceous time interval. This event was also accompanied by intrusion of granites (see below). In the underlying Hamadan Phyllite deformation prior to the regional northwest-trending Late Cretaceous - Palaeocene event has been observed in several areas in the northwestern complexly deformed sub-zone. This deformation is tentatively equated with the uplift event that formed the angular unconformity at the base of the Cretaceous succession (see Chapter 6).

In the Hamadan region, Berberian and Alavi-Tehrani (1977) identified northwest-trending folds and axial planar schistosity that predated the regional Late Cretaceous - Palaeocene structures (see above). In the area 35 km southeast of Hamadan (see above), an early deformation was found characterised by recumbent isoclinal folds, not recognisable in every outcrop, with axial plane schistosity (Figure 5.11c, d). These folds plunge gently and axial plane schistosity has an east-west strike. In the study area, D_1 formed tight to isoclinal folds with an axial planar schistosity dipping to the east (see Chapter 3).

A prograde amphibolite-greenschist facies metamorphic event was associated

with D_1 in the study area (see Chapter 4). A similar metamorphic event has also been found in the Hamadan area by Berberian and Alavi-Tehrani (1977). It is therefore recognised that metamorphism of the northwestern complexly deformed sub-zone is syndeformational and related to the Late Jurassic - Early Cretaceous and Late Cretaceous - Palaeocene regional deformations. In contrast Alavi (1994) related metamorphism to extensional tectonics associated with opening of Neo-Tethys, but no evidence for extensional metamorphic complexes has been found in the present study.

Late Jurassic - Early Cretaceous metamorphism has also been established for southeastern Sanandaj-Sirjan Zone. West of Sirjan (Figure 5.1), Jurassic rocks are affected by low-grade to moderate-grade regional metamorphism which did not affect the unconformably overlying Cretaceous rocks (Ricou 1974). K/Ar ages obtained from these metamorphic rocks range from 186 to 89 Ma (Watters and Sabzehei 1970) and an additional age of 170 ± 5 Ma based on hornblende has been obtained from amphibolite (Haynes and Reynolds 1980).

Tillman et al. (1981) studied a region of 5000 km^2 near Esfahan in the northwestern part of the Sanandaj-Sirjan Zone. They divided the region into three tectonic blocks which are separated from each other by northwest-trending high-angle reverse faults with an additional component of dextral strike-slip translation. They interpreted these structures as having formed in an earlier rift event as part of a horst and graben terrain associated with deposition of Triassic-Jurassic rocks. The faults were inverted during convergence prior to the Aptian-Albian interval, with folding of each basin (Tillman et al. 1981). Tillman et al. regarded the basement rocks of the horsts as Precambrian in age but these are now recognised as equivelents of the June Complex and of Triassic age (see Chapters 2 and 5).

Mesozoic-Cainozoic intrusive rocks of the complexly deformed sub-zone

One of the distinctive features of the Sanandaj-Sirjan Zone is that it contains Mesozoic-Cainozoic plutonic rocks that do not occur in the Zagros Fold-Thrust Belt. By contrast, most plutonic rocks in central Iran are of Cainozoic age. The plutonic rocks of the Sanandaj-Sirjan Zone are mainly granites and are all located in the complexly deformed sub-zone. In the northwestern complexly deformed zone these plutonic rocks are divided into two groups: plutons of Late Jurassic age and plutons of Late Cretaceous - Palaeocene age. In the southeastern complexly deformed sub-zone plutonic rocks of Triassic age have also been reported (Sabzehei 1974; Berberian 1977; Davoudzadeh and Weber-Diefenbach 1987); but more work is required to establish the age of these rocks.

Late Jurassic plutonic rocks of the complexly deformed zone are less abundant than younger plutonic rocks. The Almugulakh Diorite, 30 km northwest of Hamadan, (Figure 5.1, locality number 1) is dated at 144±17 Ma by the Rb/Sr method and therefore has an age close to the Jurassic-Cretaceous boundary (Valizadeh and Cantagrel 1975). The Golpaygan granodiorites, 15 km north of Golpaygan (Figure 5.1, locality number 2), have intruded the Hamadan Phyllite and clasts derived from them are found in the basal conglomerate of the Early Cretaceous succession which disconformably overlies the granodiorite (Thiele et al. 1968). 30 km southeast of Esfahan, the Kolah-Gazi Granite is overlain by the basal conglomerate of the Aptian-Albian succession (Figure 5.1, locality number 3). Small stocks of diorite in the Dehbid area (Figure 5.1, locality 4) and others ranging from granite to gabbro are exposed to the southwest of Shahrbabak (Figure 5.1, locality 5, Berberian and Berberian 1981).

Most of the Late Cretaceous - Palaeocene intrusive bodies are exposed in the Hamadan-Borujerd region of the northwestern complexly deformed sub-zone and range

in composition from gabbro to granite. The main granites are at Alvand, Borujerd, Astaneh, Aligudarz, Bouin-Miandasht and Hasn-Robat (Figures 5.1, 5.10). All these granites and granodiorites have elliptical outcrop patterns that are elongate in a northwest-southeast direction.

The Alvand Norite in the Hamadan region is dated at 88.5-78.5 Ma (Rb/Sr method) and 89.1±3 (K/Ar method); granites in the same region are dated at 65±2 Ma (Rb/Sr method) and 81±3 (K/Ar method; Valizadeh and Cantagrel 1975) with one of Early Palaeocene age dated at 64 Ma (K/Ar method, Braud 1987). 80 km to the northwest of Hamadan, a gabbro batholith, 30 km long and 10 km wide, has intruded the Hamadan Phyllite. K/Ar dates indicate an age of 38-40 Ma (Braud 1987). Clasts of these granites occur in Oligocene basal conglomerate in the Kermanshah region.

The granite to granodiorite at Borujerd has intruded the Hamadan Phyllite and is thought to be the same age as the Alvand Norite (Hajmolla-Ali et al. 1989). In the southeastern extremity of the Borujerd Granite, at Nezam-Abad village, this granite has been dated by the K/Ar method at 100 Ma (Cretaceous) and granodiorite and quartz diorite in the same area has been dated at 43-51 Ma (Farhadian 1991).

In the Aligudarz area, the Aligudarz Granite has intruded the Hamadan Phyllite and has also contact metamorphosed the basal conglomerate of the Aptian-Albian succession indicating an age younger than Aptian-Albian, possibly Late Cretaceous (Soheili et al. 1992). Farther southeast, the Bouin-Miandasht Granite (40 km south of Golpaygan) has intruded the equivalent rocks of the June Complex. This granite is identified as a calc-alkaline I-type granite based on mineralogy and Na_2O/K_2O relations and is thought to be of Late Cretaceous age (Valizadeh and Gasemi 1993).

Little detailed geochemical and petrological analysis has been undertaken on the granitic intrusions in the Sanandaj-Sirjan Zone.

Cainozoic successions

Cainozoic successions are not restricted to individual sub-zones but have their greatest extent along the southwestern margin of the Sanandaj-Sirjan Zone. In general, apart from alluvium and colluvium, Cainozoic successions are largely absent from the complexly deformed sub-zone. These Cainozoic rocks are considered to have formed as part of a continuous sedimentary basin that developed throughout the southwestern border of the Sanandaj-Sirjan Zone and has been filled with Palaeocene, Eocene and younger rocks.

In the Kermanshah region, the ophiolite, radiolarite and Bistoon sub-zones are overlain unconformably by Eocene basal conglomerate and volcanic rocks (see ophiolite sub-zone above). 60 km north-northeast of Kermanshah, the Eocene succession is well exposed (after Braud 1987) and consists of a basal conglomerate that contains abundant radiolarite clasts. The conglomerate is overlain by basalt and spilite, with pillow structures, that are overlain by volcaniclastic rocks, which are in turn overlain by pelagic red limestone. The limestone contains foraminifers, including *Globigerina* and *Globorotalia*, that indicate a late Palaeocene - Eocene age (Braud 1987). The Eocene volcanic rocks and limestone are associated with several mafic intrusions. These exposures are representative of the rocks found in the Palaeocene-Eocene succession of the Kermanshah region and extending northwestwards to Sanandaj (Figure 5.2). The Palaeocene-Eocene succession is conformably overlain by a succession of Miocene turbidites consisting of shale and sandstone (Braud 1987).

In the Dorud-Azna region (Figures 1.2, 5.7 cross sections EF and GH), the stratigraphy of a Eocene, Oligocene and Miocene succession has not been established but is known to consist of volcanic rocks, marl and marly limestone (Soheili 1992). These rocks are faulted against the radiolarite sub-zone. Between the Dorud-Azna region and the Neyriz region the Tertiary succession is locally present but has not

been documented in the literature. It has been mapped in the Eglid region (Houshmandzadeh et al. 1975) and the Shahrekord region (Zahedi et al. 1992).

In the Neyriz region, the Cainozoic strata are mostly Eocene and consist of turbidites with olive green sandstone, shale and conglomerate (Sabzehie and Eshragi 1995). The conglomerate contains abundant limestone olistoliths mostly derived from Cretaceous rocks that occur in the complexly deformed sub-zone to the northeast.

The Neogene Bakhtiari Formation is dominated by continental conglomerates and occurs along the northeastern side of the Zagros Fold-Thrust Belt (see Figure 5.12, after James and Wynd 1965; Stoneley 1975). Alavi (1994) has suggested that these conglomerates were synorogenic and derived from the uplifted Sanandaj-Sirjan Zone. Throughout the southwestern Sanandaj-Sirjan Zone, Neogene rocks are dominated by continental conglomerates and are also called the Bakhtiari Formation (Figure 5.8, after Braud 1987; Houshmandzadeh et al. 1975; Sabzehie and Eshragi 1995).

Cainozoic rocks in the southwestern Sanandaj-Sirjan Zone have been openly folded and dislocated along thrust faults. In the Kermanshah region, the Cainozoic rocks are strongly sheared and faulted subparallel to the major thrust faults (Figure 5.2). The timing of the deformation of the Palaeocene-Miocene succession is constrained to after the Miocene when all marine conditions in the Sanandaj-Sirjan Zone were terminated. Deformation must have been synchronous with deposition of Neogene strata. As noted for the Kermanshah-Borujerd region, allochthons of the Bistoon sub-zone (e.g. Garin unit) and the marginal sub-zone (Chagalvandi nappe) were emplaced by Tertiary thrusting onto the Zagros Fold-Thrust Belt.

The common absence of early Cainozoic successions in the complexly deformed sub-zone and restriction of these successions to the southwestern border of the Sanandaj-Sirjan Zone implies uplift of the former during the Cainozoic era. It is inferred that the early Cainozoic successions formed a foreland basin marginal to the

uplifted complexly deformed sub-zone. This is consistent with the presence of limestone clasts derived from the complexly deformed sub-zone in clastic rocks of the Cainozoic succession in the Neyriz region (see above).

5.3 DISCUSSION

The major palaeogeographic and tectonic event associated with the development of the Sanandaj-Sirjan Zone has been the formation of Neo-Tethys and its subsequent destruction during continental collision. Formation of Neo-Tethys in the southwestern part of the Sanandaj-Sirjan Zone has been interpreted as occurring in the Late Permian - Early Triassic and disrupted the continuous Palaeozoic succession in the northeastern part of Gondwana-Land (Şengör et al. 1988). Middle-Late Triassic to Jurassic successions of the Sanandaj-Sirjan Zone (complexly deformed sub-zone) contain abundant mafic igneous rocks (e.g. June Complex and its equivalents) and a marine turbidite succession (Hamadan Phyllite) in addition to abundant andesitic volcanic rocks in the marginal sub-zone. In contrast, the Mesozoic successions of the Zagros Fold-Thrust Belt are characterised by shallow-marine rocks with no associated igneous rocks (James and Wynd 1965; Stöcklin 1968).

A number of issues need to be addressed with respect to the geologic and tectonic history of the Sanandaj-Sirjan Zone. Firstly, the location of the Zagros suture has been debated in the literature. Secondly, the palaeogeography of the zone has not been previously clearly formulated and is now more apparent using the sub-zone subdivision applied above. Thirdly, the structural and metamorphic history has been misinterpreted and poorly documented in the past.

Zagros suture

The Zagros suture separates the passive continental margin of the Zagros Fold-

Thrust Belt (Haynes and McQuillin 1974; Berberian and King 1981) from tectonic elements to the northeast in central Iran. The Zagros suture has been traditionally recognised as occurring along the southwestern margin of the Sanandaj-Sirjan Zone (e.g. Berberian and King 1981) and is supported by this work. In contrast, Alavi (1994) inferred that the Zagros suture is located at the northeastern border of the Sanandaj-Sirjan Zone at the contact with the Urumieh-Dokhtar Magmatic Assemblage. Alavi suggested that the ophiolites of the Kermanshah and Neyriz regions had covered the passive continental margin, that included both the Sanandaj-Sirjan Zone and the Zagros Fold-Thrust Belt, and that intense thrust tectonics affected the region. The ophiolite outcrops in the Neyriz and Kermanshah regions are located 200 km southwest of the Urumieh-Dokhtar Magmatic Assemblage apparently indicating over 200 km of thrust transport prior to final disruption to form the present outcrop pattern. As much as 100 km of this shortening must have been achieved since the Miocene according to the structural model of Alavi (1994). These estimates of considerable thrust shortening seem excessive and do not match the structural history of the Sanandaj-Sirjan Zone as described in this work. Alavi (1994) also regarded the radiolarite succession along the southwestern border of the Sanandaj-Sirjan Zone as disrupted components of the ophiolite complex.

Alavi and Mahdavi (1994) argued that the location of the traditional Zagros suture, as supported in this work, separates similar metamorphosed and non-metamorphosed rock assemblages in the Nahavand-Borujerd region (e.g. the Garin unit west of Borujerd and the Chagalvandi nappe south of Borujerd). Therefore, they felt that either the main suture was at the northeastern border of the Sanandaj-Sirjan Zone or was deeply buried by thrust sheets in the Nahavand-Borujerd region.

In this thesis, the Zagros suture is recognised as being located along the southwestern margin of the ophiolite sub-zone but to the northwest of the radiolarite

and Bistoon sub-zones. Ophiolites are only recognised in the Neyriz and Kermanshah regions, elsewhere the suture occurs at the southwestern contact of the marginal sub-zone and is a faulted contact between it and the Zagros Fold-Thrust Belt. As has been documented for the Yarlung-Zangbo suture in the Himalayas (Burg and Chen 1984) the Zagros suture is not always marked by the presence of oceanic units such as ophiolites.

Stratigraphic evolution of the Sanandaj-Sirjan Zone

The radiolarite and Bistoon sub-zones have been positioned from the Late Triassic until the Late Cretaceous as two components of the distal part of the passive continental margin of the Arabian platform (after Kazmin et al. 1986; Bernoulli et al. 1990). Thus the radiolarite sub-zone is not regarded as the site of the Zagros suture. The radiolarite succession indicates deepening over time and is regarded as having formed on continental crust that was being attenuated rather than having always formed in a deep-marine environment. The Bistoon sub-zone is presently located northeast of the radiolarite sub-zone and is interpreted as the capping of an outer shallow bank of the passive margin.

The Late Jurassic - Early Cretaceous volcanic rocks of the marginal sub-zone are extensively developed along the southwestern boundary of the complexly deformed sub-zone and represent a major volcanic accumulation. Alavi (1994, p. 221, 232) has interpreted these volcanic rocks as part of a former forearc basin located along the southwestern border of the Urumieh-Dokhtar Magmatic Assemblage. In this interpretation, the volcanic succession, as for the ophiolite sub-zone, has been transported by major low-angle thrust faults over 150 km to their present location. The volcanic rocks of the marginal sub-zone, however, cannot be a forearc basin succession to the Urumieh-Dokhtar Magmatic Assemblage as the rocks of the latter

are no older than middle Eocene (Dimitrijevic 1973) whereas the volcanic rocks of the marginal sub-zone are overlain, at an angular unconformity, by an Aptian-Albian succession (see above). Thus the volcanic activity in the marginal sub-zone ceased prior to the Aptian-Albian and is unrelated to that of the Urumieh-Dokhtar Magmatic Assemblage. It is suggested that the volcanism of the marginal sub-zone is related to closure and subduction of Neo-Tethys (see Chapter 6).

The complexly deformed sub-zone consists of a thick sequence of Middle-Late Triassic - Jurassic rocks which were originally deposited in shallow-marine environments but by the Jurassic had changed to deep-marine environments of deposition. Mafic and silicic igneous activity occurred throughout the shallow-marine phase of deposition. This history is related to opening of Neo-Tethys and was produced in an extensional setting (see Chapter 6). The angular unconformity at the base of the Aptian-Albian succession in the complexly deformed sub-zone reflects uplift of the sub-zone and is related to a change in the tectonic pattern from extensional to convergent activity. Late Jurassic granitoids intruded in the Middle-Late Triassic - Jurassic successions reflect a new phase of magmatic activity accompanying the new tectonic regime (see Chapter 6).

The Cainozoic successions have been deposited in a basin between the uplifted complexly deformed sub-zone and the uplifted frontal sub-zones. The mafic volcanism and deep-water turbidite deposition of the Palaeocene-Eocene succession in the marginal sub-zone did not occur in the early Cainozoic rocks of the Zagros Fold-Thrust Belt (Figure 5.12). It is suggested that the Cainozoic basin of the southwestern Sanandaj-Sirjan Zone represented a marginal foreland basin subparallel to the Zagros Fold-Thrust Belt. The source of the mafic volcanism in this setting is anomalous and presumably is related to a general relaxation of convergence in the early Cainozoic.

Structural history of the Sanandaj-Sirjan Zone

Three main phases of deformation are recognised in the Sanandaj-Sirjan Zone: (1) Late Jurassic - Early Cretaceous uplift, intense ductile deformation and local amphibolite facies metamorphism, (2) Late Cretaceous - Palaeocene regional deformation and associated greenschist facies metamorphism, and (3) Cainozoic regional thrusting and associated folding. Plutonism was associated with the first and second deformation events in addition to regional metamorphism.

The first deformation includes the D_1 deformation of the study area and related deformation recognised in the northwestern complexly deformed sub-zone. Owing to the intensity of the second regional deformation structures related to the first deformation are less clearly recognised. The impressive sub-Cretaceous unconformity throughout the northwestern complexly deformed sub-zone is tentatively related to the ductile D_1 event of the study area. During the hiatus of the unconformity Late Jurassic - Early Cretaceous plutons were intruded. Deformation at about this time is also recognised in the marginal sub-zone where an unconformity occurs at the base of a mid-Cretaceous succession. In contrast, no deformation of this timing is recognised in the radiolarite and Bistoon sub-zones.

The second event was the major episode of deformation in the Sanandaj-Sirjan Zone and produced the pervasive west-northwesterly trending structures in the zone. Timing of the second deformation is consistent with the obduction of the ophiolites over the Zagros Fold-Thrust Belt as shown by clasts in the Maastrichtian-Palaeocene Amiran Formation (Braud 1987; Motiei 1993). Additionally, tectonic instability in the foreland in the Late Cretaceous in the Kermanshah region is related to foreland loading, flexing of the lithosphere and uplift of a perpherial bulge as the thrust sheets were emplaced southwards. The tectonic instability is shown by the deposition of olistoliths derived from the Zagros Fold-Thrust Belt (see radiolarite sub-zone).

Similar relationships are documented in western Newfoundland where limestone breccias of the Humber Arm allochthon represent the changeover from passive distal margin to foreland loading associated with the initiation of thrusting (see Cawood et al. 1988, p. 27).

Alavi (1994) inferred that the major deformation in the Sanandaj-Sirjan Zone produced large-scale composite duplex structures and imbricate thrust systems increasing in intensity to the northeast. In contrast, structural analysis of the study area in addition to the reconnaissance observation in the northwestern part of the Sanandaj-Sirjan Zone indicate that the major deformation in the complexly deformed sub-zone is reflected by map-scale west-northwesterly trending folds. These tight to isoclinal folds have a pervasive axial plane schistosity/cleavage steeply dipping to the north-northeast indicating vergence to the south-southwest.

In contrast to the inner complexly deformed sub-zone, imbricate thrust systems are widely developed in the outer part of the orogen where thrust sheets of the marginal, Bistoon, ophiolite and radiolarite sub-zones abound. This major thrust event was generated from continental collision (see Chapter 6). The implication is that at least the outer part of the Sanandaj-Sirjan Zone has a thin-skinned structural style (cf. Alavi 1994). It is clear from this work that the metamorphic rocks of the complexly deformed sub-zone have been brought to the surface from mid-crustal depths and that the deformation within the sub-zone was of a more thick-skinned character than that in the outer sub-zones.

The third regional deformation is a continuation of the thrusting that occurred in the outer Sanandaj-Sirjan Zone and has involved strata as young as Pliocene. This thrusting must also be thin-skinned in character and it is likely, although yet to be confirmed by detailed structural analysis, that the open upright folds identified in Cainozoic successions are fault-related, fault-bend and fault-propagation folds.

Considerable thrust activity is reflected by the thrust sheets (nappes) of the marginal, Bistoon and radiolarite sub-zones. During the younger deformation the inner part of the orogen has acted as a coherent mass ("tectonic bulldozer") that has pushed outward the rocks of the outer sub-zones and transported them over the Zagros Fold-Thrust Belt. Deformation in the inner part of the orogen (complexly deformed sub-zone) is characterised by mostly ductile deformation dominated by polydeformed and metamorphosed rocks that have been intruded by granitic rocks and have apparently not been affected by Cainozoic deformation.

5.4 CONCLUSIONS

Stratigraphic and structural variations in each sub-zone of the Sanandaj-Sirjan Zone reflect the tectonic significance of each sub-zone during tectonic evolution. The southwestern-most radiolarite sub-zone with shallow- to deep-marine rocks formed in a basin developed adjacent to the passive continental margin of the Arabian platform. It developed adjacent to the Bistoon sub-zone to the northeast which formed as a carbonate platform isolated from any terrigenous inputs. Several lines of evidence, including the continuous succession of the radiolarite sub-zone from the Late Triassic to the Late Cretaceous containing marine strata with olistoliths derived from the Zagros Fold-Thrust Belt and the transitional carbonate to radiolarite succession found in part of the Bistoon sub-zone, indicate that these sub-zones formed southwest of the Zagros suture. Therefore, the Late Triassic - Late Cretaceous successions of the radiolarite and Bistoon sub-zones are considered to reflect two different depositional settings in the distal passive continental margin (see also Kazmin et al. 1986).

The Sanandaj-Sirjan Zone and Zagros Fold-Thrust Belt have dissimilar Mesozoic successions. The Zagros suture occurs near the southwestern boundary of the Sanandaj-Sirjan Zone and is a major stratigraphic discontinuity between passive

(Zagros Fold-Thrust Belt) and active (Sanandaj -Sirjan Zone) continental margins of Neo-Tethys (see Chapter 6).

Extensive ductile complex folding, associated with metamorphism, affects the complexly deformed sub-zone and several deformation episodes are observed (see Chapter 3). The first deformation affected the Middle Triassic - Jurassic successions of the June Complex and Hamadan Phyllite but does not affect overlying Cretaceous successions. This deformation is partially overlapping in age with the formation of a vast accumulation of volcanic rocks in the marginal sub-zone along the southwestern border of the complexly deformed sub-zone. It is also similar in timing to the intrusion of Late Jurassic granitic plutons in the complexly deformed sub-zone.

Despite local faults at the contact of the Hamadan Phyllite and the overlying Cretaceous succession, the contact is mainly an angular unconformity and a similar unconformity occurs in the marginal sub-zone. This unconformity has not been recognised in the Zagros Fold-Thrust Belt where the Neocomian conformably overlies the Jurassic rocks (near Shiraz) with a transitional contact (Motiei 1993). The unconformity is related to folding and regional uplift including tentatively the D_1 deformation of the study area.

The major regional deformation of the Sanandaj-Sirjan Zone was of Late Cretaceous - Palaeocene age and produced pervasive west-northwest trending structures. These structures are typically verging to the south-southwest and are associated with uplift of the radiolarite, Bistoon and marginal sub-zones by thrusting which is related to continental collision (Chapter 6). Abundant plutons were emplaced during and after the second major deformation (see Chapter 3).

Metamorphism was associated with the first and second regional deformations with metamorphic minerals forming axial plane schistosities (see Chapter 4). In contrast to the suggestion of Alavi and Mahdavi (1994), it is emphasised that the

metamorphic rocks of the complexly deformed sub-zone all occur on the northeastern side of the Zagros suture.

Cainozoic successions along the southwestern border of the Sanandaj-Sirjan Zone have been affected by deformation as young as Pliocene and Quaternary. The synorogenic clastic rocks of the Zagros Fold-Thrust Belt (Figure 5.12, see also Alavi 1994, figure 17) show two distinct intervals of development: a Late Maastrichtian - Palaeocene - early Eocene interval, and a Pliocene-Quaternary interval. Both events are related to continental collision and crustal thickening associated with continuing convergence along the collision zone (see Chapter 6).

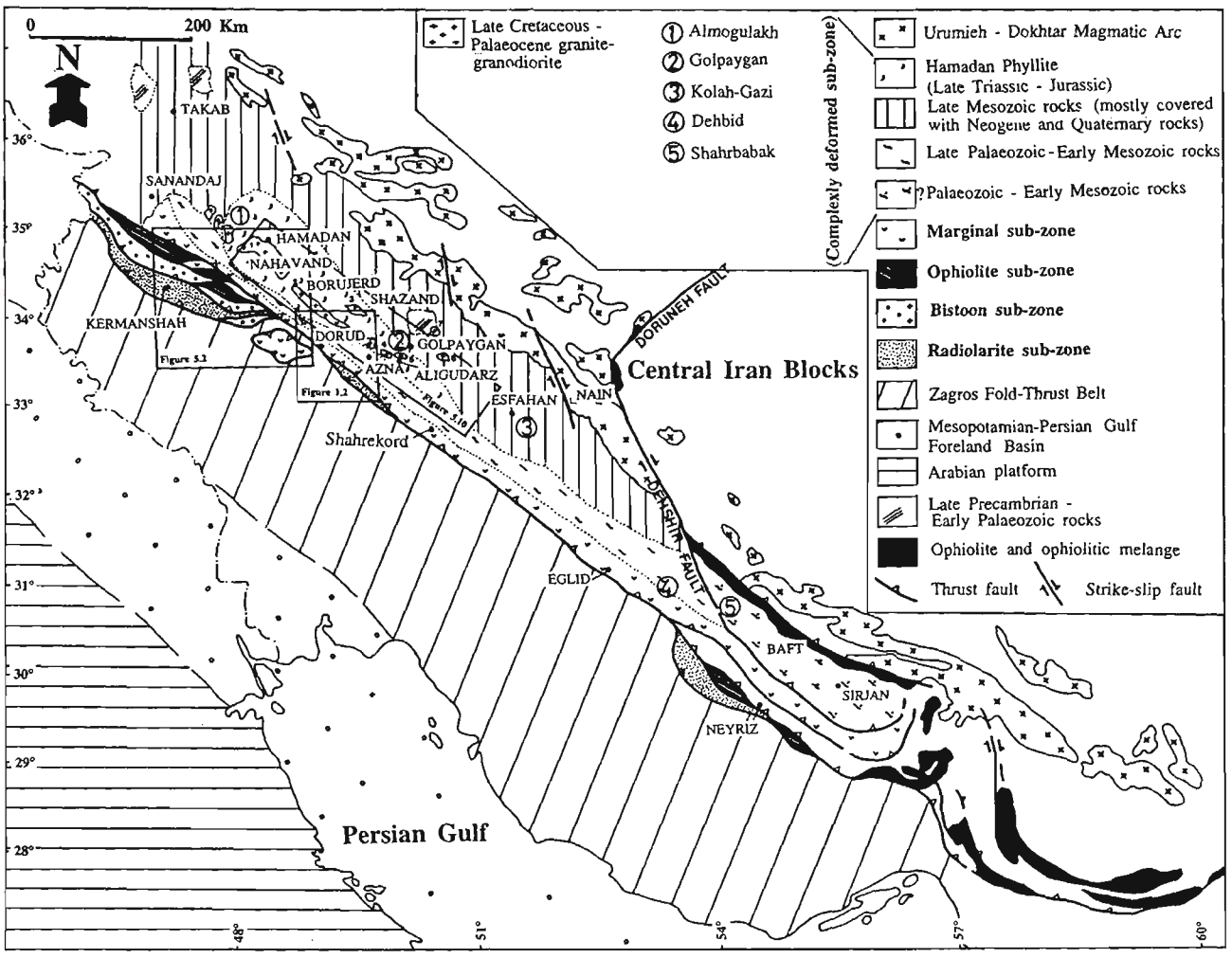

Figure 5.1 Tectonic subdivision of the Sanandaj-Sirjan Zone.

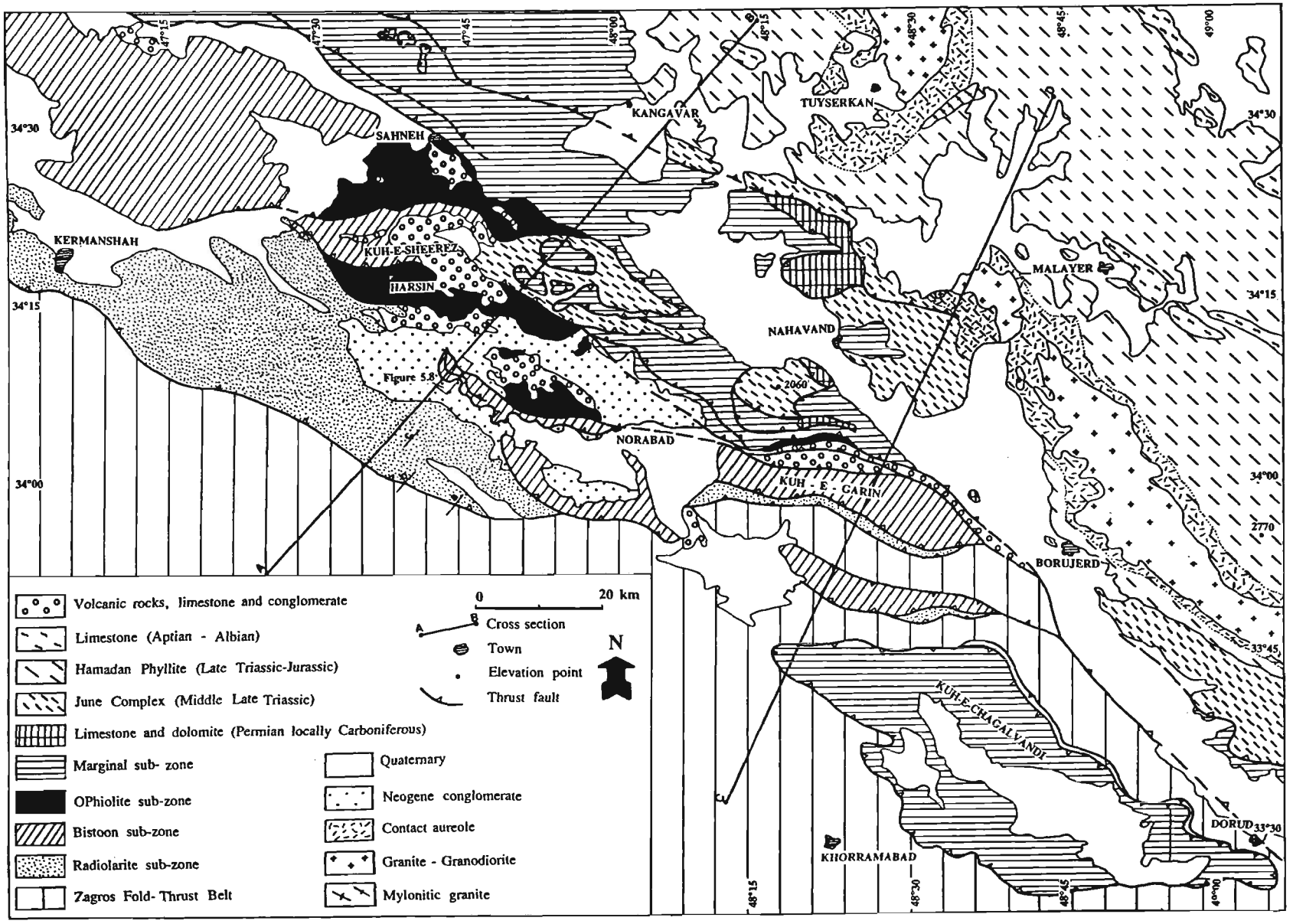

Figure 5.2 Tectonic map of the Kermanshah area.

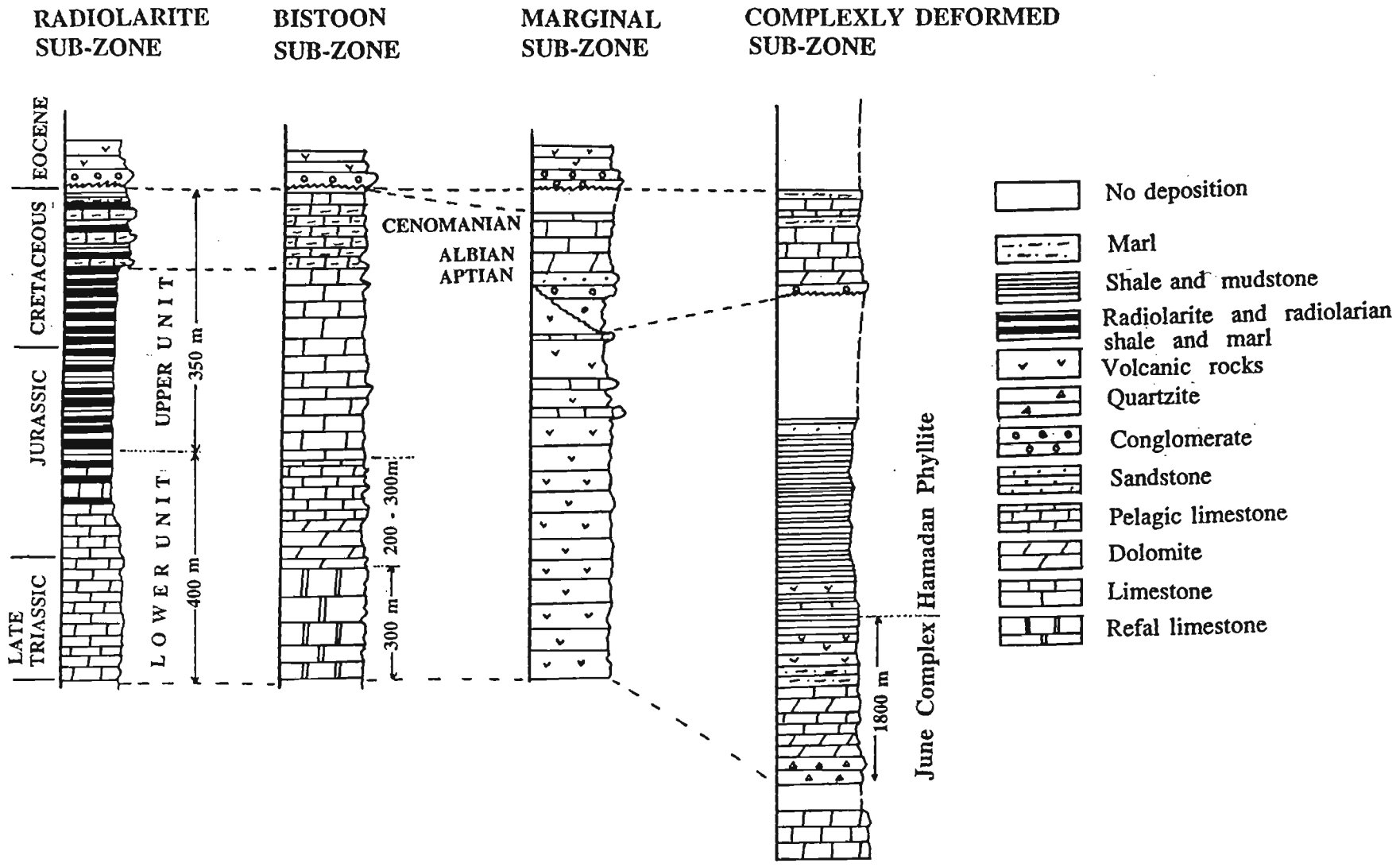

Figure 5.3 Stratigraphic columns of sub-zones in the Sanandaj-Sirjan Zone. (Note columns are not to scale.)

Figure 5.4

(a) Olistolith of limestone from the Zagros Fold-Thrust Belt (Tarbur Formation) in the radiolarite sub-zone. A bedding trace is evident in the limestone block. The right lower darker part is radiolarite surrounded by limestone. Hammer is located on the contact of radiolarite and limestone. The block is 6 m across. Location is 60 km south-southeast of Kermanshah.

(b) Radiolarite and radiolarian shale. 50 km south-southeast of Kermanshah. Note the tight overturned folds with southwest vergence.

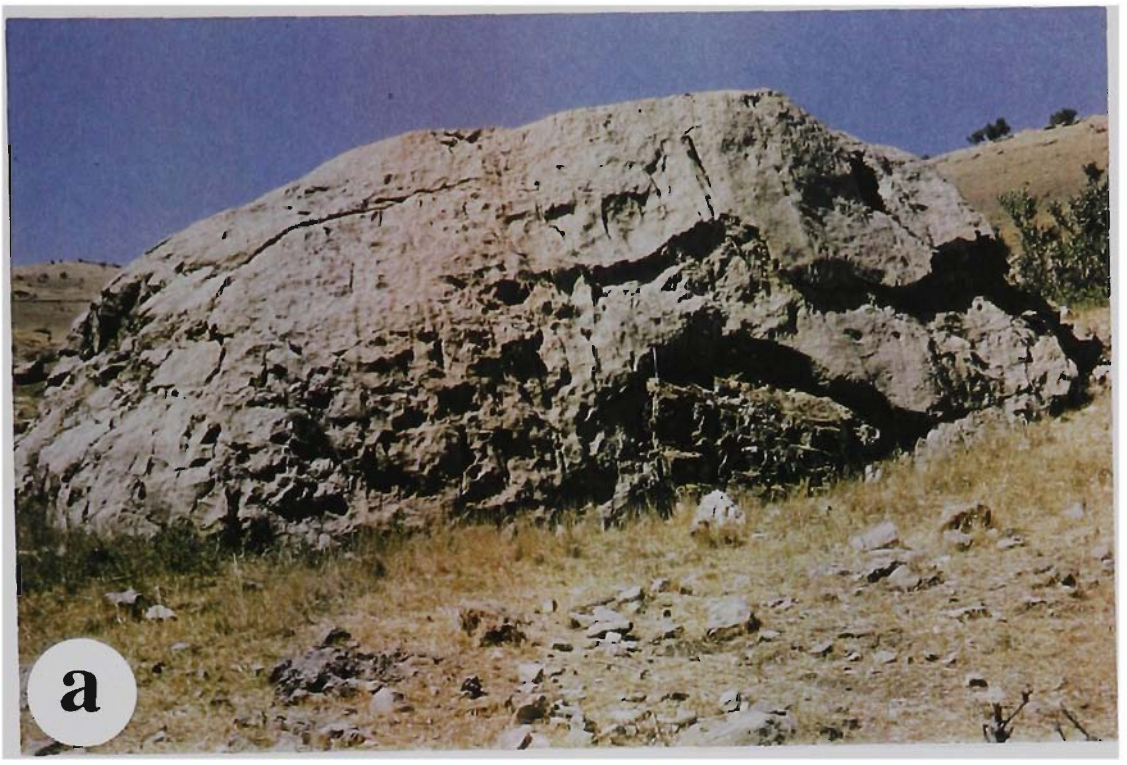
a

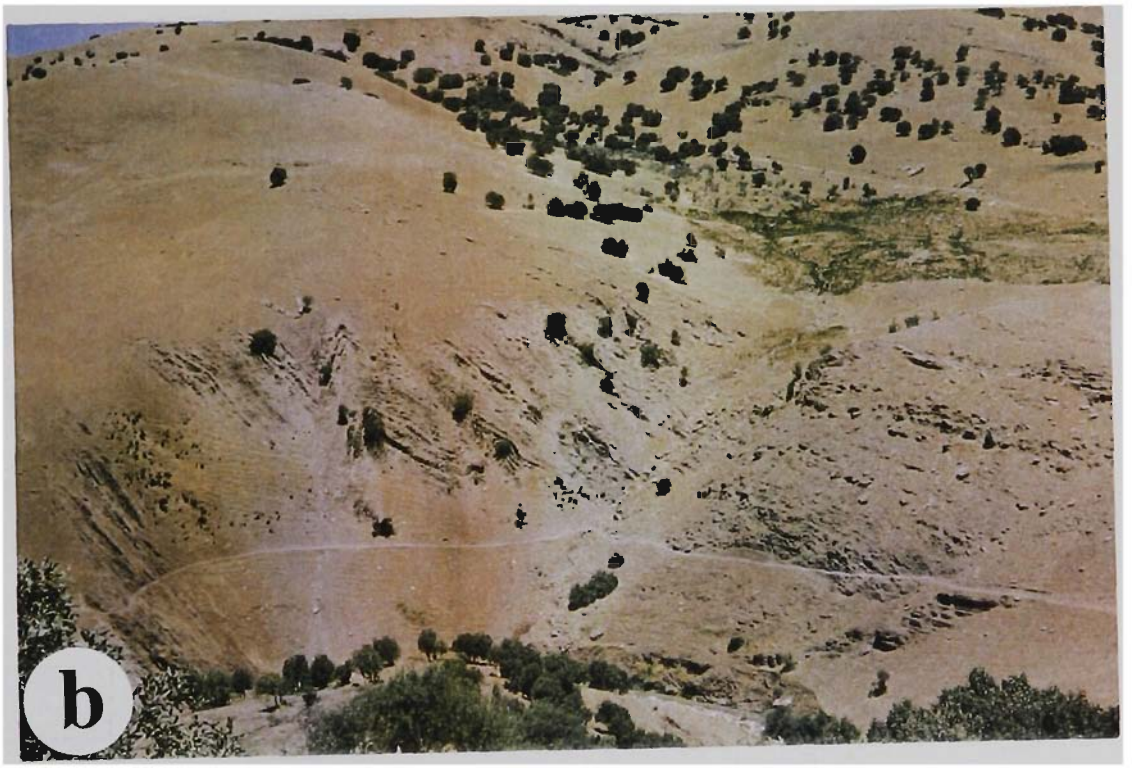
b

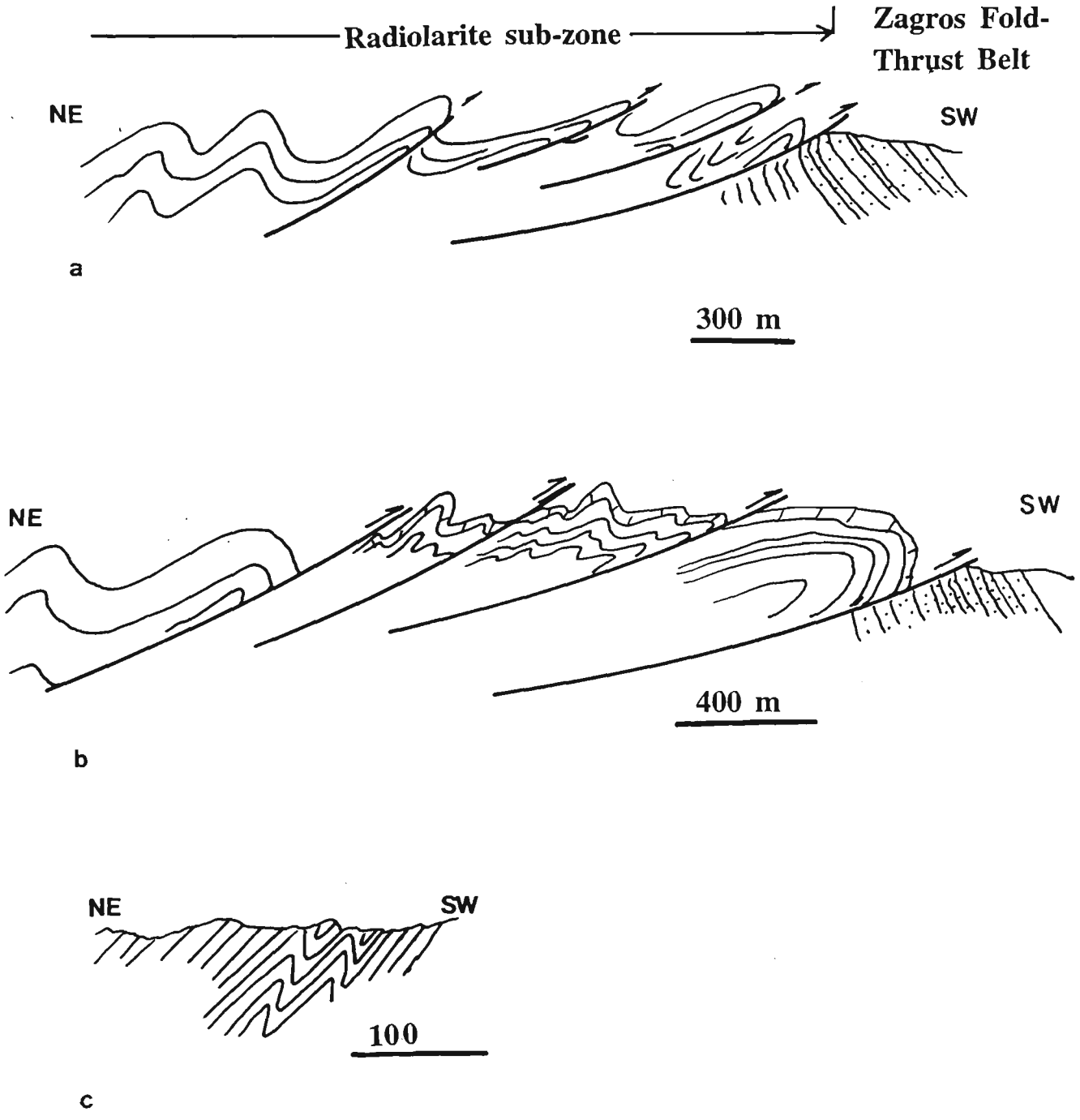

Figure 5.5 Cross-sections of the radiolarite sub-zone: (a), (b) in the vicinity of the Zagros Fold-Thrust Belt, and (c) in the central part of the sub-zone (see Figure 5.2 for locations). Horizontal scale = vertical scale.

Figure 5.6 Thrust sheet of the radiolarite sub-zone overlying the Zagros Fold-Thrust Belt, and thrust sheet of Eocene marly limestone overlying the radiolarite sub-zone. 20 km southwest of Azna, looking from east to the west. The panorama photograph is 1 km across.

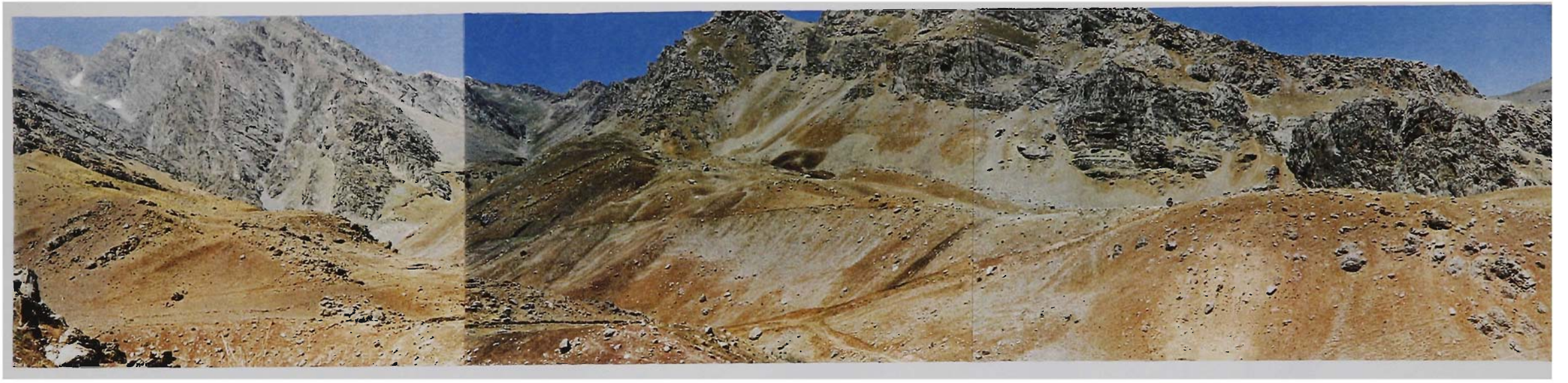

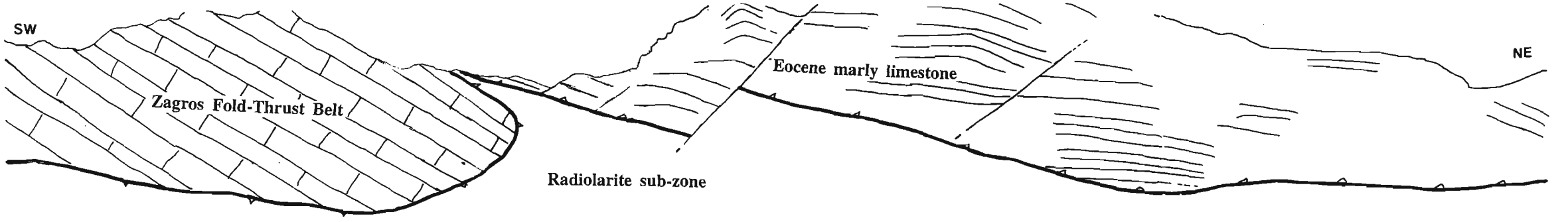
SW
Zagros Fold-Thrust Belt
Radiolarite sub-zone
Eocene marly limestone
NE

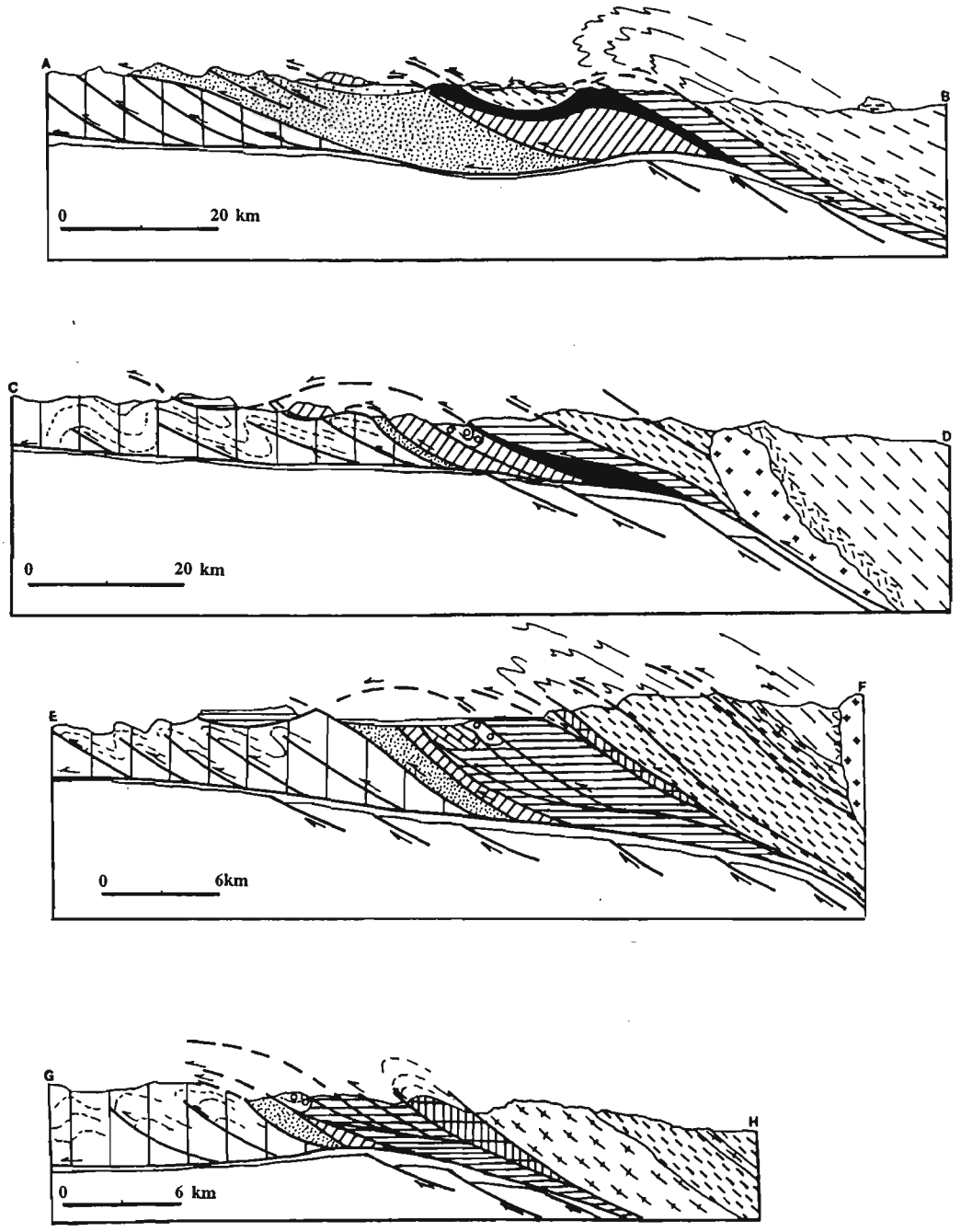

Figure 5.7 Cross-sections, see (AB and CD in Figure 5.2, EF and GH in Figure 1.2 in Chapter 1 for the location). Scale for horizontal.

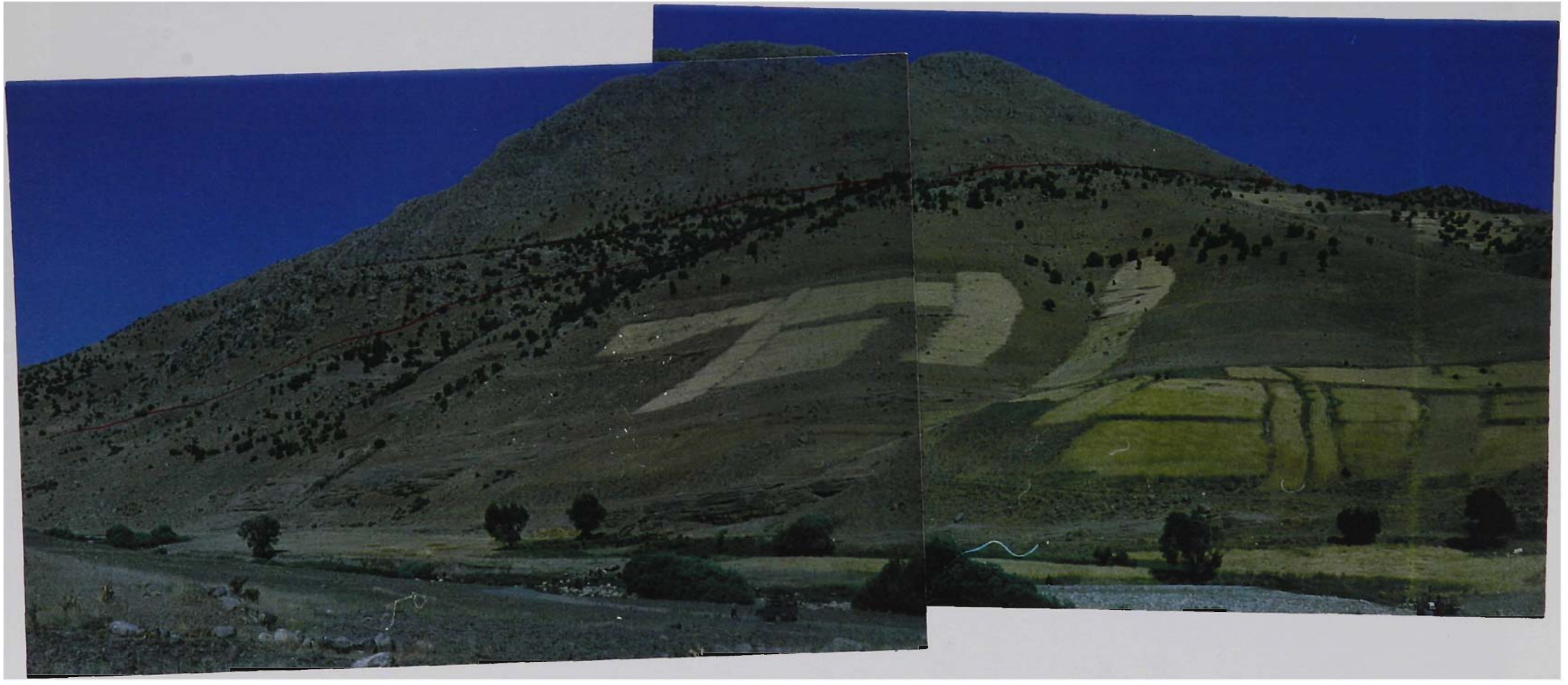

Figure 5.8 Thrust of the Bistoon sub-zone over the Pliocene Bakhtiari Formation. Photograph is 500 m across, looking from west to the east, 25 km west of Norabad (see Figure 5.2 for location).

Figure 5.9

(a) Pillow lava in ophiolite melange. 10 km west of Norabad. Lens cap is 5.5 cm in diameter.

(b) Chevron folds in pink micritic limestone. 10 km west of Norabad. Lens cap is 5.5 cm in diameter.

(c) Sheared micritic limestone with chert bands. 10 km west of Norabad. Lens cap is 5.5 cm in diameter.

(d) Marker conglomerate horizon (40-50 cm) thick with iron oxide pisoliths. 15 km northeast of Sahneh. Hand lens is 4 cm long.

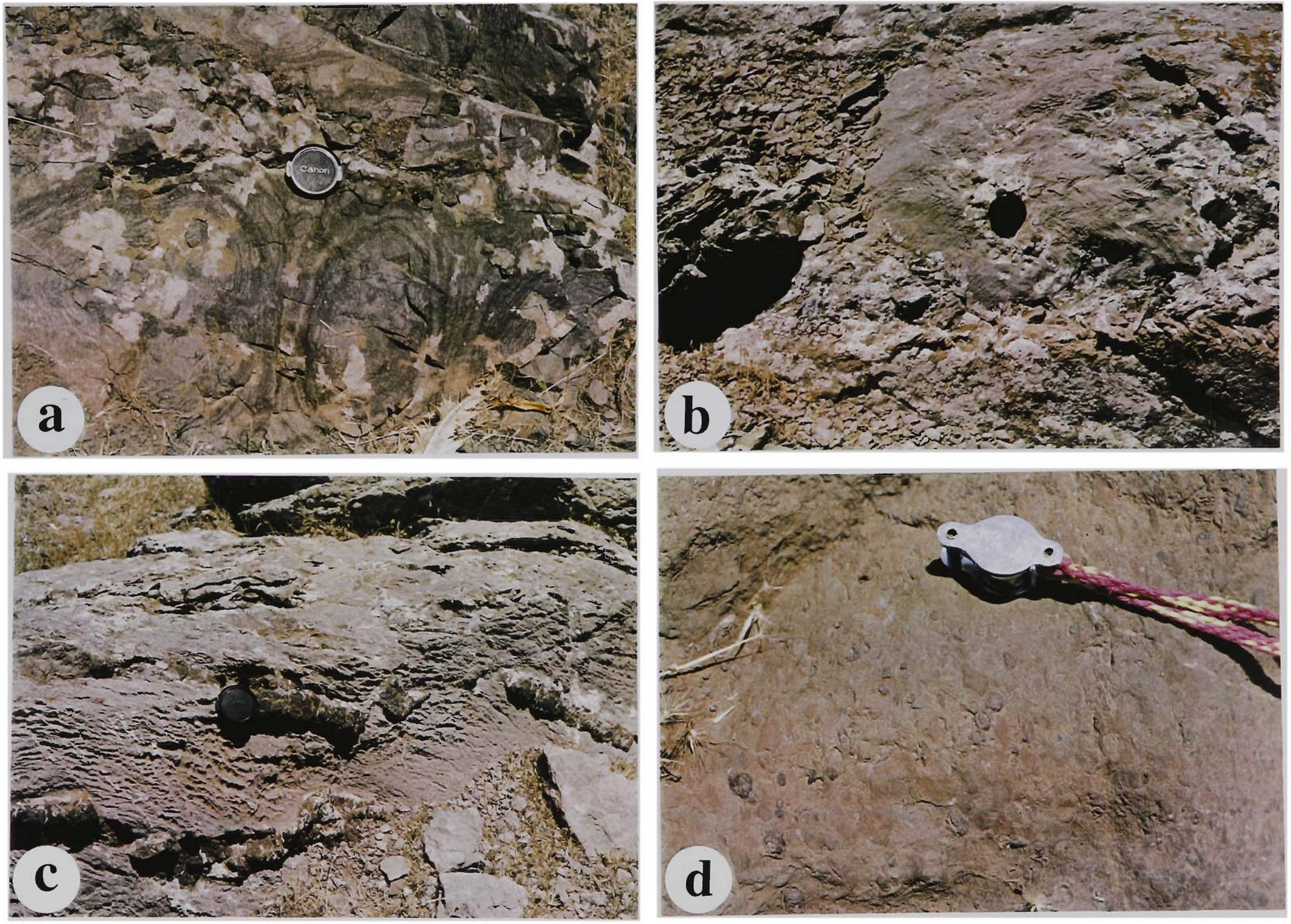
a
b
c
d

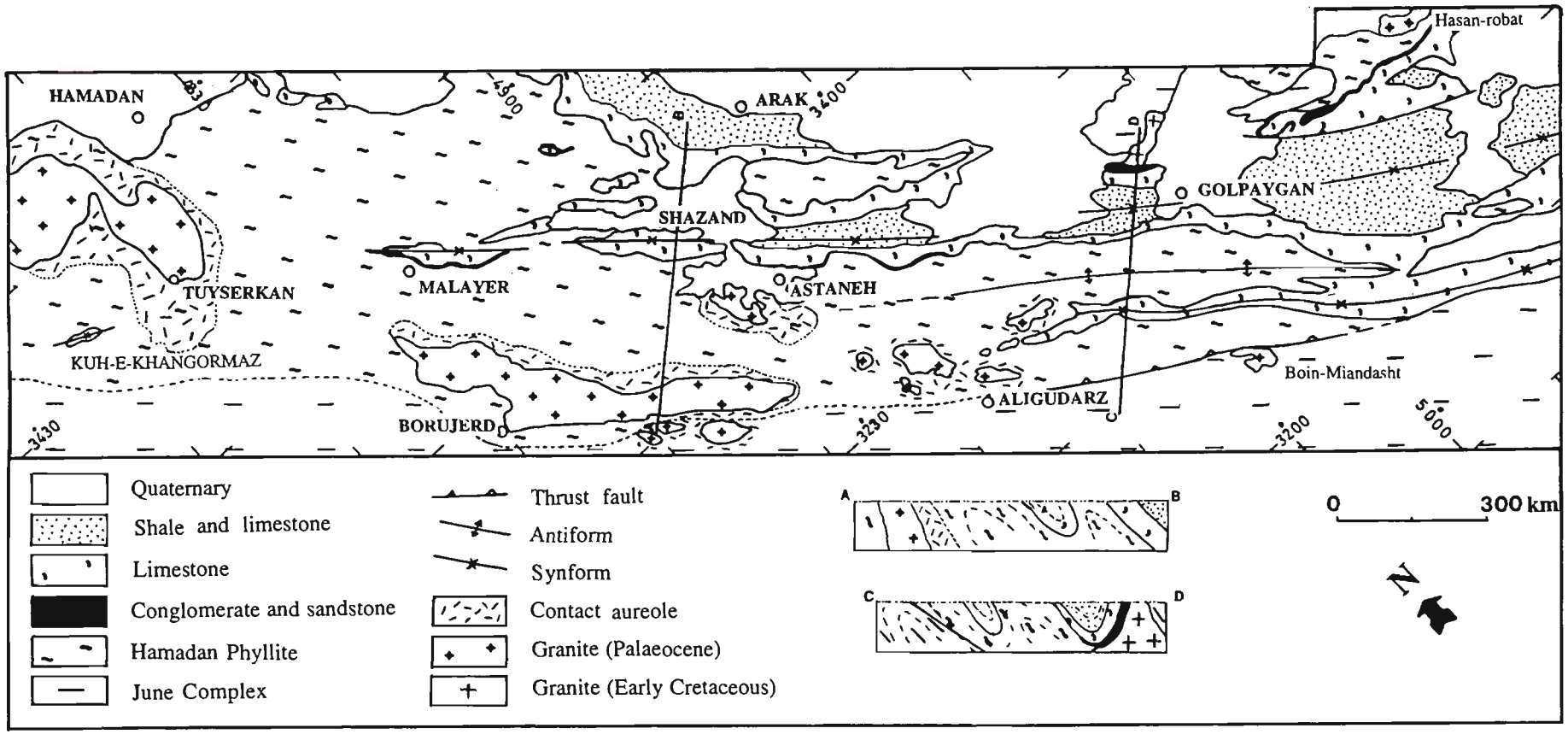

Figure 5.10 Generalised geological map of northwestern complexly deformed sub-zone showing the distribution of the Hamadan Phyllite and overlying Cretaceous successions and Palaeocene granite intrusions.

Figure 5.11

(a) Disharmonic isoclinal folds in andalusite-garnet schist. 35 km south-southeast of Hamadan. Lens cap is 5.5 cm across.

(b) Disharmonic isoclinal folds in quartz vein in the andalusite-garnet schist. 35 km south-southeast of Hamadan. Hand lens is 4 cm long.

(c) Mylonitic granitic gneiss. The dyke intruded in the gneiss and foliated with the same foliation existing in the gneiss. 25 km south-southeast of Hamadan. Compass is 15 cm long.

(d) Close view from the same mylonitic granitic gneiss in c. Pen cap is 6 cm long.

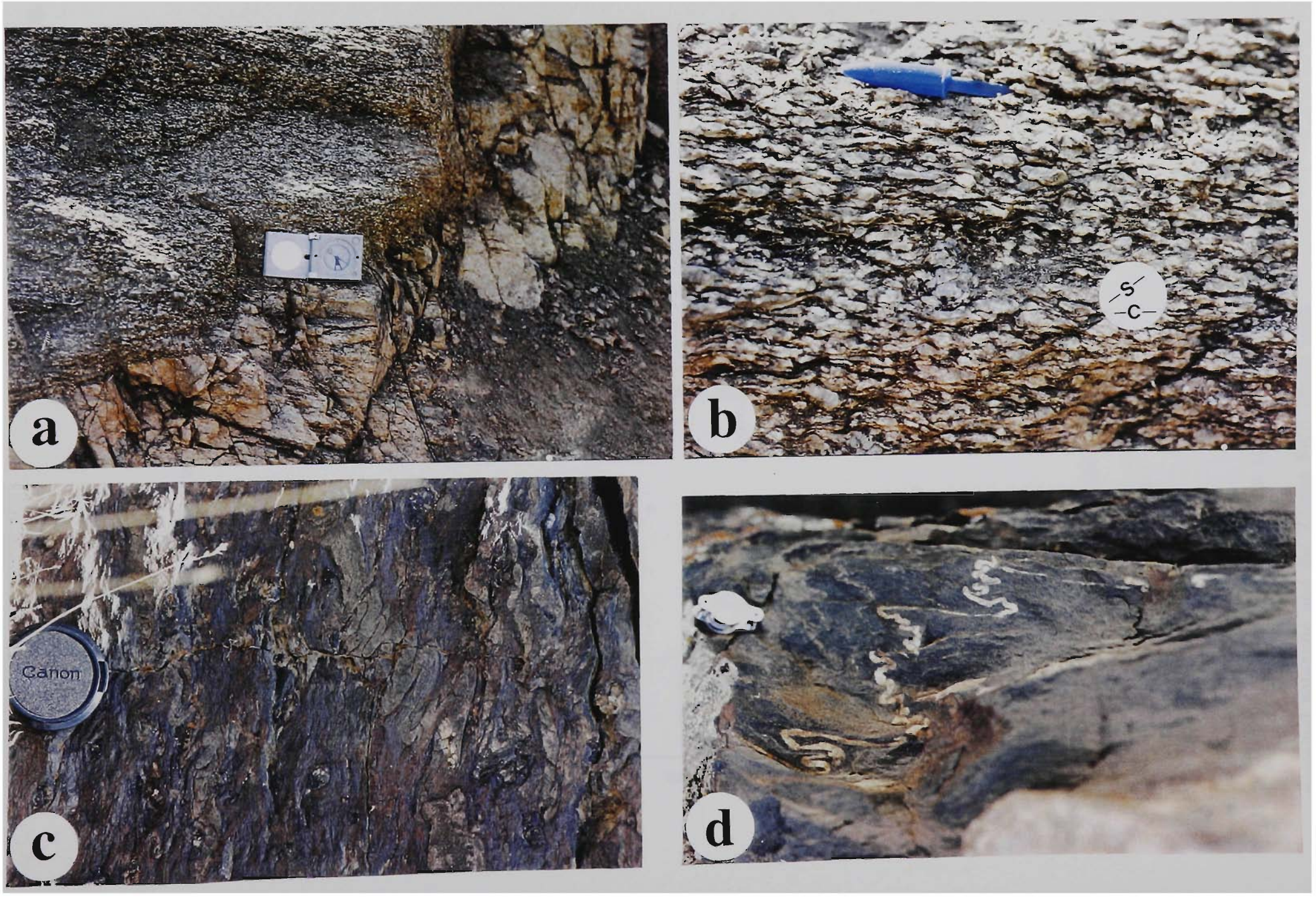
a
b
S
C
c
Canon
d

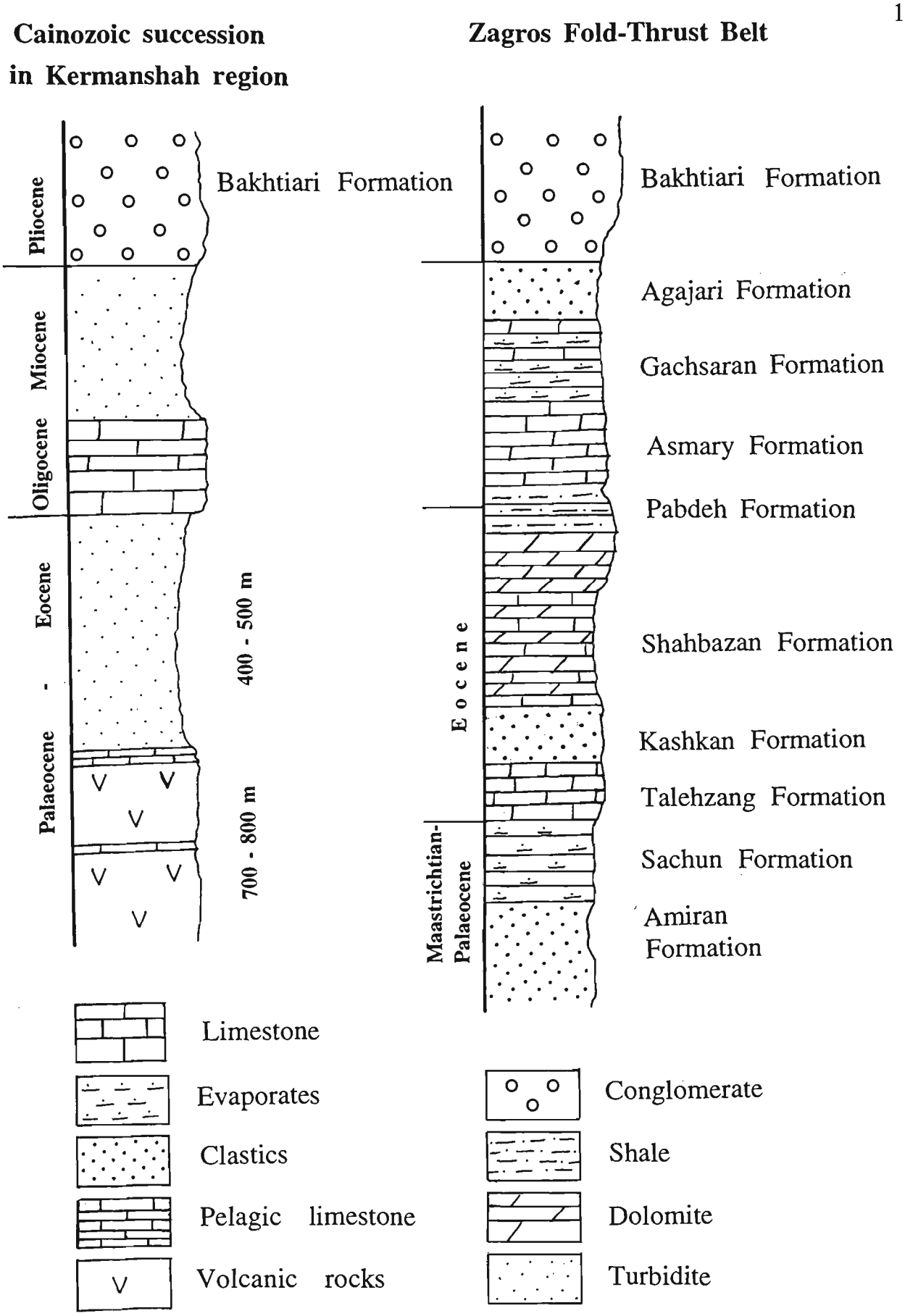

Figure 5.12 General correlation of the stratigraphy of the Cainozoic rocks of the marginal sub-zone and the Zagros Fold-Thrust Belt.

CHAPTER 6

TECTONICS

6.1 INTRODUCTION

The tectonic evolution of the Sanandaj-Sirjan Zone was controlled by opening and subsequent closure of the Neo-Tethys at the northeastern margin of Gondwana-Land (Alavi 1994). Structure, metamorphism and magmatism of the Sanandaj-Sirjan zone are related to a long history of northeast-dipping subduction and subsequent continental collision.

The Sanandaj-Sirjan Zone has been interpreted as an active continental margin of Neo-Tethys, separated from the passive continental margin of the Arabian platform by the Zagros suture (e.g. Dewey et al. 1973; Hynes and McQuillan 1974; Berberian and King 1981; Dercourt et al. 1986; Şengör 1984). In contrast, Alavi (1980, 1994) placed the Neo-Tethyan suture along the northeastern border of the Sanandaj-Sirjan Zone; in this scheme, the Sanandaj-Sirjan Zone has been considered a northeastern extension of the Arabian passive continental margin. The Sanandaj-Sirjan Zone has also been regarded as an active continental margin of Palaeo-Tethys (Şengör 1979, 1990a).

The tectonic evolution of the Sanandaj-Sirjan Zone is discussed in this chapter based on new structural and metamorphic data obtained from the study area and from a reconnaissance overview of the whole zone (see Chapter 5). The significance of stratigraphic, structural and palaeogeographic variations observed in the different sub-zones is considered along with their tectonic setting. The significance of abundant Late Jurassic - Early Cretaceous volcanic rocks in the marginal sub-zone and the extensive deformed and undeformed plutonic rocks in the complexly deformed sub-

zone is evaluated.

The tectonic evolution is discussed for three main tectonic events: (1) an extensional regime, associated with the rifting event that formed Neo-Tethys with separation of the different blocks of Iran from Gondwana-Land, (2) development of a convergent margin along the southwestern border of the Sanandaj-Sirjan Zone associated with subduction of Neo-Tethyan oceanic crust, and (3) subsequent collision of the Arabian platform along the southwestern border of the Sanandaj-Sirjan Zone. The tectonic model of Cawood and Suhr (1992), which accounts for the generation and emplacement of ophiolites in re-entrants along a sinuous passive continental margin, is applied to the ophiolite fragments at Neyriz and Kermanshah along the southwestern border of the Sanandaj-Sirjan Zone. Deformation partitioning in the Sanandaj-Sirjan Zone, associated with the major shortening event, is interpreted in terms of oblique collision. A tectonic model is applied for the oblique collision event which commenced in the Late Cretaceous and is still actively continuing at the present time.

6.2 REGIONAL TECTONICS

Tectonic evolution of the Sanandaj-Sirjan Zone has been controlled by the tectonic movements of adjacent plates since the Late Palaeozoic. Agglomeration of continental fragments had produced the supercontinent of Pangea during the early Mesozoic although the supercontinent was relatively short-lived and fragments may have begun to be rifted off during the period of the supercontinent's assembly (Scotese 1991). Veevers (1989) recognised a Middle-Late Triassic singularity at the time of Pangean assembly. It has been recognised that Neo-Tethys must have formed prior to the Pangean assembly with initial rifting in the Permian and continuing into the Triassic (Şengör et al. 1988). It has been calculated that Neo-Tethys was 2000-

4000 km wide and formed in about 70 million years in the Early Permian to Late Triassic which indicates a spreading rate of about 3 cm/yr at the longitude of Iran (Dercourt et al. 1986). Regionally, generation of the Neo-Tethyan ocean has been obscured by younger collisional events, however, it is suggested that opening of Neo-Tethys in the northwestern Sanandaj-Sirjan Zone, contrary to the reports quoted above, probably occurred in the Middle Triassic (see Tectonic Model below).

In the Early Jurassic, plate tectonic reconstructions show that parts of Eurasia lay to the north of Neo-Tethys which formed a triangular-shaped ocean widening from the west-northwest to an open ocean (Pacific Ocean) to the east-southeast and bordered to the southwest by Gondwana-Land (Figure 6.1a, after Scotese 1991). A spreading ridge formed in the Early Jurassic (approximately 180 Ma) separating the African plate from the North American plate (Scotese 1991). Tensional forces associated with the continuing breakup of Pangea resulted in sea-floor spreading forming the South Atlantic Ocean which began to open in the Valanginian (130 Ma) and enabled rotation and separation of the Afro-Arabian plate from the South American and Antarctica plates (Figure 6.1b; see Scotese 1991 for timing). The northeastward motion of the Afro-Arabian plate towards Eurasia must have been accommodated by subduction of Neo-Tethyan oceanic crust. The subduction zone was sited along the northeastern border of Neo-Tethys where earlier the Cimmerian continent had been attached to Eurasia along the Palaeo-Tethyan suture (Şengör et al. 1988). The convergent margin has been regarded as including the Sanandaj-Sirjan Zone in Iran (Figure 6.1c, see Şengör et al. 1988, 1990a). Timing of the initiation of subduction of Neo-Tethyan oceanic crust under the Cimmerian continent has been suggested as Triassic (Scotese 1991) and somewhat younger in the more complicated reconstructions of Şengör et al. (1988). The Neo-Tethyan ocean was closed in the Late Cretaceous (Turonian-Campanian) and the Afro-Arabian plate collided with

central Iran and ophiolites have been obducted over the Arabian plate margin along the Zagros suture (Berberian and King 1981; Şengör et al. 1988; Alavi 1994; Figure 6.1d, see Chapter 5).

Cainozoic Tectonic Setting

The Cainozoic tectonic evolution of the Sanandaj-Sirjan Zone has been controlled by the shape and movement of the adjacent plates. In the Neogene, the most important plate is the Arabian plate located to the south-southwest. The northeastern border of the Arabian plate is defined by the west-northwest trending Zagros suture which formed in the earlier collision of the Afro-Arabian and Eurasian (Cimmerian) plates (see above). The Zagros suture occurs from the northwest of Iran to the southeast, where it changes to a north-south trend along the Minab fault which marks the boundary between the Zagros Fold-Thrust Belt and the Makran Accretionary Complex (Figure 6.2, compiled after Alavi 1990a).

An active fault, called the "main recent fault" by Tchalenko and Braud (1974), occurs near the Zagros suture in the northwestern part of the Sanandaj-Sirjan Zone. This fault has a northwest-southeast trend but its location is poorly known as it has been inferred on the basis of earthquake focii (Jackson 1992; Berberian 1995). The fault is not shown on Figures 5.2 and 1.2. Berberian has even suggested that the "main recent fault" has displaced the Zagros suture 197 km in the Nahavand-Dorud region (see Figure 1 in Berberian 1995) and has estimated a slip rate of 40 mm/yr since the Pliocene (5 Ma). Dextral displacement along this fault of 10-60 km has also been inferred for supposedly displaced Neogene conglomerates in the same region (Berberian 1995, p. 203). These displacements have not been confirmed by regional mapping. It cannot be demonstrated that the Zagros suture is offset nearly 200 km. Neogene conglomerates are widespread in the region and may not have necessarily

been moved such long distances to their present locations. However, earthquake activity along the "main recent fault" is a result of dextral displacement as shown by rupture of alluvium and topographic features observed at the surface (see Berberian 1995, p.203). Dextral strike-slip motion along other faults in the northeastern part of the Sanandaj-Sirjan Zone (the Abadeh, Shahrbabak and Baft faults) has been determined from earthquake data and indicate ongoing dextral motion (Berberian 1981). The motion along the "main recent fault" and other active structures demonstrates a present-day dextral strike-slip movement between the Arabian plate and central Iran (Jackson 1992).

Earthquake epicentre maps (Ni and Barzangi 1986), and epicentres of the very active recent earthquakes which are located southwest of the Zagros suture, indicate currently active tectonics throughout this area (Berberian 1995). In contrast to the Zagros suture, earthquakes in the Zagros Fold-Thrust belt have lower magnitudes, thrust mechanisms and no rupture at the surface (Berberian 1995).

The northwestern boundary of the Arabian plate is defined by the Dead Sea transform fault which has had sinistral displacement of 105 km since the Miocene (Garfunkel 1981; Girdler 1990). Two phases of Neogene movement have been suggested for this strike-slip motion, the oldest was from 27 Ma to 15 Ma and the younger was from 5 Ma until the present and involved movement of 40 km (Manspeizer 1985; Barjous and Mikbel 1990). Along the southern and southwestern boundaries of the Arabian plate is the Red Sea - Gulf of Aden rift system (McKenzie et al. 1970; Le Pichon and Francheteau 1978). Faulting responsible for the rifts of the Gulf of Aden and the Red Sea commenced in the late Oligocene or early Miocene with an initial width of about 100 km in the Red Sea (Cochran 1981, 1983). Oceanic crust began to form from 10 Ma in the Gulf of Aden, with separation of the Arabian plate from the Somalian plate, and from 5 Ma in the Red Sea between the Arabian

plate and the African (Nubian) plate (Bonatti 1987).

East of the Arabian plate, India has collided with Asia in the Palaeocene and has since continued its northwards movement (Molnar and Tapponnier 1975; Tapponnier et al. 1982; Dewey et al. 1988; Harrison et al. 1992). The Chaman fault is located at the northwestern boundary of the Indian plate and has a north-south trend with a sinistral sense of displacement (Figure 6.2, Molnar and Tapponnier 1975; Dewey et al. 1988). The Indian-Asian collision has formed the Himalayan mountain range and the Tibetan plateau (Dewey et al. 1988). On a larger scale the Indian collision has been associated with extrusion tectonics with the eastward expulsion of continental fragments in front of the advancing Indian crust. This process was experimentally examined by Tapponnier et al. (1982).

The region between the Chaman Fault and the Zagros suture in east and southeast Iran consists of the Central Iran Blocks, East Iran Belt and Central Afghanistan Blocks, which are all part of the Cimmerian continent. The Arabian plate has collided to the north-northeast with the Cimmerian continent (Figure 6.2; Şengör et al. 1988; 1990a, b). This region contains two main sets of faults with north-south and east-west trends (Figure 6.2). All the east-west oriented faults are thrust faults with north-over-south displacement and all the north-south oriented faults are strike-slip faults with dextral displacement (see Alavi 1990a). This regional tectonic pattern with strike-slip and thrust faults indicates partitioning of the oblique convergence between the Arabian plate and the Turan Platform. In response to convergence of India and the Arabian plate northwards, the eastern part of the Iran adjacent to greater India is escaping southwards along the numerous north-south trending dextral strike-slip faults (Figure 6.2).

Northwest of Iran, eastern Turkey and the Caucasus have the highest elevations in western Asia and in this respect they occupy a similar position in the Arabia-

Eurasia collision to that of the Pamir-Karakoram region in the India-Eurasia collision system (Şengör and Kidd 1979; Jackson 1992). Escape tectonics occurs at a smaller scale than that in east Asia with westerly escape of the Anatolian block. Most of the earthquake events in eastern Turkey and in the northwest of Iran have slip vectors subparallel to the east-west strike of the deforming zone (Jackson 1992). This reflects dextral faulting and is causing the Anatolian block to escape to the west (Şengör et al. 1985; Jackson 1992).

6.3 TECTONIC MODEL

The tectonic model which is presented here is based on stratigraphy, structure and metamorphism in the study area and additionally from the geology of the whole Sanandaj-Sirjan zone and its regional tectonic setting. In order to discuss the deformation history in the study area at a regional scale, a series of simple palinspastic cross sections are presented (Figure 6.3). The kinematic evolution of the Sanandaj-Sirjan Zone is divided into three main tectonic events: (1) generation of the Neo-Tethyan ocean, (2) subduction and (3) collision.

(1) Generation of the Neo-Tethyan ocean

Generation of Neo-Tethys at the southwestern boundary of the Sanandaj-Sirjan Zone can be regarded as either simultaneous with the subduction of the Palaeo-Tethyan ocean or began soon after the Palaeo-Tethyan ocean was closed by collision at the northern border of the central Iran (Stöcklin 1968, 1974; Boulin 1988, 1991; Berberian and King 1981; Berberian 1983; Dercourt et al. 1986). Palaeo-Tethys was closed prior to the Late Triassic (Şengör et al. 1988; Alavi 1991b). It has been suggested that Neo-Tethys opened as it was in a back-arc position with respect to the Palaeo-Tethyan magmatic arc (Şengör et al. 1988; Şengör 1990a). It is commonly

cited that during the Late Permian - Early Triassic Neo-Tethys was created at the northeastern part of Gondwana-Land (Figure 6.3a, Şengör 1984).

The Palaeozoic stratigraphy of the Sanandaj-Sirjan Zone is the same as that for the Zagros Fold-Thrust Belt, Alborz Belt and Central Iran Blocks and reflects their location at the northern part of Gondwana-Land prior to generation of Neo-Tethys (Stöcklin 1968; Hamedi 1995). After shallow-marine sedimentary rocks were deposited in the Permian at the northeast of the Arabian platform, the Early Triassic was a time of regression under arid conditions (Berberian and King 1981). In the Mesozoic era, the stratigraphy of the Sanandaj-Sirjan Zone differs from that for the Central Iran Blocks and the Zagros Fold-Thrust Belt. In the Zagros Fold-Thrust Belt, shallow-marine deposition continued from the Permian into Tertiary times with a conformable Mesozoic succession containing no volcanic or plutonic rocks (Stöcklin 1968; Motiei 1993). In the Central Iran Blocks and the Alborz Belt, Triassic successions (e.g. Sorkh Shale and Shotori Formation) consist of dolomite and Rhaetic-Liassic coal-bearing sandstone-shale successions reflecting a continental to shallow-marine environment (Stöcklin 1968). Whereas in the Sanandaj-Sirjan Zone, the Middle-Late Triassic continental and shallow-marine sedimentary successions were interrupted by widespread magmatic activity and followed by Jurassic deep-marine sedimentation (Hamadan Phyllite). The contrast in the stratigraphy of these regions in the Triassic is consistent with the formation of Neo-Tethys at this time.

Traditionally, the Neo-Tethyan ocean has been regarded as having initiated along the southwestern border of the Sanandaj-Sirjan Zone in the Late Permian to Early Triassic (Berberian and King 1981; Şengör et al. 1988). However, the precise timing of the initiation of this event in the Sanandaj-Sirjan Zone is poorly constrained owing to the lack of a detailed stratigraphic understanding of late Palaeozoic - early Mesozoic rocks. Opening of Neo-Tethys must have been associated with prolongued

extension as is documented for the formation of new oceans (e.g. Bond and Kominz 1988). Extension to produce a new ocean is normally associated with rift-related volcanism and the development of extensional fault systems (see Veevers 1981; Lister et al. 1986).

In the Sanandaj-Sirjan Zone the association of mafic and silicic igneous rocks with shallow-marine sedimentation in the June Complex and equivalent units is considered the most likely products of this extensional activity along the northeastern margin of Neo-Tethys (Figure 6.4). The igneous activity has not been studied in any petrological detail and clearly much more work is required to establish its proposed rifted-related setting. On the southwestern margin of Neo-Tethys, igneous activity was less developed with only minor intermediate to mafic volcanism associated with deep-marine radiolarite sedimentation in parts of the radiolarite sub-zone (see Chapter 5).

Continental splitting must also have been associated with the formation of extensional structures as is well illustrated from many continental margins (see Bond and Kominz 1988). The existence of extensional fault systems is inferred from the palaeogeography of the radiolarite and Bistoon sub-zones along the southwestern margin of Neo-Tethys on the passive margin of the Arabian platform. The radiolarite sub-zone developed in a depression that is interpreted as graben-fill that had continuous sedimentation throughout the Late Triassic - Late Cretaceous interval. The Bistoon sub-zone, developed outboard of the radiolarite sub-zone, formed in a shallow-marine environment that is interpreted as a horst (see Chapter 5). Subsidence is shown by the progressive deepening of environments over time in both sub-zones (see Chapter 5) and is related to a phase of post-rift thermal subsidence (cf. Bond and Kominz 1988). The extensional structures associated with the horst and graben terrain developed in the Late Triassic. These extensional structures have not been identified in the field due to intense collision-related deformation in the Late Cretaceous and

Tertiary (see below).

On the northeastern margin of Neo-Tethys the recognition of extensional structures has also been hindered by the younger compressive deformation. In the study area, it was noted that the fault to the north of Kuh-e-June places younger over older rocks. This structure may have formed as a normal fault and was inverted during later compressional deformation (see Chapter 3). Tillman et al. (1981) have also recognised inverted normal faults in the Esfahan region (see Chapter 5). Apart from these structures, extensional faults associated with rifting along the northeastern Neo-Tethys margin have not been recognised. As noted in Chapter 5, suggestions that metamorphic rocks are related to extensional faults and uplifted metamorphic core complexes have not been substantiated in this study (cf. Alavi 1994). In the study area, a Middle-Late Triassic succession indicates sedimentation with deposition of quartz-rich detritius followed by accumulation of shallow-marine carbonate and shale with interbedded abundant volcanic rocks (June Complex). This succession and the overlying basal part of the Hamadan Phyllite may have been associated with active rifting and active normal faults as noted above. Fault-angle depressions filled with locally derived materials indicative of active rift settings (e.g. Mitchell and Reading 1986, p. 478-490) have yet to be documented. It is possible that the extensional structures were relatively minor features with the igneous activity being the main expression of extensional activity. The widespread deep-marine deposition of the Hamadan Phyllite is a dramatic change from the preceding Triassic shallow-marine environments and associated igneous activity. When this change took place is poorly constrained in time but must have occurred sometime in the Early Jurassic (see Chapter 5). The cessation of igneous activity followed by rapid deepening of the sedimentary basin is interpreted as the change from active rifting to sea-floor spreading in Neo-Tethys with thermal subsidence producing the widespread deep-

marine sedimentation along the northeastern margin.

Both passive margins of Neo-Tethys in the Sanandaj-Sirjan Zone appear to have had similar histories with Late Triassic rifting followed by a phase of thermal subsidence. The northeastern margin has had more extensive magmatic activity in contrast to the southwestern margin. Compared to other passive margin successions no breakup unconformity has been recognised associated with the formation of new sea floor in Neo-Tethys (cf. Veevers 1981). Rifting is therefore thought to have begun within the later part of the general Permian to Triassic interval indicated by Berberian and King (1981) and Şengör et al. (1988). The Permian marine rocks of the Zagros Fold-Thrust Belt and the Sanandaj-Sirjan Zone reflect deposition in a shallow epicontinental sea at the northeastern margin of Gondwana-Land followed by regression in the Early Triassic; initiation of rifting is taken as synchronous with the igneous activity in the Middle to Late Triassic.

The oceanic crust of Neo-Tethys must have formed along the site of the Zagros suture at the northeastern border of the Bistoon sub-zone and this coincides with the present site of the ophiolite sub-zone. It is suggested that sea-floor spreading probably began during the later part of the Triassic -Early Jurassic igneous activity in the northeastern passive margin preseved in the complexly deformed sub-zone. None of this supposed Early Jurassic oceanic crust is preserved and has presumably been lost during subsequent subduction (see below). The age of initiation of ocean-floor spreading in Zagros proposed here is slightly younger than that suggested by Şengör et al. (1988, p. 144) who suggested a late Triassic age.

(2) Subduction

The Neo-Tethyan ocean has developed by sea-floor spreading during the Late Triassic and Early Jurassic interval (Şengör et al. 1988). At some stage Neo-Tethys

changed from an expanding Atlantic-type ocean to a contracting ocean prior to its closure and continental collision. This changeover is probably related to the contraction of the area of Neo-Tethys that must have occurred as the Atlantic Ocean formed in the Late Jurassic with counter-clockwise rotation of Africa-Arabia towards Eurasia (see Figure 6.1, after Scotese 1991). The compressional regime began with subduction of newly formed Neo-Tethyan oceanic crust under the Sanandaj-Sirjan Zone in the Late Jurassic on the basis of geological evidence in this region (see below; also Stöcklin 1974; Leansch and Davoudzadeh 1982; Berberian and King 1981).

The Late Jurassic - Early Cretaceous andesitic volcanic rocks of the marginal sub-zone (see Chapter 5) are interpreted as the product of arc-related volcanism developed at a new active margin along the former northeastern passive margin of Neo-Tethys. The magmatic affinities of these rocks have not been investigated and future work is needed to confirm or reject their inferred subduction-related setting. In some areas of the complexly deformed sub-zone, volcanic rocks exist in the lower part of the Albian-Aptian succession (see Chapter 5) and are regarded as an extension of the magmatic arc activity. The upper part of the Hamadan Phyllite accumulated in a deep-marine setting in the backarc region at the same time as arc volcanism in the marginal sub-zone (see Chapter 2). The Late Jurassic plutonic activity in the complexly deformed sub-zone (see Chapter 5) has previously been interpreted as the product of subduction of the Neo-Tethyan oceanic crust under the Sanandaj-Sirjan Zone (Ricou et al. 1977; Berberian and Berberian 1981; Berberian 1983).

The association of these volcanic rocks with abundant shallow-marine limestone, and deep-marine backarc sedimentation, is unusual for a continental-margin magmatic arc. Andean-style arcs have widespread uplifted areas with marine deposition largely restricted to forearc basins and trenches (Cas and Wright 1987, p. 456-462). The

abundance of shallow-marine strata and some deep-marine backarc sedimentation is more typical of island arc successions (see Cas and Wright 1986). Initiation of arc magmatism on attenuated continental crust of the passive margin would account for marine conditions persisting at least during the early phase of arc activity. Over time, however, arc magmatism should have contributed to crustal thickening and emergence as is common in Andean and Sumatran continental-margin arc systems.

In contrast to many ancient arc assemblages no accretionary subduction complex and forearc basin have been recognised along the southwestern border of the volcanic arc. For example, in the Himalayan collision zone forearc basin and subduction complex rocks have been mapped discontinuously along parts of the Yalung-Zangbo suture (see Burg and Chen 1984). Forearc units are not always well represented in all subduction systems. For example, in the Honshu arc the forearc features have been tectonically removed over time as a result of tectonic erosion along the subduction zone (e.g. von Huene 1984). In parts of the Chilean subduction zone the lack of substantial forearc development has been attributed, in part, to the lack of sediment entering the system due to aridity (von Huene et al. 1985). The arc in the marginal sub-zone, and its continentwards extension into the complexly deformed sub-zone, remained in a marine setting throughout much of its history implying that crustal thickening was not occurring (see below). Alternatively, crustal thickening within the arc may have been balanced by tectonic erosion in the forearc associated with the volumetric reduction of forearc tectonic elements.

In addition to tectonic erosion it is possible that the arc system developed in the marginal sub-zone was volumetrically small due to a combination of factors such as a low angle of subduction (e.g. Jordan et al. 1983) and a relatively slower rate of subduction. The length of arc volcanism is not firmly established but must have been active for at least 40 million years (see Chapter 5, Late Jurassic up to the Aptian-

Albian) compounding the problem of the lack of adjoining detrital wedges associated with the arc system. Nevertheless the linear extent and the timing of this volcanic assemblage are the best arguements for its interpretation as a subduction-related magmatic arc.

Subduction-related deformation

In the Late Jurassic to Early Cretaceous, Neo-Tethys was closed by the subduction of oceanic crust at the active continental margin (marginal and complexly deformed sub-zones of the Sanandaj-Sirjan Zone) of central Iran. Deformation associated with the subduction is shown by intense tight to isoclinal folding of the arc basement in the study area (D_1) and in other parts of the complexly deformed sub-zone (see Chapters 3 and 5). The arc basement consisted of the rifted continental crust and the overlying passive margin succession of Neo-Tethys. During this deformation (D_1), the normal faults in basement were probably partly inverted (see also Tillman et al. 1981). In the study area, the first deformation event was simultaneous with metamorphism at amphibolite to greenschist facies conditions (see Chapter 4). Metamorphism of a similar grade and timing has also been established for other parts of the complexly deformed sub-zone (see Chapter 5).

In the Early Cretaceous, during the first deformation episode, the complexly deformed sub-zone was uplifted as shown by the absence of Early Cretaceous rocks and an unconformity underlying basal conglomerate of the Aptian-Albian succession (see Chapter 5). The first deformation and metamorphic event were not observed in the overlying Cretaceous rocks.

Convergent deformation is well documented in continental-margin arc systems and their backarc regions such as in the Andean system (e.g. Roeder 1988; Noblet et al. 1996) and the Sumatran system (e.g. Cameron et al. 1980). Uplift synchronous

with deformation of metamorphic and crystalline rocks is also documented in arc systems (e.g. Rubin et al. 1990). The association of convergent deformation, uplift of metamorphic and plutonic rocks synchronous with widespread intermediate volcanism in the marginal and complexly deformed sub-zones are considered consistent with the inferred active margin setting of the northeastern Neo-Tethyan ocean.

Crustal thickening did not occur in the long term during the evolution of this system as shown by the maintenance of marine conditions in the Late Jurassic and mid-Cretaceous. The crustal thickening that accompanied Late Jurassic - Early Cretaceous magmatism, deformation and uplift must have been counterbalanced by other processes (extensional tectonics?). In the previous section it was suggested that tectonic erosion along the subduction zone may account for the lack of forearc elements. This process would not, however, be expected to affect the main arc itself. Royden (1993) has recognised two types of continental-margin arc systems related to the presence or absence of subduction rollback. In the Early Cretaceous, the arc in the Sanandaj-Sirjan Zone may have undergone a period with an advancing convergent boundary associated with uplift, deformation and plutonism. Before and after this interval, in the Late Jurassic and mid-Cretaceous, a retreating convergent margin may have been active and arc volcanism was accompanied by widespread marine sedimentation. By implication arc magmatism and Early Cretaceous crustal thickening must have been counterbalanced by extension to explain the lack of crustal thickening.

(3) Collision

The major deformation event in the Sanandaj-Sirjan Zone (D_2) was the result of the collision of the Arabian platform with the southwestern border of this zone in the

Late Cretaceous. The collision is associated with obduction of the Zagros ophiolites over the passive continental margin of the Arabian platform (see Chapter 5).

Zagros ophiolites - generation and emplacement

Ophiolites represent displaced fragments of oceanic crust that are exposed along collision plate boundaries (Dewey and Bird 1971). Ophiolites are generated either in mid-ocean ridges or in a supra-subduction zone environment and are subsequently emplaced onto a continental margin through convergent plate interactions (Moores 1982; Moores et al. 1984; Leitch 1984; Edelman 1988; Bloomer et al. 1995). The Zagros ophiolites are the remnants of Neo-Tethyan oceanic crust emplaced along the Zagros suture in the Late Cretaceous during the collision of the passive continental margin of the Arabian plate and the active continental margin of central Iran (Sanandaj-Sirjan Zone). A variety of models has been proposed for generation and emplacement of ophiolites and no a single model has proved satisfactory (Cawood and Suhr 1992).

The location of the ophiolites in distinct areas along the Neo-Tethyan suture zone in Iran (Kermanshah in the northwest and Neyriz in the southeast, see Chapter 5), in addition to the similar age of generation and emplacement are the most significant factors in determining the tectonic history of ophiolite generation and emplacement. Radiometric ages of the Zagros ophiolites in Kermanshah and Neyriz indicate a Senonian age (see Chapter 5). The Neyriz ophiolites are overlain at an angular unconformity by the Campanian-Maastrichtian Tarbur formation and the clasts of ophiolites in Kermanshah region are seen in the Maastrichtian-Palaeocene Amiran Formation of the Zagros Fold-Thrust Belt (see Chapter 5). Therefore, based on stratigraphical evidence, the structural emplacement of the Zagros ophiolites took place prior to the late Campanian-Maastrichtian in Neyriz (Stöcklin 1974) and prior to the

Maastrichtian in Kermanshah (Braud 1987, see Chapter 5). The Semail Ophiolite has a similar age and emplacement history to the Zagros ophiolites (see Chapter 5). All these ophiolites were generated and emplaced in the Late Cretaceous (Turonian-Campanian).

Dercourt et al. (1986) suggested that ophiolite generation occurred close to the continental margin at the same time as subduction of the Neo-Tethyan spreading ridge under the southern margin of the Cimmerian continent. They argued that the ophiolites formed at a new spreading ridge very close to the northern border of the Arabian platform. This idea was mainly based on the relatively young age of ophiolite generation compared to obduction. Knipper et al. (1986) had a similiar model apart from their suggestion that the Zagros ophiolite formed as part of a southwest-facing island arc at the foot of the ancient passive margin of the Arabian platform.

A tectonic model has been suggested for the generation and obduction of the ophiolites in the Bay of Islands in western Newfoundland (Cawood and Suhr 1992). Many aspects of the Zagros and Oman ophiolites, including the generation of the ophiolites in distinct areas along the Neo-Tethyan suture, the short time interval between generation and obduction and the existence of metamorphic soles, are similar to the characteristics of the generation and emplacement history of the ophiolites in western Newfoundland. This model is applied to the generation and obduction of the Zagros ophiolites existing at Neyriz and Kermanshah.

1. The age of Neo-Tethyan ophiolites in Iran are all Late Cretaceous (see Chapter 5) and no Triassic or Jurassic ophiolite has been discovered in these regions (Berberian and King 1981; Knipper et al. 1986).

2. Ophiolite obduction closely follows ophiolite generation. The fact that the ophiolites were hot and mobile during obduction is shown by the development of metamorphic soles (see Chapter 5; Knipper et al. 1986). The higher metamorphic grade rocks (amphibolites) in metamorphic soles are commonly attributed to a phase of intraoceanic ductile thrusting.

3. Ophiolite generation and obduction requires collision with an irregular continental margin. The distinct locations of the ophiolites along the southwestern border of the Sanandaj-Sirjan Zone (Neyriz and Kermanshah regions) can be accounted for by the northeastern continental margin of the Arabian platform having had an irregular shape with re-entrants at the Neyriz and Kermanshah regions and a promontory between them (Figure 6.5). Along the southwestern border of the Sanandaj-Sirjan Zone, between Kermanshah and Neyriz, no ophiolite has been observed.

4. Ophiolite generation was synchronous with continent-continent collision. The age of the ophiolites indicates that obduction occurred soon after generation. Using the timescale of Harland et al. (1989) there was about 15 million years between generation (Senonian) and obduction of the ophiolites (pre-Campanian). A north-dipping subduction zone formed within Neo-Tethys along the southwestern border of the Sanandaj-Sirjan zone in Iran and its equivalents, in Turkey (northwest) and Oman in the southeast. Synchronous with continent-continent collision, ophiolite has been generated in the re-entrants of Kermanshah, Neyriz and Oman. Final collision resulted in widespread ophiolite obduction from western Turkey to Oman.

Based on these points the Zagros ophiolites of the Neo-Tethyan suture, at the southwestern border of the Sanandaj-Sirjan Zone, are thought to have formed from the collision of an irregular northeastern edge of the Arabian platform with the

southwestern boundary of the Sanandaj-Sirjan Zone (Figure 6.5).

Late Cretaceous - Palaeocene collision-related deformation

The trend of the structures of the second deformation is west-northwest subparallel to the trend of the Zagros suture. This deformation is the major deformation in the Sanandaj-Sirjan Zone and in the study area it is characterised by dextral pure-shear dominated transpression and deformation partitioning. The second deformation is partitioned into two different rock assemblages: (1) schist and marble, and (2) mylonitic rocks (see Chapter 3). In the schist and marble units deformation is characterised by tight to isoclinal inclined folds, with south-southwest vergence, moderately plunging to the east and thrust faults subparallel to the structural trend that cut the attenuated southwestern overturned limbs of map-scale F_2 antiforms (see Chapter 3 and 5). Inversion of pre-existing normal faults also continued during D_2. Permian and older rocks were transported by these faults such as to the north of the Kuh-e-June antiform in the study area (see Chapter 3). Deformation led to folding of early formed structures and overprinting of the early schistosity (S_1). The mylonitic rocks have a different deformation style with formation of a mylonitic foliation (parallel to S_2) and a prominent mineral stretching lineation (see Chapter 3). Strike-slip dextral shear with a west-northwest trend is indicated by shear-sense indicators in the mylonitic rocks. Syn-D_2 granities were intruded and deformed during dextral shearing. The geometric patterns of these plutons (e.g. the Galeh-Doz pluton in the study area) are related to the shearing where S-shaped fissures have controlled their emplacement (see Chapter 3).

D_2 was associated with low-grade metamorphism. Petrological and microstructural data from tectonites, record a metamorphic event with greenschist facies conditions overprinting the higher grade earlier event (see Chapter 4).

Retrogression of the moderate-grade metamorphosed rocks (amphibolite facies) was due to uplift as these rocks were brought to shallower depths in the crust during the collision event.

Deformation partitioning associated with the second deformation is accounted for by the overall tectonic setting with the west-northwest trending Sanandaj-Sirjan Zone at the northeastern boundary of the Arabian platform oblique to the compression direction (north-northeast, cf. Teyssier et al. 1995). The transpressional tectonic regime produced compression across the zone by motion of the Afro-Arabian plate to the north-northeast (see Regional Tectonics). Horizontal stress (σ_1) was generated by the motion of the Afro-Arabian plate pushing central Iran at the southwestern border of the Sanandaj-Sirjan Zone. The northeastern boundary of the Arabian plate strikes 060° and makes an angle of about 70° with the stress direction. Therefore, following Teyssier et al. (1995), the deformation is divided into two components, a normal compression and a dextral shear (Figure 6.6). The shortening axis of the pure shear component is perpendicular to the shear plane and progressive deformation causes the rock mass to elongate parallel to the shear plane (see Chapter 3).

Silicic plutonism occurring during and in the final stages of the Late Cretaceous - Palaeocene collision is thought to be related to a combination of factors. Firstly, the occurrence of gabbroic to granodioritic compositions is consistent with some magma derivation from the mantle and possibly reflects magmatism related to the final stages of subduction during the collision (cf. Pitcher 1993, p. 117). Secondly, crustal thickening associated with the collision would enable partial melting in the lower crust and would form the more leucocratic granitic rocks (e.g. Searle et al. 1993).

Collision-related structures are documented in many orogenic belts and are particularly well developed in the Himalayas and formed associated with collision of

the Indian plate with Asia at about 40 Ma (e.g. Burg and Chen 1984). Deformation through the frontal and main part of the range has produced a crustal-scale wedge with the development of major low-angle thrusts (e.g. Coward 1990). Collision-related deformation in the northern part of the Indian plate is shown by intense deformation with refolded largescale recumbent folds and associated syn-metamorphic ductile thrusts (e.g. Burg and Chen 1984). In contrast the synmetamorphic structures of the Sanandaj-Sirjan Zone are more inclined and show an overall less intense deformation pattern.

Neogene collision-related deformation

Opening of the Red Sea and the Gulf of Aden has resulted in the rotation of Arabia with respect to Africa (Nubia and Somalia) since 30 Ma (McKenzie et al. 1970; Bonatti 1987). This plate movement has been responsible for oblique convergence between the Arabian plate and central Iran and has resulted in dextral transpression along the Sanandaj-Sirjan Zone. Deformation partitioning, which has been well established in association with D_2 in the study area (see Chapter 3), is also inferred for tectonic development of the Sanandaj-Sirjan Zone during the Neogene and is still actively continuing. As for the D_2 event, deformation is partitioned into compression normal to the zone and dextral strike-slip motion along it (see Chapter 3; after theory of Tikoff and Teyssier 1994; Teyssier et al. 1995).

Compression normal to the Zagros Orogen is reflected by further collision and Neogene deformation. Deformation and uplift is documented by the synorogenic siliciclastics which consist mostly of conglomerate in the Zagros Fold-Thrust Belt and along the southwestern border of the Sanandaj-Sirjan Zone (see Chapter 5). These rocks are of late Miocene and to Recent age and indicate that uplift was synchronous with opening of the Red Sea and the Gulf of Aden. This uplift is associated with

reactivation of west-northwest trending thrusts that are south-southwest vergent in the Sanandaj-Sirjan Zone, especially in the marginal, ophiolite, Bistoon and radiolarite sub-zones and has involved Cainozoic rocks (see Chapter 5). Thrusting has been active in Neogene times as shown by the timing of thrust faults in the Sanandaj-Sirjan Zone, e.g. thrust faults transported rocks of the marginal sub-zone over Neogene rocks (see Chapter 5, Figures 5.6, 7). Several thrust faults transported the Bistoon sub-zone over the radiolarite sub-zone and the Zagros Fold-Thrust Belt (see Chapter 5). Thrust sheets of the Bistoon sub-zone occur on top of the Pliocene Bakhtiari formation (Pliocene, Figure 5.7). To the southwest, deformation has affected the Zagros Fold-Thrust belt, which is the youngest affect of this collision event (Berberian 1995).

Dextral motion in the Sanandaj-Sirjan Zone is shown by transcurrent displacement along the Zagros suture as has been demonstrated for the "main recent fault" in the northwestern part zone (Berberian 1981, 1995). Oblique convergence is also shown by the development of dextral north-south trending faults that cut the Urumieh-Dokhtar Magmatic Assemblage and associated dextral transcurrent motion along all north-south trending faults between the Chaman fault and the Zagros suture (Figure 6.2). These movements are considered the result of north-northeast motion of the Arabian plate (Figure 6.6).

The Neogene phase of thrusting and crustal thickening in the Sanandaj-Sirjan Zone is similar to the Tertiary tectonic development of the Himalayas with incorporation of early Cainozoic marine rocks in the deforming thrust wedge. Tertiary collision-related structures of the northwestern Himalaya are characterised by a southwest-vergent nappe piles (Steck et al. 1993). The youngest marine rocks incorporated in these nappes are marl and limestones of early Eocene age (Steck et al. 1993).

6.4 DISCUSSION

A generalised ideal tectonic model (Hatcher and Williams 1986) has been applied to the Zagros orogenic belt by Hooper et al. (1994). The application of this ideal model to the Zagros orogen is based on their synthesis of previously published data. They have accepted the thin-skinned tectonic character for the Zagros Fold-Thrust Belt (after Alavi 1994) and proposed that the Sanandaj-Sirjan Zone is an allochthon thrust over the old Arabian margin. As discussed in Chapter 5 the structure of the Sanandaj-Sirjan Zone consists of major thrust slices in the southwest with more thick-skinned features developed in the complexly deformed sub-zone.

In addition to the previous discussion (see Chapter 5), here additional structural and tectonic aspects of the Zagros orogen are considered.

1. A compilation of seismic data by Seber et al. (1997) indicates that the crustal thickness of the Zagros Fold-Thrust Belt is 50 km and decreases gradually towards the northeast with a crustal thickness of 35 km under the northeastern border of the Sanandaj-Sirjan Zone and central Iran (Figure 6.7; Seber et al. 1997). In contrast, Alavi (1994) suggested that the thickest part of the Sanandaj-Sirjan Zone occurred in the northeast which was considered supportive of the location of the Zagros suture in this region. It is now clear that the thickest crust beneath the Sanandaj-Sirjan Zone occurs in the southwest at the location of the Zagros suture as supported in this study (see Chapter 5). The southwestern part also contains the most widespread thrust sheets of both Late Cretaceous and Neogene age in the Sanandaj-Sirjan Zone.

2. Alavi's (1994) suggestion that the Neo-Tethyan suture in western Iran is located at the northeastern border of the Sanandaj-Sirjan Zone was supported by his interpretation that ophiolitic melange of the Nain-Baft suture is a continuation of the

Neo-Tethyan suture. The Nain-Baft suture is located at the northeastern border of the Sanandaj-Sirjan Zone to the east of the Dehshir Fault (see Figure 5.1 in Chapter 5). In fact, these ophiolitic melanges do not continue to the northwest along the northeastern border of the Sanandaj-Sirjan Zone. Instead they occur along the Dehshir fault and extend from Nain to the northeast along the Doruneh fault (see Figure 5.1 in Chapter 5). These ophiolitic melanges are regarded as part of the ophiolites that surround the central Iran microcontinent (see Stöcklin 1974; Leansch and Davoudzadeh 1982).

In a study, based on trace and major element chemical data collected from volcanic rocks in 3 different parts of the Urumieh-Dokhtar Magmatic Assemblage, Moradian (1997) concluded that volcanic rocks of the Nain-Baft sector differ from those of the Urumieh-Nain sector of the Urumieh-Dokhtar Magmatic Assemblage. He suggested that the volcanic rocks of the Nain-Baft sector had been derived from melting of subducted oceanic crust of the Nain-Baft ocean which were part of the ocean near the Central Iran Blocks (Dercourt et al. 1986; Şengör et al. 1988; Şengör 1990a). In contrast, the volcanic rocks of the Urumieh-Nain sector are not related to melting of any subducted oceanic slab (Moradian 1997).

3. The Urumieh-Dokhtar Magmatic Assemblage postdates the subduction of the Neo-Tethyan oceanic crust which had started in the Late Jurassic and continued up to subsequent collision in the Late Cretaceous (see Chapter 5). The Urumieh-Nain sector of the Urumieh-Dokhtar Magmatic Assemblage contains extensive volcanic and plutonic rocks with a continuous succession from the middle Eocene until the Quaternary (Dimitrijevic 1973; Amidi 1984) and represents a post-collisional magmatic assemblage (see Moradian 1977).

6.5 CONCLUSIONS

Tectonic evolution of the Sanandaj-Sirjan Zone has been involved with the generation of the Neo-Tethys, followed by subduction and subsequent collision with the northeastern margin of the Arabian platform. Continental rifting started in the Middle-Late Triassic in the northwestern Sanandaj-Sirjan Zone and was followed by sea-floor spreading in the latest Triassic to Early Jurassic interval. Continental rifting in northeastern Gondwana-Land is generally attributed to the Late Permian to Early Triassic interval with sea-floor spreading in the Late Triassic causing rotation of the Cimmerian to the northeast (see Şengör et al. 1988).

Subduction of Neo-Tethyan oceanic crust was probably a result of the counter-clockwise rotation of the Africa-Arabia towards Eurasia associated with the generation of the Atlantic Ocean in the Late Jurassic. The subduction of the Neo-Tethyan oceanic crust under the southwestern border of the Eurasia (Cimmerian), in the Sanandaj-Sirjan Zone, caused the development of the Late Jurassic - Early Cretaceous andesitic volcanic rocks (volcanic arc of the marginal sub-zone), deformation (D_1 of the study area), associated prograde metamorphism (greenschist-amphibolite) and plutonic rocks. Limited uplift was associated with subduction with the arc mainly developed in a shallow-marine setting.

The major structures in the Sanandaj-Sirjan Zone were the result of the oblique collision of this zone with the Arabian platform in the Late Cretaceous. Dextral transpression is documented with deformation partitioning during the second deformation event (D_2). D_2 structures are characterised by the development of intense folding with south-southwest vergence and mylonitic rocks. Syn-tectonic granitic intrusions were strongly mylonitised. The mylonites contain dextral shear-sense indicators. Low-grade greenschist metamorphic rocks are developed during D_2 and the higher-grade minerals of the first metamorphism were retrogressed. During the

collision there was uplift, erosion and unloading simultaneous with deformation to produce exposure of the metamorphic core. The ophiolites of the Neyriz and Kermanshah regions indicate obduction of oceanic fragments along the Zagros suture. The location of the ophiolites in distinct areas (Oman, Neyriz and Kermanshah) in addition to the similar age of generation and emplacement reflects an irregular northeastern edge to the passive continental margin (Arabian Platform).

Deformation of the Sanandaj-Sirjan Zone has continued into the Cainozoic synchronous with opening of the Red Sea and the Gulf of Aden. The north-northeast motion of the Arabian platform resulted in the continuation of oblique collision and dextral transpression. Deformation partitioning continued and is demonstrated by compression normal to the Sanandaj-Sirjan Zone and dextral strike-slip motion during the Neogene (e.g. the "main recent fault"). Synorogenic conglomerates developed in the southwestern border of the Sanandaj-Sirjan Zone and the Zagros Fold-Thrust Belt, reflect this deformation and uplift. Compression during the Neogene is demonstrated by the abundant thrust faults involving Cainozoic successions in the southwestern border of the Sanandaj-Sirjan Zone that transported different sub-zones over the Zagros-Fold-Thrust Belt.

Neogene transpression is reflected regionally throughout eastern Iran by dextral motion along all north-south trending faults and thrust motion along all west-northwest trending faults between the Chaman fault to the east and the Zagros suture. This results from ongoing north-northeast motion of the Arabian plate.

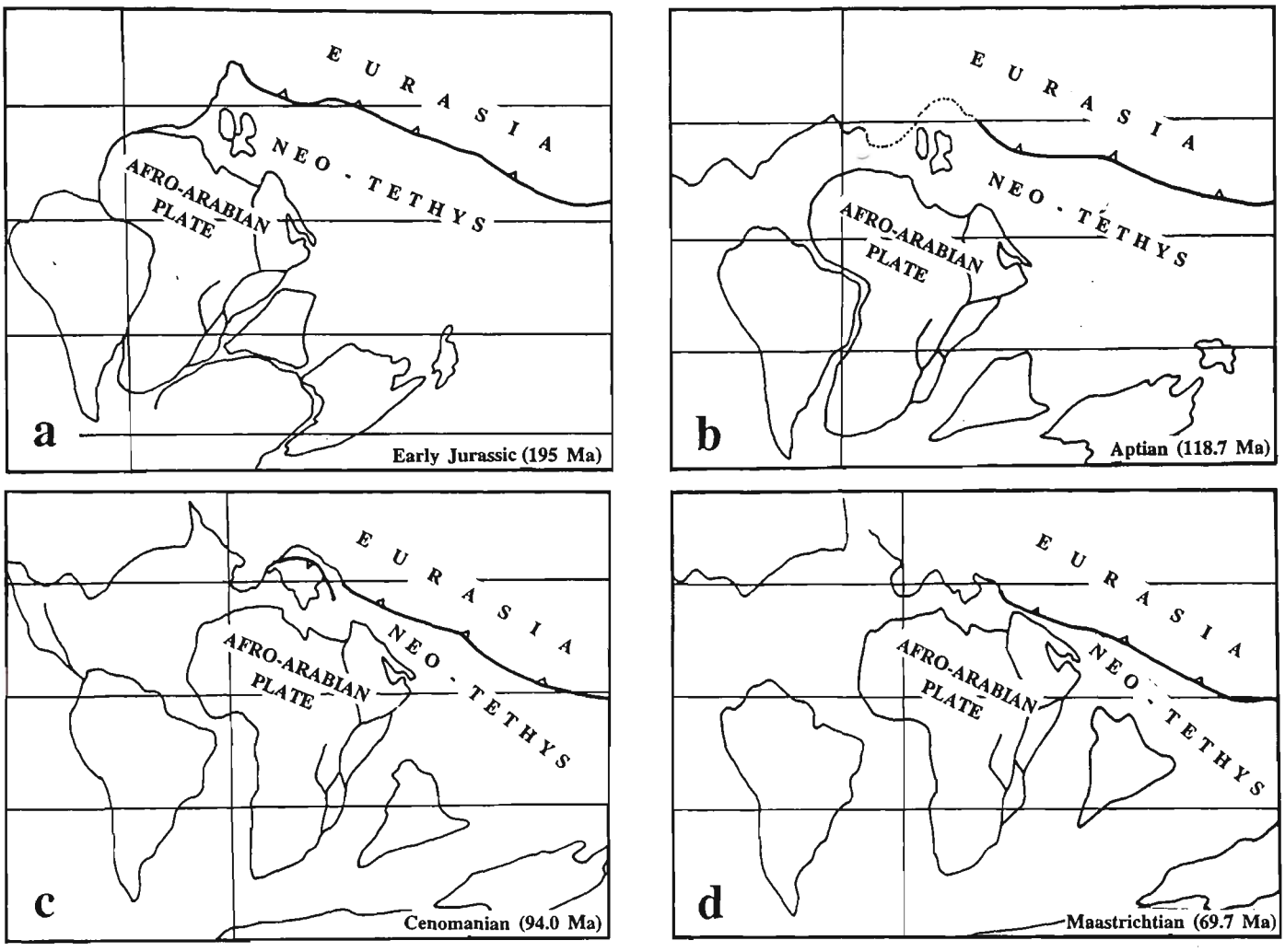

Figure 6.1 Plate tectonic reconstruction for the (a) Early Jurassic (b) Early Cretaceous (c) Middle Cretaceous (d) Late Cretaceous (modified after Scotese 1991).

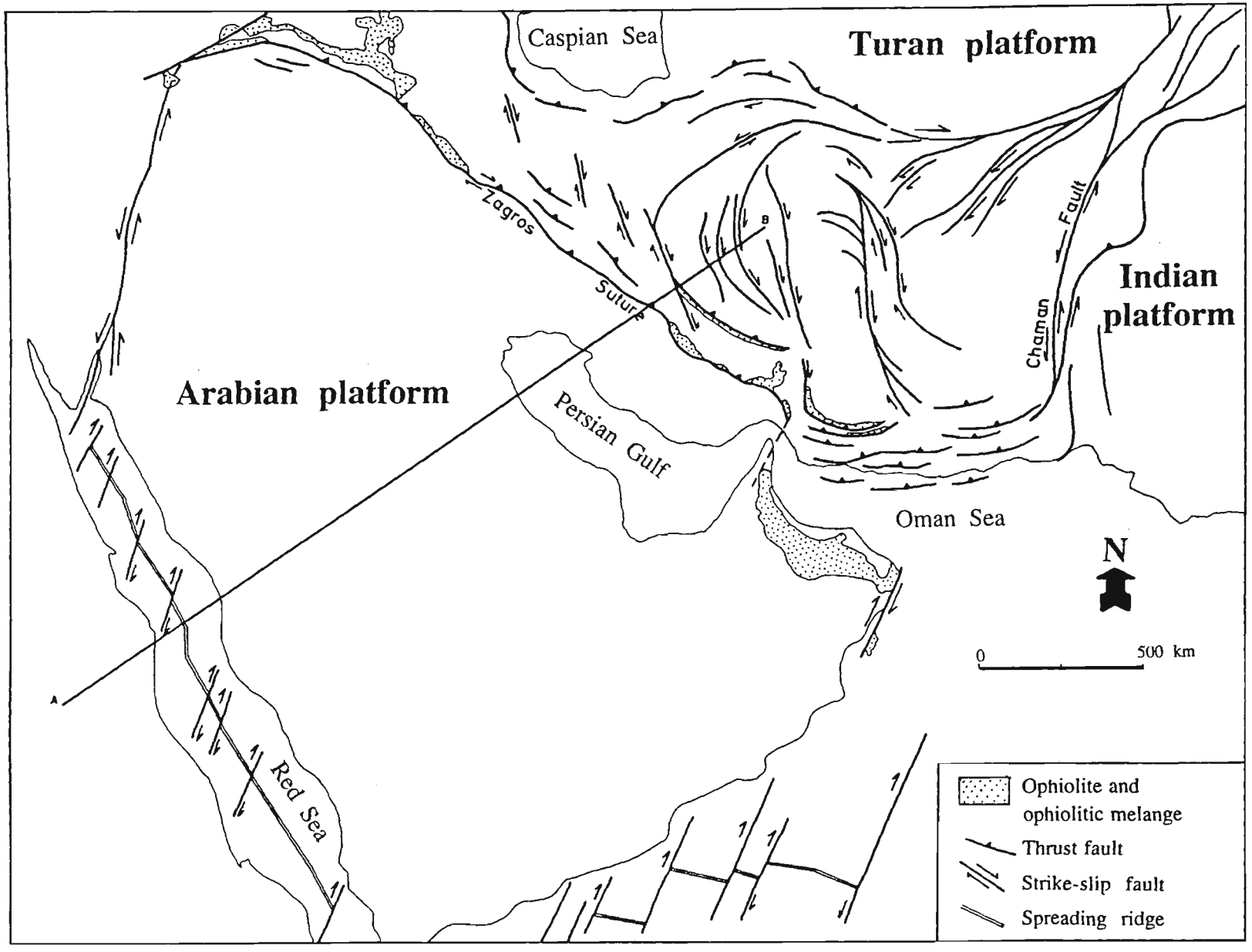

Figure 6.2 Simplified tectonic map of the Middle East with active plate boundaries and major faults.

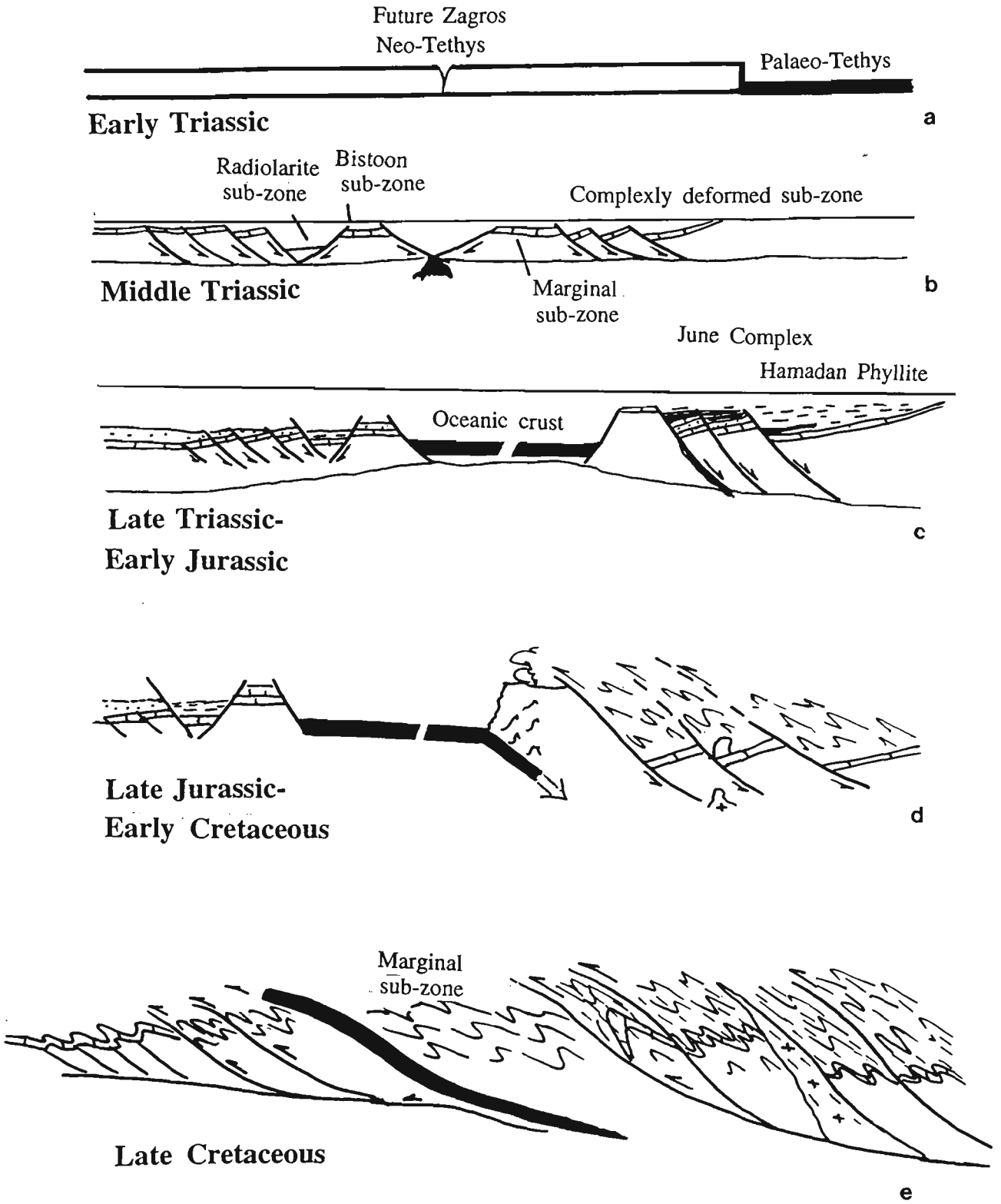

Figure 6.3 Schematic cross sections along the Zagros Orogen showing the tectonic evolution of the Sanandaj-Sirjan Zone.

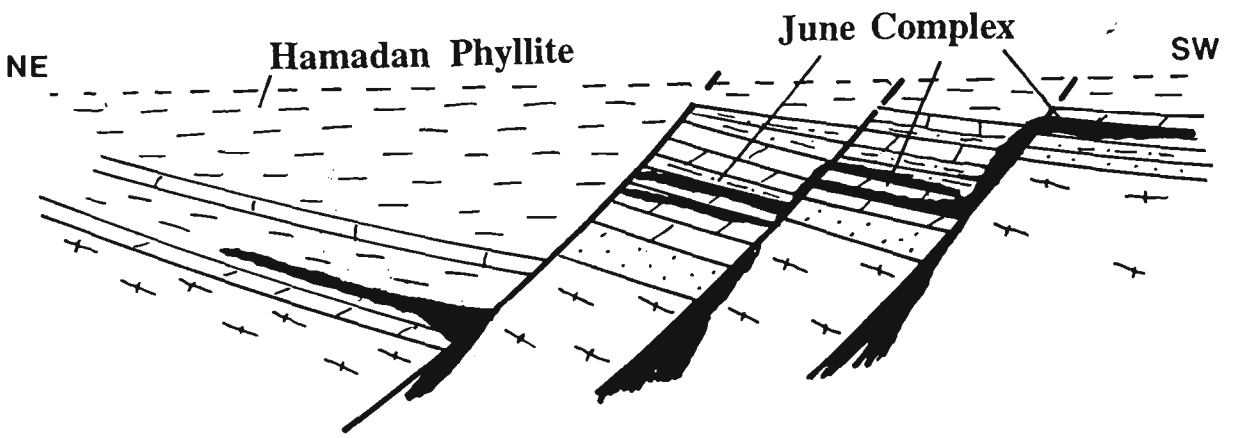

Figure 6.4 Proposed distribution of Mesozoic half graben structures in Dorud-Azna region. Rifted basement consists of Permian and older rocks.

Figure 6.5 Schematic tectonic map illustrating the position of re-entrants and promontories along the southwestern boundary of the Sanandaj-Sirjan Zone.

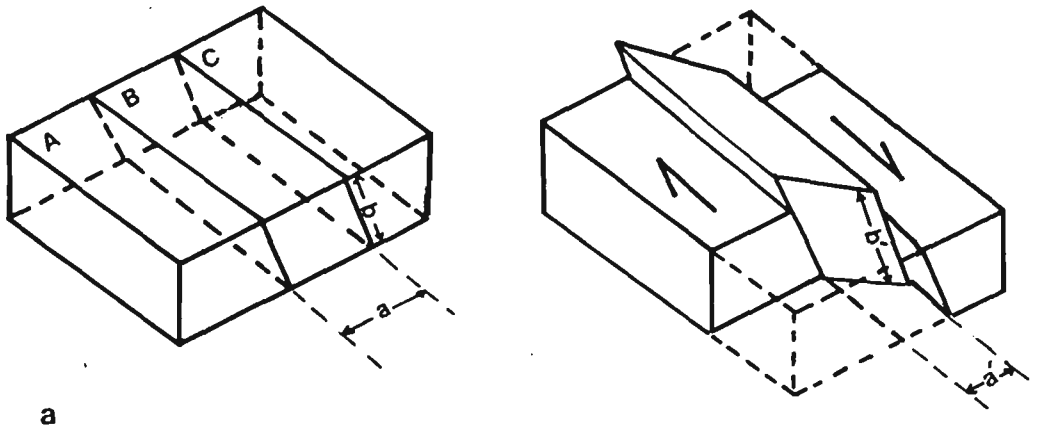

a

A Arabian platform
B Sanandaj-Sirjan Zone
C central Iran

$a > a'$
$b < b'$

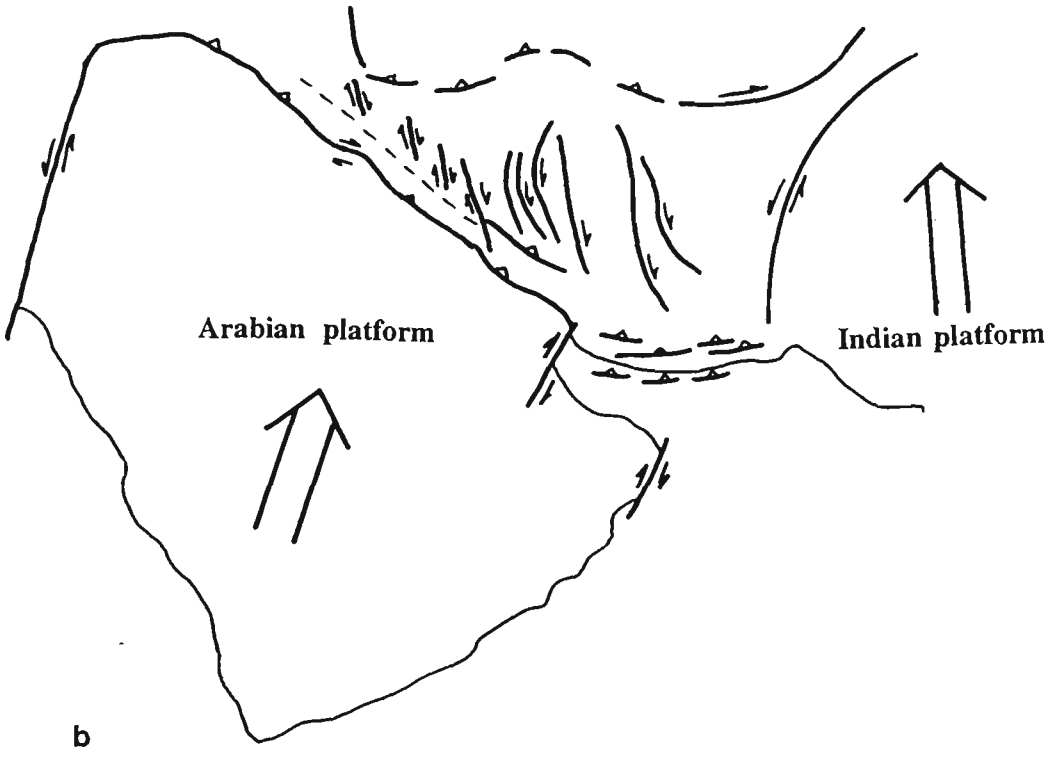

b

Figure 6.6

(a) Transpression tectonic model is schematically illustrated by block diagram.

(b) The main compression orientation due to north-northeastern motion of the Arabian platform.

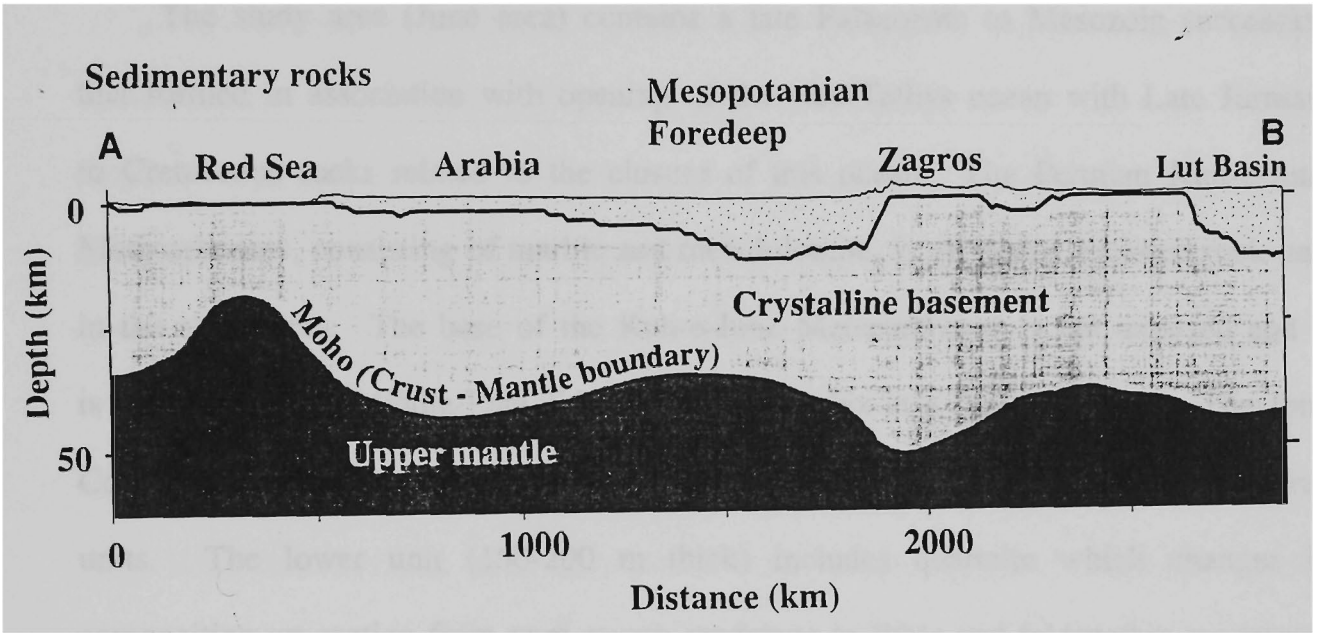

Figure 6.7 Crustal scale profile showing change of crust-mantle boundary and the thickness of sedimentary cover. Note the thickest crust under the frontal part of the Zagros Fold-Thrust Belt which decreases towards the Sanandaj-Sirjan Zone and central Iran. See the location in Figure 6.2 (after Seber et al. 1997).

CHAPTER 7

SUMMARY

7.1 STRATIGRAPHY

The study area (June area) contains a late Palaeozoic to Mesozoic succession that formed in association with opening of the Neo-Tethys ocean with Late Jurassic to Cretaceous rocks related to the closure of this ocean. The Permian Kuh-e-June Metacarbonate, consisting of marble and metadolomite, is the oldest exposed rock unit in the study area. The base of the Kuh-e-June Metacarbonate is not exposed and it is overlain by the Middle-Late Triassic June Complex at a faulted contact. The June Complex comprises most of the outcrops in the study area and is divided into three units. The lower unit (150-200 m thick) includes quartzite which changes in composition up section from pure quartz sandstone to lithic and feldspathic sandstone. Quartzite is locally interbedded with metadolomite containing chert bands and nodules. The middle unit consists of metacarbonate, quartzite and schist up to 600 m thick and is the thickest unit of the June Complex. This unit contains a marker horizon, the Darijan Marble Member, which divides the middle unit into two parts. The upper unit is estimated at 600 m thick and consists of greenstone, including amphibolite and epidote-amphibolite schist. This unit appears to have a transitional contact with overlying Late Triassic - Jurassic Hamadan Phyllite.

Hamadan Phyllite is exposed in the northeastern part of the study area and consists of black phyllite and slate that are regularly interbedded with marble layers in the lower part. More than 2 km thickness is estimated for the Hamadan Phyllite which occupies a vast area of the northwestern Sanandaj-Sirjan Zone. Late Jurassic - Early Cretaceous Teadar volcanic rocks consist of andesitic lava and pyroclastic rocks that are exposed in the southwest of the study area. The base of the Teadar volcanic

rocks is not exposed and the true thickness is unknown. The upper contact is faulted with overlying Aptian-Albian recrystallised limestone at Suraneh village. The successions are intruded by silicic and mafic intrusive rocks. The Galeh-Doz granitic gneiss is a syn-tectonic intrusion and is strongly mylonitised.

The Permian and Triassic rocks were deposited in mainly shallow-marine environments with a major episode of igneous activity in the Middle-Late Triassic. Jurassic rocks of the Hamadan Phyllite reflect deposition in deep-marine environments that in their upper part were synchronous with intermediate volcanism to the southwest.

7.2 STRUCTURE

Four deformations have been recognised in the study area with the most significant being D_2. Tight to isoclinal F_1 moderately plunge to the northeast and axial planes dip moderately to steeply to the east with variable strikes. S_1 axial plane schistosity is strongly overprinted by F_2 with development of type 2 and 3 refold patterns at macroscopic and mesoscopic scales.

West-northwest trending tight to isoclinal F_2 with strongly developed axial plane schistosity are sub-coaxial with F_1. Lithological layers in limb areas of many F_2 folds are partially attenuated and/or dismembered. Boudinage and pinch-and-swell structures are aligned parallel to S_2. Extensive mylonites, including syn-deformational granitic plutons, were developed during D_2. Mylonitic rocks have strongly developed foliation sub-parallel to the S_2 schistosity and a west-northwest trending subhorizontal stretching lineation. The geometry of D_2 structures indicates that both shortening and dextral strike-slip shearing played major roles during D_2. D_2 is partitioned in two different rock types: (a) schist and marble, (b) mylonite. This process reflects the different responses of these rock units to the dextral transpression. Abundant shear-sense

indicators demonstrate dextral strike-slip shearing in the mylonites. Dextral transpression led to the horizontal shortening and extension of the rock masses in the west-northwest direction. This accompanied the southwestward thrusting responsible for major folding in the schist and marble unit. The outcrop pattern, as well as the strong D_2 mylonitic fabrics, in the Galeh-Doz granitic gneiss indicate syn-D_2 emplacement of this pluton. Dextral shearing controlled emplacement and formed the S-shaped geometry of the Galeh-Doz pluton.

The third deformation is characterised by upright, close to open folds moderately plunging to the east and with an axial plane crenulation cleavage, vertical or steeply dipping to the north-northeast. The last deformation consists of open, upright folds with northeast-southwest trending axial planes. Folds plunge gently both to northeast and southwest.

It is concluded that during D_2, structures were produced in a pure-shear dominated transpressional tectonic regime with compression in a north-northeast to south-southwest direction and dextral shearing in a west-northwest orientation. Thrust faults and folds in schist and marble unit with south-southwest vergence are the result of the compression. Mylonitic rocks containing steeply dipping foliation to the north-northeast, west-northwesterly-oriented subhorizontal stretching lineation and shear-sense fabrics all reflect the dextral shearing.

7.2 METAMORPHISM

Two phases of regional metamorphism have been observed in the study area and are tentatively recognised throughout the Sanandaj-Sirjan Zone: (a) prograde metamorphism associated with D_1, and (b) retrograde metamorphism which affected the prograde metamorphic rocks during D_2. Metamorphosed rocks are divided into two types: metabasite and metasedimentary rocks. Metabasites are at amphibolite,

epidote-amphibolite and greenschist facies whereas the metasedimentary rocks are at greenschist facies. During the first deformation event, the rocks reached peak metamorphic conditions in the amphibolite facies.

The prograde metamorphism (M_1) and first deformation episode (D_1) were synchronous as shown by the development of metamorphic minerals along S_1. S_1 is observed in the Middle-Late Triassic June Complex and the Late Triassic - Jurassic Hamadan Phyllite, but it has not been identified in the Cretaceous rocks. The retrograde metamorphism (M_2) was simultaneous with D_2 as shown by the widespread development of retrograde mineral assemblages along S_2. Garnet porphyroblasts contain no inclusion trails and are wrapped around by S_2 indicating syn-D_2 growth. Also, D_2 has affected the Cretaceous rocks in contrast to D_1.

The prograde metamorphism has been associated with the subduction-related orogeny during the D_1 event. The rocks were uplifted and cooled during subsequent collision (D_2). Deformed syn-kinematic plutons are characterised by weak contact aureoles (e.g. Galeh-Doz pluton). The M_2 metamorphic event is associated with D_2 and intrusion of syntectonic plutons and formed during Late Cretaceous collision.

7.3 TECTONICS

The Sanandaj-Sirjan Zone was generated by the opening of the Neo-Tethys ocean in the Late Permian - Early Triassic and developed as an active continental margin during subduction and subsequent collision. Five sub-zones have been identified for the Sanandaj-Sirjan Zone and are based on stratigraphic, structural, and metamorphic characteristics.

The radiolarite sub-zone at the southwestern margin of the Sanandaj-Sirjan Zone. This sub-zone contains shallow-marine to deep-marine successions with olistoliths derived from the Zagros Fold-Thrust Belt and some rift-related volcanic activity. To

the northeast is the Bistoon sub-zone with a shallow-marine carbonate succession of Late Triassic - Late Cretaceous age. Farther northeast is the ophiolite sub-zone with well-developed Late Cretaceous ophiolites in the Neyriz and Kermanshah regions. The Zagros suture divides the passive continental margin (Arabian platform) from the marginal and complexly deformed sub-zones of the Sanandaj-Sirjan Zone and is defined by the ophiolite sub-zone. The Zagros ophiolites are thought to have formed in re-entrants along the passive margin of the Arabian platform. Abundant Late Jurassic-Early Cretaceous andesitic volcanic rocks have erupted in the marginal sub-zone. The complexly deformed sub-zone has developed to the northeast of the marginal sub-zone contains the northeastern passive margin of Neo-Tethys which has been affected by subsequent multiple deformation, metamorphism and plutonism.

Compressive deformation in the Sanandaj-Sirjan Zone began in the Late Jurassic by subduction of Neo-Tethyan oceanic crust due to the opening of the Atlantic Ocean and counter-clockwise rotation of the Afro-Arabian continent. This event was associated with formation of the volcanic arc in the marginal sub-zone and the development of the first deformation and associated metamorphism in the complexly deformed sub-zone.

The Late Cretaceous collision is defined by the major deformation (D_2) with west-northwesterly-trending structures and intrusion of syn-deformational plutonic rocks in the complexly deformed sub-zone. Partitioning of D_2 into occurred into domains of dextral shearing and domains with normal compression formed from dextral transpression due to oblique convergence. The present regional tectonic pattern of the Zagros Orogen is a continuation of a similar tectonic regime to the Late Cretaceous collision with deformation partitioned into compression normal to the zone (i.e. thrusting) and dextral strike-slip faulting parallel to the zone.

REFERENCES

ALAVI, M., 1980. Tectono-stratigraphic evolution of the Zagrosides of Iran. *Geology* **8**, 144-149.

ALAVI, M., 1991a. Tectonic map of the Middle East (1:2900 000). *Geological Survey of Iran.*

ALAVI, M., 1991b. Sedimentary and structural characteristics of the Palaeo-Tethys remnants in northeastern Iran. *Geological Society of America Bulletin* **103**, 983-992.

ALAVI, M., 1992. Thrust tectonics of the Binalood region, NE Iran. *Tectonics* **11**, 360-370.

ALAVI, M., 1994. Tectonics of the Zagros Orogenic belt of Iran: new data and interpretations. *Tectonophysics* **229**, 211-238.

ALAVI, M., AND MAHDAVI, M.A., 1994. Stratigraphy and structure of the Nahavand region in western Iran and their implications for the Zagros tectonics. *Geological Magazine* **131**, 43-47.

ALAVI-NAINI, M., HAJIAN J., AMIDI, M. AND BLOURCHI, H., 1982. Geology of Takab-Saein-Qaleh quadrangle. *Geological Survey of Iran* report number 50.

AMIDI, S.M., (Compiler), 1984. Geological map of the Saveh quadrangle, scale 1:250 000. *Geological Survey of Iran.*

AMIDI, S.M., AND MAJIDI, B., (COMPILERS), 1977. Geological map of the Hamadan quadrangle, scale 1:250 000. *Geological Survey of Iran.*

BARD, J.P., 1980. *Microtextures of Igneous and Metamorphic Rocks*, D. Reidal Publishing Company, 264 p.

BARJOUS, M., AND MIKBEL, SH., 1990. Tectonic evolution of the Gulf of Agabeh-Dead Sea transform fault system. *Tectonophysics* **180**, 49-59.

BECHENNEC, F., LE METOUR, J., RABU, D., BOURDILLON-DE-GRISSAC, CH., DE WEVER, P., BEURRIER, M. AND VILLEY, M., 1990. The Hawasina Nappes: stratigraphy, palaeogeography and structural evolution of a fragment of the south-Tethyan passive continental margin. **In** Robertson, A.H.F., Searle, M.P., and Ries, A.C., (eds). The geology and Tectonics of the Oman Region. *Geological Society of London Special Publication* **49**, 213-225.

BERBERIAN, F., AND BERBERIAN, M., 1981. Tectono-plutonic episodes in Iran. **In**: Gupta, H.K., and Delang, F.M., (eds). *Zagros, Hindu Kush, Himalaya geodynamics Evolution* **3**, 5-32.

BERBERIAN, M., 1977. Three phases of metamorphism in Haji-Abad quadrangle (southern extremity of the Sanandaj-Sirjan structural Zone): A palaeotectonic discussion. **In** Contribution of the seismotectonics of Iran (part III). Edited by M. Berberian, *Geological Survey of Iran* report number **40**, 239-260.

BERBERIAN, M., 1981. Active Faulting and tectonics of Iran. **In** Gupta, H.K., and Delnay, F.M., (eds). *Zagros, Hindu Kush, Himalalia Geodynamics Evolution* **3**, 33-69.

BERBERIAN M., 1983. The southern Caspian: A compressional depression floored by a trapped, modified oceanic crust. *Canadian Journal of Earth Science* **20**, 163-183.

BERBERIAN, M., 1995. Master "blind" thrust faults hidden under the Zagros folds: active basement tectonics and surface morphotectonics. *Tectonophysics* **241**, 1933-224.

BERBERIAN, M. AND ALAVI-TEHRANI, N., 1977. Structural Analyses of Hamadan Metamorphic Tectonites. **In** Contribution to the Seismotectonics of Iran (part 3). Edited by M. Berberian. *Geological Survey of Iran* report number **40**, 239-260.

BERBERIAN, M., AND KING, G.C., 1981. Towards a palaeogeography and tectonics evolution of Iran. *Canadian Journal of Earth Science* **18**, 210-265.

BERBERIAN, M., AND NOGOLE, M.A.A., 1974. Preliminary explanatory text of the geology of Dh Sard Khabr maps with tectonics of the area (two geological maps, 1:100,000, from the Hajiabad quadrangle map). *Geological Survey of Iran* internal report, 60 pages.

BERNOULLI, D., WEISSERT, H., 1987. The upper Hawasina nappes in the central Oman Mountains: stratigraphy, palinspastics and sequence of nappe emplacement. *Geodinamica Acta* **1**, 47-58.

BERNOULLI, D., WEISSERT, H., AND BLOME, C.D., 1990. Evolution of the Triassic Hawasina Basin, Central Oman Mountains. **In** Robertson, A.H.F., Searle, M.P., and Ries, A.C., (eds). The geology and Tectonics of the Oman Region. *Geological Society of London Special Publication* **49**, 189-203.

BERTHE, D., CHOUKROUNE, P., AND JEGOUZO, P., 1979. Orthogneiss, mylonite and non coaxial deformation of granites: the example of the south Armorican Shear Zone. *Journal of Structural Geology* **1**, 31-42.

BERTHIER, F., BLLIAUT, J.P., HALBRONN, B., AND MAURIZOT, P., 1974.

Étude stratigraphique, pétrologique et structurale de la région de Khorramabad (Zagros Iran). Thèse, *3 ème cycle, université scientifique et Médicale de Gronoble, France.*

BLENDINGER, W., VAN VLIET, A. AND HUGHES CARKE, M.W., 1990. Updoming, rifting and continental margin development during the Late Palaeozoic in northern Oman. **In** Robertson, A.H.F., Searle, M.P., and Ries, A.C., (eds). The geology and Tectonics of the Oman Region. *Geological Society of London Special Publication* **49**, 27-38.

BLOOMER, S.H., TAYLOR, B., MACLEOD, CJ., STERN, R.J., FRYER, P., HAWKINS, J.W., AND JOHNSON, L., 1995. Early volcanism and the ophiolite problem: a perspective from drilling in the western Pacific. **In** Taylor, B., and Natland, J., (eds). Active margins and marginal basins of the western Pacific *American Geophysical Union.* Geophysical Monograph **88**, 1-30.

BONATTI, E., 1987. Oceanic evolution, rifting or drifting in the Red Sea? *Nature* **330**, 692-693.

BOND, G.C., AND KOMINS, M.A., 1988. Evolution of thought on passive continental margins from the origin of geosynclinal theory (~1860) to the present. *Geological Society of America Bulletin* **100**, 1909-1933.

BOULIN, J., 1988. Hercynian and Eocimmerian events in Afghanistan and adjoining regions. *Tectonophysics* **148**, 253-278.

BOULIN, J., 1991. Structures in Southwest Asia and evolution of the eastern Tethys. *Tectonophysics* **196**, 211-267.

BRAUD, J., 1987. Paleogéographique, magmatique et structurale de la region Kermanshah, Iran. *Thèse de étate, Université de Paris, France, 489p.*

BRUN, J.P., AND PONS, J., 1981. Strain pattern of pluton emplacement in a crust undergoing non-coaxial deformation, Sierra Morena, Southern Spain. *Journal of Structural Geology* **3**, 219-229.

BURG, J.P. AND CHENG, G.M., 1984. Tectonics and structural zonation of southern Tibet, China. *Nature* **311**, 219-223.

BURG, J.P., AND WILSON, C.J.L., 1988. A Kinematic analysis of the southernmost part of the Bega Batholith. *Australian Journal of Earth Sciences* **35**, 1-13.

CAMERON, N.R., CLARKE, M.C.G., ALDISS, D.T., ASPDEN, J.A., AND DJUNUDDIN, A., 1980. The geological evolution of Northern Sumatra. *Proceedings Indonesian Petroleum Association, ninth annual Convention, May*

1980.

CASTRO, A., 1986. Structural pattern ascent model in the Central Extremadura batholith, Hercynian belt, Spain. *Journal of Structural Geology* **8**, 633-645.

CAWOOD, P.A., AND SUHR, G., 1992. Generation and obduction of ophiolites: Constraints from the Bay of Islands complex, western Newfoundland. *Tectonics* **11**, 884-897.

CAWOOD, P.A., GREEN, F.K., AND CALON, T.J., 1990. Origin of culminations within the southeast Oman Mountains at Jebal Majhool and Ibra Dome. **In** Robertson, A.H.F., Searle, M.P., and Ries, A.C., (eds). The geology and Tectonics of the Oman Region. *Geological Society of London Special Publication* **49**, 429-445.

CAWOOD, P.A., WILLIAMS, H., O'BRIEN, S.J., AND O'NEILL, P.P., 1988. Field trip guidebook, trip A1. A geologic cross-section of the appalachian orogen. *Geological Association of Canada, Mineralogical Association of Canada and Canadian Society of Petroleum Geologists.*

CAS, R.A.F., AND WRIGHT, J.V., 1987. *Volcanic successions, modern and ancient,* Allen & Unwin, London.

CHOUKROUNE, P., AND GAPAIS, D., 1983. Strain pattern in the Aar Granite (Central Alps): orthogneiss developed by bulk inhomogeneous flattening. *Journal of Structural Geology* **5**, 411-418.

COCHRAN, J.R., 1981. The gulf of Aden: Structure and evolution of a young oceanic basin and continental margin. *Journal of geophysical research* **86**, 263-287.

COCHRAN, J.R., 1983. A model for development of Red Sea. *American association of petroleum geophysics Bulletin* **67**, 41-69.

COLLINS, W.J., AND VERNON, R.H., 1991. Orogeny associated with anticlockwise P-T-t paths: Evidence from low-P, high-T metamorphic terranes in the Arunta inlier, central Australia. *Geology* **19**, 835-838.

COLLINS, W.J., VERNON, R.H., AND CLARKE, G.L., 1991. Discrete Proterozoic structural terranes associated with low-P, high-T metamorphism, Anmatjira Range, Arunta Inlier, central Australia: tectonic implications. *Journal of Structural Geology* **13**, 1157-1171.

COLMAN-SADD, S.P., 1982. Two stages continental collision and plate driving forces. *Tectonophysics* **90**, 263-282.

COWARD, M., 1990. Continental collision. **In** Hancock, P.L., (ed.). *Continental deformation*, Pergamon Press.

CURTIS, M.L., 1997. Gondwanian age dextral transpression and spatial kinematic partitioning within the Heritage Range, Ellsworth Mountains, West Antarctica. *Tectonics* **16**, 172-181.

DAVOUDZADEH, M., AND WEBER-DIEFENBACH, K., 1987. Contribution to the palaeogeography, stratigraphy and tectonics of the upper Palaeozoic of Iran. *Neues Jahrbuch Fur Geologie und Palaontologie Abhandlungen, Stuttgart* **175**, 121-146.

DAVOUDZADEH, M., LEANCH, G., AND WEBER-DIEFENBACH, K., 1986. Contribution to the palaeogeography, stratigraphy and tectonics of the upper Infracambrian and lower Palaeozoic of Iran. *Neues Jahrbuch Fur Geologie und Palaontologie Abhandlungen, Stuttgart* **172**, 245-269.

DEHGAN, M., 1947. Sur l'âge mesozoique de la zone de Hamadan (Iran septentrional). *C.R. Academic Science Paris* **224**, 1516-1518.

DERCOURT, J., ZONENSHAIN, L.P., RICOU, L.E., KAZMIN, V.G., LE PICON, X., KNIPPER, A.L., GRANDJACQUET, C., SBORTSHIKOV, I.M., GEYSSANY, J., LEPVERIER, C., PECHERSKY, D.H., BOULIN, J., SIBUET, J.C., SAVOSTIN, L.A., SOROKHTIN, O., WESTPHAL, M., BAZHENOV, M.L., LAUER, L.P., AND BIJU-DUVAL, B., 1986. Geological evolution of the Tethys belt from the Atlantic to the Pamirs since the Lias. *Tectonophysics* **123**, 241-315.

DEWEY, J.F., AND BIRD, J.M., 1971. Origin and emplacement of the ophiolites suite: Appalachian Ophiolites in Newfoundland, *journal of Geophysical research* **76**, 3179-3206.

DEWEY, J.F., PITMAN, W.C., RYAN, W.B.F., AND BONIN, J., 1973. Plate tectonics and the evolution of the Alpine system. *Geological Society of America Bulletin* **84**, 3137-3180.

DEWEY, J.F., SHACKELTON, R.M., CHENGFA, C., YIYIN, S., 1988. The tectonic evolution of the Tibetan Plateau. *Phil. Trans. R. Soc. London. A* **327**, 379-443.

DIMITRIJEVIC, M.D., 1973. The geology of the Kerman region. *Geological Survey of Iran* 334 p.

EDELMAN, S.H., 1988. Ophiolite generation and emplacement by rapid subduction

hinge retreat on a continent-bearing plate. *Geology* **16**, 311-313.

EL-SHAZLY, A.K., AND COLEMAN, R.G., 1990. Metamorphism in the Oman Mountains in relation to the Semail ophiolite emplacement. **In** Robertson, A.H.F., Searle, M.P., and Ries, A.C., (eds). The geology and Tectonics of the Oman Region. *Geological Society of London Special Publication* **49**, 473-493.

ESHRAGI, S. in press. Geological map of Tuyserkan, scale: 1:100 000. *Geological Survey of Iran.*

FALCON, N.L., 1969. Problems of the relationship between surface structure and deep displacements illustrated by the Zagros range. *Geological Society of London special publication* **3**, 9-26.

FALCON, N.L., 1974. Southern Iran Zagros mountains. *Geological Society of London special publication* **4**, 194-211.

FARHADIAN, M.B., 1991. Geochemistry and mineralogy of the Nezam-Abad Granite. MSc. Thesis, University of Tehran, Iran.

GARFUNKEL, Z., 1981. Internal structure of the Dead Sea leaky transform (rift) in relation to plate kinematics. *Tectonophysics* **80**, 81-108.

GILLEN, C., 1982. *Metamorphic geology, an introduction to tectonic and metamorphic processes*, George Allen & Unwin (publishers) ltd, UK.

GIRDLER, R.W., 1990. The Dead Sea transform fault system. *Tectonophysics* **180**, 1-13.

GLENNIE, K.W., BOEUF, M.G.A., HUGHES CLARKE, M.W., MOODY-STUART, M., PILAAR, W.F.H., AND REINHARDT, B.M., 1973. Late Cretaceous nappes in Oman mountains and their geological evolution. *American Association of Petroleum Geologists Bulletin* **57**, 5-27.

GLENNIE, K.W., BOEUF, M.G.A., HUGHES CLARKE, M.W., MOODY-STUART, M., PILAAR, W.F.H., AND REINHARDT, B.M., 1974. Geology of the Oman Mountains. Verhandelingen van het Koninklijk Nederlands Geologisch Mynbouw-Kundig Genootschap. Volume **31**, The Hague, Martinus Nijhoff.

GOLDSTEIN A.G., 1988. Factors affecting the kinematic interpretation of asymmetric boudinage in shear zones. *Journal of Structural Geology* **10**, 707-715.

GOSH S.K., 1993. *Structural Geology, fundamentals and modern developments.* Pergamon Press, UK.

GUINEBERTEAU, B., BOUCHEZ, J.L., VIGNERESSE, J.L., 1987. The Mortange

granite pluton (France) emplaced by pull-apart along a shear zone: Structural and gravimetric arguments and regional implication. *Geological Society of America Bulletin* **99**, 763-770.

HAJMOLLA-ALI, A., HUSSEINI, M., FARHADIAN, M.B., AND SEDAGAT, E., 1989. Geological map of the Borujerd area, Scale 1:100 000 sheet number 5757. *Geological Survey of Iran.*

HALLAM, A., 1976. Geology and plate tectonics interpretation of the sediments of the Mesozoic radiolarite-ophiolite complex in the Neyriz region, southern Iran. *Geological society of America Bulletin* **87**, 47-52.

HAMEDI, M.A., 1995. Lower Palaeozoic Sedimentology and Stratigraphy of the Kerman region, East-Central Iran. PHd thesis, 176 pages.

HANMER, S., 1986. Asymmetrical pull-aparts and foliation fish as kinematic indicators. *Journal of Structural Geology* **8**, 111-122.

HANMER, S., AND PASSCHIER, C., 1991. Shear-sense indicators: a review. *Geological Survey of Canada, paper 90-117.*

HARISON, T.M., COPELAND, P., KIDD, W.S.F., AND YIN, A., 1992. Raising Tibet. *Science* **255**, 1663-1670.

HARLAND, W.B., ARMSTRONG, R.L., COX, A.V., CRAIG, L.E., SMITH, A.G., AND SMITH, D.G., 1989. *A geologic time scale 1989*, Cambridge University Press, 263 p.

HATCHER, R.D., AND WILLIAMS, R.T., 1986. Mechanical model for single thrust sheets Part 1: Crystalline thrust sheets and their relationships to the mechanical/thermal behaviour of orogenic belts. *Geological Society of America Bulletin* **97**, 975-985.

HAYNES, S.J., AND McQUILLAN, H., 1974. Evolution of the Zagros Suture Zone, southern Iran. *Geological Society of America Bulletin* **85**, 739-744.

HAYNES, S.J., AND REYNOLDS, P.H., 1980. Early development of Tethys and Jurassic ophiolite displacement. *Nature* **283**, 561-563.

HOOPER, R.J., BARON, I., HATCHER, R.D. AND AGAH, S., 1994. The development of the southern Tethyan margin in Iran after the break-up of Gondwana-land, implications for the Zagros hydrocarbon province. *Geoscience, Scientific Quarterly Journal, Geological Survey of Iran* **4**, Number 13 Autumn, 72-85.

HOUSHMANDZADEH, A.R., OHANIAN, T., SAHANDI, M.R., TARAZ, H.,

AGANABATI, A., SOHEILI, M., AZARM, F., AND HAMDI, B., 1975. Geological map of Eglid, scale 1:250 000, *Geological Survey of Iran.*

HUCKRIEDE, R., KURSTEN, M. AND VENZLAF, H., 1962. Zur Geologie zwischen Kerman und Sagand (Iran). *Beihefte zum Geologisches Jahrbuch* **51**. 197 p.

HUSSEINI, M.I., 1989. Tectonic and Deposition Model of Late Precambrian Arabian and Adjoining Plates. *The American Association of Petroleum Geologists Bulletin* **73**, 1117-1131.

HUTTON, D.H,W., 1982. A tectonic model for the emplacement of the main Donegal granite, Northwest Irland. *Jounal of Geological Society of London* **139**, 615-631.

HUTTON, D.H.W, 1988. Granite emplacement mechanisms and tectonic controls: inferences from deformation studies. *Transactions of the Royal Society of Edinburgh: Earth Sciences* **79**, 245-255.

JACKSON, J.A., 1992. Partitioning of strike-slip and convergent motion between Eurasia and Arabia in eastern Turkey and the Caucasus. *Journal of Geophysical Research* **97**, 12471-12479.

JACKSON, J.A., AND McKENZIE, D.P., 1984. Active tectonics of the Alpine-Himalayan belt between western Turkey and Pakistan. *Geophysical journal* **77**, 185-264.

JACKSON, J.A., AND McKENZIE D.P., 1988. The relationship between plate motions and seismic moment tensors, and the rates of active deformation in the Mediterranean and Middle East. *Gephysical journal* **93**, 45-73.

JAFARIAN, M.B., in press. The geological map of the Malayer area. *Geological Survey of Iran.*

JAMES, N.P., AND STEVENS, P.K., 1986. Stratigraphy and correlations of the Cambro-Ordovician Cow Head Group, western Newfounland, *Geological Survey of Canada Bulletin* 366, 143p.

JAMES, J.A., AND WYND, J.G., 1965. Stratigraphic nomenclature of Iranian oil consortium agreement area. *American Association of Petroleum Geologists Bulletin* **49**, 2182-2245

JAMIESON, R.A., AND BEAUMONT, C., 1988. Deformation and P-T-t paths in Convergent Orogens. **In** Nisbet, E.G., and Fowler, C.M.R., (eds). Short course on heat, metamorphism and tectonics Volume 14. *Mineralogical Association of*

Canada. St. Johns, Newfoundland.

JORDAN, T.E.,, ISACKS, B.L., ALLMENDINGER, R.W., BREWER, J.A., RAMOS, V.A., AND ANDO, C.J., 1983. Andean tectonics related to geometry of subducted Nazca plate. *Geological Society of America Bulletin* **94**, 341-361.

KAZMIN, V.G., RICOU, L.F., AND SBORTSHIKOV, I.M., 1986. Structure and evolution of the passive margin of the eastern Tethys. *Tectonophysics* **123**, 153-179.

KHOLGI, M.H., 1984. Late Triassic-Jurassic age from the Hamadan Phyllite in Lakan area (90 km west-northwest of Golpaygan). *Geological Survey of Iran*, internal report in farsi, 9 pages.

KNIPPER, A., RICOU, L.E., AND DERCOURT, J., 1986. Ophiolites as indicators of the geodynamic evolution of the Tethyan ocean. *Tectonophysics* **123**, 213-240.

LANPHERE, M.A., AND PAMIC, J., 1983. Ar^{40}/Ar^{39} ages and tectonic setting of ophiolite from the Neyriz area. Southeast Zagros range, Iran. *Tectonophysics* **96**, 245-256.

LEANSCH, G., AND DAVOUDZADEH, M., 1982. Ophiolites in Iran. *Neues Jahrbuch Fur Geologie und Palaontologie*, Mh., **1982**, 306-320.

LEITCH, E. C., 1984. Island arc elements and arc-related ophiolites. *Tectonophysics* **106**, 177-203.

LE METOUR, J., RABU, D., TEGYER, M., BECHENNEC, F., BEURRIER, M., AND UILLEY, M., 1990. Subduction and obduction: two stages in the Eo-Alpine tectonometamorphic evolution of the Oman Mountains. **In** Robertson, A.H.F., Searle, M.P., and Ries, A.C., (eds). The geology and Tectonics of the Oman Region. *Geological Society of London Special Publication* **49**, 327-341.

LE PICHON, X., AND FRANCHETEAU, J., 1978. A plate tectonic analysis of the Red Sea-Gulf of Aden area. *Tectonophysics* **46**, 369-406.

LISTER, G.S., ETHERIDGE, M.A., SYMONDS, P.A., 1986. Detachment faulting and the evolution of passive continental margins. *Geology* **14**, 246-250.

LISTER, G.S., AND SNOKE, A.W., 1984. S-C Mylonites. *Journal of Structural Geology* **6**, 617-638.

LUX, D.R., DE YOREO, J.J., GUIDOTTI, C.V., AND DECKER, E.R., 1986. Role of plutonism in metamorphic belt formation. *Nature* **323**, 794-797.

MAHDAVI, M.A., HUSSEINI-DOOST, J., AND ALAVI, M., 1992. Geological map

of the Nahavand area, scale 100 000, *Geological Survey of Iran*, sheet number 5658.

McCALL, G.J.H., 1985. Area report, east Iran project, area number 1, north Makran and south Baluchestan. *Geological Survey of Iran*, report number 57, 643 p., 2 maps.

McCALL, G.J.H., AND KIDD, R.G.W., 1982. The Makran, southeastern Iran: anatomy of a convergent plate margin active from Cretaceous to Present. **In** Legett, J., (ed.). Trench-Fore-arc Geology. *Geological Society of London, Special Publication* **10**, 387-397.

McKENZIE, D.P., DAVIES, D., AND MOLNAR, P., 1970. Plate tectonics of the Read Sea and East Africa. *Nature* **226**, 243-248.

MANSPEIZER, W., 1985. The Dead Sea rift: impact of climate and tectonism on Pleistocene and Holocene sedimentation. **in** Biddle, K.T., and Christie-Blick, N., (eds). Strike-slip deformation, basin formation, and sedimentation. *Society of Economic palaeontologists and mineralogists, special publication number 37.*

MARSHAK, S., AND MITRA, G., 1988. *Basic methods of structural geology*, Prentice-Hall Inc.

MITCHELL, A.H.G., AND READING, H.G., 1986. Sedimentation and tectonics. **In** Reading, h.g., (ed.). *Sedimentary environments and facies*, Blackwell scientific publications.

MOHAJJEL, M., 1992. Geological map of the Golpaygan area, scale 1:100 000. *Geological Survey of Iran*, sheet number 6056.

MOLNAR, P., AND TAPPONNIER, P., 1975. Cenozoic tectonics of Asia: Effects of a continental collision, *Science* **189**, 419-426.

MOORES, E.M., 1982. Origin and emplacement of ophiolites: *Reviews of Geophysics and Space Physics* **20**, 735-760.

MOORES, E.M., ROBINSON, P.T., MALPAS, J., AND XENOPHONOTOS, C., 1984. Model for the origin of the Troodos massif, Cyprus, and other mideast ophiolites. *Geology* **12**, 500-503.

MORADIAN, A., 1997. Geochemistry, geochronology and petrography of feldspathoid-bearing rocks in the Urumieh-Dokhtar Volcanic Belt, Iran. Phd thesis, University of Wollongong, Australia.

MOTIEI, H., 1993. Stratigraphy of the Zagros. *Geological Survey of Iran*, 536 p.

MURPHY, F.C., 1987. Late Caledonian granitoids and timing of deformation in the

Iapetus suture zone of eastern Ireland. *Geological Magazine* **124**, 135-142.

NABAVI, M.H., 1974. A preface to the Geology of Iran (in Farsi). *Geological Survey of Iran.*

NI, J., AND BARAZANGI, M., 1986. Seismotectonics of the Zagros Continental Collision Zone and a Comparison with Himalayas. *Journal of Geophysical Research* **91**, No. B6, 8205-8218.

NOBLET, C., LAVENU, A., MAROCCO, R., 1996. Concept of continuum as opposed to periodic tectonism in the Andes. *Tectonophysics* **255**, 65-78.

PASSCHIER C.W., AND SIMPSON C., 1986. Porphyroclast systems as kinematic indicators. *Journal of Structural Geology* **8**, 831-843.

PATERSON, S.R., VERNON, R.H., AND TOBISCH, O.T., 1989. A review criteria for determining magmatic and solid-state foliations in granitoids. *Journal of Structural Geology* **11**, 349-363.

PATERSON, S.R., BRUDOS, T., FOWLER, K., CARLSON, C. BISHOP, K., AND VERNON, R., 1991. Papoose Flat pluton: Forceful expansion or postemplacement deformation? *Geology* **19**, 324-327.

PATERSON, S.R., TOBISCH, O.T., AND MORAND, V.J., 1990. The influence of large ductile shear zones on the emplacement and deformation of the Wyangala Batholith, SE Australia. *Journal of Structural Geology* **12**, 639-650.

PATERSON, S.B., AND TOBISCH, O.T., 1988. Using pluton ages to date regional deformations: Problems with commonly used criteria. *Geology* **16**, 1108-1111.

PITCHER, W.S., 1993. *The nature and origin of granite*, Blackie Academic & Professional.

POLAT, A., AND CASEY, F., 1995. A structural record of the emplacement of the Pozanti-Karsanti ophiolite onto the Menderes-Taurus block in the late Cretaceous, eastern Taurides, Turkey. *Journal of Structural Geology* **17**, 1673-1688.

PRICE, N.J., AND COSGROVE, J.W., 1990. *Analysis of geological structures*, Cambridge University press.

RAMSAY J.G., 1967. *Folding and fracturing of rocks*, New York, McGraw-Hill.

RAMSAY J.G., AND HUBER M.I., 1987. *The techniques of modern structural geology. Volume 2: Folds and fractures*, Academic Press, London.

REYER, D., AND MOHAFEZ, S., 1972. A first contribution of the NIOC-ERAP agreements to the knowledge of Iranian geology. Technip, Paris, 1-58.

RICOU, L.E., 1971. Le croissant ophiolitique péri-arabe. Une ceinture de nappes misses en place au Crétacé superiéur. *Revue de Geographie Physique et de Geologie Dynamique* **13**, 327-350.

RICOU, L.E., 1974. L' évolution géologique de la région de Neyriz (Zagros Iranien) et l' évolution structurale des Zagrides. *Thèse de état, Université de Orsay, France.*

RICOU, L.E., BRAUD, J., AND BRUNN, J.A., 1977. Le Zagros. Mémories de la Societe Géologique de France. Hors. Sér., **8**, 33-52.

ROBERTSON, A.H.F., AND SEARLE, M.P., 1990. The northern Oman Tethyan continental margin: stratigraphy, structure, concepts and controversies. **In** Robertson, A.H.F., Searle, M.P., and Ries, A.C., (eds). The geology and Tectonics of the Oman Region. *Geological Society of London Special Publication* **49**, 27-38.

ROEDER, D., 1988. Andean-age structures of eastern Cordillera (Provience of La Paz, Bolivia). *Tectonics* **7**, 23-39.

ROYDEN, L.H., 1993. The tectonic expression slab pull at continental convergent boundaries. *Tectonics* **12**, 303-325.

RUBIN, C.M., SALEEBY, J.B., DARREL, S.C., BRANDON, M.T., AND McGRODER, M.F., 1990. Regionally extensive mid-Cretaceous west-vergent thrust system in the northwestern Cordillera: Implications for continent-margin tectonism. *Geology* **18**, 276-280.

SABZEHIE, M., 1974. Les melange ophiolitques de la région de Esfandagheh. Thèse d' état, *Université Scientifique et Médicale de Grenoble, France*, 306 p.

SABZEHIE, M., AND ESHRAGI, S., 1995. Geological map of the Neyriz. 1:100,000 *Geological Survey of Iran.*

SAHANDI, M.R., HUSSEINI-DOOST, J., RADFAR, J., AND MOHAJJEL, M., in press. The geological map of the Shazand area, scale 1:00 000. *Geological Survey of Iran.*

SAMANI, B., 1992. Introducing riftogenic Saghand Formation and its stratigraphical position in the Precambrian of Iran. **In** The 11th Symposium on Geoscience, *Geological Survey of Iran*, 24-30.

SAMANI, B., ZHUYI, G., XUETAO, G., AND CHUAN, T., 1994. Geology of Precambrian in central Iran; on the context of stratigraphy, magmatism and metamorphism. *Scientific quarterly journal* **3**, number 10, 40-63.

SANDERSON, D.J., AND MARCHINI, W.R.D., 1984. Transpression. *Journal of Structural Geology* **6**, 449-454.

SCOTESE, C.R., 1991. Jurassic and Cretaceous plate tectonic reconstructions. *Palaeogeography, Palaeoclimatology, Palaeoecology* **87**, 493-501.

SEARLE, M.P., AND GRAHAM, G.M., 1982. 'Oman Exotics' oceanic carbonate build-ups associated with early stages of continental rifting. *Geology* **10**, 43-59.

SEBER, D., VALLVE, M., SANDVOL, E., STEER, D. AND BARZANGI, M., 1997. Middle East tectonics: applications of Geographic Information Systems (GIS). *GSA today* **7**, 2-6.

ŞENGöR, A.M.C., 1990b. Plate tectonics and orogenic research after 25 years: A Tethyan perspective. *Earth science reviews* **27**, 1-201.

ŞENGöR, A.M.C., ALTMER, D., CIN, A., USTAOMER, T., AND HSU, K.J., 1988. Origin and assembly of the Tethyside orogenic collage at the expense of Gondwana Land. **In** Audley-Chales, M.G., and Hallam, A., (eds). Gondwana and Tethys. *Geological society of London Special Publication* **37**, 119-181.

ŞENGöR, A.M.C., 1990a. A new model for the late Palaeozoic-Mesozoic tectonic evolution of Iran and implications for Oman. **In** Robertson, A.H.F., Searle, M.P., and Ries, A.C., (eds). The geology and Tectonics of the Oman Region. *Geological Society of London Special Publication* **49**, 797-831.

ŞENGöR, A.M.C., AND KIDD, W.S.F., 1979. Post-collitional tectonics of the Turkish-Iranian plateau and A comparison with Tibet. *Tectonophysics* **55**, 361-376.

ŞENGöR, A.M.C., 1979. Mid-Mesozoic closure of Permo-Triassic Tethys and its implications. *Nature* **279**, 590-593.

ŞENGöR, A.M.C., 1984. The Cimmeride orogenic system and tectonics of Eurasia. *Geological Society of America, special paper* **195**, 82p.

ŞENGöR, A.M.C., GORUR, N., AND SARGOGLU, F., 1985. Strike-slip faulting and related basin formation in zones of tectonic escape: Turkey as a case study. **In** Biddle, K.T., and Christie-Blick, N., (eds). Strike-slip deformation, basin formation and sedimentation. *Society of Economic Palaeontologists and Mineralogists Special Publication* **37**, 227-265.

SENGUPTA, S., 1983. Folding of boudinaged layers. *Journal of Structural Geology* **5**, 197-210.

SEARLE, M.P., METSALFE, R.P., REX, A.J., AND NORRY, M.J., 1993. Field relations, petrogenesis and emplacement of the Bhagirathi leucogranite, Garhwal Himalaya. **In** Treloar, P.J., and Searle, M.P., (eds). Himalayan tectonics, *Geological Society of London, special publication No 74*, 429-444.

SHAHIDI, A.R., AND NAZARI, B., in press. Geological map of the Harsin area, scale 100 000, *Geological Survey of Iran.*

SIMPSON, C., AND SCHMID, S.M., 1983. An evaluation of criteria to deduce the sense of movement in sheared rocks. *Geological Society of America Bulletin* **94**, 1281-1288.

SOHEILI, M., (Compiler) 1992. Geological map of the Khorramabad, scale 1:250 000. *Geological Survey of Iran.*

SOHEILI, M., JAFARIAN, M.B., AND ABDOLLAHE, M.R., 1992. Geological map of the Aligudarz area. *Geological Survey of Iran* 1:100 000 series sheet number 5956.

STECK, A., SPRING, L., VANNAY, J.C., MASSON, H., BUCHER, H., STUTZ, E., MARCHANT, R. AND TIECHE, J.C., 1993. The tectonic evolution of the Northwestern Himalya in eastern Ladakh and Lahul, India. **In** Treloar, P.J., and Searle, M.P., (eds). Himalayan tectonics, *Geological Society of London, special publication No 74*, 265-276.

STöCKLIN, J., 1974. Possible ancient continental margins in Iran. **In** Buk, C.A., and Darke, C.L., (eds). *The geology of continental margins. Springer, New York*, 873-887.

STöCKLIN, J., 1968. Structural history and tectonics of Iran; a review. *American Association of Petroleum Geologists Bulletin* **52**, 1229-1258.

STöCKLIN, J., AND SETUDEHNIA, A.D., 1991. Stratigraphic Lexicon of Iran. *Geological Survey of Iran, Report 18.*

STONELEY, R., 1975. On the origin and ophiolite complexes in the southern Tethys region. *Tectonophysics* **25**, 303-322.

SUPPE, J., 1985. *Principles of structural geology*, Prentice Hall, Englewood Cliffs, New Jersy.

TAKAGI, H., 1986. Implications of mylonitic microstructures for the geotectonic evolution of the Median Tectonic Line, central Japan. *Journal of Structural Geology* **8**, 3-14.

TAKIN, M., 1972. Iranian geology and continental drift in the Middle East. *Nature* **235**, 147-150.

TAPPONNIER, P, PELTZER, G., LE DAIN, A. Y., ARMIJO, R., AND COBBOLD, P., 1982. Propagating extrusion tectonics in Asia: New insights from simple experiments with plasticine. *Geology* **10**, 611-616.

TEYSSIER, C., TIKOFF, B., AND MARKLEY, M., 1995. Oblique plate motion and continental tectonics. *Geology* **23**, 447-450.

TCHALENKO, J.S., AND BRAUD, J., 1974. Seismicity and structure of the Zagros (Iran): The main Recent Fault between 33° and 35° N. *Philos. Trans. Royal Society of London* **277**, 1-25.

THIELE, O., 1966. Zum Alter der Metamorphose in Zentral Iran. *Mitt. Geol. Ges. Wien*, **58**, 87 101.

THIELE, O., ALAVI-NAINI, M., ASSEFI, R., HOUSHMANDZADEH, A., SEYED-EMAMI, K., AND ZAHEDI, M., 1968. Explanatory text of the Golpaygan quadrangle map. *Geological Survey of Iran*, Quadrangle Number E_7, scale 1:250 000, 24p.

TIKOFF, B., AND TEYSSIER, C., 1994. Strain modelling of displacement-field partitioning in transpressional orogens. *Journal of Structural Geology* **16**, 1575-1588.

TILLMAN, J.E., POOSTI, A., ROSSELLO, S., AND ECKERT, A., 1981. Structural Evolution of Sanandaj-Sirjan Ranges Near Esfahan, Iran. *American Association of Petroleum Geology* **65**, 674-687.

TOBISCH, O.T., AND PATERSON, S.R., 1990. The Yarra granite: An intradeformational pluton associated with ductile thrusting, Lachlan Fold Belt, southeastern Australia. *Geological Society of America Bulletin* **102**, 693-703.

TURNER, F.J., 1981. *Metamorphic petrology: mineralogical, field and tectonic aspects*, New York: McGraw-Hill Book Company.

VAEZIPOUR, M.J., AND EGLIMI, B., 1984. Ammonite from the Lakan area (90 km west-northwest of Golpaygan). *Geological Survey of Iran*, internal report in farsi.

VALIZADEH, M.V., AND CANTAGREL, J.M., 1975. Prèmieres données radiométricques (K-Ar et Rb-Sr) sur les micas du complexe magmatique du Mont Alvand, Près Hamadan (Iran occidental). *Comptes Rendus, Academie des Sciences Paris, Série D*, **281**, 1083-1086.

VALIZADEH, M.V., AND GHASEMI, H., 1993. Petrogenesis of granitoid massif of Buin-Miandasht, Southeastern Aligudarz. *Geosciences, Scientific Quarterly Journal, Geological Survey of Iran*, **2**, number 7 Spring.

VEEVERS, J.J., 1981. Morphotectonics of rifted continental margins in Embryo (East Africa), youth (Africa-Arabia), and maturity (Australia). *Journal of Geology* **89**, 57-82.

VEEVERS, J.J., 1989. Middle-Late Triassic (230 ± Ma) singularity in the stratigraphic and magmatic history of the Pangean heat anomaly. *Geology* **17**, 784-787.

VERNON, R.H., 1976. *Metamorphic processes, reactions and microstructure development*, George Allen & Unwin (publishers) Ltd, UK, 247 pages.

von HUENE, R., 1984. Tectonic processes along the front of modern convergent margins - Research of the past decade. *Ann. Rev. Earth Planet. Sci.* **12**, 359-381.

von HUENE, R., KULM, L.D., AND MILLER, J., 1985. structure of the frontal part of the Andean convergent margin. *Journal of Geophysical Research* **90**, 5429-5442.

WATTERS, W.A., AND SABZEHIE, M., 1970. Preliminary report, geology and petrography of the metamorphic and igneous complex of the central part of the Neyriz quadrangle. *Geological Survey of Iran*, Internal report.

WELLS, A.J., 1969. The crush zone of the Iranian Zagros mountains and its implications. *Geological Magazine* **106**, 385-394.

WERNICKE B., AND BURCHFIEL, B.C., 1982. Modes of extensional tectonics. *Journal of Structural Geology* **4**, 105-115.

WHITE, R.S., ROSS, D.A., 1979. Tectonic of the western Gulf of Oman. *Journal of Geophysical Research* **84**, 3479-3489.

WHITE, S.H., BURROWS, S.E., CARRERAS, J., SHAW, N.D., AND HUMPHREYS, F.J., 1980. On mylonites in ductile shear zones. *Journal of Structural Geology* **2**, 175-187.

WILLIAMS, H., HISCOTT, R.N., 1987. Deformation of the lapetus rift-drift transition in western Newfoundland. *Geology* **15**, 1044-1047.

WILSON, G., AND COSGROVE, J.W., 1982. *Introduction to small-scale geological structures*, Allen & Unwin, London.

WORLEY, B.A., AND WILSON, C.J.L., 1996. Deformation partitioning and foliation

reactivation during transpressional orogenesis, an example from the Central Longmen Shan, China. *Journal of Structural Geology* **18**, 395-411.

YARDLEY, B.W.D., MACKENZI, W.S., AND GUILFORD, C., 1990. *Atlas of metamorphic rocks and their textures*, Longman Scientific & Technical, UK, 120 p.

ZAHEDI, M., SAMADIAN, M., AMIDI, M., AND TATAVOUSIAN, Sh., 1978. Geological map of the Esfahan, scale 1:250 000, *Geological Survey of Iran.*

ZAHEDI, M., RAHMATI-ILKHCHI, M., AND VAEZIPOUR, J., 1992. Geological map of the Shahrekord, scale 1:250 000. *Geological Survey of Iran.*

Rock No.	Field No.	TS No.	Description	Locality	Formation	Age
R16559	P17	1	Quartzite	Papion	June Complex	Middle-Late Triassic
R16560	P19	2	Muscovite schist	Papion	June Complex	Middle-Late Triassic
R16561	19	3	Muscovite schist	Papion	June Complex	Middle-Late Triassic
R16562	23	4	Chlorite-epidote schist	Zageh-Bala	June Complex	Middle-Late Triassic
R16563	27	5	Metagabbro	Zageh-Bala	June Complex	Middle-Late Triassic
R16564	28a	6	Mylonitic granite	Meydanak		Palaeocene
R16565	28b	7	Mylonitic granite	Meydanak		Palaeocene
R16566	28c	8	Mylonitic granite	Meydanak		Palaeocene
R16567	28d	9	Mylonitic granite	Meydanak		Palaeocene
R16568	30a	10	Schist	Darijune-Bala	June Complex	Middle-Late Triassic
R16569	P31	11	Calcite mylonite	Darijune-Bala	June Complex	Middle-Late Triassic
R16570	32	12	Calcite mylonite	Darijune-Bala	June Complex	Middle-Late Triassic
R16571	33	13	Metasandstone	Darijune-Bala	June Complex	Middle-Late Triassic
R16572	42	14	Dolerite	Darijune-Paein		
R16573	45	15	Amphibolite	Zageh-Bala	June Complex	Middle-Late Triassic
R16574	49	16	Schist	Zageh-Bala	June Complex	Middle-Late Triassic
R16575	52	17	Schist	Zageh-Bala	June Complex	Middle-Late Triassic
R16576	63	18	Metasandstone	Papion	June Complex	Middle-Late Triassic
R16577	66a	19	Muscovite schist	Papion	June Complex	Middle-Late Triassic
R16578	66b	20	Muscovite schist	Papion	June Complex	Middle-Late Triassic
R16579	66c	21	Muscovite schist	Papion	June Complex	Middle-Late Triassic
R16580	70	22	Schist	Papion	June Complex	Middle-Late Triassic
R16581	78	23	Dolerite	Papion	June Complex	Middle-Late Triassic
R16582	87	24	Dolerite	Papion	June Complex	Middle-Late Triassic
R16583	102	25	Marble	Papion	June Complex	Middle-Late Triassic
R16584	P106	26	Amphibolite	Zageh-Bala	June Complex	Middle-Late Triassic
R16585	P106a	27	Amphibolite	Zageh-Bala	June Complex	Middle-Late Triassic
R16586	P106b	28	Amphibolite	Zageh-Bala	June Complex	Middle-Late Triassic
R16587	120a	29	Muscovite schist	Darijune-Bala	June Complex	Middle-Late Triassic
R16588	120b	30	Muscovite schist	Darijune-Bala	June Complex	Middle-Late Triassic
R16589	122	31	Metavolcanic rokc	Teadar	Teadar volcanics	L. Jurassic - E.Creta.
R16590	122a	32	Metavolcanic rokc	Teadar	Teadar volcanics	L. Jurassic - E.Creta.
R16591	122b	33	Metavolcanic rokc	Teadar	Teadar volcanics	L. Jurassic - E.Creta.
R16592	134	34	Garnet-biotite schist	Zageh-Bala	June Complex	Middle-Late Triassic
R16593	134a	35	Garnet-biotite schist	Zageh-Bala	June Complex	Middle-Late Triassic
R16594	134b	36	Garnet-biotite schist	Zageh-Bala	June Complex	Middle-Late Triassic
R16595	135a	37	Schist	Zageh-Bala	June Complex	Middle-Late Triassic
R16596	135b	38	Schist	Zageh-Bala	June Complex	Middle-Late Triassic
R16597	142a	39	Ultramylonite	Ag-Bolag	Hamadan Phyllite	Late Triassic-Jurassic
R16598	142b	40	Ultramylonite	Ag-Bolag	Hamadan Phyllite	Late Triassic-Jurassic
R16599	143	41	Schist	Ag-Bolag	June Complex	Middle-Late Triassic
R16600	150	42	Quartzite	Bavaki	June Complex	Middle-Late Triassic
R16601	165a	43	Muscovite schist	Masud-Abad	June Complex	Middle-Late Triassic
R16602	165b	44	Muscovite schist	Masud-Abad	June Complex	Middle-Late Triassic
R16603	165c	45	Muscovite schist	Masud-Abad	June Complex	Middle-Late Triassic
R16604	171	46	Mylonitic granite	Masud-Abad		Palaeocene
R16605	171a	47	Mylonitic granite	Masud-Abad		Palaeocene
R16606	171b	48	Mylonitic granite	Masud-Abad	June Complex	Middle-Late Triassic
R16607	203	49	Mylonitic granite	Masud-Abad	June Complex	Middle-Late Triassic
R16608	209	50	Amphibolite	Masud-Abad	June Complex	Middle-Late Triassic
R16609	215	51	Metagabbro	Bavaki	June Complex	Middle-Late Triassic
R16610	338	52	Quartzite	Masud-Abad	June Complex	Middle-Late Triassic
R16611	352a	53	Mylonitic amphibolite	Dareh-Zooleh	June Complex	Middle-Late Triassic
R16612	352b	54	Mylonitic amphibolite	Dareh-Zooleh	June Complex	Middle-Late Triassic
R16613	401	55	Amphibolite	Bavaki	June Complex	Middle-Late Triassic
R16614	417	56	Dolerite	Baraftab-Deraz		
R16615	422	57	Ultramylonite	Baraftab-Deraz	June Complex	Middle-Late Triassic
R16616	447	58	Mylonitic granite	Dareh-Zooleh		Palaeocene

R16617	470	59	Quartzite	Dareh-Zooleh	Hamadan Phyllite	Late Triassic-Jurassic
R16618	472	60	Amphibolite	Dareh-Zooleh	Hamadan Phyllite	Late Triassic-Jurassic
R16619	475	61	Dolerite	Dareh-Zooleh	Hamadan Phyllite	Late Triassic-Jurassic
R16620	482	62	Meta sandstone	Deh-Haji	June Complex	Middle-Late Triassic
R16621	488	63	Ultramylonite	Deh-Haji	Hamadan Phyllite	Late Triassic-Jurassic
R16622	502	64	Muscovite schist	Deh-Haji	June Complex	Middle-Late Triassic
R16623	578	65	Schist	Papion	June Complex	Middle-Late Triassic
R16624	711	66	Schist	Papion	June Complex	Middle-Late Triassic
R16625	747	67	Garnet-biotite schist	Shur-Shur	June Complex	Middle-Late Triassic
R16626	778	68	Schist	Choubdar	June Complex	Middle-Late Triassic
R16627	808	69	Amphibolite	Zageh-Bala	June Complex	Middle-Late Triassic
R16628	813	70	Amphibolite	Zageh-Bala	June Complex	Middle-Late Triassic
R16629	813a	71	Amphibolite	Zageh-Bala	June Complex	Middle-Late Triassic
R16630	813b	72	Amphibolite	Zageh-Bala	June Complex	Middle-Late Triassic
R16631	829	73	mylonitic granite	Zageh-Bala		Palaeocene
R16632	847	74	Schist	Galeh-Gurchak	June Complex	Middle-Late Triassic
R16633	848	75	mylonitic granite	Galeh-Gurchak		Palaeocene
R16634	873	76	Metavolcanic rock	Galeh-Gurchak	June Complex	Middle-Late Triassic
R16635	914	77	Marble	Darijune-Bala	June Complex	Middle-Late Triassic
R16636	951	78	Muscovite schist	Ag-Bolag	June Complex	Middle-Late Triassic
R16637	957	79	Muscovite-biotite schist	Ag-Bolag	June Complex	Middle-Late Triassic
R16638	972	80	Amphibolite	Ag-Bolag	Hamadan Phyllite	Late Triassic-Jurassic
R16639	998a	81	mylonitic granite	Ag-Bolag	June Complex	Middle-Late Triassic
R16640	998b	82	mylonitic granite	Ag-Bolag		Palaeocene
R16641	1001	83	mylonitic granite	Ag-Bolag		Palaeocene
R16642	1052	84	mylonitic granite	Ag-Bolag		Palaeocene
R16643	1089	85	Chlorite-actinolite schist	Darijune-Bala	June Complex	Middle-Late Triassic
R16644	1125	86	schist	Darijune-Paein	June Complex	Middle-Late Triassic
R16645	377	87	marble	Kuh-e-June		Permian
R16646	143b	88	schist	Ag-Bolag	June Complex	Middle-Late Triassic
R16647	21	89	Metagabbro	Zageh-Bala	June Complex	Middle-Late Triassic
R16648	158	90	Mylonitic granite	Galeh-Doz		Palaeocene

Alluvium
Conglomerate
Travertine
Dolerite
GalehDoz mylonitic granite
Suraneh Limestone (Cretaceous)
Teadar volcanic rocks (Late Jurassic-Early Cretaceous)
Hamadan Phyllite (Late Triassic Jurassic)
Silicic metaigneous rocks
Amphibolite
Metadolomite and marble
Schist
Darijan Marble
Quartzite
Kuh-e-June Metacarbonate (Permian)
June Complex (Middle Late Triassic)

F fold axis I intersection lineation
F fold axis I intersection lineation
S schistosity
S schistosity
F fold
S crenulation cleavage
AS1
AS2
AS3
D stretching lineation
Anticline
Overturned antiform with plunge direction
Overturned synform with plunge direction
Thrust fault
Covered
Strike-slip fault
Younging direction
Fossil locality
Cross section
Village
Contact
Creek
Approximate cotact
Road
Track
Spring
Mine
Bedding
Upright younging determined
Overturned
Structure line
Elevation point in metre

GHOUBDAR-E BALA
CHESHMEH-NARGES THRUST
KUH-E-SIAH
MALHAMDAR
DEH-NASIR
GALEH-NO
DOUAB
DAREH-ZOOLEH
SARAB
AQ-BOLAGH
ODEH-MOSA
DEH-HAJI
ZAGEH BALA
SHUR-SHUR
DARIJUNE-BALA
MEYDANAK
PAPOMI
DARIJUNE PAEIN
BARAFTAB-DERAZ
PIRKHALIL
GALEH-GURCHAK THRUST
KUH-E-JUNE
TEADAR
SURANEH
SERENGEH
JUNE
RAZAKI
CHAGA-MOOSHAN
CHESHMEH-HARES THRUST
KUH-E-SEFID
ABBAS-ABAD
MASUD-ABAD

NNE SSW
NNE SSW

(MAP)
STRUCTURE OF THE JUNE AREA, DORUD AZNA REGION, SANANDAJ-SIRJAN ZONE, IRAN
M. MOHAJJEL
Scale 1:20 000

V

V • 17

SURANEH

V

V

KUH-E-SEFID

NNE

SSW

2300

2100

1900

M

N

S_1

S_2

KUH-E-SEFID

NNE

SSW

2600

2400

2200

2000

L

O

S_3

S_2

S_1